Receptor-mediated activation and pharmacological inhibition of heterotrimeric G proteins

Dissertation

zur

Erlangung des Doktorgrades (Dr. rer. nat)

der

Mathemathisch-Naturwissenschaftlichen Fakultät

der

Rheinischen Friedrich-Wilhelms-Universität Bonn

vorgelegt von

Jan Hendrik Voß

aus

Dinslaken

Bonn, 2022

Angefertigt mit Genehmigung der Mathematisch-Naturwissenschaftlichen Fakultät der Rheinischen Friedrich-Wilhelms-Universität Bonn

1. Gutachtertin:	Prof. Dr. Christa E. Müller
2. Gutachterin:	PD Dr. Anke Schiedel
Tag der Promotion:	08.11.2022
Erscheinungsjahr:	2022

Table of Contents

1. Abstract 1

2. Introduction 2

2.1. An introduction to G protein-coupled receptors 3

2.1.1. Phylogeny of GPCRs 4

2.1.2. The three-dimensional structure and dynamics of GPCRs 5

2.1.3. GPCR function 9

2.1.4. Fundamental principles of GPCR pharmacology 12

2.1.5. Pharmacological characterization of ligand binding and functional responses of GPCRs 13

2.2. A short overview on heterotrimeric G proteins 16

2.2.1. Physiological effects of $G\alpha_{q/11}$ proteins 16

2.2.2. Pharmacology of macrocyclic $G\alpha_{q/11}$ protein inhibitors 18

3. Heterotrimeric G protein α-subunits - structures, peptide-derived inhibitors, and mechanisms 19

4. Unraveling binding mechanism and kinetics of macrocyclic $G\alpha_q$ protein inhibitors 21

5. Structure-affinity and structure-residence time relationships of macrocyclic $G\alpha_{q/11}$ protein inhibitors 24

5.1. Results and discussion 26

5.2. Materials and Methods 40

6. Imaging of $G\alpha_{q/11}$ protein expression by autoradiography 44

6.1. Results 45

6.2. Discussion 51

6.3. Materials and Methods 53

7. Agonist-dependent coupling of the promiscuous adenosine A_{2B} receptor to Gα protein subunits 56

8. Using novel BRET-based biosensors to detect coupling of the adenosine-activated $A_{2B}AR$ 59

8.1 Results and discussion 59

8.2 Methods 67

9. Summary 69

9.1. Studies on binding mechanism and binding kinetics of macrocyclic $G\alpha_{q/11}$ protein inhibitors 69

9.2. Gα protein activation profile of the adenosine A_{2B} receptor 74

10. References 78

11. Acknowledgements 100

12. List of abbreviations 102

13. Appendix 105

13.1. Appendix A – Heterotrimeric G protein α-subunits - structures, peptide-derived inhibitors, and mechanisms 106

13.2. Appendix B – Unraveling binding mechanism and kinetics of macrocyclic $G\alpha_q$ protein inhibitors 127

13.3. Appendix C – Agonist-dependent coupling of the promiscuous adenosine A_{2B} receptor to Gα protein subunits 167

1. Abstract

Heterotrimeric guanine-nucleotide binding proteins (G proteins) are key signal transducers in animal and human cells, where they forward signals transmitted by active G protein-coupled receptors (GPCRs) and trigger intracellular signaling cascades. This thesis presents pharmacological studies on (i) macrocyclic $G\alpha_{q/11}$ protein inhibitors and (ii) on the Gα protein activation by the adenosine A_{2B} receptor ($A_{2B}AR$), a promiscuous GPCR.

(i) The structurally related natural products YM-254890 (YM) and FR900359 (FR) are potent and selective inhibitors of the $G\alpha_{q/11}$ protein family. Recently, our group developed tritium-labeled derivatives, which display large differences in residence time, despite having a similar affinity for the $G\alpha_q$ protein. We identified lipophilic interactions between the inhibitor binding site and an isopropyl group, which is exclusively present in FR and its derivatives, as the molecular basis for the long residence time of the FR-derived radioligand. Furthermore, our data suggest a complex binding mechanism of macrocyclic $G\alpha_q$ protein inhibitors, involving a conformational selection step. The proposed mechanism was supported by molecular dynamics simulation studies. Next, we established structure-affinity relationships and structure-residence time relationships of a series of YM and FR derivatives. Additionally, YM- and FR-derived radioligands were employed to analyze the $G\alpha_{q/11}$ protein expression in mouse tissues by autoradiography.

(ii) The $A_{2B}AR$ constitutes a promising drug target for the immunotherapy of cancer. Its physiological functions, however, remain enigmatic. Here, we determine the Gα protein activation fingerprint of the $A_{2B}AR$ by calcium mobilization assays and novel BRET assay systems. In summary, we found that the $A_{2B}AR$ is a promiscuous receptor, which activated nearly all Gα protein subunits. However, it did so with varying degrees of efficacy. It couples most efficaciously to $G\alpha_s$, $G\alpha_{15}$, and $G\alpha_{12}$ proteins, but activates all other Gα proteins with submaximal efficacy (< 50% of control receptors). Importantly, each employed agonist displays a different Gα coupling profile. Finally, both the expression levels of the Gα protein and the GPCR are decisive for effective coupling of the $A_{2B}AR$ to a certain Gα protein.

Altogether, this work provides profound insights into the molecular pharmacology of macrocyclic $G\alpha_q$ protein inhibitors, focusing on their binding kinetics – a parameter which is gaining recognition in drug design. Furthermore, we created a Gα protein coupling profile of the $A_{2B}AR$ and identified relevant parameters that influence $A_{2B}AR$-mediated Gα activation to gain more insight into $A_{2B}AR$ signal transmission.

2. Introduction

The exchange of information is vital in any complex system, be it in a living organism or for example in a computer network. Information can be encoded and transmitted in many different ways, e.g. language and images, but also – especially in a biological context – by electric currents and molecules. Information must be intelligible to be put to use, and therefore it needs to be perceived and interpreted. To this end, a living cell requires structures to sense and to process information presented in whichever way. By analogy, a tape recorder requires both a microphone to sense the voice of a singer and also a tape to record the audio track. If these necessary structures are not present, information cannot be utilized. The human body, for example, lacks sensory structures for infrared light, which are present in other animals, such as snakes and tilapia. In metazoa and fungi, the possibly most important microsensors for extracellular stimuli – small molecules, peptides, and proteins, but also e.g. photons – are G protein-coupled receptors (GPCRs). In particular, the purpose of GPCRs is the propagation of signals across cellular membranes. They capture chemical information from the extracellular space and forward it into the intracellular space, where it is further processed, integrated, and ultimately responded to by the cell.

When activated by a cognate agonist, the first contact partner for an activated GPCR is commonly a member of the family of heterotrimeric guanine nucleotide binding proteins (G proteins), which initiates an intracellular signaling cascade that invokes a response dependent on the GPCR and G protein activated by the stimulus. As the GPCR-G protein axis is crucial for cells to perceive their environment, it is frequently targeted by drugs which activate or block a given GPCR – either to simulate information that otherwise would not be there, or to render the cell blind to information that is actually present – with great success, as roughly a third of marketed drugs acts via GPCRs, thereby contributing largely to overall health in our society.

The following introduction provides a general overview to GPCRs in the first part and to G proteins in the second part to convey fundamentals required for the understanding of published research articles and chapters included in this thesis. The work presented in this thesis was performed in one part on the pharmacology of macrocyclic $G\alpha_q$ protein inhibitors (sections 3-6), and in another part on the G protein coupling of the adenosine A_{2B} receptor (sections 7-8).

2.1. An introduction to G protein-coupled receptors

GPCRs are the largest family of membrane proteins, consisting of over 800 genes in humans [1]. All members of the GPCR gene family share a common architecture of seven transmembrane helices spanning across the membrane, hence they are also known as 7-transmembrane domain receptors. GPCRs facilitate communication between the extracellular and intracellular space. Specifically, GPCRs sense and bind extracellular molecules and propagate a stimulus across the cell membrane into the intracellular space, eliciting a response from the cell. Accordingly, the binding site for GPCR ligands is located on the extracellular side of the seven-transmembrane helix bundle. Upon binding of an agonist, the intracellular portion of the GPCR rearranges into an active GPCR conformation. Here, effector proteins – heterotrimeric G proteins and β-arrestins – can bind to the active GPCR and forward the receptor signal into the cell by interacting with respective effectors. While there are over 800 GPCR genes known in human, far fewer intracellular binding partners are described – namely 16 G protein α subunits (Gα) and 4 arrestins –, thus signaling converges on the layer of GPCR effectors.

Due to the high count of individual receptors, their involvement in a multitude of physiological and pathophysiological processes, their complex pharmacology and signaling, and their well-accessible extracellular binding site, GPCRs constitute valuable drug targets allowing finely tuned pharmacological interventions. Nevertheless, a wide range of GPCRs is currently understudied – endogenous ligands, i.e. the body's own agonists, for a plentitude of GPCRs are still unidentified (orphan GPCRs) [2], potent and specific ligands are lacking (undrugged GPCRs) [3], or the physiology of a GPCR is poorly understood with regard to its downstream signaling. Consequently, GPCRs remain a priority research field in cellular biology, pharmacology, and drug development.

This introduction will focus mainly on GPCRs, starting with their phylogeny, general architecture and structure, and further discusses their function, pharmacology, methods to measure GPCR activity, and current research questions. It is followed by a brief introduction on G proteins; a more comprehensive summary on G proteins is provided in section 3 by the review article "Heterotrimeric G protein α-subunits – structures, peptide-derived inhibitors, and mechanisms" [4].

2.1.1. Phylogeny of GPCRs

There are five major classes of GPCRs, which are clustered based on their sequence similarity. These classes are termed class A (rhodopsin-like GPCRs), class B (secretin-like and adhesion receptors), class C (metabotropic glutamate-like receptors), class D (Ste2-like fungal pheromone receptors, which do not exist in human), and class F (frizzled receptors) [1]. A phylogenetic tree is shown in **Figure 1** [5]. The cluster of class A, rhodopsin-like GPCRs includes around 700 receptor genes, out of which approximately 400 belong to the group of olfactory receptors. In humans, the class A cluster is larger than the other clusters combined [6], and it is further divided into α, β, γ, and δ-branches based on sequence similarity [1].

A common denominator for all GPCRs is the seven transmembrane helix structure with an extracellular N-terminus and an intracellular C-terminus. Ligand and effector binding sites and loop residues constitute more variable receptor regions, while the helical domains are, generally speaking, more conserved. Each class of GPCRs displays characteristic features, e.g. class C receptors have a prominent extracellular domain containing a ligand binding site [7]. Receptors associated with the same endogenous agonist are closely related, even if individual receptors within the receptor family engage distinct signaling pathways, as it is the case for e.g. adenosine receptors or aminergic receptors (see **Figure 1**) [8].

Although the gene family of GPCRs is the largest among membrane proteins [1], key residues are well-conserved throughout the GPCR family. The Ballesteros-Weinstein nomenclature for residue labeling is used to compare structural elements between different receptors [9]: the most conserved residue X within helix *n* is labeled in superscript as $X^{n.50}$; residues N-terminal from $X^{n.50}$ within the same helix are labeled with decreasing numbers, C-terminal residues are vice versa labeled with increasing numbers. For example, the DRY-motif of the adenosine A_{2A} receptor ($A_{2A}AR$) would be labeled as $D^{3.49}$, $R^{3.50}$, and $Y^{3.51}$ instead of D101, R102, and Y103.

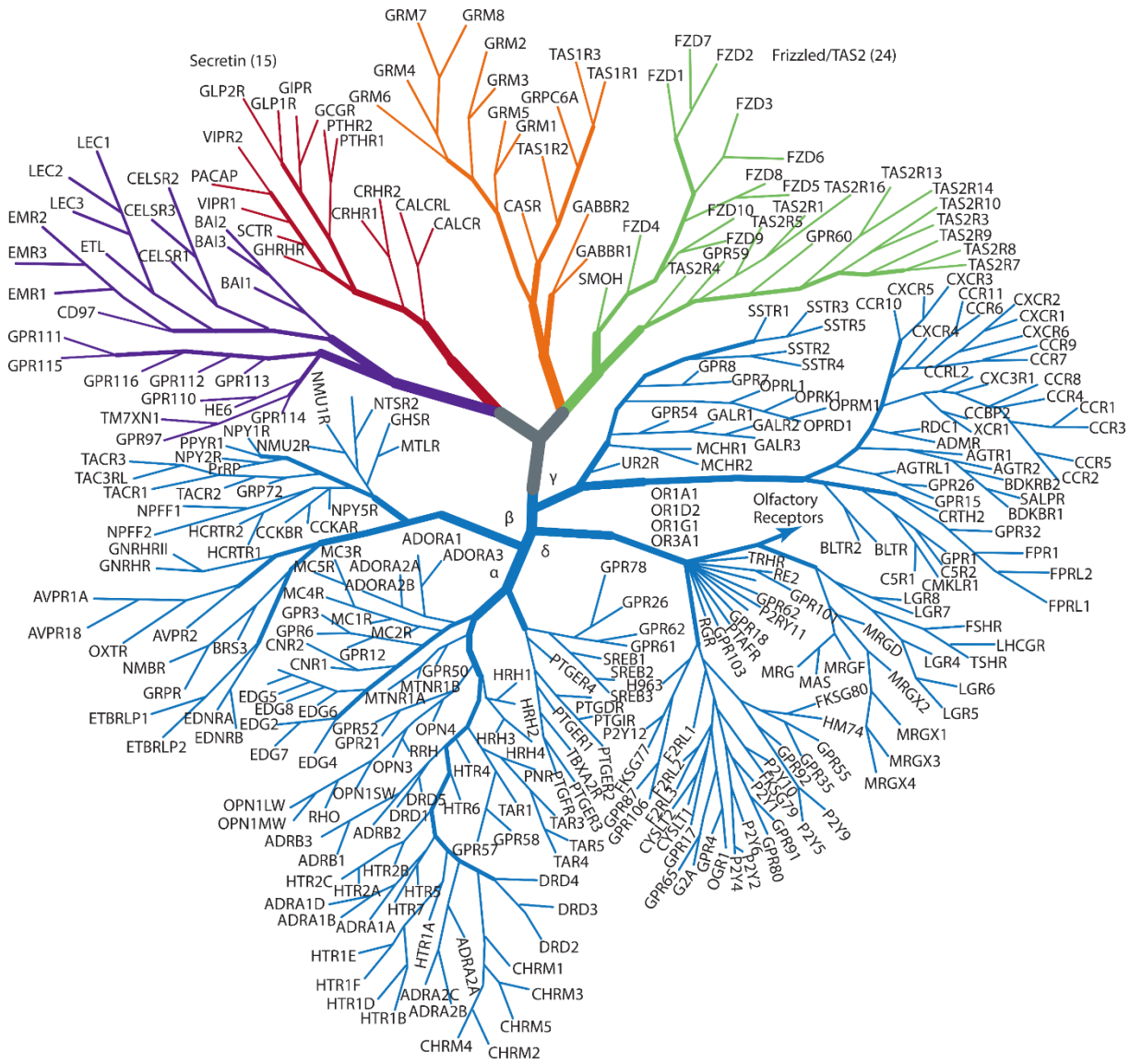

Figure 1: Phylogenic tree of human GPCRs. The over 800 human GPCRs are classified into the class A rhodopsin-like receptors (further divided into the α, β, γ, and δ-branches), the class B adhesion (purple) and secretin (red) family receptors, the class C glutamate receptor family receptors (orange), and the class F Frizzled/TAS2-receptors (green). The image was taken from Stevens *et al.* and modified by Andhika B. Mahardhika [5].

2.1.2. The three-dimensional structure and dynamics of GPCRs

The structure of a biomolecule at a given time determines its function [10], therefore structural biology, physiology, and pharmacology of a protein of interest are intertwined. This section introduces to structural biology and dynamics common to GPCRs in general, paying special attention to the ligand binding site, the activation mechanism, and the intracellular site of GPCRs.

Structural biology – namely X-ray crystallography [11, 12] and, more recently, cryogenic electron microscopy (cryo-EM) [13] – has brought tremendous advances to GPCR research. Ligand-bound GPCR structures are of great use for structure-based drug design, and comparisons of active and

inactive structures have contributed to unveiling the activation mechanism of GPCRs and revealed interaction patterns with G proteins and β-arrestins [14]. Importantly, GPCRs are highly flexible proteins that can adopt countless conformations [15], which are commonly clustered into inactive, active, and intermediate conformations. Conformations captured by structural biology efforts typically require to be ligand-bound and deliver a snapshot of a GPCR in a relatively stable conformation: these are either inactive, antagonist-bound GPCR structures or agonist-bound structures of a GPCR alone or in complex with a G protein or β-arrestin. Currently, 788 structures of 136 unique receptors are resolved, out of which 91 are in complex with an effector protein (August 2022, Source: gpcrdb.org [16, 17]); in turn, structural information on approximately three quarters of the non-olfactory GPCRome is not available yet, emphasizing the need for further structural biology efforts to aid drug development.

GPCRs generally consist of a bundle of seven helices spanning the membrane. The seven helices are connected by three intra- and three extracellular loops (ICLs, ECLs). The ligand binding pocket is located within the cavity between the seven transmembrane domains near the extracellular side of the receptor (see **Figure 2A**), rendering it easily accessible for extracellular molecules as they do not have to penetrate the cellular membrane. The variety of ligands recognized by GPCRs ranges from peptides and small organic molecules to ions and photons and is reflected by high structural diversity between GPCR families in the upper portion of the receptor [18]. Henceforth, the ligand binding sites of GPCRs are characteristic for each receptor, e. g. within the family of rhodopsin-like GPCRs, aminergic receptor ligands bind deep within the 7TM bundle [19], the adenosine binding site of the adenosine A_{2A} receptor requires interaction with at least one ECL2 residue side chain [20], while the chemokine CXCR4 receptor has a large and shallow binding region at the extracellular receptor face [21], making it easily accessible for large peptide ligands (**Figure 2 B**). Receptors binding the same ligand commonly share a similar binding site (at least ~50-60% identity), which may however be fully conserved as it is the case with the β_1- and β_2-adrenergic receptors [18, 19, 22].

In contrast to the ligand binding site, residues essential for GPCR activation are more conserved across GPCR families and they are located in the helix bundles or on the intracellular half of the receptor [23]. A hallmark feature of GPCR activation is the outward movement of the transmembrane helix 6 (TM6, visualized in **Figure 2 C**), which creates space for effector proteins to enter the resulting cavity on the intracellular side of the receptor. Notably, this displacement is more pronounced in the presence of a G protein, which provides a structural basis for the stabilization of an active GPCR state (and the detectable increase of agonist affinity) by G proteins when comparing agonist-activated GPCR structures in the absence and presence of a Gα subunits, e.g. PDB 6GDG [24] and 2YDV [25] for the NECA-activated A_{2A}AR. The mechanism of agonist-induced (or spontaneously occurring) activation is well-understood in class A GPCRs. It is

mediated by conformational changes in evolutionarily conserved microswitches [23, 26]. Key microswitches are e.g. the DRY motif, the sodium binding pocket at $D^{2.50}$ and $S^{3.39}$ [20, 27], and the NPxxY motif ($N^{7.49}$, $P^{7.50}$, $Y^{7.53}$). These motifs forward the signal into the intracellular space by interconnecting the ligand binding pocket and the intracellular face of the receptor [23]. Ultimately, the ionic lock between $R^{3.50}$ and $E^{6.30}$ is broken, which allows the outward movement of TM6 by approximately 10 Å in case of the $A_{2A}AR$ (**Figure 2 D**). Importantly, the activation mechanisms of non-class A GPCRs may be different [28].

In summary, ligand binding allosterically propagates conformational changes to the very other end of the receptor via conserved activation mechanisms, composed of a network of microswitches, enabling effector protein binding to the active GPCR. This general pattern holds true for most GPCRs, but – considering the variety of receptors – there may be exceptions from these rules.

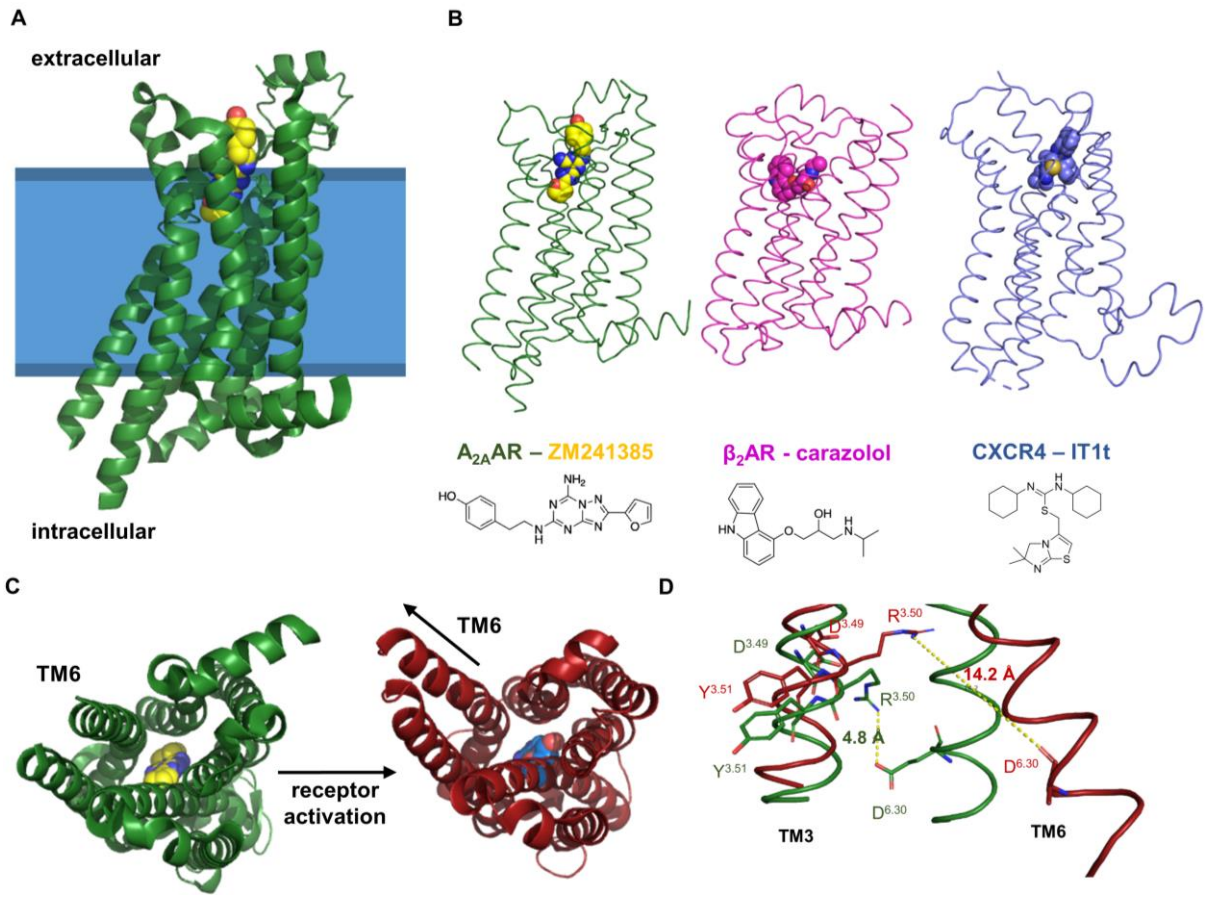

Figure 2. Three-dimensional structure of GPCRs bound to different ligands and effector proteins. **A**. Side view of an inactive receptor (green) bound to an antagonist (yellow, $A_{2A}AR$ bound to ZM241385, PDB 4EIY [20]). The ligand binding site is located near the extracellular face of the receptor, while effector molecules bind on the intracellular side of the membrane (illustrated in blue). **B**. Comparison of the position of the ligand binding site in three different antagonist-bound class A GPCRs. From left to right: $A_{2A}AR$ (green) in complex with ZM241385 (yellow, PDB 4EIY [20]), β_2 adrenergic receptor bound to carazolol (magenta, PDB 2RH1 [22]), chemokine CXCR4 receptor bound to IT1t (blue, PDB 3ODU [21]). **C**. Intracellular perspective of the inactive and active $A_{2A}AR$. Receptor activation leads to a change at

the intracellular half of the receptor, which allows binding of effector proteins. When transitioning from an inactive state (green, PDB 4EIY [20]) to an active state (red, PDB 6GDG [24], $A_{2A}AR$ bound to 5'-*N*-ethylcarboxamidoadenosine (blue)), the most prominent conformational change is the outward movement of TM6. **D**. Close-up of the ionic lock between TM3 and TM6 from a lateral perspective. Superposition of the inactive (green) and active (red) $A_{2A}AR$ displays a 10Å outward movement of the intracellular end of TM6. The DRY motif in helix 3 and $D^{6.30}$ in helix 6 are depicted as sticks, the distance was measured between the carbonyl-O of $D^{6.30}$ and the η1-N atom of $R^{3.50}$.

As visualized in **Figure 2 C+D**, the outward movement of TM6 creates a cavity at the intracellular side of the receptor, which can be occupied by effector proteins. The two main classes of GPCR effector proteins are heterotrimeric G proteins and β-arrestins (see also section 2.1.3). When Gα proteins bind to active GPCRs, their C-terminal α5 helix enters the cavity at the intracellular side of the GPCR (visualized for the $A_{2A}AR$-$G\alpha_s\beta_1\gamma_2$ complex in **Figure 3 A**). The interactions between G protein and receptor differ depending on the Gα protein family, to which the receptor couples [29]. Different receptors coupling to the same Gα protein subfamily may display different G protein binding modes [30], and additionally, the same receptor can form stable complexes with more than one Gα protein, as demonstrated by structures of the glucagon receptor or the human cholecystokinin 1 receptor [31, 32]. Individual receptors may display peculiar G protein binding features, such as pre-coupling in an inactive receptor state, as it was shown for the serotonin $5HT_7$ receptor [33].

Similar to the α5 helix of Gα proteins, the finger loop of β-arrestin enters the intracellular cavity of an active GPCR (**Figure 3 B**), while the central loop, the lariat loop, and the C-loop of β-arrestin form additional contacts with the receptor [34]. The binding of β-arrestins commonly requires phosphorylation of the C-terminal receptor tail by GPCR kinases (GRKs), and – in analogy to the binding of the Gα subunit – the orientation of arrestins in GPCR-arrestin complexes can differ significantly [34–36]. In fact, even the same receptor can interact with a β-arrestin in more than one stable conformation as demonstrated for the neurotensin 1 receptor in complex with human β-arrestin 1 [37]. Lately, the structure of a GPCR-G protein-β-arrestin megaplex, proposed to play a role in endosomal GPCR signaling, has been determined [38, 39]. In addition to structures of GPCRs in complex with G proteins and arrestins, there was a case of a non-conventional GPCR coupling captured by cryo-EM, namely the GPR158-regulator of G protein signaling (RGS) 7-$G\beta_5$ complex [40].

GPCR effector recognition is a current research topic, which is moving forward quickly due to the emergence of the cryo-EM technology that enables researchers to capture large protein complexes in multiple conformations at atom-scale resolution. Several structures of GPCR-G protein or GPCR-arrestin complexes have been published, and common features of GPCRs have been delineated with the help of structural biology. However, several key questions remain unanswered or partially answered, e.g. what is the structural basis for partial or biased agonism [41]? Which mechanisms are universal to all GPCRs and which are, on the contrary, features of individual

GPCRs? How do receptors develop selectivity for multiple G protein α subunits to couple with and what are the structural requirements for this selectivity? Some of these questions may be answered by solving more structures, however, even large amounts of structural data may be insufficient to answer more practice-oriented questions such as 'how to develop drugs stabilizing a receptor conformation beneficial for a clinically relevant condition?'.

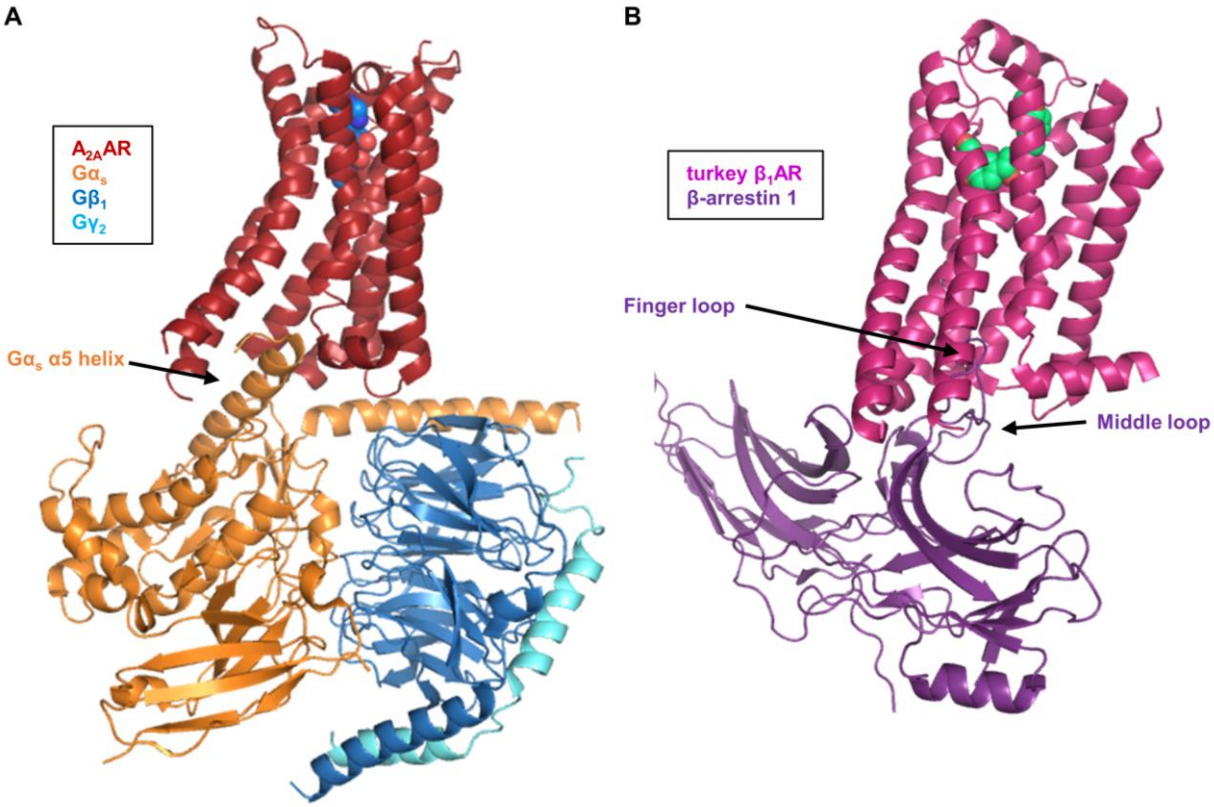

Figure 3: **A**. An active GPCR bound to a heterotrimeric G protein (NECA-activated (blue spheres) $A_{2A}AR$ in complex with $G\alpha_s$ (orange), $G\beta_1$ (blue), and $G\gamma_2$ (light blue), PDB 6GDG). The C-terminal α5-helix of the $G\alpha_s$ protein enters a cavity in the receptor opened up by the outward movement of TM6. **B**. Active GPCR (formoterol-activated (green) turkey β_1-adrenoceptor, magenta, PDB 6TKO [35]) in complex with β-arrestin 1 (dark purple). The finger loop of β-arrestin 1 is inserted close to TM7 into the intracellular cavity of the active receptor.

2.1.3. GPCR function

To trigger an effect in a cell, an active GPCR initiates a signaling cascade starting with the activation of a G protein. In this section, the best-described signaling cascades will be introduced and current research questions regarding GPCR signaling will be outlined. GPCR signaling is more complex than linear signaling cascades suggest, e.g. due to crosstalk between multiple intracellular signaling cascades (e.g. extracellular signal-regulated kinases (ERK) 1/2 activation by multiple Gα proteins), the adoption of multiple conformational states by a receptor that cannot be simply labeled as "off" or "on" [42], promiscuous G protein coupling of GPCRs [8, 43, 44], homo-

and heteromerization of GPCRs [45, 46], and spatiotemporal compartmentalization of signaling proteins [47, 48]. As a result, the same compound acting via the same receptor subtype may not cause the same effect in different cell types, tissues, and animal models [49]. Therefore, the effect of each ligand at each individual receptor in each system deserves careful investigation.

The impact of GPCRs on cellular physiology is closely tied to their canonical effector proteins, heterotrimeric G proteins. G proteins consist of α, β and γ subunits. The Gα protein family is divided into four subfamilies – $G\alpha_s$, $G\alpha_{i/o}$, $G\alpha_{q/11}$, and $G\alpha_{12/13}$ – according to their sequence homology [50]. In total, 16 Gα subunits are encoded by the human genome [50]. The Gα subunit is the key determinant for the downstream signaling of a heterotrimeric G protein, however the associated Gβγ subunits can additionally activate separate effector proteins [51, 52]. While the role of distinct Gα proteins is mostly well-characterized, the roles of distinct Gβ and Gγ subunits are only gradually unveiled [53]. When interacting with an active GPCR, nucleotide exchange from guanosine diphosphate (GDP) to guanosine triphosphate (GTP) in the Gα protein subunit occurs via a conserved intra-protein network of allosteric interactions in a fashion similar to GPCRs [54, 55]. The active, GTP-bound Gα protein dissociates from the Gβγ-dimer, which it is bound to in the inactive GDP-bound state, allowing effector recognition [56]. Depending on the signaling cascade of each Gα protein, the respective responses are triggered in the cell: $G\alpha_s$ proteins increase intracellular cAMP production by activation of adenylate cyclase [57], while $G\alpha_{i/o}$ proteins counteract intracellular cAMP production by adenylate cyclase inhibition. $G\alpha_{q/11}$ proteins increase intracellular calcium mobilization by activation of phospholipase C [58]. $G\alpha_{12/13}$ proteins interact with small GTPase guanine exchange factors (RhoGEFs) and affect the cytoskeletal architecture of a cell [59, 60].

The coupling of GPCRs to Gα proteins is of great importance for their function and their pharmacology. It has long been known that several GPCRs can activate more than one Gα protein family. Lately, large-scale investigation of GPCR-Gα protein coupling has been facilitated by the development of novel methods to directly detect the activation of each individual Gα protein subunit on the G protein level (see section 2.1.5). Two studies independently screened the Gα protein activation patterns of a wide range of GPCRs [8, 43], identified 101 novel couplings, and found that a surprisingly large amount of GPCRs can activate more than one Gα protein family. In fact, 13 GPCRs were identified which activate all Gα protein families in both studies, e.g. the B2 bradykinin receptor, the orexin 2 receptor, and the cholecystokinin A receptor [43, 61] . A key question is which of these couplings are "productive", *i.e.* cause a cellular response and are not merely observed in highly artificial assay systems, and what processes, e.g. spatiotemporal proximity between GPCR and Gα subunit or expression levels [47], govern functional selectivity of one Gα signaling pathway over another in a living organism. Additionally, the agonist chosen for GPCR activation can bias the signaling towards certain Gα protein pathways [62, 63], which

highlights the relevance of Gα protein coupling determination of GPCR agonists in drug development.

Aside from G proteins, members of the arrestin family directly interact with activated GPCRs. Arrestins can bind to receptors, which were phosphorylated by GPCR kinases (GRKs) as a consequence of prolonged receptor activation, and lead to clathrin-mediated internalization and desensitization of GPCRs [64, 65]. The human genome encodes four arrestins, two of which (arrestin 1 and 4) are exclusively expressed in the retina. The other two arrestins (arrestin 2 and 3), also termed β-arrestins 1 and 2, are widely expressed in the human body and interact with a wide spectrum of phosphorylated GPCRs [66]. However, the role of β-arrestins is likely not limited to GPCR internalization and desensitization: internalized GPCRs have been shown to continue signaling from the endosome [67], and the role of β-arrestins in GPCR signaling is currently intensely debated [68]. On the one hand, β-arrestins may act primarily as scaffolding protein and require the presence of active Gα proteins to induce an intracellular effect [69, 70], on the other hand, β-arrestins may play a G protein-independent role in signaling processes [42, 71–73]. The exceptional case of so-called arrestin-coupled receptors (receptors that do not activate any Gα protein, but effectively recruit β-arrestins) suggests a role of β-arrestins beyond receptor internalization [74]. GPCR-effector interactions are sketched in **Figure 4**.

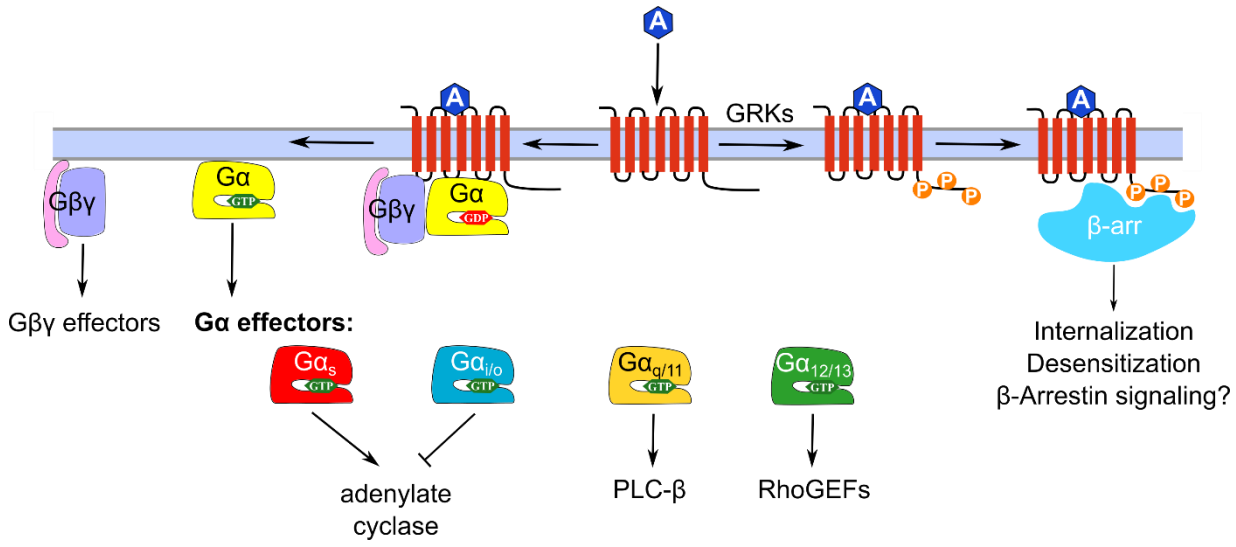

Figure 4. Overview of GPCR signaling pathways. An agonist (blue)-activated GPCR (red) facilitates nucleotide exchange from GDP to GTP in heterotrimeric G proteins (left side) resulting in G protein heterotrimer dissociation. The Gβγ dimer and the Gα subunit interact with their effector proteins; the best-known effector proteins for each Gα subfamily are depicted. After sustained GPCR activation, GRKs can phosphorylate the C-terminal receptor tail (right side), facilitating β-arrestin binding.

2.1.4. Fundamental principles of GPCR pharmacology

This chapter provides a brief introduction to the molecular pharmacology of GPCRs, which can be interpreted as the science of the interaction between a ligand (in biochemistry and pharmacology defined as a compound physically interacting with a protein to serve a biological purpose) and a receptor. The most prominent parameters to characterize a ligand in GPCR pharmacology are affinity, potency, and efficacy. The binding affinity describes the physical interaction strength between a ligand and a receptor and is expressed as K_D (or K_i) value, which is defined as the concentration required for a ligand to occupy half of the available receptor binding sites. The binding affinity, however, is not indicative of the function of a ligand, i.e. whether it activates or inactivates the receptor. Potency describes the concentration required for a half-maximum response in a given functional assay system and is usually expressed as EC_{50}- or IC_{50}-value, respectively – the ligand concentration required for a half-maximum activating or inhibiting response. Efficacy describes the maximum effect of an agonist in a given assay system; the associated E_{max} value (the intensity of the maximum response in a particular assay system) is either presented in an absolute, assay-specific readout (e.g. fluorescence intensity, bioluminescence resonance energy transfer (BRET) ratio shifts, pmol accumulated cAMP) or as a percentage relative to a reference compound, e.g. the endogenous agonist, or reference signal, e.g. the maximum signal elicited by a receptor that is known to activate the signal pathway of interest.

Compounds that bind to the same binding site as the endogenous ligand are named orthosteric ligands, while compounds binding to other regions of the receptor are called allosteric ligands. As mentioned in section 2.1.3, GPCR conformations are commonly regarded to be either active, i.e. facilitating downstream signaling, or inactive, i.e. not allowing downstream signaling. However, receptors can also be partially activated, e.g. activating downstream signaling proteins, but with a submaximal efficacy. And additionally, certain ligands stabilize the inactive conformation of a GPCR and thereby suppress spontaneous receptor activation; such antagonists are termed inverse agonists. To sum up, orthosteric ligands are grouped into full agonists, partial agonists, neutral antagonists, and inverse agonists based on the degree to which they activate or inactivate the receptor. The pharmacology of orthosteric agonists is illustrated schematically in **Figure 5 A**. Allosteric binders can act in an agonistic or antagonistic manner by themselves or modulate the efficacy and potency of orthosteric ligands in a positive or negative manner [75].

Ligand bias (or functional selectivity) commonly refers to a ligands, which are more efficacious or more potent in one signaling pathway over another. Biased ligands stabilize a receptor conformation which preferentially activates one signaling pathway over another, e.g. G protein activation over β-arrestin recruitment or one Gα protein over another Gα protein, as illustrated in the example shown in **Figure 5 B**. Biased agonists that induce a functional selectivity by activating

one signaling pathway over another promise finely tuned drug action: Recently, a G protein-biased μ-opioid receptor agonist, TRV130, has been clinically approved for pain management, supposedly with reduced side effects compared to conventional opiates [76–78]. Biased therapeutics acting via the κ-opioid receptor and angiotensin II type 1 receptor are investigated in clinical trials [79, 80].

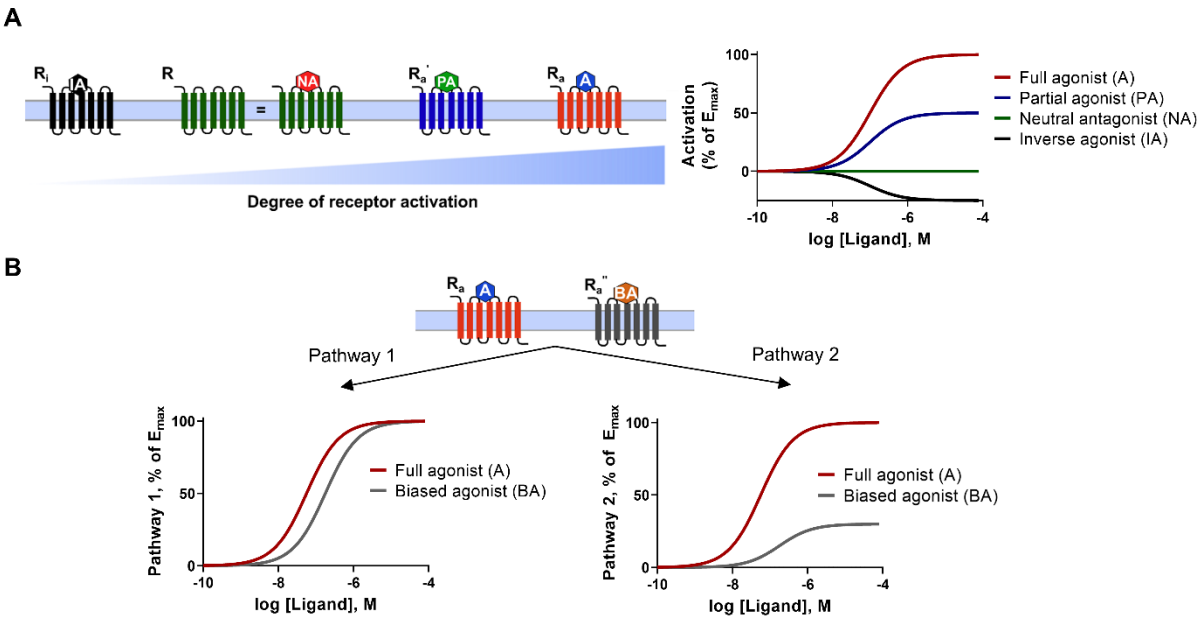

Figure 5. Pharmacological properties of GPCR ligands. **A**. The conformational ensembles of a receptor R stabilized by different ligands with distinct properties, sorted by an ascending degree of receptor activation (left), and their respective concentration-response curves (right) **B**. Visualization of biased signaling. The full agonist A yields a fully efficacious concentration-response curve (red) in both pathways. The biased agonist BA induces a yields a fully efficacious concentration response curve in a pathway 1 assay readout, but is three times less efficacious than the full agonist in pathway 2 assay readouts. All curves were simulated with GraphPad Prism v 8.0.

2.1.5. Pharmacological characterization of ligand binding and functional responses of GPCRs

Pharmacological experiments typically characterize either properties of ligand binding to a target protein or measure a functional response within a biological context to determine the above-mentioned parameters affinity, potency, and/or efficacy. A binding assay directly determines parameters of the physical interaction between ligand and protein, namely affinity and ligand binding kinetics. Binding assays are commonly performed *in vitro* and frequently rely on a radioisotope- or fluorescence-labeled ligand, whose binding constants are either directly measured or that is used to quantify binding parameters of unlabeled ligands competing at the same binding site [81]. Two other popular methods to determine binding constants are isothermal titration calorimetry [82] and surface plasmon resonance [83].

Functional assays focus on the response of a biological system following the stimulation or inhibition of a target protein, in this case a GPCR, and should be able to quantitatively measure both potency and efficacy of a compound in the investigated signaling pathway. Classical pharmacological assays record responses to receptor activation or blockade in intact tissue, e.g. in organ baths, or quantify cellular responses downstream of the receptor, such as 3',5'-cyclic adenosine monophosphate (cAMP) accumulation or intracellular calcium mobilization. More recent assay systems rely on artificial probes that do not occur in nature (e.g. modified receptors or effector proteins), allowing a precise identification of directly interacting effector proteins involved in a given signaling process. For example, treatment of an isolated aorta with endothelin-1 will lead to vascular contraction [84]. This is linked to intracellular calcium mobilization and cAMP accumulation, detectable by the stimulation of immortalized cells (over)expressing the endothelin A (ET_A) receptor with endothelin [85]. On the Gα protein level, the ET_A receptor can couple to virtually all Gα subunits, including the $G\alpha_{i/o}$-family which should theoretically inhibit cAMP formation [8]. Direct measurement of G protein activation therefore provides detailed information on possible GPCR-Gα interactions, but some of those may actually not be meaningful in living tissue and only theoretically possible in an artificial system using e.g. receptor overexpression and modified (e.g. luciferase- and GFP-tagged) biosensor proteins.

Currently, rapid advances in the dissection of Gα protein signaling pathways are possible due to the generation of BRET-based probes. Available biosensors were recently reviewed by Wright & Bouvier [86]. Three examples for novel methodologies suitable for monitoring activation of individual Gα protein subunits are (i) the TRUPATH $BRET^2$ assay system, which measures the dissociation of the G protein heterotrimer by means of a luciferase-tagged Gα subunit and a green fluorescent protein (GFP)-tagged Gγ subunit [87] and is based on the so-called Gaby-biosensors developed in the early 2000s [88, 89], (ii) the transforming growth factor-α (TGF-α) shedding assay, which measures the activity of soluble alkaline phosphatase (AP)-tagged TGF-α upon $G\alpha_{q/11/12/13}$ protein activation [8, 90], and (iii) the effector membrane translocator assay, where the recruitment of a luciferase-tagged Gα effector protein to the membrane is measured after GPCR-agonist induced Gα protein activation [43, 67]. These three examples are visualized in **Figure 6 A-C**.

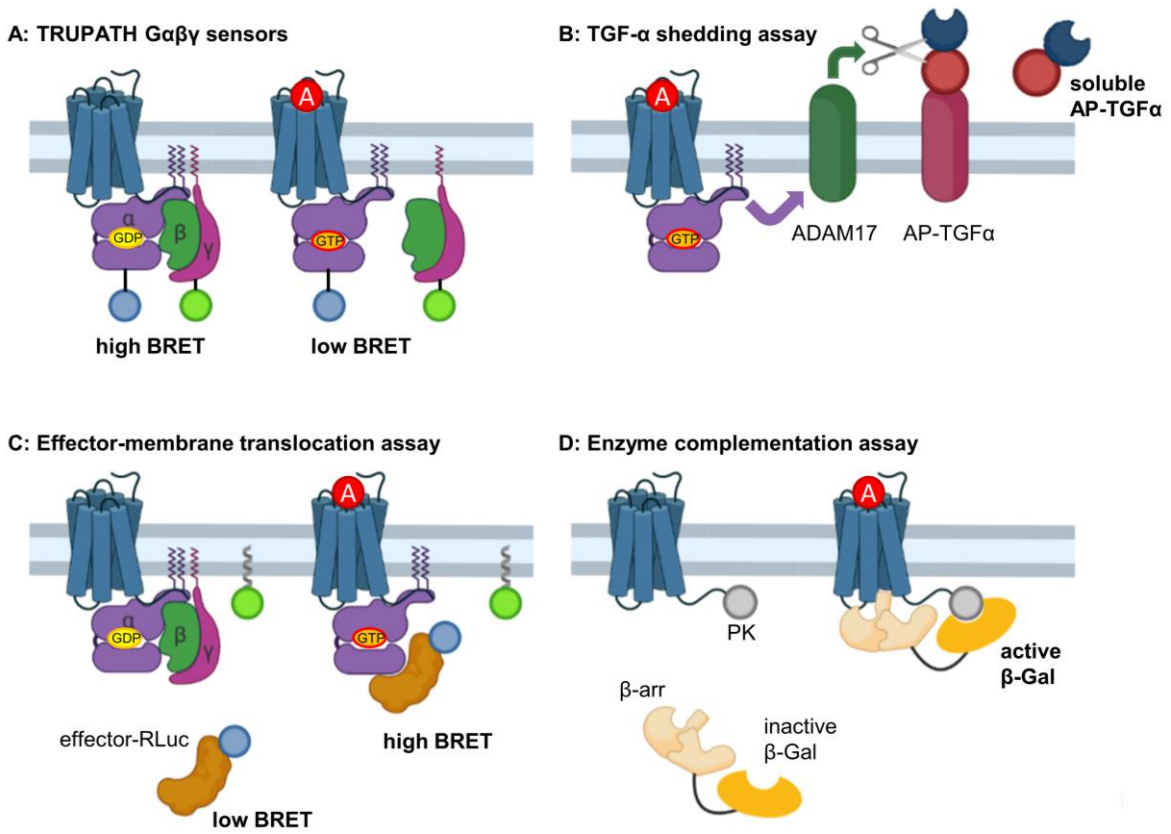

Figure 6. Examples for assay methods detecting G protein and β-arrestin activation via biosensors. **A**. TRUPATH Gαβγ biosensors [87] dissociate from each other after successful activation of a Gα protein subunit by an agonist (A)-activated GPCR, whereupon the measured BRET ratio decreases. **B**. In the TGF-α shedding assay, the agonist-activated GPCR recruits a G protein (of the $G\alpha_{q/11}$ or $G\alpha_{12/13}$ subfamily), which interacts with ADAM17, a protease cleaving membrane-bound AP-tagged TGF-α. The activity of the soluble AP is quantified by substrate conversion [90]. **C**. In the effector-membrane translocation assay, a renilla luciferase (RLuc)-tagged Gα effector protein is recruited to the membrane upon Gα activation. As a BRET acceptor is tethered to the membrane, the BRET ratio increases upon Gα activation [43]. **D**. Example for an enzyme complementation assay (DiscoverX PathHunter®): The activation of a ProLink(PK)-tagged GPCR recruits β-arrestin, tagged with an inactive β-galactosidase (β-Gal), to the receptor. The inactive β-Gal combined with the PK tag forms an active enzyme, which oxidizes a light-emitting substrate. Illustration created with biorender.com.

Similar to the measurement of Gα protein activation, detection of β-arrestin recruitment typically relies on β-arrestin biosensors, most of which are based on the BRET technology or on enzyme complementation (see **Figure 6 D** for an example of an enzyme complementation assay detecting β-arrestin recruitment). All assay systems require either modifications to the receptor C-terminus (such as insertion of a vasopressin V_2 receptor sequence, which is known to efficiently recruit β-arrestin) [91], and insertion of an enzyme fragment or protein tag [92, 93]) or modification of the β-arrestin (mostly addition of protein tags, such as luciferases [93, 94], fluorescent tags [93], nanoluciferase fragments [95, 96], or tobacco rattle virus protease [97]).

2.2. A short overview on heterotrimeric G proteins

An activated GPCR primarily interacts with two major classes of proteins: Heterotrimeric G proteins and arrestins. As this thesis focuses on G proteins, a short section of this introduction will be dedicated to their introduction, although a more comprehensive summary will be given in a review article introduced in section 3. This chapter provides a very brief overview on G proteins in general, focusing mainly on the $G\alpha_{q/11}$ protein family, and the pharmacology of macrocyclic $G\alpha_{q/11}$ protein inhibitors.

G proteins are the initial intracellular interaction partners of active GPCRs. They are attached to the intracellular leaflet of the plasma membrane, anchored by post-translationally attached lipids (myristoylation and palmitoylation at the N-terminus of Gα subunits, prenylation at the C-terminus of Gγ subunits [98]). Theoretically, a large number of G protein heterotrimers can form, as the human genome encodes for 16 Gα proteins, 5 Gβ proteins, and 13 Gγ proteins. The Gα protein subunit is the key determinant for both receptor and effector recognition. There are four families of Gα proteins, grouped according to their sequence similarity [50]. The $G\alpha_s$ family includes $G\alpha_s$ and $G\alpha_{olf}$ proteins, the $G\alpha_{i/o}$ family comprises $G\alpha_{i1}$, $G\alpha_{i2}$, $G\alpha_{i3}$, $G\alpha_o$ and $G\alpha_z$ proteins as well as the three visual and gustatory transducins, the $G\alpha_{q/11}$ family includes the $G\alpha_q$, $G\alpha_{11}$, $G\alpha_{14}$, and $G\alpha_{15}$ proteins, and the $G\alpha_{12/13}$ family consists of the $G\alpha_{12}$ and the $G\alpha_{13}$ protein. Within each family, both receptor and effector recognition patterns are similar (see also section 2.1.3) [43, 61]. The role of different Gβγ combinations in G protein signaling is slowly being elucidated, but remains mostly enigmatic at present [99].

G proteins can be imagined to work similarly to a switch: in the off-position, the Gα protein is bound to GDP and associates with the Gβγ dimer, which prevents interaction with effector proteins. Engaging an activated GPCR via the α5-helix of the Gα protein promotes nucleotide exchange from GDP to GTP, resulting in conformational changes in the so-called switch regions of the Gα proteins. In the GTP-bound state, the Gα protein is active; it releases the Gβγ dimer (which can in turn engage its own range of effector proteins [51]) and binds effector proteins that ultimately lead to a cellular response. Due to an intrinsic GTPase activity, GTP is hydrolyzed to GDP, which sets the Gα switch to the off-position again. The GTPase activity can be accelerated by certain effector proteins and RGS proteins [53, 100].

2.2.1. Physiological effects of $G\alpha_{q/11}$ proteins

Proteins of the $G\alpha_{q/11}$ family can interact with several effector proteins and can therefore affect cells in a number of ways. The most prominent interaction partner for the $G\alpha_{q/11}$ protein family belong to the phospholipase C-β (PLC-β) family. Upon interaction with active $G\alpha_{q/11}$ proteins, PLC-β hydrolyzes the membrane component phosphatidylinositol bisphosphate to inositol

trisphosphate (IP_3) and diacylglycerol (DAG). IP_3 diffuses into the cytoplasm, where it triggers intracellular calcium mobilization from the endoplasmic reticulum (ER) by binding to members of the ryanodine-inositol trisphosphate receptor family, large membrane glycoproteins inserted into the ER membrane [101, 102]. DAG remains in the plasma membrane, where it directly activates members of the the protein kinase C (PKC) family [103]. It is worth mentioning that free Gβγ subunits can also activate PLC-β [104], but require the presence of active $G\alpha_{q/11}$ proteins [52].

Next to the major canonical $G\alpha_{q/11}$ signaling pathway via PLC-β, several other direct $G\alpha_{q/11}$ interaction partners have been described. Interactions with GRK2, p63RhoGEF, several GPCRs, and RGS2/8 were resolved by X-ray crystallography [105–108]. Other proteins, such as phosphoinositol 3 kinase, protein kinase ζ, mitogen/extracellular signal-regulated kinase 5, Bruton's tyrosine kinase, and transient receptor potential cation channel subfamily M member 8 have been characterized as effector proteins downstream of $G\alpha_{q/11}$ proteins, reviewed in [109]. The broad range of proteins affected directly or indirectly by $G\alpha_{q/11}$ proteins underlines their important function in cellular signaling and physiology.

Deactivation of $G\alpha_{q/11}$ proteins occurs either by spontaneous or effector-promoted hydrolysis of bound GTP. While the GTP hydrolysis rate of purified $G\alpha_q$ proteins is rather slow [110], it can be accelerated by up to 1,000-2,000-fold by the addition of PLC-β or RGS4 to a reconstituted system, resulting in a $G\alpha_q$ deactivation half-life of 25-75 ms [100]. Addition of Gβγ subunits to this system blocks the GTPase-activating function of PLC-β, likely in a competitive manner [111]. The careful regulation mechanisms imply that $G\alpha_q$ activation/deactivation by GPCRs and GTPase-activating proteins is under strict spatiotemporal control in order to maintain a steady-state $G\alpha_{q/11}$ signaling amplitude, *i.e.* once activated, a single GTP-bound $G\alpha_q$ protein can only interact with a limited number of effector protein(s) before GTP is hydrolyzed [100]. Dysregulation of $G\alpha_{q/11}$ signaling, e.g. by constitutively active $G\alpha_{q/11}$ R183 or Q209 mutants, can drive oncogenic signaling in uveal melanoma [112, 113].

A further intriguing interaction partner for $G\alpha_{q/11}$ proteins is Ric-8, which was initially believed to be a GTP-dependent, non-receptor guanine-nucleotide exchange factor for $G\alpha_q$ proteins [114, 115]. However, it is more likely to act as a chaperone guiding $G\alpha_q$ protein folding [116–118]. Apparently, Ric-8 itself is not a GTP-dependent protein, but GTP binding to the naïve $G\alpha_q$ protein leads to release of the now mature $G\alpha_q$ protein from the Ric-8 protein instead, as demonstrated by X-ray crystallography [119]. Ric-8 assisted folding greatly increases the yield of recombinantly expressed $G\alpha_q$ proteins from non-mammalian cell culture and is often used to enable heterologous $G\alpha_q$ protein expression, e.g. in structural biology projects [120].

2.2.2. Pharmacology of macrocyclic $G\alpha_{q/11}$ protein inhibitors

Similar to other Gα proteins, $G\alpha_{q/11}$ proteins were considered to be undruggable for a long period of time. The only efficacious Gα protein inhibitor used in basic research was pertussis toxin, which inhibited receptor-mediated nucleotide exchange in $G\alpha_{i/o}$ proteins by covalent modification of a C-terminal cysteine residue [121]; other Gα proteins were not amenable to pharmacological inhibition. The discovery of macrocyclic $G\alpha_{q/11}$ protein inhibitors can be considered a breakthrough in GPCR pharmacology. Potent and selective inhibition of the $G\alpha_{q/11}$ protein family enables direct investigation of their role in signal transduction and in pathologies. There are three reviews published on macrocyclic $G\alpha_q$ protein inhibitors, discussed from either a chemical [122], a biosynthesis-focused [123], and a pharmacological perspective [124].

First described in 1988 in a plant extract from *Ardisia crenata*, but thoroughly characterized only in 2015, FR900359 (FR) is a highly potent, cell-permeable inhibitor that blocks $G\alpha_q$, $G\alpha_{11}$, $G\alpha_{14}$, but not $G\alpha_{15/16}$ or any other Gα proteins [125, 126]. The biosynthesis pathway of FR was recently resolved and involves two non-ribosomal peptide synthase assembly lines [127, 128]. The closely related natural product YM-254890 (YM) shares the pharmacological profile of FR, and was first described as a platelet aggregation inhibitor isolated from a strain of *Chromobacterium sp. QS3666* [129, 130]. Total synthesis of YM, FR, and several novel derivatives was achieved in 2016 and awarded by a prize of 100,000$ [131].

A crystal structure of the GDP-bound $G\alpha_q\beta_1\gamma_2$ protein in complex with YM was published in 2010, demonstrating binding to the Switch I/linker I region of the $G\alpha_q$ protein [132]. The shared mechanism of action of both $G\alpha_{q/11}$ protein inhibitors, FR and YM, is based on prevention of nucleotide exchange in $G\alpha_q$ proteins, which results in permanently GDP-bound, inactive $G\alpha_{q/11}$ proteins that cannot engage downstream effector proteins [126, 132]. FR and YM are highly selective for $G\alpha_q$, $G\alpha_{11}$, and $G\alpha_{14}$ proteins, showing only minor inhibition of $G\alpha_{15}$ proteins and no further off-target effects [133, 134].

Macrocyclic $G\alpha_{q/11}$ protein inhibitors have been investigated in disease models, such as uveal melanoma, a malignancy of the eye which is driven by constitutively active $G\alpha_q$ proteins, asthma bronchiale, and in adipose tissue differentiation [135], and were lately proposed to amplify morphine-induced analgesia [136]. In several independent studies of uveal melanoma cells, FR efficaciously blocked signaling by constitutively active $G\alpha_q$ Q209L/P mutants [137–139]. In asthma bronchiale, FR induced strong airway relaxation, superior to conventional treatments [140] and lasting for up to 72 h [141]. However, systemic $G\alpha_{q/11}$ protein inhibition can lead to toxic side effects (cardiovascular, impaired locomotion [136, 140]) in animals, which might be overcome in the future by targeted drug delivery or application, and YM and FR have been shown to accumulate in several peripheral organs [136, 141, 142].

3. Heterotrimeric G protein α-subunits - structures, peptide-derived inhibitors, and mechanisms

Jan H. Voss and Christa E. Müller

Curr. Med. Chem. **2022**, Online ahead of print. doi: 10.2174/0929867329666220308112424

Introduction

Heterotrimeric G proteins are the primary interaction partners at the intracellular domain of GPCRs. They forward information provided by activated GPCRs into the cell. While there are over 800 genes encoding GPCRs in human, there are only 16 genes encoding G protein α subunits – the component of the trimeric G protein that interacts closely with the GPCR and most downstream effector proteins. These 16 genes are grouped into four different families of Gα proteins by sequence homology – $G\alpha_s$, $G\alpha_{i/o}$, $G\alpha_{q/11}$, and $G\alpha_{12/13}$ [50]. Each family interacts with a distinct range of effector proteins, however, interactions of family members are similar [143].

In its inactive state, the Gα protein is bound to GDP and associates with the Gβγ dimer. When interacting with an activated GPCR, GDP is exchanged for GTP, resulting in a conformational rearrangement of so-called switch regions of the Gα subunit, and ultimately in dissociation of the Gα protein from the Gβγ dimer, which can then both interact with their effector proteins [144]. Bound GTP is hydrolyzed to GDP by the intrinsic hydrolytic activity of the Gα subunit, which can further be enhanced by GTPase-activating proteins (GAPs), e.g. several effector proteins and members of the RGS family [110]. The inactive, GDP-bound Gα subunit cannot associate with effector proteins anymore, but forms the inactive G protein heterotrimer by re-binding to the Gβγ dimer.

As GPCR signaling converges on the level of G proteins, inhibition of G protein function has been proposed for the treatment of multifactorial diseases, e.g. cancer, *asthma bronchiale*, pain, and pulmonary hypertension [136, 140, 145, 146], to name only a few. Compared to tremendously successful drug development efforts targeting GPCRs, the development of compounds and peptides targeting G proteins has so far been less fruitful. For long time, the only reliable G protein inhibitor was the $G\alpha_{i/o}$ protein inhibitor pertussis toxin [121]. In the past decade, selective and potent $G\alpha_{q/11}$ protein inhibitors, YM [129] and FR [125], came into use in pharmacological studies and further contributed to unveil the G protein signaling patterns of GPCRs [43, 49, 147]. The great demand of these compounds emphasizes the necessity of further G protein inhibitors for basic research with different selectivity profiles, which is underlined by a recent publication from a pharmaceutical company describing novel YM-254890 analogues [148].

This review article aims to summarize both well-known and understudied compounds, mainly peptides, for which a G protein modulatory activity has been described. Additionally, all compounds are presented in a tabular form, providing chemical structures and peptide sequences, which facilitates a quick overview of G protein modulator structure, mode of action, and literature references.

Summary and outlook

The article starts out with a general introduction into G proteins, with a main focus on the phylogeny, structure, and function of Gα proteins. An analysis of co-crystal structures of Gα proteins and their effector proteins provides detailed insight into protein-protein interactions by Gα proteins, the secondary structural elements of the Gα protein involved, and the Gα subunit selectivity of these interactions.

Based on the functional principle of G proteins, we cluster four pharmacological approaches to G protein modulation: (i) blockade of GPCR-G protein interaction, (ii) modulation of the nucleotide exchange process, (iii) blockade of their interaction with effector proteins, and (iv) modulation of the GTP hydrolysis rate. For each of the four approaches listed above, exemplary compounds are listed; their mechanism of action and the experimental validation is described in brief with reference to the original literature. When applicable, co-crystal structures of G protein and modulator are displayed to visualize the respective mode of action. We consider competition with the guanine nucleotide at its binding site a difficult approach of G protein inhibition due to the high affinity of GTP for its binding site and the large intracellular nucleotide concentration.

Several of the compounds listed – such as the aforementioned pertussis toxin, YM, and FR – have proven to be invaluable as pharmacological tool compounds, however the majority of the other compounds has never been utilized out of the original publication describing them. This points to major problems with regards to potency, selectivity, and cell membrane permeation, and further emphasizes the need for drug discovery efforts targeting heterotrimeric G proteins, enabling research on understudied Gα protein subunits such as $G\alpha_{12/13}$ or the atypical $G\alpha_{15}$ protein in native systems.

Author contribution

The author prepared all figures in the manuscript, analyzed the literature, and wrote main text under supervision of and with contributions by Prof. Christa E. Müller.

4. Unraveling binding mechanism and kinetics of macrocyclic $G\alpha_q$ protein inhibitors

Jan H. Voss, Jessica Nagel, Muhammad Rafehi, Ramon Guixà-González, Davide Malfacini, Julian Patt, Stefan Kehraus, Asuka Inoue, Gabriele M. König, Evi Kostenis, Xavier Deupi, Vigneshwaran Namasivayam, Christa E. Müller

Pharmacol. Res. **2021**, 173, 105880, doi: 10.1016/j.phrs.2021.105880

Introduction

Heterotrimeric G proteins act as switches forwarding signals from activated GPCRs into the inside of the cell [143]. The family of G protein α subunits is divided into four families ($G\alpha_s$, $G\alpha_{i/o}$, $G\alpha_{q/11}$, and $G\alpha_{12/}$13. The $G\alpha_{q/11}$ protein family consists of four members – $G\alpha_q$, $G\alpha_{11}$, $G\alpha_{14}$, and $G\alpha_{15}$ [50]. Activation of $G\alpha_{q/11}$ family proteins is associated with the activation of phospholipase C [58, 149], which in turn produces the second messenger molecules diacylglycerol and inositol trisphosphate from the membrane component phosphatidylinositol-4,5-bisphosphate, leading to liberation of calcium from the endoplasmic reticulum and activation of the PKC family

Over the past years, the macrocyclic $G\alpha_{q/11}$ protein inhibitors YM and FR have attracted large interest as potent and selective inhibitors of the $G\alpha_q$, $G\alpha_{11}$, and $G\alpha_{14}$ proteins, not showing inhibition of the $G\alpha_{15}$ protein [126, 150]. Both compounds were investigated *in vivo* to treat complex, $G\alpha_{q/11}$-driven disease conditions such as *asthma bronchiale* [140], and uveal melanoma [137, 139], and also constitute indispensable tools in molecular pharmacology, allowing researchers to dissect the contribution of $G\alpha_{q/11}$ proteins to various GPCR signals [43, 147]. Both inhibitors act by blocking the rate-limiting GDP dissociation step in the G protein activation cycle; thereby, the G protein is arrested in an inactive state independent of GPCR signals [126].

YM and FR share an almost identical chemical structure, which differs only in two substituents: Relative to YM, FR harbors larger lipophilic groups in two positions, which we termed anchors 1 and 2. In a previous study, our group developed a radioligand binding assay using tritiated derivatives of YM and FR [151]. While both compounds appeared to have similar affinities in competition and saturation binding assays, the more lipophilic FR-derived radioligand displays an approximately 20-fold longer residence time at the $G\alpha_q$ protein as determined in human platelet membranes [151]. This project initially aimed to elaborate the molecular mechanism behind the major residence time differences between those similar compounds.

Summary and outlook

To investigate the contribution of single amino acids to the binding of macrocyclic $G\alpha_{q/11}$ inhibitors, we have mutated several amino acids within the binding pocket of YM and FR of the $G\alpha_q$ protein. The mutations were picked based on docking studies of YM and FR. Mutant $G\alpha_q$ proteins were stably expressed in human embryonic kidney 293 (HEK 293) cells which were depleted by the genes coding for the $G\alpha_{q/11}$ proteins by clustered regularly interspaced short palindromic repeats (CRISPR)/Cas9 gene editing. Membrane preparations of these cells were analyzed in radioligand binding assays. Using the YM-derived radioligand [^{3}H]PSB-16254-YM, we determined the affinity of the radioligand to all generated $G\alpha_q$ mutants. At most mutant $G\alpha_q$ proteins, [^{3}H]PSB-16254-YM displayed an affinity similar to the wild-type (wt) $G\alpha_q$, however, high-affinity radioligand binding was abolished when key residues were mutated (e.g. F75K, I190F/W). The inhibitory potency in orthogonal calcium mobilization assays closely correlated with the affinity determined in radioligand binding assays. $G\alpha_q$ protein mutants, which did not bind the radioligand, displayed a significantly decreased inhibitory potency in calcium mobilization assays. $G\alpha_q$ protein expression was in parallel verified by Western blotting.

In kinetic binding experiments, all mutant $G\alpha_q$ proteins displayed a similar association rate compared to the wt $G\alpha_q$ protein using both the YM- and FR-derived radioligands. However, the dissociation rate was greatly increased by virtually all mutations introduced to the $G\alpha_q$ protein. This effect was more pronounced for the slowly-dissociating FR-derived radioligand [^{3}H]PSB-15900-FR, for which the dissociation was accelerated by more than a 100-fold at some $G\alpha_q$ protein mutants. Mutations around the isopropyl anchor 2 of FR caused a more severe acceleration of radioligand dissociation, emphasizing the large contribution of lipophilic interactions between anchor 2 and proximate residues to the long residence time of FR.

Dissociation constants determined by homologous competition binding assays and saturation binding did not correlate well with those obtained by kinetic binding assays in case of [^{3}H]PSB-15900-FR. Especially at wt $G\alpha_q$ proteins and mutants, at which the radioligand displayed a long residence time, the affinity of [^{3}H]PSB-15900-FR to the $G\alpha_q$ protein may have been significantly underestimated by equilibrium binding assays. In contrast, kinetic and competition K_D values were virtually identical for [^{3}H]PSB-16254. Association experiments performed with multiple concentrations of both radioligands resulted in an exponential decrease of the observed association rate, k_{obs}. This finding is commonly associated with a multi-step binding mechanism involving a conformational selection step. Molecular dynamics simulation of the heterotrimeric G_q protein in the presence and absence of FR suggested that inhibitor binding requires a tilt of the αA helix in the helical domain of the Gαq protein to prevent a steric clash between FR and the respective helix. Furthermore, these simulations showed that inhibitor binding may stabilize the

loop between the αB and the αC helices in the helical domain of the $G\alpha_q$ protein and could also have a direct effect on the GDP-binding P-loop as supported by relative entropy analysis.

In summary, this work delineates key interactions between FR or YM and the $G\alpha_q$ protein resulting in a long residence time of FR by a site-directed mutagenesis study. Several of the mutated residues, at which the residence time of [^{3}H]PSB-15900-FR is dramatically decreased, are proposed to form lipophilic interactions with the isopropyl anchor 2 of FR. Additionally, a detailed investigation of the binding mode of both radioligands suggests that macrocyclic $G\alpha_q$ protein inhibitors engage the wt $G\alpha_q$ protein via a complex binding procedure involving a conformational selection step. This finding was backed by molecular dynamics simulations. The present study furthermore demonstrates the importance of in-depth kinetic investigations to obtain a full picture of ligand binding parameters, which is of broad interest, as the significance of kinetic constants is increasingly recognized in drug discovery [152].

Author contribution

The author performed molecular biology experiments, protein expression, pharmacological assays with the exception of kinetic radioligand binding assays, and analyzed data. Furthermore, the author was involved in selecting mutations in the $G\alpha_q$ binding pocket, created figures, and wrote the manuscript in cooperation with Christa E. Müller and all co-authors.

5. Structure-affinity and structure-residence time relationships of macrocyclic $G\alpha_{q/11}$ protein inhibitors

The macrocyclic core of FR is composed of seven building blocks: phenyllactic acid, dehydroalanine, two alanine residues, threonine, and two β-hydroxy-leucine (β-HyLeu) residues. In YM, one of the β-HyLeu residues is exchanged for a threonine residue. Several residues of the macrocyclic core are modified, e.g. by *N*- or *O*-methylation and acetylation. Additionally, another β-HyLeu residue is attached to the free OH-group of a β-HyLeu residue of the cyclic core structure, which contributes greatly to the binding affinity of FR, and presumably also of YM [127]. In addition to YM and FR, several other derivatives and analogs have been described, which were either obtained by total synthesis [131, 153–155], extraction from *A. crenata* [156], or from recombinant bacterial cultures [127, 157]. These derivatives mostly contain an unaltered macrocyclic core structure, but harbor different modifications of the core or the branched β-HyLeu side chain. So far, most of them have only been tested in a functional assay system, e.g. for inhibition of inositol phosphate accumulation.

We have used the FR-derived radiotracer [^{3}H]PSB-15900-FR to determine the affinity and binding kinetics of 17 derivatives and analogs of YM and FR (see **Figure 7** for structures). Binding affinities were determined in competition binding assays, while binding kinetics were determined by competition-association binding assays. In competition-association binding assays, a fixed concentration of radioligand and competitor are mixed, followed by the addition of protein and incubation for various time periods. The resulting curve plots specific binding over time and the curve shape allows to determine on- and off-kinetics of the unlabeled competitor, if kinetic parameters of the radioligand and the number of binding sites within the protein are known. The analysis was performed according to the protocol of Motulsky and Mahan [158]. Structure-affinity and structure-residence time relationships for macrocyclic $G\alpha_{q/11}$ inhibitors were derived, which represent valuable data for further drug design.

FR derivatives

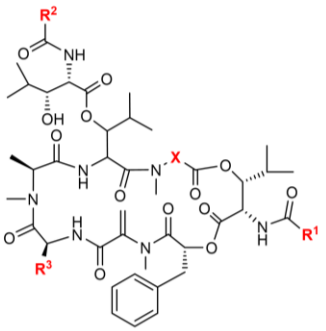

Compound	R^1	R^2	R^3	X	pK_i	τ
FR900359	CH_3	C_2H_5	CH_3		8.73	466
FR-1	C_2H_4OH	C_2H_5	CH_3		8.20	524
FR-2	CH_3	CH_3	CH_3		8.74	547
FR-3	C_2H_5	C_2H_5	CH_3		7.87	72
FR-4	CH_3	C_2H_5	C_2H_5		7.87	72
FR-6	CH_3	C_2H_5	CH_3		7.25	n.d.

FR- and YM-derived radioligands

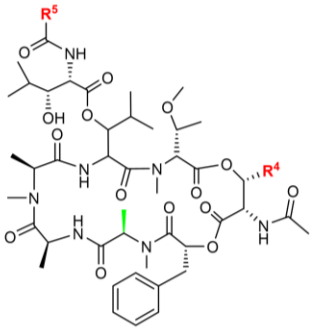

Compound	R^4	R^5	pK_D	τ
[^{3}H]PSB-15900	$C(CH_3)_2$	C_2H_5	8.19	131
[^{3}H]PSB-16254	CH_3	CH_3	7.80	6

YM derivatives with modifications at the β-OH-Leu side chain

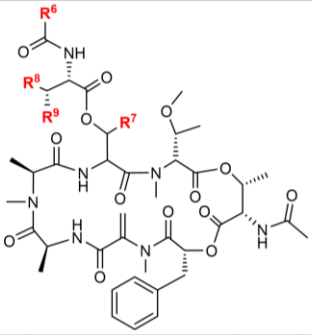

Compound	R^6	R^7	R^8	R^{19}	pK_i	τ
YM-254890	CH_3	$CH(CH_3)_2$	$CH(CH_3)_2$	OH	8.23	57
YM-7	CH_3	$CH(CH_3)_2$	CH_3	OH	6.45	n.d.
YM-8	CH_3	CH_3	$CH(CH_3)_2$	OH	6.43	n.d.
YM-9	CH_3	$CH(CH_3)_2$	$CH(CH_3)_2$	H	5.77	n.d.
YM-10	C_2H_5	$CH(CH_3)_2$	$CH(CH_3)_2$	OH	7.68	72

YM derivatives with modifications at alanine residues or the macrocylic core

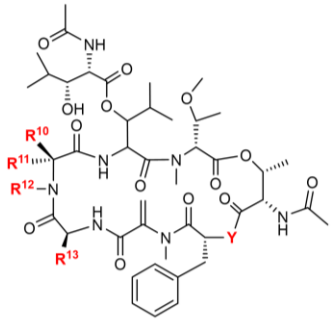

Compound	R^{10}	R^{11}	R^{12}	R^{13}	Y	pK_i	τ
YM-254890	CH_3	H	CH_3	CH_3	O	8.23	57
YM-1	CH_3	H	H	CH_3	O	6.27	n.d.
YM-3	CH_3	H	CH_3	CH_3	NH	5.57	n.d.
YM-11	$CH(CH_3)_2$	H	CH_3	CH_3	O	6.62	n.d.
YM-12	H	H	CH_3	CH_3	O	7.15	8
YM-13	H	CH_3	CH_3	CH_3	O	7.23	17
YM-14	CH_2Ph	H	CH_3	CH_3	O	7.54	14
YM-15	CH_3	H	CH_3	$CH(CH_3)_2$	O	7.02	n.d.
YM-18	CH_3	H	CH_3	CH_2Ph	O	7.88	55

Figure 7: Chemical structures, affinity values (pK_i, pK_D), and residence times (τ, in min) of FR, YM, and all characterized derivatives and analogs. n.d., not determined.

5.1. Results and discussion

Characterization of HEK293 membranes expressing the $G\alpha_q$ protein

To assess the affinity and binding kinetics of unlabeled $G\alpha_{q/11}$ protein inhibitors, we initially re-determined the affinity and binding kinetics of the radiolabeled FR derivative [^{3}H]PSB-15900-FR at HEK293 membranes exclusively expressing the $G\alpha_q$ protein (HEK293-$G\alpha_q$ membrane preparations). This was required for further calculations of pK_i values and kinetic parameters of unlabeled compounds measured under identical conditions. In this series of experiments, we determined a pK_D value of 8.19 for [^{3}H]PSB-15900-FR and a maximum binding capacity (B_{max}) of 27.5 pmol/mg per mg of protein (**Figure 8 A**), which was consistent with previously published data [159]. In association experiments, an observed association rate (k_{obs}) of 0.086 min^{-1} was determined for [^{3}H]PSB-15900-FR, resulting in a corresponding association half-life of 11.3 min (**Figure 8 B**), and in dissociation experiments, a dissociation rate (k_{off}) of 0.0078 min^{-1} was determined, resulting in a dissociation half-life (ln(2)/k_{off}) of 91.0 min and a residence time (τ; 1/k_{off}) of 131 min, respectively (**Figure 8 C**).

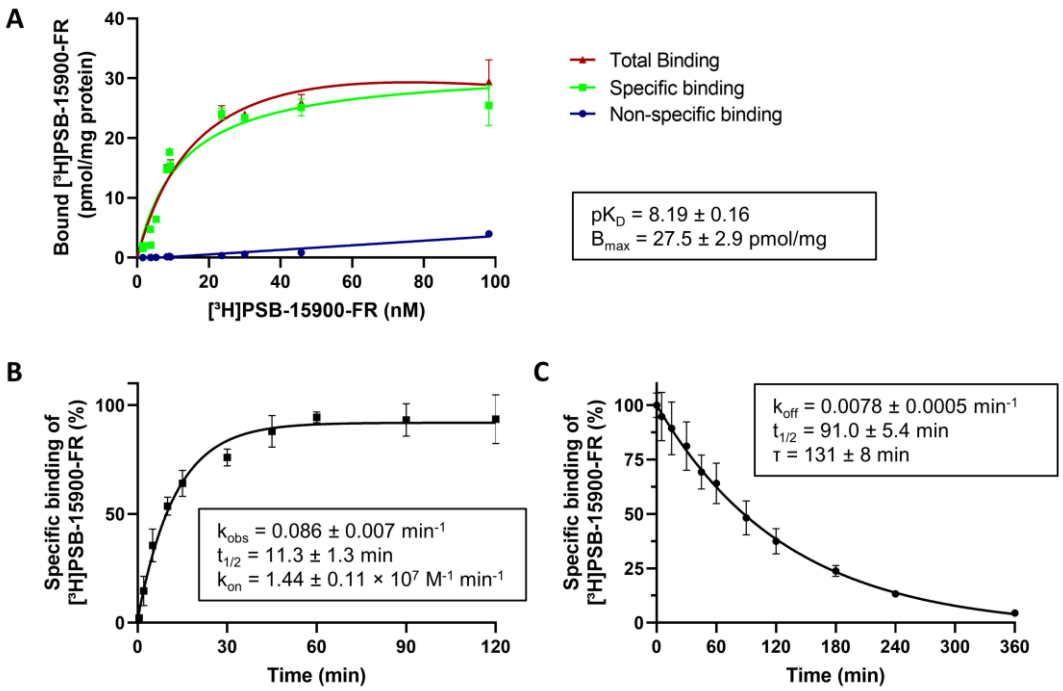

Figure 8: Characterization of HEK293-$G\alpha_q$ membrane preparations. **A**. Saturation binding experiments of different concentrations of [^{3}H]PSB-15900-FR to HEK293 $G\alpha_q$ membranes (25 µg of protein). The following values were determined: pK_D = 8.19 ± 0.16, B_{max} = 27.5 ± 2.9 pmol/mg. **B**. Association kinetics of [^{3}H]PSB-15900-FR (5 nM) to HEK293 $G\alpha_q$ membrane preparations. The observed association rate k_{obs} was 0.080 ± 0.006 min-1, resulting in an association half-life (ln 2/k_{obs}) of 8.71 ± 0.60 min and an k_{on} of 1.44 ± 0.11 × 107 M-1 min-1. **C**. Dissociation kinetics of [^{3}H]PSB-15900-FR to HEK293 $G\alpha_q$ membrane preparations. The dissociation rate k_{off} was determined as 0.0078 ± 0.0005 min^{-1} resulting in a dissociation half-life (ln 2/k_{off}) of 91.0 ± 5.4 min and a residence time (1/k_{off}) of 131 ± 8 min. All data points are shown as mean ± SD from three experiments, performed in duplicate.

Determining binding affinities of YM and FR derivatives

Subsequently, binding affinities of FR and YM derivatives were determined by competition binding experiments using HEK293-$G\alpha_q$ membrane preparations (**Figure 9**, **Table 1**). Due to the slow dissociation kinetics of [^{3}H]PSB-15900-FR, we incubated all competition binding assays for three hours at 37°C to reach equilibrium. The originally described compounds FR and YM displayed high affinity for the $G\alpha_q$ protein (pK$_i$ FR = 8.73, pK$_i$ YM = 8.23), which were virtually identical to previously described values [151]. The FR derivative FR-2 showed the same high affinity at the $G\alpha_q$ protein as FR, and FR-1 was slightly, but not significantly, less affine (pK$_i$ FR-1 = 8.20, pK$_i$ FR-2 = 8.74, **Figure 9A**). The replacement of the propionic acid side chain for the acetic acid side chain in FR-2 and the hydroxylation in FR-1 are therefore well-tolerated modifications to FR. A 3:1 mixture of FR-3 and FR-4, each bearing an ethyl group instead of a methyl group at different sites of the macrocycle, did not display a significantly lower affinity (pK$_i$ FR-3/4 = 7.87, **Figure 9 A**) than the parent compound FR either. In contrast, elimination of the methoxy side chain in FR-6 (pK$_i$ FR-6 = 7.25, **Figure 9 A**) resulted in a significantly decreased binding affinity relative to the parent compound FR. The binding affinities of the radioligands [^{3}H]PSB-15900-FR and [^{3}H]PSB-16254-YM were pK$_D$ = 8.19 and pK$_D$ = 7.80, respectively (determined by saturation binding [159]), which is slightly lower (about 0.5 log-units) than the affinities of non-hydrogenated FR and YM.

Most of the investigated YM derivatives displayed significantly decreased affinities when compared to the parent compound YM (**Figure 9 E**). In particular, derivatives YM-1, 3, 7, 8, and 9 showed pK$_i$ values ranging from 5.57 – 6.45 (**Figure 9 B,C**), which were much lower than that of the parent compound (pK$_i$ YM, 8.23). The N-demethylation of an alanine residue in YM-1 (pK$_i$ YM-1, 6.27) results in an approx. 100-fold loss of affinity compared to YM. While large parts of the contact surface between macrocyclic $G\alpha_q$ protein inhibitors and the $G\alpha_q$ proteins are lipophilic, the few polar interactions are essential for high-affinity binding as demonstrated by the huge loss in affinity for YM-3 (pK$_i$ YM-3, 5.57), in which an ester bond in the macrocyclic backbone was changed to an amide bond. The exchange of an isopropyl group for a methyl group in the β-HyLeu side chain resulted in a nearly 100-fold reduction of the binding affinity of YM-7 (pK$_i$ YM-7, 6.45) and YM-8 (pK$_i$ YM-8, 6.43) compared to YM. Similarly, removing the hydroxyl moiety in the side chain dramatically reduced the affinity of YM-9 (pK$_i$ YM-9, 5.77). YM-10, which contains the propionyl residue of FR in the β-HyLeu, instead of the acetyl group of YM, retained a relatively high binding affinity (pK$_i$ YM-10, 7.68, **Figure 9 C**), which was not significantly different from YM. The derivatives YM-11, 12, 13, 14, 15, and 18 contained modifications of YM's alanine residues and displayed high binding affinities ranging from pK$_i$, 6.62 to 7.88 (see **Figure 9 C,D**). Exchange of the methyl group of one of the alanine residues for an isopropyl group (YM-11), its removal

(YM-12), or its steric inversion (YM-13) reduced the affinities to pK_i YM-11, 6.62, pK_i YM-12, 7.15, and pK_i YM-13, 7.22. Interestingly, replacing it with a bulky benzyl side chain in YM-14 (pK_i YM-14, 7.54) did not result in a significant reduction of the binding affinity compared to YM. Similarly, at the other alanine residue, replacing the methyl residue with an isopropyl group in YM-15 (pK_i YM- 15, 7.02) led to a significantly reduced the binding affinity, while introduction of a benzyl group in YM-18 (pK_i YM- 18, 7.88) did not.

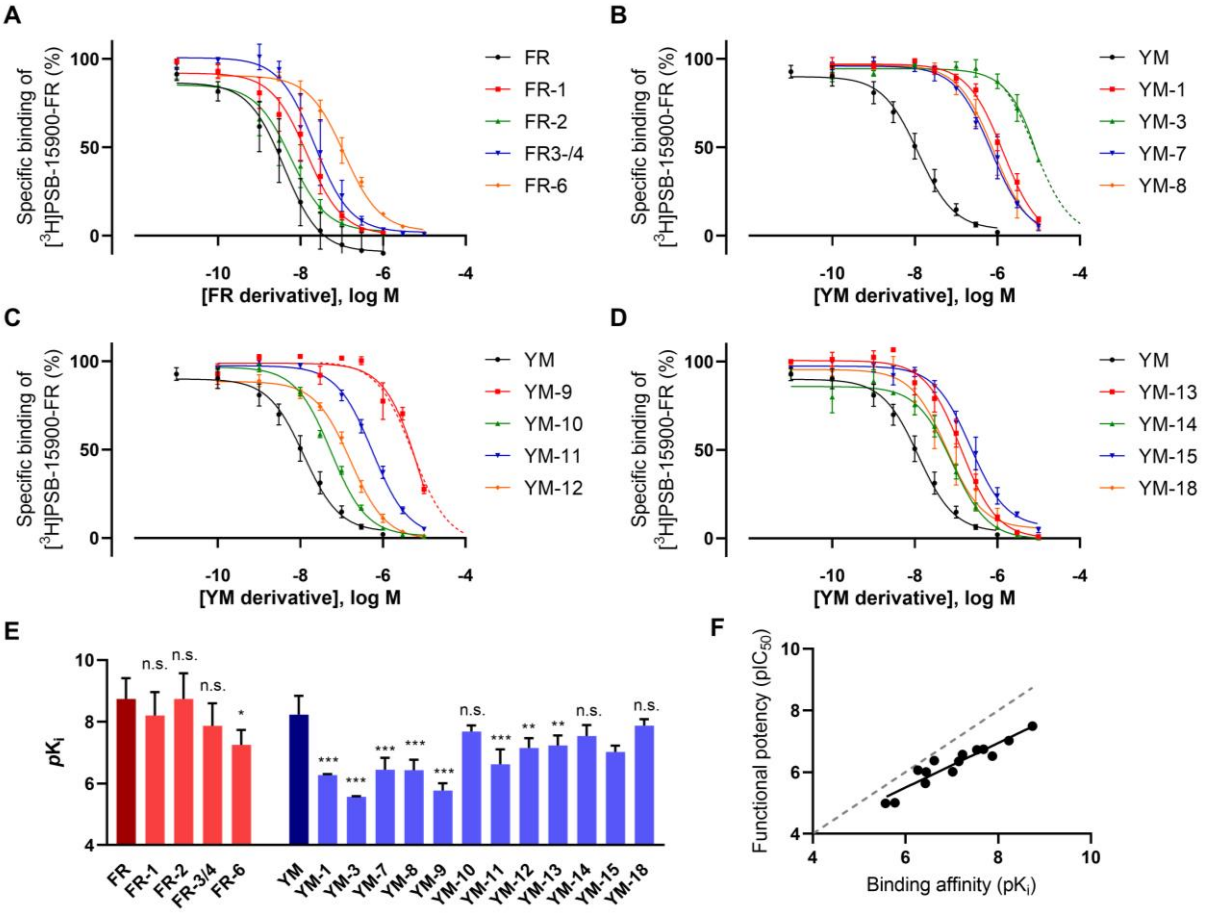

Figure 9: Characterization of FR and YM derivatives in radioligand binding assays versus [^{3}H]PSB-15900-FR. Competition binding experiments of (**A**) FR and its derivatives, (**B**) YM and its derivatives YM-1, YM-3, YM-7, and YM-8, (**C**) YM and its derivatives YM-9 to YM-12 , and (**D**) YM and its derivatives YM-13, YM-14, YM-15, and YM-18 versus [^{3}H]PSB-15900. **E**. pK_i values of FR, YM, and all investigated derivatives as determined in competition binding assays. For affinity values see **Table 1**. Significance levels were obtained from a one-way ANOVA with multiple comparisons (FR derivatives were compared to FR, YM derivatives were compared to YM) using Dunnett's post-hoc test; $p > 0.05$ not significant (n.s.), $p < 0.05$ *; $p < 0.01$ **; $p < 0.001$ ***. **F**. Correlation of affinity data from competition binding assays with functional data from previously performed IP_1 assays; slope = 0.72, $R^2 = 0.89$ [131, 153, 154], an ideal line (slope = 1) is plotted in light grey for comparison.

Affinity data obtained from radioligand binding assays showed a linear correlation with potencies from published functional assays (R^2 = 0.89, **Figure 9F**). However, pK_i values determined in binding studies were notably higher than pIC_{50} values determined in the functional assays [131, 153, 154], especially for more potent inhibitors. Ligand binding may possibly not have reached equilibrium in functional assays, therefore the potency may have been underestimated.

Table 1: Affinities of FR and YM derivatives and analogs determined in competition binding assays versus [^{3}H]PSB-15900-FR compared to published potencies determined in functional assays.

	Affinity (pK_i ± SD)	**Potency (pIC_{50})**
FR900359	8.73 ± 0.68	7.49[3]
FR-1	8.20 ± 0.74	n.d.
FR-2	8.74 ± 0.82	n.d.
FR-3/4	7.87 ± 0.72	n.d.
FR-6	7.25 ± 0.48	5.56[4]
[^{3}H]PSB-15900	8.19 ± 0.16[1]	n.d.
YM-254890	8.23 ± 0.48	7.02[3]
YM-1	6.27 ± 0.03	6.06[3]
YM-3	5.57 ± 0.02	4.99[3]
YM-7	6.45 ± 0.38	6.00[3]
YM-8	6.43 ± 0.35	5.63[3]
YM-9	5.77 ± 0.24	5.01[3]
YM-10	7.68 ± 0.20	6.74[3]
YM-11	6.62 ± 0.48	6.38[5]
YM-12	7.15 ± 0.31	6.35[5]
YM-13	7.23 ± 0.33	6.57[5]
YM-14	7.54 ± 0.36	6.72[5]
YM-15	7.02 ± 0.20	6.01[5]
YM-18	7.88 ± 0.22	6.52[5]
[^{3}H]PSB-16254	7.80[2]	n.d.

Data is expressed as mean ± SD from 3-6 independent experiments, performed in duplicate.
[1] pK_D value determined by saturation binding
[2] pK_D value determined by saturation binding [159]
[3] determined by IP_1 accumulation assays [131]
[4] determined by dynamic mass redistribution [157]
[5] determined by IP_1 accumulation assays [153]

Establishment of a competition-association binding assay

To determine the binding kinetics of FR- and YM-derivatives, we established a competition-association binding assay. Initially, competition-association assays were performed with fixed concentrations of 50 nM of unlabeled FR or YM and 5 nM of either [^{3}H]PSB-15900-FR or [^{3}H]PSB-16254-YM, using HEK293-$G\alpha_q$ membrane preparations or human platelet membrane preparations as a $G\alpha_q$ protein source (**Figure 10 A,B**). At HEK293-$G\alpha_q$ membranes, each combination of radioligand and unlabeled competitor resulted in different curve shapes, from

which dissociation rate constants for YM and FR could reliably be quantified by the model of Motulsky and Mahan [158]. In platelet membranes, an equilibrium of radioligand binding was reached almost instantly for FR versus [^{3}H]PSB-15900-FR and YM versus [^{3}H]PSB-16254-YM (**Figure 10 B**), therefore it was not possible to calculate kinetic parameters from these experiments. Furthermore, the assay window was far lower when using platelet membranes. For subsequent experiments we utilized a combination of HEK293-Gα_q membranes and [^{3}H]PSB-15900-FR due to the large assay window and the pronounced differences in curve shape in competition-association assays with YM and FR, which enabled the determination of kinetic binding constants.

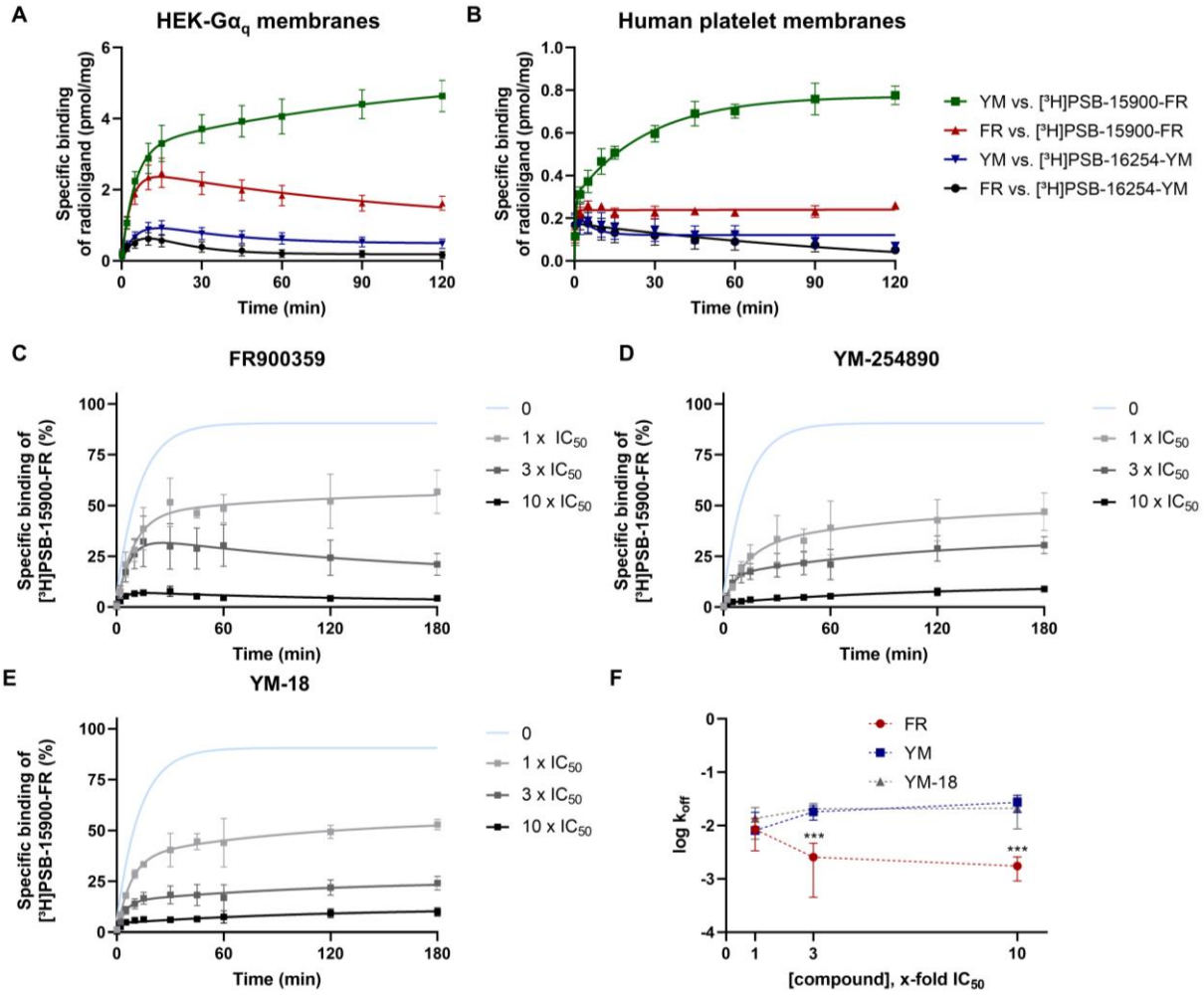

Figure 10: Selecting appropriate conditions (protein source, radioligand, and competitor concentration) for the establishment of competition-association binding assays. A, B. Competition-association binding assays with the FR-derived radioligand [^{3}H]PSB-15900-FR and the YM-derived radioligand [^{3}H]PSB-16254-YM at (**A**) HEK293-Gα_q membrane preparations and (**B**) human platelet membranes (25 µg of protein per vial). **C-E**. Competition-association binding assays of [^{3}H]PSB-15900-FR versus the indicated competitor (**C**. FR, **D**. YM, **E**. YM-18) at 1, 3, and 10-fold their IC_{50} concentration. The inhibitor-free association curve is displayed in light blue. **F**. The correlation between competitor concentration of FR (red), YM (blue), and YM-18 (gray) and log k_{off} as determined by the "Kinetics of competitive binding"-fit in Prism 8.4.0. All data are shown as mean ± SD from 3-4 independent experiments performed in duplicate.

When the unlabeled competitor dissociates from the protein faster than the radioligand, specific binding of the radioligand increases with time (see curve of YM vs [^{3}H]PSB-15900-FR in **Figure 10 A**). In contrast, the specific binding reaches a maximum followed by a decrease, striving towards an equilibrium, when the competitor dissociate slower than the radioligand (see all other curves in **Figure 10 A**). If the kinetic properties of radioligand and competitor are essentially identical, the curve would have the shape of a one-phase association. **Figure 10 A** clearly shows that non-hydrogenated FR and YM display a faster dissociation than their respective tritiated radioligands, [^{3}H]PSB-15900-FR and [^{3}H]PSB-16254-YM.

Next, we determined appropriate competitor concentration for measuring kinetic rate constants. Three different competitor concentrations, 1-, 3- and 10-fold of the IC_{50} value (**Figure 10 C-E**) of FR, YM, and the high-affinity YM-derivative YM-18, were employed. Interestingly, the determined log k_{off} values for FR, YM, and YM-18 were essentially identical at competitor concentrations of 1-fold IC_{50}. At 3- and 10-fold IC_{50} concentrations, the log k_{off} of FR was largely different from the log k_{off} of YM and YM-18 (**Figure 10 F**). Increasing the competitor concentration from 3-fold IC_{50} to 10-fold IC_{50} did not significantly affect the determined log k_{off} values. The authors of a study quantifying the dissociation rates of muscarinic M_3 receptor ligands had observed, similar to us, that a competitor concentration > 1x IC_{50} was necessary to obtain kinetic parameters for unlabeled compounds [160], probably due to the small effect of low inhibitor concentrations on the kinetics of radioligand binding. We decided to use a 3-fold IC_{50} concentration for competition-association experiments, which allowed us to determine kinetic binding parameters, while providing a large window of specific binding.

Competition-association binding experiments

Applying the optimized assay conditions, competition-association binding experiments were performed with $G\alpha_q$ protein inhibitors that had pK_i values > 7 to establish structure-kinetics relationships (**Figure 11**, **Table 2**). We determined k_{off} values, kinetic rate indices (obtained by dividing specific binding at 15 min by specific binding at 180 min) [161], and residence times (τ; in min) (all values are listed in **Table 2**).

FR and its derivatives FR-1 and FR-2 displayed extremely slow dissociation from the $G\alpha_q$ protein at 37° C (**Figure 11A-C**), with residence times of > 400 min, which did not differ significantly from each other. The structural modifications (extended, hydroxylated side chain R^1 in FR-1, and replacement of the propionyl by an acetyl group (R^2) in FR-2; see also **Figure 7**) did not affect the unbinding kinetics. As indicated by the curve shapes, all other tested compounds dissociated faster from the $G\alpha_q$ protein than [^{3}H]PSB-15900-FR. This suggests that the isopropyl group present in FR and its derivatives is pivotal for a long residence time. However, the isopropyl group is not sufficient for a long residence time. For instance, the mixture of FR-3/4, which both harbor

ethyl groups instead of methyl groups in different positions of the backbone, dissociates from the $G\alpha_q$ protein with a residence time of τ = 72 min (**Figure 11 D)**.

The parent compound YM displayed a residence time of 57 min (**Figure 11 E**). The derivative YM-10, which contains a propionylation of the β-HyLeu side chain (like FR) instead of an acetylation like YM, displayed a non-significantly increased residence time of 72 min. YM-12, YM-13, and YM-14, all of which are modified at one of the two alanine residues of YM, dissociated quickly from the $G\alpha_q$ protein (**Figure 11 G-I**). YM-18, which is benzylated at the other Ala residue of YM, shares an almost identical residence time with YM (**Figure 11 J**).

Table 2: k_{off} values (min^{-1}), kinetic rate indices (KRI), and residence times (τ) determined for unlabeled FR and YM derivatives and analogs.

	k_{off} (min^{-1})	**Kinetic rate index (KRI)**	**Residence time τ (min)**
FR	$2.56 \pm 1.32 \times 10^{-3}$	1.62 ± 0.28	466 ± 296
FR-1	$1.37 \pm 0.72 \times 10^{-3}$	1.83 ± 0.15	524 ± 181 (n.s.)
FR-2	$1.85 \pm 0.15 \times 10^{-3}$	1.58 ± 0.12	547 ± 70 (n.s.)
FR-3/4	$1.48 \pm 0.24 \times 10^{-2}$	0.72 ± 0.03	72 ± 21 (***)
[^{3}H]PSB-15900	$7.8 \pm 0.5 \times 10^{-3}$	n.d.	131 ± 8 (**)
YM	$1.82 \pm 0.22 \times 10^{-2}$	0.57 ± 0.03	57 ± 12
YM-10	$1.50 \pm 0.26 \times 10^{-2}$	0.62 ± 0.07	72 ± 22 (n.s.)
YM-12	$1.26 \pm 0.13 \times 10^{-1}$	0.21 ± 0.01	8 ± 2 (***)
YM-13	$6.37 \pm 1.29 \times 10^{-2}$	0.32 ± 0.04	17 ± 5 (*)
YM-14	$7.35 \pm 1.04 \times 10^{-2}$	0.32 ± 0.04	14 ± 4 (*)
YM-18	$2.07 \pm 0.33 \times 10^{-2}$	0.69 ± 0.02	55 ± 13 (n.s.)
[^{3}H]PSB-16254[1]	1.77×10^{-1}	n.d.	6 (***)

Data was obtained by competition-association assays using a three-fold IC_{50} concentration of test compound versus ~ 5 nM [^{3}H]PSB-15900-FR. Values are presented as means ± SD of 3-4 independent experiments performed in duplicate; n.d. not determined. Significance levels were obtained from a one-way ANOVA with multiple comparisons (FR derivatives were compared to FR, YM derivatives were compared to YM) using Dunnett's post-hoc test; $p > 0.05$ not significant (n.s.), $p < 0.05$ *; $p < 0.01$ **; $p < 0.001$ ***.

[1] Taken from [159]

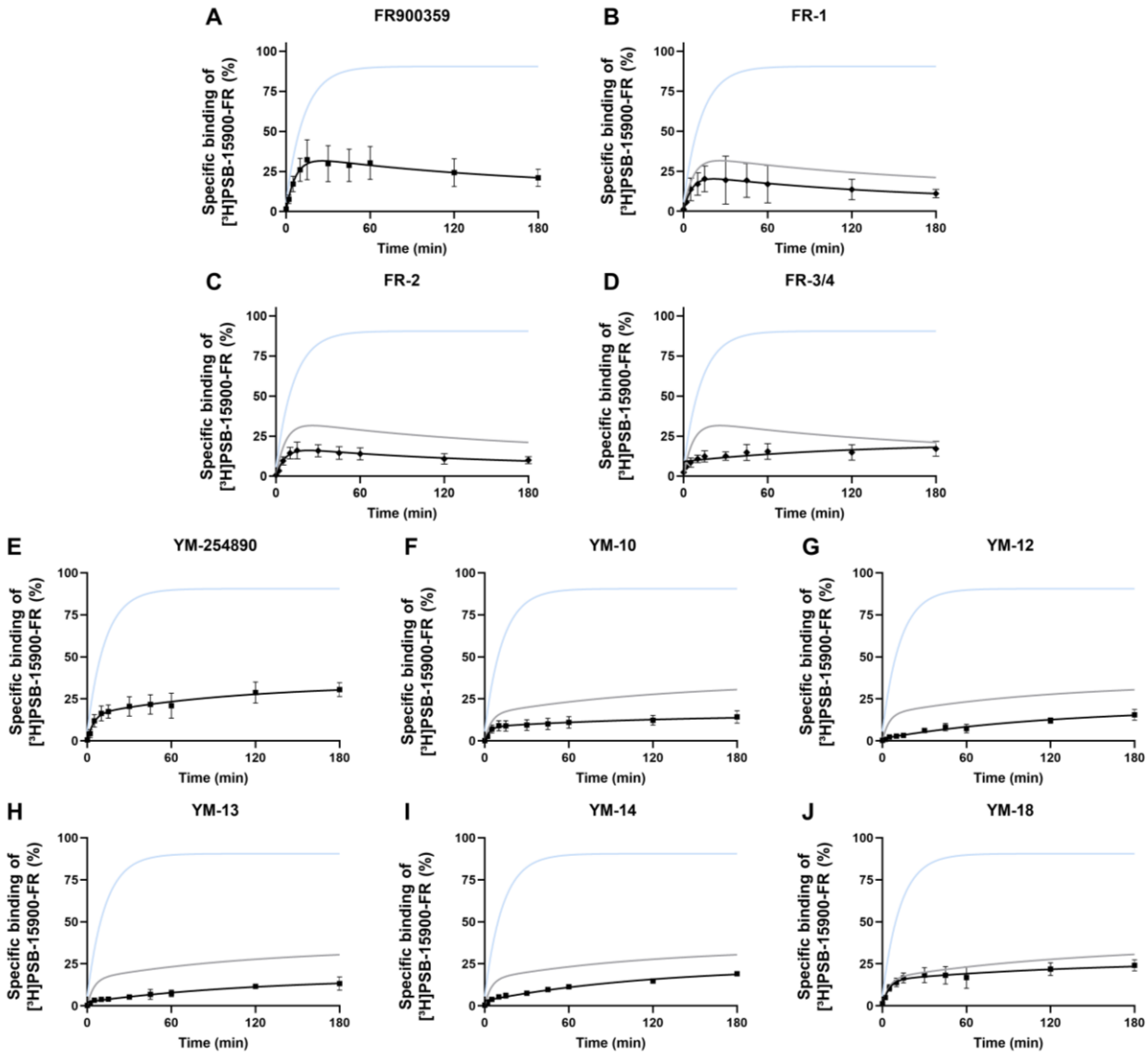

Figure 11: Competition association assays for the determination of the residence time of $G\alpha_q$ inhibitors. The curve of the indicated compound is shown in black, the curve of competitor-free [^{3}H]PSB-15900-FR association is displayed in blue and the curve of either FR (for FR-derived compounds) or YM (for YM-derived compounds) is displayed in gray for reference. **A-D**. Competition association curves of FR derivatives (**A**. FR, **B**. FR-1, **C**. FR-2, **D**. FR-3/4). **E-J**. Competition association curves of YM derivatives and analogs (**E**. YM, **F**. YM-10, **G**. YM-12, **H**. YM-13, **I**. YM-14, **J**. YM-18). Displayed values are means ± SD of 3-4 independent experiments performed in duplicate.

Structure-affinity relationships

Macrocyclic $G\alpha_q$ inhibitors bind to a cleft between the $G\alpha_q$ protein and the associated Gβ subunit (**Figure 12 A**), however no direct interaction with the Gβ subunit was observed in a co-crystal structure of YM and $G\alpha_q\beta_1\gamma_2$ [132, 151]. The pharmacophore of $G\alpha_q$ protein inhibitors is rather complex and involves all building blocks of the macrocyclic depsipeptides with exception of the two alanine residues, which do not directly interact with the $G\alpha_q$ protein [162]. The macrocyclic $G\alpha_q$ protein inhibitors feature multiple lipophilic interactions with the wide binding pocket at the switch I/linker I region of the $G\alpha_q$ protein, and only few polar contacts, e.g. hydrogen bonds between Arg60 and the ester bond of the phenyllactic acid residue, or the amide nitrogen of Glu191 and the free hydroxyl group of the β-HyLeu side chain. An interaction map of YM with surrounding residues is displayed in **Figure 12 B**.

As previously observed in functional assays, most modifications to the parent compounds YM and FR impaired their potency in inhibiting $G\alpha_q$ proteins [131, 153–156]. In the present study, we observed that functional potency of the macrocyclic $G\alpha_q$ protein inhibitors correlated well with their binding affinity (**Figure 9 F**), suggesting that the modifications that reduced the functional potency of YM or FR derivatives reduced their binding affinity and not e.g. their cell membrane permeability. Nevertheless, the potency was underestimated (compared to the binding affinity) in highly potent/affine compounds (slope 0.73), which might be explained by non-equilibrium conditions in functional assays.

FR-1 and FR-2 were found to bind to the $G\alpha_q$ protein with similar affinity as FR (pK_i FR-1, 8.20; FR-2, 8.74; FR, 8.73). Both the extension of the *N*-acetyl side chain at the macrocyclic backbone in FR-1 and the exchange of a propionyl group for an acetyl group at the branched β-HyLeu side chain in FR-2 did not result in a disruption or loss of contacts to the $G\alpha_q$ protein. The extended side chain of FR-1 points towards the aqueous phase and likely does not interact with the $G\alpha_q$ protein. The truncated side chain of FR-2 is located in a rather wide pocket in proximity to Glu191 and Tyr192, which permits flexible movements of this part of the β-HyLeu side chain. The FR-3/4 mixture displayed a moderate, yet not significant decrease in affinity compared to FR (pK_i FR-3/4, 7.87; FR, 8.73). Structural differences to the parent compound are minor, there is namely an exchange of methyl groups for ethyl groups in parts of the molecule that do not appear to interact with the $G\alpha_q$ protein, but rather point towards the aqueous compartment. It is worth noting that already minor modifications of the molecules can affect their conformation and their conformational stability in solution, which may in turn also affect binding to the $G\alpha_q$ protein [163]. The elimination of methanol in the side chain of FR-6 resulted in a major decrease in affinity (pK_i FR-6, 7.25), presumably due to decreased contacts with a hydrophobic pocket formed by Leu78, Val182, Val184, and Pro185.

Loss of the aforementioned polar contacts between macrocyclic $G\alpha_q$ inhibitors and the protein resulted in a major reduction in affinity as seen with YM-3 (pK_i YM-3, 5.57; YM, 8.23; exchange of the ester bond for an amide disrupts the hydrogen bond to Arg60) and YM-9 (pK_i YM-9, 5.77; removing the hydroxyl group in the side chain disrupted hydrogen bonds with the amide of Glu191).

N-Demethylation in YM-1 (pK_i YM-1, 6.27) also resulted in a major decrease in affinity, which may be explained by conformational destabilization of the macrocycle, as the methyl group appears to points towards the solvent. Other modifications of the backbone present in derivatives YM-11 to YM-15 and YM-18 were better tolerated and resulted mostly in a slight to moderate reduction of affinity (pK_i YM-11, 6.62; YM-12, 7.15; YM-13, 7.23; YM-14, 7.54; YM-15, 7.02; YM-18, 7.88). Replacement of side chain methyl groups with isopropyl moieties in the two alanine building blocks (YM-11, YM-15) was less well tolerated than the addition of larger, lipophilic benzyl groups (YM-14, YM-18). Removing a side chain methyl group (YM-12) or inverting its configuration (YM-13) led to an approximately 10-fold decrease in affinity. In summary, modification of the alanine decreases the affinity of the compounds, even though these residues should point to the solvent. Interestingly, only the addition of bulky benzyl groups (YM-14, YM-18) does not result in a significant affinity decrease.

In the compounds YM-7 and YM-8, isopropyl moieties within the branched β-HyLeu side chain were replaced by methyl groups, leading to reduced affinity by almost two orders of magnitude (pK_i YM-7, 6.45; YM-8, 6.43; YM, 8.23). The isopropyl group missing in YM-7 may form lipophilic interactions with the side chains of Ile189 and Ile190, while the isopropyl group missing in YM-8 presumably interacts with the side chains of Thr187 and Ile190. The extension of the acetyl to a propionyl residue in YM-10 was well tolerated (pK_i YM-10, 7.68), which was to be expected as this moiety is also present in FR and its derivatives (with the exception of FR-2).

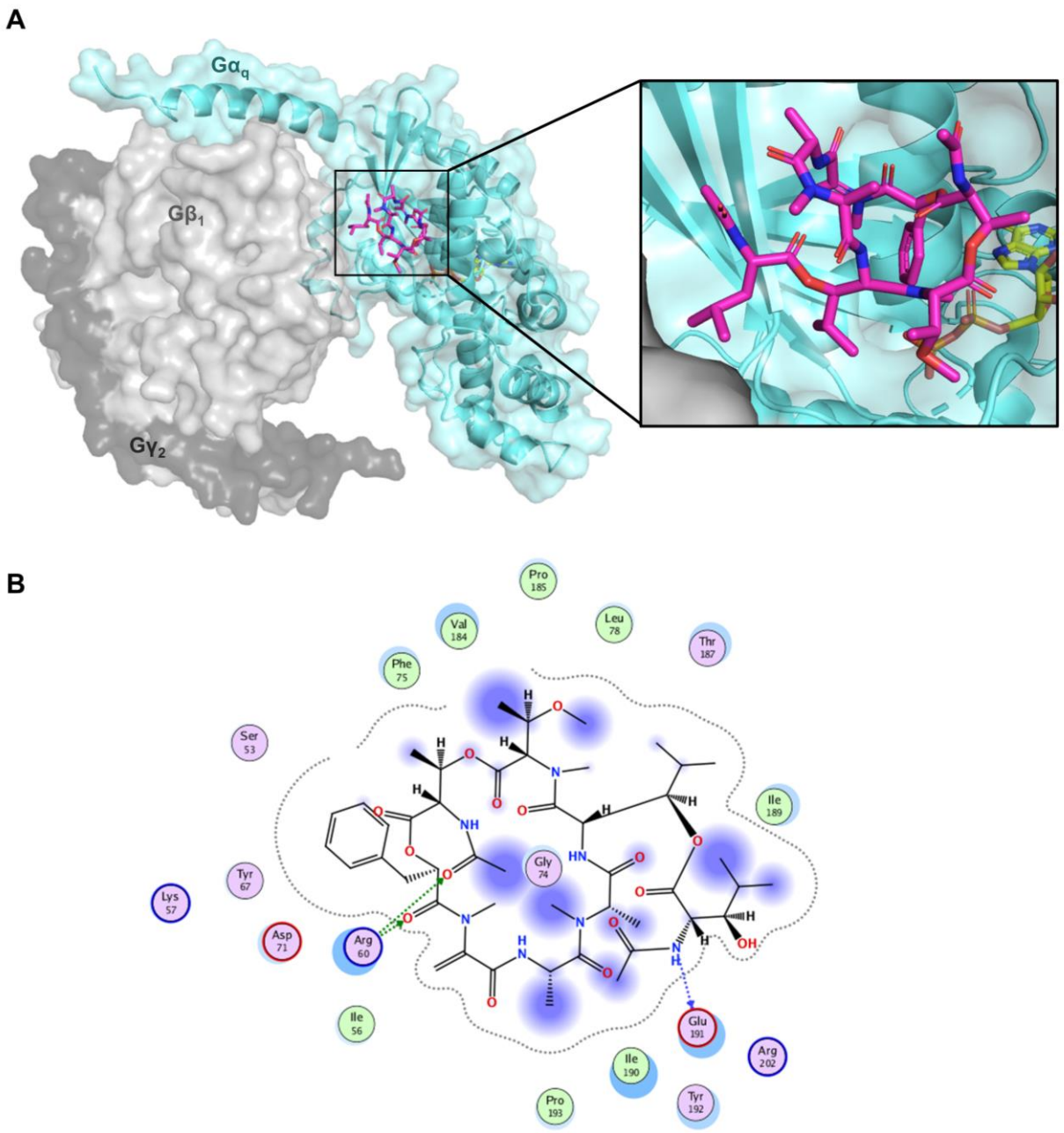

Figure 12: Binding site of macrocyclic $G\alpha_q$ protein inhibitors and inhibitor-protein interactions. **A**. Binding site of YM (magenta) at the heterotrimeric $G\alpha_q\beta_1\gamma_2$ protein ($G\alpha_q$ cyan, $G\beta_1$ light gray, $G\gamma_2$ dark gray) as determined by X-ray crystallography (PDB 3AH8) [132]. GDP is shown in yellow. A close-up illustrating the binding pose of YM at the membrane is displayed at the right. **B**. 2D-ligand interaction diagram of YM at the binding pocket of the $G\alpha_q$ protein, generated by MOE (Chemical Computing Group, Cambridge, UK).

Structure-residence time relationships

The residence time of compounds is a major determinant for the duration of their pharmacological effects; even when eliminated from the blood stream, slow-dissociating compounds may still be bound to their target. Inhibition of airway contraction by FR in mice has previously been shown to persist for as long as 96 h, while YM effects were significantly shorter [141] – both the effect of YM and FR apparently carried on for far longer than its residence time, possibly due to rebinding [164].

We have now observed that the dissociation kinetics of the radioligands [^{3}H]PSB-15900-FR and [^{3}H]PSB-16254-YM are not identical to those of their parent, non-hydrogenated compounds (**Figure 10 A**). Hydrogenation of the exocyclic double bond drastically shortened the residence times as observed for the tritiated radioligands (τ FR = 466 min vs. τ [^{3}H]PSB-15900-FR 131 min, ~4-fold difference; τ YM = 57 min vs. τ [^{3}H]PSB-16254-YM = 6 min, ~10-fold difference). The faster-dissociating YM was impacted by the hydrogenation of the double bond even more strongly. The electron-rich C=C-bond may undergo π-π interactions with the proximate Tyr192. Thus, due to their strongly differing dissociation kinetics, it is not adequate to treat the parent compounds and their derived radioligands as equivalents.

The residence time τ of FR-1 and FR-2 (τ FR-1, 524 min; τ FR-2, 547 min) is not significantly different from that residence time of the parent compound FR (τ FR, 466 min). This implies that the prolonged residence time of FR compared to YM is not caused by the propionyl group present in FR (replaced by an acetyl group in YM and FR-2, previously termed lipophilic "anchor 1" [159]), but rather by the isopropyl moiety at the core of FR („anchor 2" [159]). Consistent with this finding, exchange of the acetyl group for a propionyl residue in YM-10 prolonged the residence time of YM only by approx. 25% (τ YM-10, 72 min vs. τ YM, 57 min). The mixture of FR-3 and FR-4 dissociated significantly faster from the $G\alpha_q$ protein than the parent compound (τ FR-3/4 = 72 min vs. τ FR = 466 min). As the compounds could not be separated and are present in a 3:1 ratio of FR-3/FR-4 mixture, structural modifications cannot be directly correlated with changes in residence time.

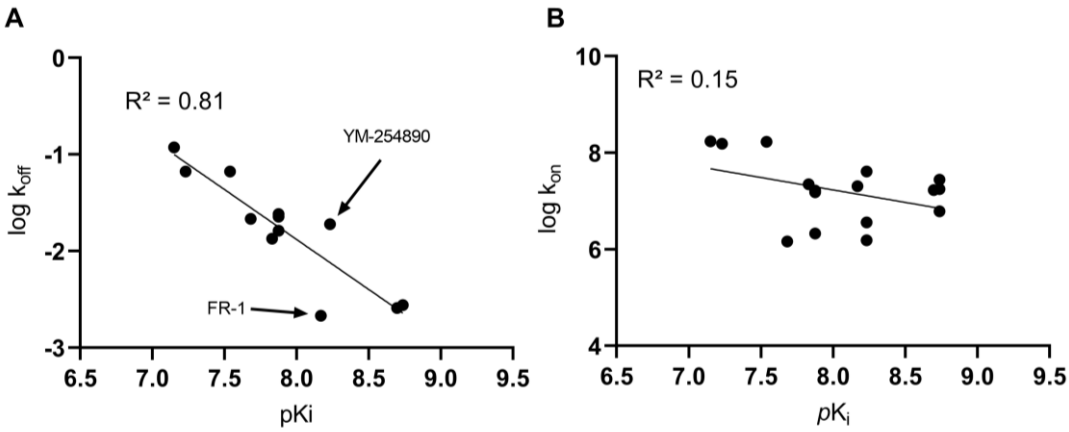

Figure 13: Correlations between (**A**) affinity (pK_i) and dissociation rate (log k_{off}), and (**B**) affinity (pK_i) and association rate (log k_{on}).

Among the YM derivatives and analogs, only YM-10 (see above), YM-12, YM-13, YM-14, and YM-18 displayed sufficiently high affinities to allow for competition-association studies. Removing a methyl group of an alanine building block (in YM-12) reduced the residence time drastically from 57 min for YM to 8 min for YM-12. Inverting its configuration or extending the methyl group to a benzyl group in YM-13, or YM-14, respectively, resulted in similar residence times of 17 and 14 min, respectively. Replacing the methyl group in the other alanine group with a benzyl group had no significant effect on the residence time (τ YM-18, 55 min), as compared to YM. Even though modifications of the alanine residues were well-tolerated in terms of affinity, most of them (with the exception of the addition of a benzyl group in YM-18) still resulted in notably decreased residence times.

Overall, dissociation rates (expressed as log k_{off}) and affinities (pK_i value) showed a good correlation for the investigated YM and FR derivatives (R^2 = 0.81, **Figure 13 A**). Two outliers were detected: YM dissociated faster than other compounds of similar affinity, and FR-1 displayed a longer residence time than compounds of a similar affinity. The KRI correlated well with log k_{off} (R^2 = 0.87, not shown). The KRI can be determined from only two incubation time points and therefore allows simple, but nevertheless quite accurate determination of the dissociation rate [161]. There was no correlation between the calculated k_{on} value determined by competition-association experiments and the affinity of a compound (**Figure 13 B**). However, the calculation of on-rates by competition-association experiments may be inaccurate, as macrocyclic $G\alpha_q$ protein inhibitors bind via a conformational selection mechanism [159].

Discussion

Altogether, steep structure-affinity and structure-residence time relationships were observed. Also, affinity and dissociation kinetics (expressed as log k_{off}) displayed a good linear correlation (**Figure 13**). The longest residence times were determined for FR and its derivatives FR-1 and FR-2, which emphasizes the major contribution of this isopropyl group exclusively present in FR and its derivatives to long-lasting $G\alpha_q$ protein inhibition. Well-tolerated changes to the inhibitor structure (in terms of both affinity and residence time) are exclusively located in parts of the molecule, which do not interact with the $G\alpha_q$ protein, but point towards the ambient aqueous phase (e.g. in FR-1, FR-2, YM-10, YM-18; **Figure 12 B**). However, abolishing single lipophilic contacts results in major decreases in affinity and residence time (e.g. in YM-7, YM-8, YM-12). Similarly, hydrogenation of the double bond largely decreases the compounds' residence time (compare YM and FR with their respective hydrogenated radioligands, **Figure 10 A**), and slightly lowers their affinity similar affinity (saturation pK_D of [^{3}H]PSB-15900-FR = 8.19, competition pK_i of FR = 8.73; saturation pK_D of [^{3}H]PSB-16254-YM = 7.80, competition pK_i of YM = 8.23). Affinity values determined by competition binding experiments may however even underestimate the real affinity of very slow-dissociating compounds such as FR, FR-1, and FR-2, which would require enormous incubation times to reach equilibrium due to their pseudo-irreversible binding to the $G\alpha_q$ protein [159]. Despite the potentially reactive partial structure (Michael acceptor) present in YM and FR, previous studies clearly demonstrated reversible binding of both compounds to the $G\alpha_q$ protein [126, 151]. Increasing the lipophilicity of the molecule does not necessarily result in higher affinity or residence time as shown by the reduced affinity of FR-3/4, YM-11, and YM-15 (see **Table 2**). In a previous study we have shown that many single-residue mutations greatly accelerate dissociation of YM- and FR-derived radioligands from the $G\alpha_q$ protein [159]. Combined with our findings from the present study, we conclude that the long-lasting inhibition of $G\alpha_q$ proteins by FR is based on a network of interactions, which is easily disturbed by modifications to both the protein and the inhibitor.

Due to the complexity of ligand-protein interactions involved, we consider it challenging to use the scaffold of YM or FR to inhibit Gα proteins outside of the $G\alpha_{q/11}$ family with high potency and selectivity. On the other hand, $G\alpha_{15}$ and $G\alpha_s$ proteins with high affinity for YM and FR were generated and characterized in functional assays [165, 166]. Step-by-step mutagenesis of the $G\alpha_{15}$ protein inhibitor binding site to that of the $G\alpha_q$ protein reveals that fewer mutations are required to render the $G\alpha_{15}$ protein sensitive to the slow-dissociating FR than to the faster-dissociating YM [165].

It is worth noting that the model of Motulsky and Mahan treats ligand binding as a one-step process to a single conformation of the target protein [158]. This model does not fit ideally to the binding process of YM and FR at Gα proteins: While inhibitor dissociation apparently occurs via a one-step unbinding, association involves a conformational selection step of the $G\alpha_q$ protein, which is rate-limiting to inhibitor association, and renders the determination of a k_{on} value in the sense of a one-step binding model impossible [159]. Accordingly, on-rates of macrocyclic $G\alpha_q$ protein inhibitors determined by the Motulsky-Mahan model in competition association assays do not correlate with affinities (**Figure 13C**). Therefore, we do not consider this experimental approach valid for the determination of association rate constants of macrocyclic $G\alpha_q$ protein inhibitors.

Summary and outlook

In summary, we analyzed structure-affinity relationships and a structure-residence time relationships for a series of macrocyclic $G\alpha_q$ protein inhibitors. Importantly, we discovered that YM and FR kinetically behave very differently from their respective hydrogenated radioligands. Both affinities and residence times (which correlate well with each other) of macrocyclic $G\alpha_q$ protein inhibitors are parameters that depend even on subtle structural modifications. Generally speaking, FR and its derivatives display both higher affinities and longer residence times than YM and its derivatives, which highlights the importance of the isopropyl group exclusively present in FR for long-lasting high-affinity inhibition of the $G\alpha_q$ protein.

5.2. Materials and Methods

Chemicals and materials

YM-254890 was purchased from Wako Chemicals (Neuss, Germany). FR900359 and its analogs were isolated from *A. crenata* or recombinantly produced in *C. vacinii* as previously described [126, 156, 157]. YM analogs were synthesized as previously described [131, 153]. The radiolabeled FR- and YM-derivatives [^{3}H]PSB-15900-FR (28 Ci mmol^{-1}) and [^{3}H]PSB-16254-YM (31 Ci mmol^{-1}) were obtained by catalytic hydrogenation of FR, or YM, respectively, with tritium gas (Pharmaron UK Ltd, Cardiff, UK) [151]. Assay tubes and cell culture materials were purchased from Sarstedt (Nümbrecht, Germany). Cell culture medium was purchased from Gibco (ThermoFisher, Waltham, MA), fetal calf serum (FCS) and antibiotics were obtained from PAN Biotech (Aidenbach, Germany). Further chemicals were purchased from SigmaAldrich (Merck, Darmstadt, Germany) or Roth (Karlsruhe, Germany).

Cell culture

Cells were cultured at 37°C and 5% CO_2 in Dulbecco's Modified Eagle Medium (DMEM), supplemented with 10% FCS, penicillin (100 U ml^{-1}), and streptomycin (0.1 mg ml^{-1}). HEK293 cells (human, female) were edited by CRISPR/Cas9 to delete the *GNAQ* and *GNA11* genes encoding the $G\alpha_q$ and $G\alpha_{11}$ protein subunits [126]. Cells were retrovirally transfected to overexpress the $G\alpha_q$ protein as previously described [151, 159]. Transfected cells were cultured in the presence of 0.2 mg ml^{-1} G418. At 70% confluency, cells were passaged by trypsination. Routine checks for mycoplasma contamination (detection by polymerase chain reaction (PCR)) were consistently negative.

Cell membrane preparation

Recombinant HEK293 cells were seeded into cell culture dishes and incubated till confluency. The medium was discarded and the cells were frozen at -20°C overnight. The next day, cells were thawed, detached with a rubber scraper, and harvested after adding 2 ml of 5 mM Tris-HCl plus 2 mM Na-EDTA buffer, pH 7.4, per dish. The suspension was subsequently homogenized using an UltraTurrax® (IKA Labortechnik, Staufen, Germany) for 1 min at level 4. Cell debris and nuclei were removed by a 10 min centrifugation at 1,000 *g*; the pellet (P1) was discarded. The supernatant (S1) was then centrifuged again for 1 h at 48,000 *g*, the pellet (P2) was resuspended and washed with 50 mM Tris-HCl pH 7.4 and then again centrifuged for 1 h at 48,000 *g*. After discarding the supernatant, the pellet was resuspended in 50 mM Tris-HCl, pH 7.4, and aliquots were stored at -80° C until use.

Saturation binding experiments

Affinity (K_D) and maximum binding capacity (B_{max}) of the radiolabeled FR-derivative [^{3}H]PSB-15900-FR were determined by saturation binding experiments. All binding assays employed a Tris-HCl buffer of pH 7.4, and experiments were performed in a total volume of 200 µl per sample. Multiple concentrations of [^{3}H]PSB-15900-FR were co-incubated with HEK293 cell membranes expressing the $G\alpha_q$ protein (25 µg of protein) in the presence of 5 µl of DMSO to assess total radioligand binding, or in the presence of unlabeled FR in dimethylufoxide (DMSO) (final concentration: 5 µM) to assess non-specific radioligand binding. The assay was incubated for 3 h at 37°C before the incubation was rapidly terminated by vacuum filtration through GF/C glass fiber filters. Filters were washed three times with 3.5 ml of ice-cold Tris-HCl buffer, pH 7.4, supplemented with 0.1% bovine serum albumin (BSA) and 0.1 % Tween 20. Filters were then transferred to scintillation vials and incubated with 2.5 ml of scintillation cocktail (LumaSafe®) for 9 h before they were counted in a liquid scintillation counter at 53-55% counting efficiency.

To determine K_D and B_{max} values, non-specific binding (determined in counts per minute (cpm)) were subtracted from total binding (in cpm) to calculate the specific binding of the radioligand. Values were calculated from the "Saturation binding: One site – specific binding" equation implemented in GraphPad Prism 8.4.0 (GraphPad, San Diego, CA, USA). Data are presented in pmol of bound radioligand per mg of protein, determined by the method of Lowry [167].

Competition binding experiments

The binding affinity of macrocyclic $G\alpha_q$ inhibitors was determined by competition binding experiments. Multiple concentrations of test compound, dissolved in DMSO, were co-incubated with radioligand (5 nM) and HEK293 $G\alpha_q$ membrane preparations (25 µg protein) for 3 h at 37° C. All other assay components were identical to those used in saturation binding assays. Samples were harvested and evaluated as described in the paragraph "Saturation binding experiments".

Raw data were normalized to total binding (DMSO control) = 100% and non-specific binding (5 µM of unlabeled FR) = 0%. K_i values and IC_{50} values were determined by the respective equations ("Binding – competitive: One site – Fit K_i / Fit IC_{50}). The K_D value of [^{3}H]PSB-15900-FR, determined by saturation binding, was used for the calculation of K_i values.

Kinetic binding experiments

In the course of this study, we performed association, dissociation, and competition-association experiments to measure the kinetics of [^{3}H]PSB-15900-FR as well as unlabeled compounds.

In association and competition-association experiments, membrane preparations (25 µg of protein) were added at several time points to a mixture of buffer, radioligand (5 nM), and DMSO or competitor dissolved in DMSO (final competitor concentration: 3 x IC_{50} if not mentioned otherwise, final DMSO concentration 2.5%). Non-specific binding was determined in parallel as described in the previous sections. The maximum incubation period was 3 h at 37°C. Incubation was performed with gentle shaking.

In dissociation experiments, radioligand, protein, and buffer were pre-incubated for 1 h at 37°C. Subsequently, an excess of unlabeled FR (final concentration: 5 µM) was added to the samples at several time points during the incubation period of 6 h at 37°C.

Samples were harvested and counted as described in section "Saturation binding experiments". For association and dissociation experiments, data was normalized (non-specific binding = 0%, highest cpm = 100%) and fit to a single exponential association function or an exponential decay function, respectively, to retrieve the observed association rate constant k_{obs} and the dissociation rate k_{off}. Half-lives ($t_{1/2}$) were calculated by ln(2)/k; residence time (τ) is $1/k_{off}$.

For competition-association binding experiments, the "Kinetics of competitive binding"-fit was employed according to the model of Motulsky and Mahan [158]. Ligand and radioligand concentrations were fixed according to the employed concentrations; B_{max}, k_{on}, and k_{off} were fixed at experimentally determined values from saturation, association, and dissociation binding experiments. On- and off-rates of the unlabeled compound were left unconstrained. For dissociation experiments, data was fit to a one phase exponential decay model after subtraction of non-specific binding and normalization (0% = 0 cpm, 100% = highest cpm) to obtain k_{off} values and dissociation $t_{1/2}$.

Data evaluation

All data points were obtained in three or more replicate experiments, each performed in duplicate. The exact number of experiments is given in the figure legends. Data is presented as mean ± SD if not otherwise noted. Statistical comparisons between two values were performed by an unpaired *t*-test, comparisons between more than two mean values were carried out by a one-way analysis of variance (ANOVA) followed by Dunnett's post-hoc test. Significance levels were determined according to *p*-values as follows: $p < 0.05$ (*) statistically significant, $p < 0.01$ (**) very statistically significant, $p < 0.001$ (***) extremely statistically significant.

6. Imaging of $G\alpha_{q/11}$ protein expression by autoradiography

Heterotrimeric guanine nucleotide-binding proteins ("G proteins") play a key role in cellular signaling by transmitting information from activated G protein-coupled receptors (GPCRs) to intracellular effectors. G proteins consist of three subunits, termed α, β, and γ [144]. The Gα protein subunit is the main interaction partner for GPCRs as well as effector proteins. There are four families of Gα proteins, $G\alpha_s$, $G\alpha_{i/o}$, $G\alpha_{q/11}$, and $G\alpha_{12/13}$ proteins, each of which is associated with distinct intracellular signaling pathways [50, 143]. The $G\alpha_{q/11}$ protein family comprises four members ($G\alpha_q$, $G\alpha_{11}$, $G\alpha_{14}$, and $G\alpha_{15}$), which link active GPCRs to phospholipase C-β (PLC-β) activation. PLC-β hydrolyzes phosphatidylinositol-4,5-bisphosphate to inositol trisphosphate (IP_3) and diacylglycerol (DAG), inducing calcium mobilization and protein kinase C activation [58, 149, 168]. $G\alpha_q$ and $G\alpha_{11}$ proteins are ubiquitously expressed and share a sequence identity of 90% (determined by pairwise sequence alignment of canonical sequences deposited in UniProt [169, 170]), and are regarded as functionally equivalent with respect to receptor interactions [43]. The $G\alpha_{14}$ protein shares 80% sequence identity with the $G\alpha_q$ protein. Its mRNA widely transcribed, showing the highest transcription levels in endocrine tissues [171]. It is activated mostly by the same GPCRs as the $G\alpha_q$ protein [8, 43]. The $G\alpha_{15}$ protein shows the largest evolutionary distance to the $G\alpha_q$ protein, sharing only 54% of its sequence identity. Its expression is limited to the hematopoietic system, which suggests a specific role for the $G\alpha_{15}$ protein in immune function [172, 173]. The $G\alpha_{15}$ protein is activated by a wider range of GPCRs and is therefore considered to be a promiscuous Gα protein [8, 43, 174].

$G\alpha_{q/11}$ proteins are vital signal transducers in mammalian cells [175] that can be activated by approx. 45% of therapeutically relevant human GPCRs [43]. Hyperactivation of $G\alpha_{q/11}$mediated signaling pathways plays a role in several diseases, such as uveal melanoma [113, 137], asthma bronchiale [140], pulmonary hypertension [176], and cardiac hypertrophy [177]. The macrocyclic $G\alpha_{q/11}$ protein inhibitors YM-254890 (YM) and FR900359 (FR) were previously shown to bind to $G\alpha_q$, $G\alpha_{11}$, and $G\alpha_{14}$ proteins with high affinity, low non-specific binding, and, in the case of FR, a long residence time [151] (see also section **Fehler! Verweisquelle konnte nicht gefunden werden.**). FR had displayed a ~1000-fold lower potency at the $G\alpha_{15}$ protein, while YM did not inhibit the $G\alpha_{15}$ protein at all [165]. Both compounds had shown no off-target effects, even at high inhibitor concentrations [133]. Accordingly, their tritiated radioligands had shown low non-specific binding [151]. Therefore, derivatives of YM and FR may have ideal properties for the development of a [^{18}F]-labeled diagnostic positron emission tomography (PET) tracer to detect pathologies, which display significantly increased $G\alpha_{q/11}$ protein expression relative to the surrounding tissue.

In this study, we investigate the suitability of macrocyclic $G\alpha_{q/11}$ protein inhibitors as *in vitro* diagnostics to evaluate $G\alpha_{q/11}$ protein expression and distribution in different organs and tissues, and to identify disease conditions which show up- or downregulation of $G\alpha_{q/11}$ protein expression. To this end, we performed autoradiography experiments with tissue samples obtained from mice, using the FR- and YM-derived radioligands [^{3}H]PSB-15900-FR and [^{3}H]PSB-16254-YM. Additionally, we determined the expression of $G\alpha_{q/11}$ proteins in lungs and hearts of mice with acute *asthma bronchiale* (preparation of mice by J. Dietrich). In future studies, we plan to analyze the $G\alpha_{q/11}$ protein expression in samples of various human cancer types relative to the surrounding tissue.

6.1. Results

The expression of $G\alpha_{q/11}$ proteins was determined by autoradiography experiments in brain, lung, heart, liver, kidney, pancreas, and spleen sections obtained from healthy female CD 1 mice. In order to compare both employed radioligands, we incubated brain sections with the FR-derived [^{3}H]PSB-15900-FR and the YM-derived [^{3}H]PSB-16254-YM (**Figure 14 A+B**). Both radiotracers displayed high average total binding and minimal non-specific binding, which was determined in the presence of 5 µM FR900359. Furthermore, both radioligands showed identical binding patterns to different brain regions. Brain sections were additionally stained with cresyl violet (Nissl staining; blue staining of basophilic molecules, e.g. RNA and DNA, thereby labeling neuron cell bodies) and hematoxylin-eosin (blue staining of basophilic structures and red staining of eosinophilic structures) (**Figure 14 C**). In the hippocampus (HA) and the cerebellum (CB), radioligand binding correlated inversely with the Nissl-staining, *i.e.* cell body-rich regions displayed low radioligand binding, while regions mostly composed of nerve fibers bound high amounts of radioligand.

The expression of $G\alpha_{q/11}$ proteins was calculated by densitrometric analysis (**Figure 14 D**, see method section for details), resulting in an average $G\alpha_{q/11}$ expression in the brain of 1.12 pmol per mg tissue (determined for binding of [^{3}H]PSB-15900-FR). Increased radioligand binding was found in the dentate gyrus (DG), hippocampal areas (HA), and the molecular of the cerebellum. Cortex (CO) and striatum (ST) displayed $G\alpha_{q/11}$ protein expression levels similar to the average binding of the brain, while the superior colliculus (SC) and the bright areas of the cerebellum (composed of the Purkinje cell layer, granular cell layer, and white matter) showed lower $G\alpha_{q/11}$ protein expression.

Both radioligands can be considered as suitable for autoradiography studies due to their high affinity, low nonspecific binding, and their ability to discriminate between regions with lower and higher $G\alpha_{q/11}$ protein expression in the brain. Because of similar preliminary results for both

radioligands, we decided to continue autoradiography studies using [^{3}H]PSB-15900-FR due to its longer residence time at the $G\alpha_q$ protein [151, 159].

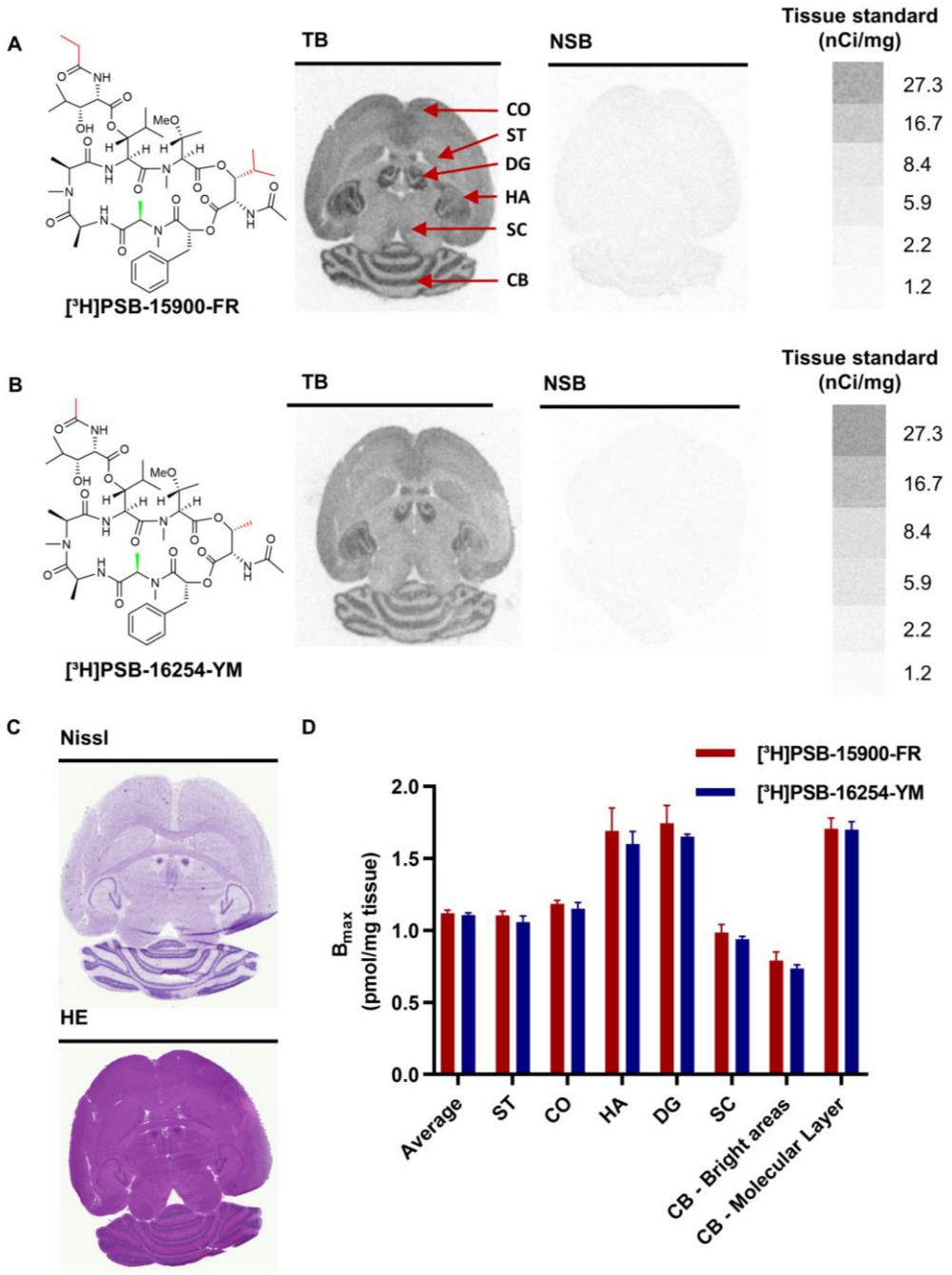

Figure 14: Structural formulas of the radioligands and representative autoradiography images of mouse brain sections, incubated with (**A**) [^{3}H]PSB-15900-FR and (**B**) [^{3}H]PSB-16254-YM. Images display total radioligand binding (TB) and non-specific binding (NSB; determined in presence of 5 µM FR). Organ slices were incubated with 10 nM of the indicated radioligand for 1 h at room temperature. Tissue equivalent standards for each radioligand are displayed on the right. (**C**) Brain sections stained with cresyl violet (Nissl) and hematoxylin-eosin (HE). (**D**) B_{max} values obtained by densitometric analysis of radioligand binding. CO, cortex; ST, striatum; DG, dentate gyrus; HA, hippocampus; SC, superior colliculus; CB, cerebellum.

Expression levels and distribution of $G\alpha_{q/11}$ proteins were further determined in tissue slices of lung, heart, liver, kidney, spleen, and pancreas using [^{3}H]PSB-15900-FR (see **Figure 15** for images of total radioligand binding, nonspecific binding and HE-staining). In lung tissue, [^{3}H]PSB-15900-FR displayed lower specific binding as compared to the brain. The radioligand displayed higher binding to the lung parenchyma compared to the tissue surrounding bronchi and blood vessels (indicated as "airways", see **Figure 15 A**). In hearts, we observed low, homogeneous binding of [^{3}H]PSB-15900-FR to the muscle tissue with occasional dark spots, corresponding to blood clots in the ventricles (**Figure 15 B**).

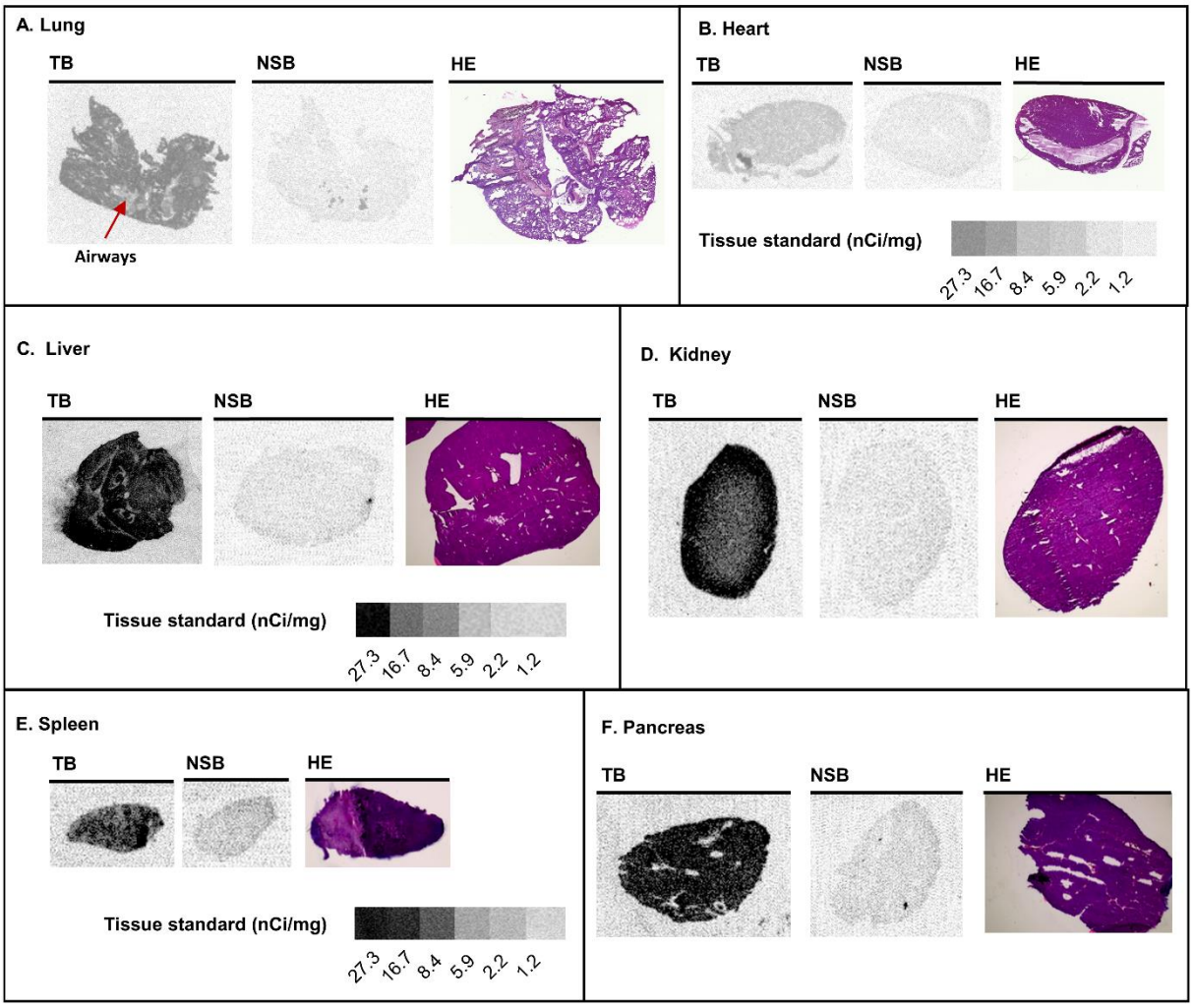

Figure 15: Representative images of tissue sections obtained from healthy female CD1 mice showing total radioligand binding (TB), non-specific binding (NSB; determined in presence of 5 µM FR) and hematoxylin-eosin staining (HE) of (**A**) lung, (**B**) heart, (**C**) liver, (**D**) kidney, (**E**) spleen, and (**F**) pancreas. Organ slices were incubated with 10 nM [^{3}H]PSB-15900-FR for 1 h at room temperature. Tissue equivalent standards are displayed below the respective panels.

Liver tissue sections displayed a high density of radioligand binding, which was mostly homogenous, but contained structures displaying lower $G\alpha_{q/11}$ protein expression (**Figure 15 C**). These might represent bile ducts, vessels, or artifacts from cryosectioning (see HE-staining in **Figure 15 C**). Kidney sections displayed very high binding of the radioligand to the renal cortex, but lower binding to the medulla, which might originate from the lower cell density in the collecting duct system in the center of the kidney (**Figure 15 D**).

Spleen sections displayed rather homogeneous [^{3}H]PSB-15900-FR binding of an intermediate intensity (**Figure 15 E**). In sections of the pancreas, high levels of homogeneous radioligand binding were observed. Areas displaying no specific binding correspond to excretory ducts and septa, which subdivide the pancreas into irregular lobes (see **Figure 15 F**).

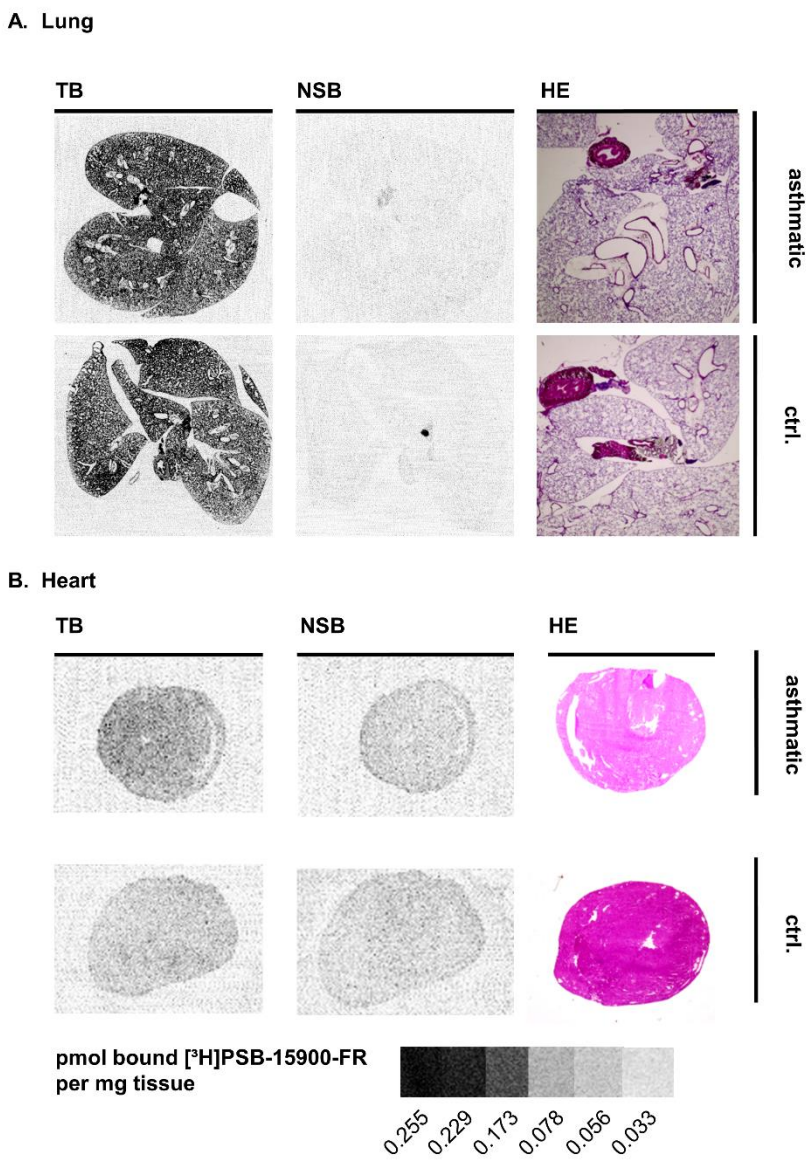

Figure 16: Representative images of (**A**) lung and (**B**) heart tissue sections obtained from BALB/c mice, which were either exposed to ovalbumin to induce symptoms of acute asthma (asthmatic) or were left untreated (ctrl.). TB, total radioligand binding; NSB, non-specific binding (determined in the presence of 5 µM FR), HE, hematoxylin-eosin staining. For autoradiography, organ slices were incubated with 10 nM [^{3}H]PSB-15900-FR for 1 h at room temperature. Tissue equivalent standards are displayed at the bottom.

Inhalation of FR had prevented bronchoconstriction in mice with ovalbumin-induced acute *asthma bronchiale* [140]. Thus, we imaged the $G\alpha_{q/11}$ distribution in lung and heart sections of BALB/c mice in this asthma model and compared it to untreated BALB/c mice (**Figure 16**). Lungs were filled with a mixture of polyvinyl alcohol and phosphate-buffered saline (PBS) before cryosectioning to prevent the collapse of the lungs during mounting to the slide. Similar to sections of healthy lung tissue, the radioligand bound mainly to lung parenchyma and the tissue surrounding bronchi and vessels exhibited lower radioligand binding. There was no clear difference visible between the lungs of mice with induced asthma and untreated mice (**Figure 16 A**). HE-stained close-ups of lung tissue did not show notable differences in the lung tissue between asthmatic and healthy mice (**Figure 16 A**). Heart sections of mice with acute asthma displayed low, homogeneous levels of radioligand binding, similar to control mice (**Figure 16 B**).

All autoradiography images were analyzed by densitometry to quantify the expression of $G\alpha_{q/11}$ proteins in each tissue section (see methods section). All B_{max} values obtained by autoradiography imaging of tissue sections using [^{3}H]PSB-15900-FR are plotted in **Figure 17**; exact values are presented in **Table 3**.

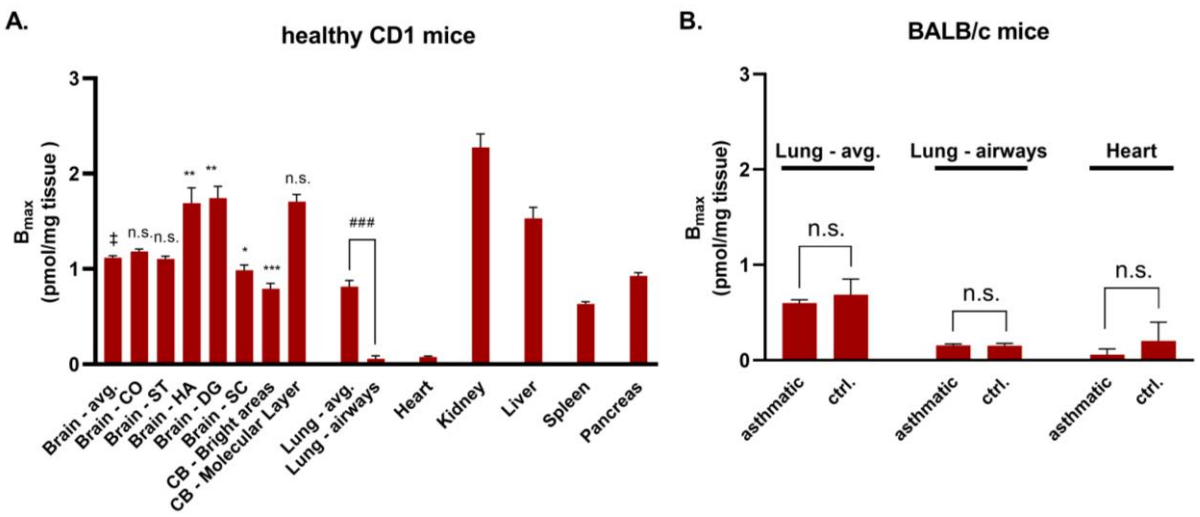

Figure 17: $G\alpha_{q/11}$ protein expression (B_{max}, given in pmol $G\alpha_{q/11}$ proteins per mg tissue) of (**A**) tissues obtained from healthy female CD1 mice, and (**B**) BALB/c mice treated with ovalbumin to induce symptoms of acute asthma (asthmatic) or untreated BALB/c mice (ctrl.). Values are presented as mean ± SEM from three (A) or two (B) individual animals, each measured at least in triplicate. avg., average; CO, cortex; ST, striatum; HA, hippocampus; DG, dentate gyrus; CB, cerebellum. Comparisons between two mean values were performed by an unpaired, two-sided t test (lung); if more than two mean values were compared, a one-way ANOVA with Dunnett's post-hoc test was employed, in which all means were compared to the tissue average (brain). Significance levels are defined as follow: n.s., $p > 0.05$; *, $p < 0.05$; **, $p < 0.01$, ***, $p < 0.001$, the reference value is indicated with ‡. The significance level of the direct comparison between lung average and airways is denoted with # instead of *.

Table 3: B_{max} values (pmol of $G\alpha_{q/11}$ proteins per mg tissue) obtained from autoradiography experiments in different mouse organs.

CD1 mice	**B_{max} ± SEM (pmol/mg of tissue)**
Brain – average	1.12 ± 0.02
Brain – striatum	1.11 ± 0.03
Brain – cortex	1.18 ± 0.02
Brain – hip. sulc.	1.69 ± 0.16
Brain – gyr. dent.	1.74 ± 0.12
Brain – superior colliculus	0.99 ± 0.06
Cerebellum – Bright areas	0.79 ± 0.06
Cerebellum – Molecular layer	1.71 ± 0.07
Lung – average	0.81 ± 0.07
Lung – airways	0.06 ± 0.03
Heart	0.08 ± 0.01
Kidney	2.27 ± 0.14
Liver	1.53 ± 0.12
Spleen	0.63 ± 0.02
Pancreas	0.93 ± 0.04
BALB/c mice	
Lung asthmatic – full	0.60 ± 0.04
Lung control – full	0.69 ± 0.17
Lung asthmatic – airways	0.16 ± 0.02
Lung control – airways	0.15 ± 0.02
Heart – asthmatic	0.06 ± 0.06
Heart – control	0.21 ± 0.19

In brain sections of healthy CD1 mice, the average $G\alpha_{q/11}$ protein expression was found to be 1.12 pmol/mg of tissue, which was not significantly different from the expression levels in cortex (CO, 1.18 pmol/mg), striatum (ST, 1.11 pmol/mg), and superior colliculus (SC, 0.99 pmol/mg). The hippocampal areas (HA, 1.69 pmol/mg), dentate gyrus (DG, 1.74 pmol/mg), and the molecular layer of the cerebellum (1.71 pmol/mg), which is composed of Purkinje cell dendrites, parallel fibers, and Bergman glia cells, expressed significantly more $G\alpha_{q/11}$ proteins than the brain average (**Figure 17 A**). In contrast, the Purkinje cell layer, granular layer, and white matter of the cerebellum expressed significantly less $G\alpha_{q/11}$ proteins (CB – Bright areas, 0.79 pmol/mg). The $G\alpha_{q/11}$ protein expression in the lung was on average significantly higher than in the tissue that surrounds the bronchi and vessels (denoted as "airways"; 0.81 pmol/mg in average lung tissue, 0.06 pmol/mg in airway, $p < 0.001$, two-sided t-test). Across all investigated organs and tissues, the $G\alpha_{q/11}$ protein expression levels in healthy CD1 mice can be ranked as follows: kidney > liver > brain > pancreas > lung > spleen >> heart (**Figure 17 A**).

In the model of acute asthma, we detected no significant difference in $G\alpha_{q/11}$ protein expression between lung sections of treated and untreated BALB/c mice (asthmatic, 0.60 pmol/mg; ctrl., 0.69 pmol/mg; see **Figure 17 B**). Similarly, we detected no different $G\alpha_{q/11}$ protein expression levels when focusing on the tissue that surrounds bronchi and vessels ("airways"; asthmatic, 0.16 pmol/mg; ctrl., 0.15 pmol/mg). In heart sections, the mean difference in $G\alpha_{q/11}$ protein expression

between healthy and asthmatic was not significant due to the high variance in radioligand binding to heart sections of untreated animals. Furthermore, $G\alpha_{q/11}$ protein expression levels in lung and heart sections of BALB/c mice were not significantly different from those determined in CD1 mice.

6.2. Discussion

In this study, we imaged the expression of $G\alpha_{q/11}$ proteins in several organs of healthy CD1 mice by autoradiography. Additionally, we compared the $G\alpha_{q/11}$ protein expression levels in lung and heart of mice with and without ovalbumin-induced *asthma brochiale*. The aim of the study was quantify the expression levels of $G\alpha_{q/11}$ proteins in diverse tissues in heath and disease. Radiotracers for autoradiography require a high binding affinity, and preferably a long residence at the target protein accompanied by low off-target and non-specific binding.

Initial experiments showed that both radioligands, [^{3}H]PSB-15900-FR and [^{3}H]PSB-16254-YM, were suitable for autoradiography experiments. Both of them displayed high affinity binding to all investigated tissues, and nearly no non-specific binding after addition of high concentrations (5 µM) of FR. The quantification of $G\alpha_{q/11}$ protein expression in brain sections delivered virtually identical results for both radioligands (**Figure 14 D**). Furthermore, both radioligands showed identical binding patterns in the brain, allowing a distinction between adjacent brain regions that expressed different levels of $G\alpha_{q/11}$ proteins. As both radioligands appeared to be equivalent, we continued to use [^{3}H]PSB-15900-FR for further experiments due to its longer residence time. Expression levels of $G\alpha_{q/11}$ proteins were highly similar in lung and heart tissue sections of different mouse strains (CD1 and BALB/c), which also indicates that the determination of $G\alpha_{q/11}$ protein expression by autoradiography using [^{3}H]PSB-15900-FR is highly reproducible between unrelated series of experiments.

We have used [^{3}H]PSB-15900-FR to quantify the expression levels of $G\alpha_{q/11}$ proteins and to image their distribution within several organs. Kidney, liver, pancreas, lung, spleen, and heart displayed decreasing $G\alpha_{q/11}$ protein expression in this order in organs obtained from healthy CD1 mice (**Figure 17 A**, **Table 3**). The expression of $G\alpha_{q/11}$ proteins ranged between 0.63 and 2.27 pmol per mg tissue, except for heart tissue, where $G\alpha_{q/11}$ proteins are expressed in a lower density of 0.08 pmol/mg. The native expression of $G\alpha_{q/11}$ proteins is therefore very high when compared to the typical expression levels of GPCRs in native tissue.

While radioligand binding was distributed evenly in most organs, brain and lung sections (and to some extent also kidney, liver, and pancreas sections) displayed notable differences of radioligand binding according to substructures (**Figure 14**, **Figure 15**, **Figure 16**). In lung tissue, we could discriminate between the main tissue and tissue surrounding bronchi and blood vessels

(indicated as "airways"). We found a significant, approx. 15-fold lower expression of $G\alpha_{q/11}$ proteins in the airways (excluding vessel/bronchi cavities) than in lung parenchyma in both CD1 mice and BALB/c mice (**Figure 17**). Brain sections clearly displayed a heterogeneous distribution of radioligand binding with substructures being discernable. Above-average expression of $G\alpha_{q/11}$ proteins was detected in the dentate gyrus and the hippocampal areas. The hippocampal areas and the dentate gyrus (which is also part of the hippocampus) are best-known to play a pivotal role in memory formation [178]. In the cerebellum, the cell body-rich Purkinje cell layer, the subjacent granular layer, and the white matter displayed only a very low $G\alpha_{q/11}$ protein expression, but the molecular layer of the cerebellum displayed increased $G\alpha_{q/11}$ protein expression relative to the brain average. The molecular layer is mainly composed of dendritic trees of Purkinje cells, parallel fibers of granule cells, and Bergmann glia. Previously, $G\alpha_q$ protein expression had been confirmed in the molecular layer and in the Purkinje cells of the mouse cerebellum by real-time polymerase chain reaction [179], and distinct roles for $G\alpha_q$ and $G\alpha_{11}$ proteins with regard to signal transmission of metabotropic glutamate receptors in Purkinje cell signaling were suggested [180].

As $G\alpha_{q/11}$ proteins are involved in the signal transmission in *asthma bronchiale* [140], we compared the $G\alpha_{q/11}$ protein expression in heart and lung sections of BALB/c mice with induced asthma to that of untreated mice. However, no significant difference of $G\alpha_{q/11}$ protein expression was observed between healthy and asthmatic mice – neither in the lung average, nor in the airways, or the heart. This indicates that (i) acute asthma does not induce an increase of $G\alpha_{q/11}$ protein expression during its pathogenesis and airway constriction is rather caused by hyperactivation of $G\alpha_{q/11}$ proteins and not by overexpression, or (ii) $G\alpha_{q/11}$ protein expression is only increased in a few layers of bronchial endothelial cells and is therefore not detectable by autoradiography due to the limited resolution of ~12 µm per pixel. Since we used a model of acute asthma, airway remodeling – a feature of persistent asthma [181] – and lung fibrosis cannot be expected to play a significant role.

$G\alpha_{q/11}$ proteins are considered to be ubiquitously expressed and are involved in signal transduction downstream of many receptors [43, 143]. However, correlating $G\alpha_{q/11}$ protein expression levels with the importance or number of physiological signaling pathways present in an organ appears to be difficult, e.g. $G\alpha_q$ signaling in the heart is vital [175, 182], despite the low protein expression levels detected in this study. Furthermore, it is worth mentioning that both radioligands cannot discriminate between $G\alpha_q$, $G\alpha_{11}$, and $G\alpha_{14}$ proteins as they bind all of them with a virtually identical affinity [151]. Further tissues from disease models will be investigated in due course.

6.3. Materials and Methods

Organs from CD1 mice

Female CD1 wild-type mice were housed with ad libitum chow and water supply under a normal circadian rhythm. At the age of 10 weeks, mice were killed by cervical dislocation. Respective organs were harvested from three healthy animals, frozen in isopentane and stored at -20° C until use.

Acute asthma model and preparation of fixated lung tissue.

Female BALB/c mice were housed with ad libitum chow and water supply under a normal circadian rhythm until an age of 10 weeks. On day 0 and day 14, mice were sensibilized by intraperitoneal injection of 20 µg ovalbumin. At day 21, 22, and 23, mice were challenged by nebulized 1% ovalbumin solution. Mice were sacrificed at day 24. Control mice were untreated.

To fixate lung tissue, the trachea was dissected and punctured and the lung was filled with modified OCT compound (100 mL Hank's balanced salt solution (HBSS) with 10 g polyvinyl alcohol, heated in a microwave; when cooled down to room temperature, 8 ml polypropylene glycol 2000 and 100 mg sodium azide were added) and sealed with a thread. Heart and lung were removed from the mice, washed with HBSS, and separated afterwards. Organs were snap-frozen in liquid nitrogen and stored at -80° C until cryosectioning.

Cryosectioning

Frozen organs were adjusted to the temperature of the cryostat (Microm HM560, Thermo Scientific, Waltham, MA, USA) and mounted on a carrier plate with Tissue-Tek® O.C.T.™ compound (Sakura Finetek, Alphen an de Rijn, NL). The organs were trimmed until tissue slices spanned the entire cross-section of the respective organ. Slices with a thickness of 10 µm (lung: 16 µm) were cut and mounted onto a room-tempered slide (2-4 slices per slide). Tissues slices were dried for 60 min and stored at -20° C.

Histological staining of samples

Slices of each harvested organ were stained by Nissl-staining and Hematoxylin-Eosin(HE)-Staining. For Nissl-staining, slices were thawed, dried, and the tissue slices were covered in Nissl staining solution (1.5% cresyl violet in aqueous ammonium acetate buffer, pH 4.6) for 5 min. The slides were subsequently rinsed and flushed with deionized water, differentiated in 70% and 100% ethanol, rinsed, and dried. HE staining was performed with an HE-staining kit (BIOZOL, Eching, Germany). Dried tissue slices were covered in Hematoxylin staining solution for 5 min, rinsed with deionized water briefly, and incubated in warm tap water for 3-5 min. Slides were

dipped in 100% ethanol for 10 seconds and subsequently incubated with Eosin Y solution for 3 min. After rinsing the slides with 100% ethanol, they were dehydrated with 100% ethanol for 3 min and dried. When dry, the cover slip was mounted onto the tissue section with NeoMount (Merck Millipore, Burlington, MA, USA) and fixed with a weight until the mounting medium solidified. Each slide was scanned in high resolution.

Autoradiography

Radioligand ([^{3}H]PSB-15900-FR, 28 Ci mmol^{-1}, [^{3}H]PSB-16254-YM, 31 Ci mmol^{-1}) solutions were prepared in autoradiography buffer (25 mM Tris, 120 mM NaCl, 5 mM KCl, 2 mM $CaCl_2$, 1 mM $MgCl_2$; pH_{RT} 7.4) at a final concentration of 10 nM. For the determination of total binding, 1% DMSO was added to the solution. Non-specific binding was recorded in the presence of 5 µM FR900359 (final DMSO concentration: 1%). Slides mounted with cryosectioned tissue slices were thawed, dried, and pre-treated with autoradiography buffer for 15 minutes. Excess buffer was removed from the slides. When dry, the slides were covered in radioligand solution for 60 min. Subsequently, radioligand solution was decanted and the slides were flushed with ice-cold 50 mM Tris, pH 7.4 twice for 2 min per step. Buffer salts were removed by dipping all slides in ice-cold deionized water for 10 seconds. Each organ was analyzed in triplicate (organs were harvested from 3 individual mice; 2 individual mice for experiments with asthmatic mice) and for each harvested organ, 2 slides of total binding and 2 slides of non-specific binding were imaged. Afterwards, slides were mounted onto a phosphoplate (BAS TR2025, FUJIFILM, Minato, Japan) and incubated for 3 weeks before scanning the plates.

Densitometric analysis

Images of the scanned plates were analyzed with AIDA (v 4.27). Each pixel in the obtained image had a size of 12.61 µm * 12.61 µm. Regions of interest (ROI) were manually defined within each tissue section. Generally, the average gray scale intensity of each ROI was determined; in lung and brain sections, the average gray scale intensity of discernible substructures was determined as well. ROIs were defined from the autoradiograms alone. A calibration curve of tritium standards (ART0123B/C; American Radiolabeled Chemicals, St. Louis, USA) with a known activity (in nCi/mg of tissue equivalent[1]) were used to transform gray scale intensity of the image into activity per mg of tissue (in nCi per mg of tissue). Taking into account the specific activity of the radioligand, this value is transformed into pmol radioligand bound per mg tissue. Subsequently, the non-specific binding was subtracted from total binding of the samples to obtain the specific

[1] Tissue equivalent: Tritium standards have a known activity, which is expressed in nCi/mg of tissue equivalent, *i.e.* issue that displays the same grey scale intensity as a standard, contains the same amount of activity (in nCi/mg of tissue) as the standard does. It is not required to weigh the organs and/or approximate the volume of the sections in [^{3}H]-autoradiography, because a large fraction of β-radiation emitted from radioligand bound to the sample is absorbed by the sample itself, and does not reach the imaging plate [183, 184].

radioligand binding per mg of tissue. Considering the K_D values of each radioligand (pK_D [^{3}H]PSB-15900-FR, 7.92; pK_D [^{3}H]PSB-16254-YM,7.80; determined by saturation binding to HEK cell membranes expressing the $G\alpha_q$ protein at 37°C [159]), and the actual concentration of radioligand, B_{max} values (in pmol $G\alpha_{q/11}$ proteins per mg of tissue) were calculated for each region of interest using a one-sire saturation binding model.

Numeric values were further analyzed in GraphPad PRISM 8.4.0 (GraphPad, San Diego, CA, USA). When evaluating the statistical significance of a difference between two means, an unpaired t-test was used (if necessary corrected for multiple comparisons). Significance analysis among three or more mean values was computed with a one-way analysis of variance (ANOVA). Dunnett's post-hoc test was employed to obtain significance levels of each mean compared to a reference mean value. Statistical significance was presented as follows: $p < 0.05$, *; $p < 0.01$, **, $p < 0.001$, ***.

Mouse brain regions were identified with help of Prof. Karl Schilling (Anatomisches Institut, UK Bonn) and the Mouse Brain Atlas (retrieved at www.mbl.org in June 2022).

7. Agonist-dependent coupling of the promiscuous adenosine A_{2B} receptor to Gα protein subunits

Jan Hendrik Voss, Andhika B. Mahardhika, Asuka Inoue, Christa E. Müller

ACS Pharmacol. Transl. Sci. **2022**, 5, 5, 373-386, doi: 10.1021/acsptsci.2c00020

Introduction

The adenosine A_{2B} receptor (A_{2B}AR) is a GPCR of the rhodopsin-like GPCR family. It is widely expressed in the human body in a low density, and its physiological functions still remain enigmatic. In contrast to the other AR subtypes (A_1-, A_{2A}-, and A_3AR), the A_{2B}AR binds adenosine with a low, micromolar affinity. Due to its upregulation in several pathological conditions, such as hypoxia, inflammation, and cancer [185–187], the A_{2B}AR constitutes a promising drug target, however, A_{2B}AR signaling pathways appear to be diverse and are not well understood.

Ligand-activated GPCRs engage heterotrimeric G proteins to forward signals into the cell. When activated, the Gα protein exchanges bound GDP for GTP and dissociates from the Gβγ-dimer. In its active, GTP-bound conformation, the Gα protein engages effector proteins. The 16 human Gα proteins are grouped into four subfamilies ($G\alpha_s$, $G\alpha_{i/o}$, $G\alpha_{q/11}$, and $G\alpha_{12/13}$), which interact with distinct effector proteins and whose activation thus results in different effects within the cell [50, 143].

GPCRs can couple to more than one specific Gα subunit, and additionally, different agonists can preferentially activate one signaling pathway over another – a phenomenon termed functional selectivity or biased signaling [42]. Due to advances in assay development and the discovery of the CRISPR-Cas9 technology, it has become feasible to dissect G protein activation by a GPCR, either by the use of biosensors or by selective expression of single Gα proteins. GPCR-G protein coupling data for the A_{2B}AR has been contradictory so far: Canonically, the A_{2B}AR couples primarily to $G\alpha_s$ proteins and secondarily to members of the $G\alpha_{q/11}$ family [49, 188]; very few reports of A_{2B}AR coupling to the $G\alpha_{i/o}$ family have been published [189, 190]. A large GPCR-G protein coupling screening performed by Inoue *et al.* [191] discovered coupling of the adenosine-activated A_{2B}AR to virtually all proteins with exception of the $G\alpha_{15}$ protein, while another study by Avet *et al.* [43] found exclusively A_{2B}AR coupling to $G\alpha_s$ and $G\alpha_{15}$ proteins.

In this study, we examined coupling of the $A_{2B}AR$ to the $G\alpha_{q/11}$ protein family ($G\alpha_q$, $G\alpha_{11}$, $G\alpha_{14}$, $G\alpha_{15}$) in calcium mobilization assays using HEK293 cells selectively expressing only a single $G\alpha_{q/11}$ family member. Additionally, we profiled $A_{2B}AR$ coupling to all Gα proteins by the TRUPATH $BRET^2$ assay kit. We used three agonists to activate the receptor: adenosine, its metabolically more stable analog NECA, and the non-nucleosidic partial agonist BAY 60-6583. Moreover, we investigated the impact of adenosine deaminase (ADA) on ligand potency and efficacy.

Summary and outlook

In calcium mobilization assays, adenosine and NECA led to calcium mobilization in cells expressing the $G\alpha_q$ or $G\alpha_{15}$ proteins, but not in cells expressing $G\alpha_{11}$ and $G\alpha_{14}$ proteins. NECA activated the $G\alpha_{15}$ protein with a notably higher potency than the $G\alpha_q$ protein. BAY 60-6583 did not activate any $G\alpha_{q/11}$ family protein at native $A_{2B}AR$ expression, but overexpression of the receptor led to a partial calcium mobilization by BAY 60-6583, as exemplarily shown in HEK-$G\alpha_{15}$ cells. This suggests a key role of expression levels of receptors, and putatively also of G protein subunits and downstream effector proteins, for the effective coupling measured in a living system.

In $BRET^2$ experiments, the adenosine-activated $A_{2B}AR$ turned out to be a promiscuous receptor, which can activate most Gα proteins (with the exception of the gustatory Gα subunit; the $G\alpha_{14}$ protein could not be investigated) with similar potencies, albeit with large differences in efficacy (relative to control receptors known to strongly activate the respective Gα protein subunits). Similarly, NECA can activate the same range of Gα subunits, but shows a preference regarding its potency and efficacy towards $G\alpha_s$, $G\alpha_{15}$, and $G\alpha_{i1-3}$ proteins. The partial agonist BAY exclusively activated $G\alpha_s$, $G\alpha_{15}$, and $G\alpha_{12}$ proteins, displaying full efficacy at the $G\alpha_{15}$ protein, but only partial efficacy at $G\alpha_s$ and $G\alpha_{12}$ proteins.

Additionally, we investigated the role of ADA on the potency and efficacy of $A_{2B}AR$ signaling by NECA and BAY 60-6583 via $G\alpha_q$, $G\alpha_{11}$, $G\alpha_{15}$, and $G\alpha_s$ proteins and found an increased potency and efficacy for both ligands at the $G\alpha_{15}$ protein in the presence of ADA. Conversely, a somewhat decreased efficacy (and unaltered potency) was observed at the $G\alpha_s$ protein. We attribute this to allosteric effects of ADA at the $A_{2B}AR$, which were previously described to bind to each other [192–194].

In this study, we systematically assessed the G protein coupling of a single receptor (the $A_{2B}AR$) activated by several agonists, and we profiled the functional selectivity of these ligands towards Gα protein pathways. A key focus of this study was the evaluation of the efficacy of $A_{2B}AR$-G protein coupling: while the receptor can activate nearly all Gα subunits, it activates them with different efficacies. Low efficacy may however not translate into efficacious downstream signaling of the respective Gα subunits under physiological conditions. Additionally, the efficacy depends

on the employed agonist. By comparing efficacies to control receptors, we attempted to generate a "global" efficacy score for the $A_{2B}AR$, which does not merely compare agonists with one another, but instead relies on well-described, efficacious GPCR-G protein couplings for comparison. Future work in this direction may delineate determinants for receptor-G protein coupling efficacy and potency.

We conclude that the $A_{2B}AR$ is a promiscuous receptor, which preferentially activates $G\alpha_s$, $G\alpha_{15}$, and $G\alpha_{12}$ proteins. Additionally, each agonist displays a characteristic coupling fingerprint. Thus, the choice of agonist is of major importance for biological studies on the $A_{2B}AR$, as no synthetic agonist will completely imitate adenosine action.

Author contribution

The author performed all experiments in the manuscript with the exception of $BRET^2$ assays of control receptors and the generation of cell lines selectively expressing $G\alpha_{q/11}$ family proteins. Additionally, the author prepared all figures included in the manuscript and supporting information, and wrote the manuscript in cooperation with Christa E. Müller.

8. Using novel BRET-based biosensors to detect coupling of the adenosine-activated $A_{2B}AR$

During a research stay in the laboratory of Prof. Dr. Michel Bouvier, Institute for Research in Immunology and Cancer, Montreal, Canada, Gα protein coupling of the adenosine-activated $A_{2B}AR$ was further studied by novel BRET-based biosensors, named enhanced bystander BRET (ebBRET), effector membrane translocator assay (EMTA) biosensors (see section 2.1.5 for assay principles), and GPCR kinase (GRK)-Gγ co-localization assays. Briefly, ebBRET assays measure a BRET ratio between an RLucII-tagged G protein or β-arrestin and rGFP-CAAX (a membrane-anchored polybasic sequence with the prenylated CAAX box from the KRAS protein fused to rGFP). EMTA biosensors detect recruitment of RLucII-tagged Gα protein effectors to the cell membrane by measuring a BRET ratio between the effector-RLucII and rGFP-CAAX. GRK-Gγ co-localization assays measure an increase of BRET ratio between Gγ-RLucII and GRK-GFP10 upon GPCR agonist-promoted dissociation of heterotrimeric G proteins. Additionally, PKC activation and DAG production downstream of $A_{2B}AR$ receptor activation were monitored by respective biosensors.

We have previously shown that the G protein activation fingerprint of the $A_{2B}AR$ is dependent on the employed agonist (see section 7 and 13.3). All assay data on $A_{2B}AR$-induced Gα protein activation presented in this chapter were exclusively generated using the endogenous agonist adenosine. The employed BRET assays can only detect "productive coupling", i.e. GPCR-Gα interactions which lead to Gα protein activation, but not "unproductive coupling", i.e. physical interaction between receptor and G protein that does not lead to G protein activation (as e.g. described for the vasopressin 2 receptor – $G\alpha_{12}$ protein interaction [195]).

8.1 Results and discussion

EbBRET and EMTA assays were performed with the $A_{2B}AR$ and compared to a control receptor to determine the Gα protein activation fingerprint of the $A_{2B}AR$ in this assay system (see **Figure 18** for curves). cDNA amounts used for transfection were previously established by the Bouvier group (**Table 4**). We detected recruitment of $G\alpha_s$, $G\alpha_{15}$, and $G\alpha_z$ effector biosensors to the plasma membrane upon stimulation of the $A_{2B}AR$ with adenosine. Results for other Gα subunits such as $G\alpha_{oA/B}$, $G\alpha_{12}$, and $G\alpha_{14}$ were ambiguous and displayed, if at all, a very weak efficacy of the adenosine-activated $A_{2B}AR$ at these subunits. No recruitment of β-arrestins was observed. Potencies and efficacies (relative to the control receptor), if applicable, are listed in

Table 5.

Table 4: cDNA amounts of transfected biosensor cDNAs used per 3.5 × 10^5 cells. Amounts of receptor and renilla GFP (rGFP)-CAAX cDNA were 200 and 500 ng per 3.5 × 10^5 cells, respectively.

Biosensor + Gα protein	Biosensor cDNA (ng)	Gα cDNA (ng)
p63-RLucII + $G\alpha_{q/11/14}$	10	64
p63-RLucII + $G\alpha_{15}$	10	15
PDZ-RLucII + $G\alpha_{12/13}$	40	40
Rap1GAP-RLucII + $G\alpha_{i/o}$	5	60
Rap1GAP-RLucII + $G\alpha_z$	10	20
β-arrestin1/2-RLucII[1]	5	-
$G\alpha_s$67-RLucII	10	-

[1] Instead of Gα cDNA, 20 ng GRK2 cDNA was co-transfected per 3.5 × 10^5 cells.

Table 5: pEC_{50} values and efficacy relative to control receptors[a] of the adenosine-activated $A_{2B}AR$ at multiple Gα proteins using GENTA or ebBRET biosensors.

Biosensor + Gα protein	pEC_{50} ± SEM	Efficacy (% of ctrl.) ± SEM
p63-RLucII + $G\alpha_{15}$	6.34 ± 0.39	71 ± 19
PDZ-RLucII + $G\alpha_{12}$	5.27 ± 0.28	27 ± 14
Rap1GAP-RLucII + $G\alpha_{oA}$	4.83 ± 0.01	30 ± 12
Rap1GAP-RLucII + $G\alpha_{oB}$	5.05 ± 0.16	24 ± 10
Rap1GAP-RLucII + $G\alpha_z$	5.42 ± 0.10	73 ± 20
$G\alpha_s$67-RLucII	5.98 ± 0.00	78 ± 0

[a] The following control receptor-ligand combinations were used: p63-RLucII + $G\alpha_{15}$ – serotonin-activated $5HT_{2A}$ receptor; PDZ-RLucII + $G\alpha_{12}$ – U44619-activated TPα receptor; Rap1GAP-RLucII + $G\alpha_{i/o}$ proteins – dopamine-activated D_2 receptor; $G\alpha_s$67-RLucII – serotonin-activated $5HT_{7A}$ receptor.

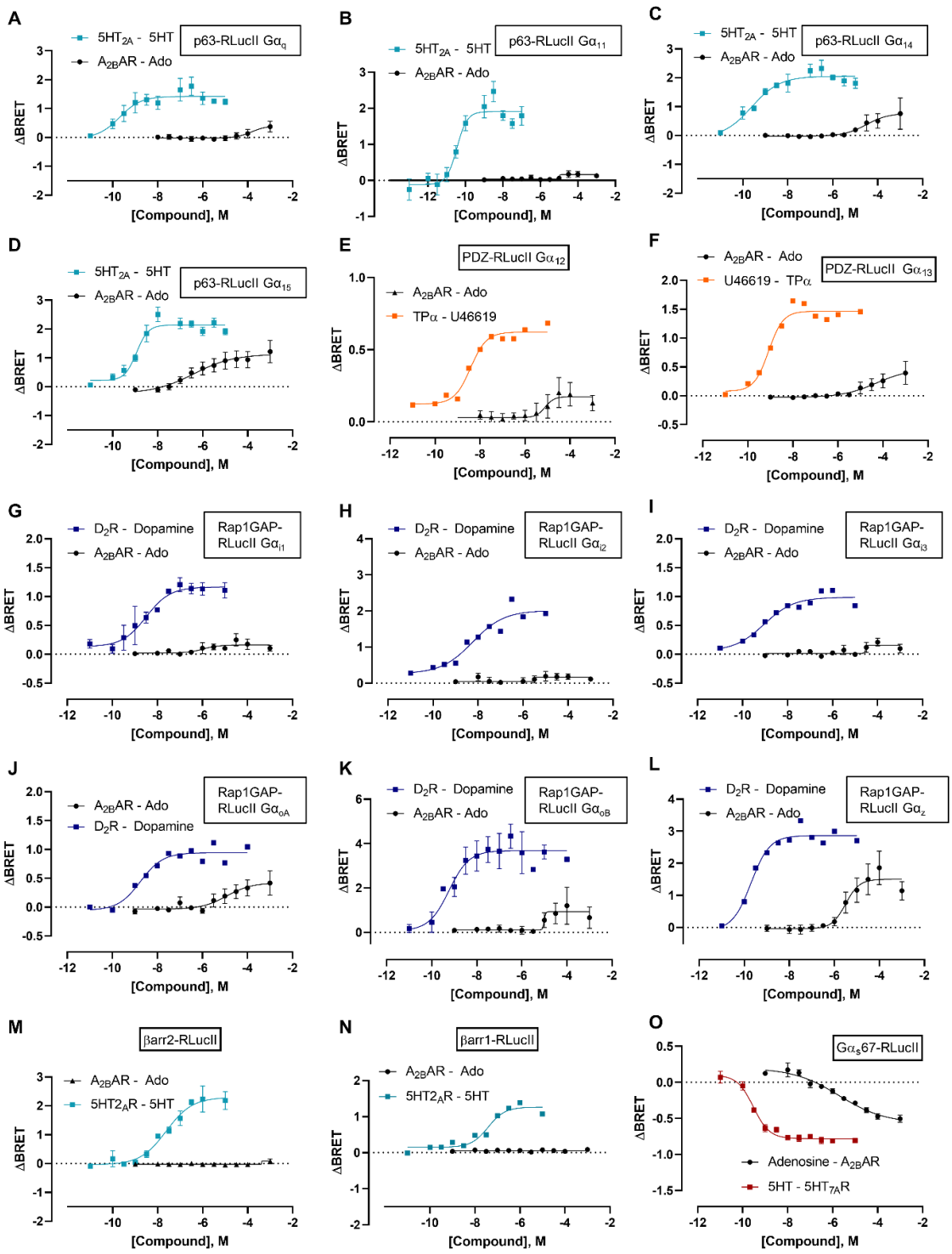

Figure 18: Concentration-response curves displaying agonist-promoted BRET ratio shift (ΔBRET) of the adenosine-activated $A_{2B}AR$ (black) and a control receptor (colored) at various ebBRET/GEMTA biosensor-Gα protein combinations. **A-D.** p63-RLucII – rGFP-CAAX BRET ratios of the $G\alpha_{q/11}$ family (**A.** $G\alpha_q$, **B.** $G\alpha_{11}$, **C.** $G\alpha_{14}$, **D.** $G\alpha_{15}$), using the serotonin-activated $5HT_{2A}$-receptor as control. **E-F.** PDZ-RLucII – rGFP-CAAX BRET ratios with $G\alpha_{12}$ (**E**) and $G\alpha_{13}$ (**F**), using the U46619-activated TPα receptor as control. **G-L.** Rap1GAP-RLucII – rGFP-CAAX BRET ratios of the $G\alpha_{i/o}$-family (**G.** $G\alpha_{i1}$, **H.** $G\alpha_{i2}$, **I.** $G\alpha_{i3}$, **J.** $G\alpha_{oA}$, **K.** $G\alpha_{oB}$. **L.** $G\alpha_z$). **M-O.** ebBRET assays plotting βarr1-RLucII (**M**), βarr2-RLucII (**N**), $G\alpha_s67$-RLucII (**O**) – rGFP-CAAX ratios, using the $5HT_{2A}$ receptor (**M**,**N**) or the $5HT_{7A}$ receptor (**O**) as a control.

Previous experiments performed with the same biosensors [43] only detected $G\alpha_s$ and $G\alpha_{15}$ protein activation by the adenosine-activated $A_{2B}AR$. Here, we additionally detected activation of the $G\alpha_z$ protein by the adenosine-activated $A_{2B}AR$. It is worth mentioning that the concentration-response curves of adenosine displayed a Hill slope of 0.5 at the $G\alpha_{15}$ and $G\alpha_s$ protein, but a regular Hill slope of 1 at the $G\alpha_z$ protein, which might hint at a role of receptor dimerization in $A_{2B}AR$ pharmacology. A curve with a hill slope of 0.5 is more flat than a typical sigmoidal curve with a hill slope of 1, theoretically meaning that 2 "ligand equivalents" are required for 1 "signal equivalent", i.e. 2 molecules of adenosine would be required for the formation of one active complex when signaling via $G\alpha_s$ and $G\alpha_{15}$ proteins, but not when signaling via $G\alpha_z$ proteins. Dimerization of the $A_{2B}AR$ with the related $A_{2A}AR$ has previously been demonstrated [45]. However, there are no published data on $A_{2B}AR$ homodimerization, and the expression levels of all other adenosine receptors are negligible in HEK293 cells [196].

Furthermore, very minor activation of the $G\alpha_{q/11}$ family and $G\alpha_{oA/B}$ proteins was observed with a low efficacy relative to a control receptor. In contrast to these data, results obtained with the TRUPATH $G\alpha\beta\gamma$ assay [44] or the TGF-shedding assay [8] suggested that the $A_{2B}AR$ is a promiscuous receptor that can couple to virtually all $G\alpha$ protein subunits. Due to this discrepancy, the assay conditions were optimized by adapting the amount of $G\alpha$-encoding cDNA for transfection (**Figure 19**). The BRET ratio was determined at a single, high concentration of adenosine (100 µM), from which the buffer value was subtracted to obtain ΔBRET values. ΔBRET values > 0.5 are considered as productive coupling in these assays (see dotted lines in **Figure 19**).

Increasing the amount of cDNA used for transfection revealed productive coupling of the $A_{2B}AR$ to $G\alpha_{12/13}$ and $G\alpha_{i/o}$ family proteins (**Figure 19 A-H**), which required high expression levels of $G\alpha$ proteins. In contrast, $G\alpha$ proteins efficaciously activated by the $A_{2B}AR$, such as $G\alpha_{15}$ and $G\alpha_z$ proteins (**Figure 19 F**,**I**) require only very low amounts of cDNA to result in high BRET ratio shifts. Data for $G\alpha_{14}$ displayed high BRET ratio shifts at all $G\alpha_{14}$ expression levels in these experiments, which is contradictory to previous experiments (see **Figure 18 C**, **Figure 19 J**). Further replicates are required for a conclusive interpretation. A systematic investigation of the impact of receptor and $G\alpha$ protein activation on coupling, efficacy, and ligand potency will help to identify conditions for efficient $A_{2B}AR$-$G\alpha$ coupling.

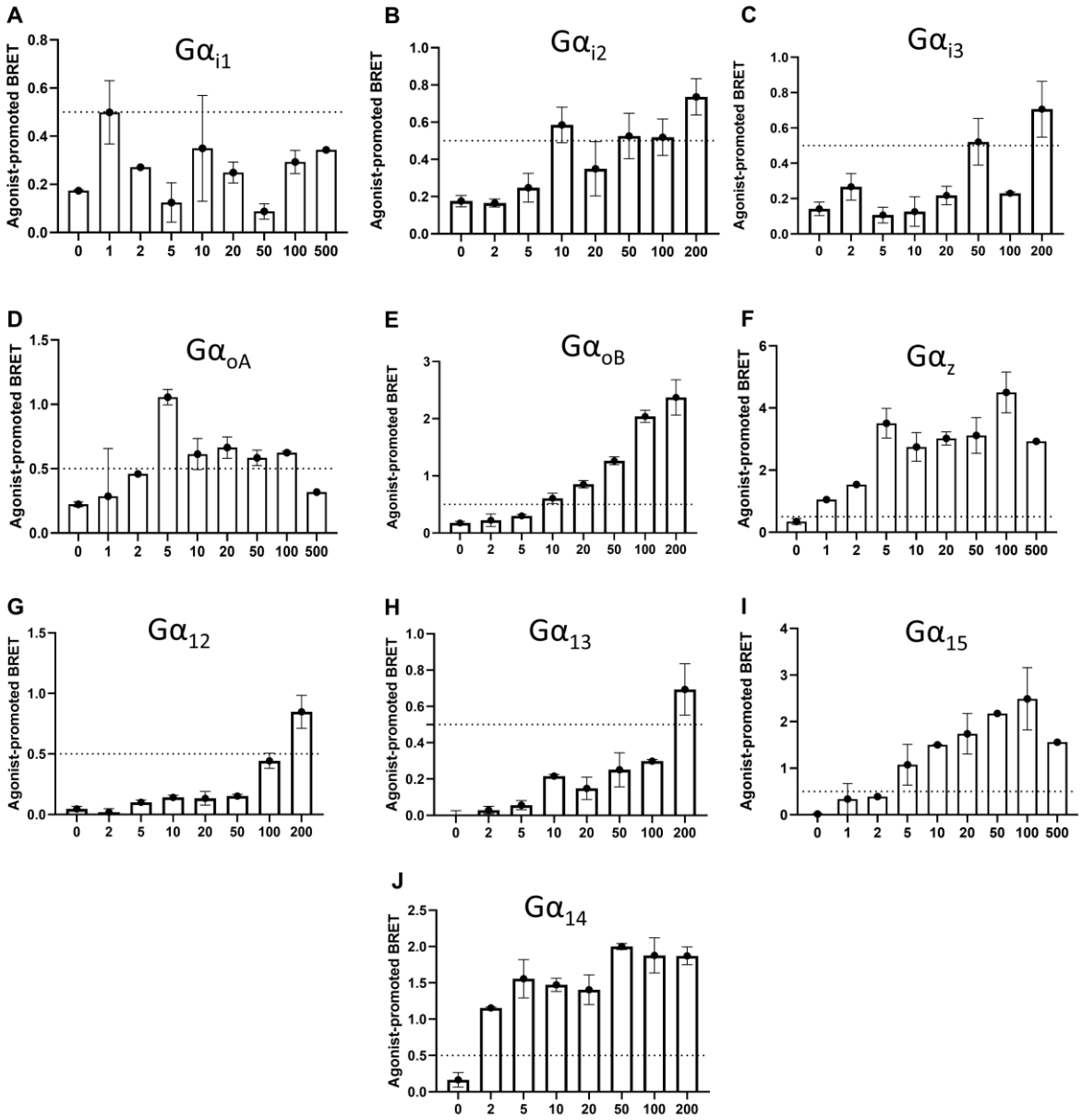

Figure 19: Gα-cDNA titration experiments, displaying the agonist-promoted BRET ratio at several Gα-cDNA amounts (indicated as ng of cDNA per ml cells). Receptor, rGFP-CAAX, and effector-RLucII amounts remained constant. An agonist-promoted BRET ratio shift of 0.5, threshold for successful Gα protein activation, is indicated by a dotted line. Shown data was obtained in two independent experiments performed in duplicate.

Biosensors detecting PKC activation or DAG accumulation were used to take a closer look at the activation of proteins downstream of $G\alpha_{q/11}$ family proteins by the $A_{2B}AR$ (**Figure 20**). We compared results of the $A_{2B}AR$ to the angiotensin II type 1 (AT_1) receptor, which is known to strongly activate $G\alpha_{q/11}$ family proteins. Both receptors were co-expressed with $G\alpha_q$ proteins (weak activation by the $A_{2B}AR$, strong PKC activator), $G\alpha_z$ proteins (strong activation by the $A_{2B}AR$, no PKC activator), and $G\alpha_{15}$ proteins (strong activation by the $A_{2B}AR$, strong PKC activator) or no Gα subunit at all, either in the presence or absence of $G\beta_1\gamma_1$ cDNA (100 ng of each cDNA per 3.5 ×

10^6 cells). While AT_1R stimulation with angiotensin II resulted in a strong BRET shift under all conditions, $A_{2B}AR$ activation required expression of the $G\alpha_{15}$ protein for PKC activation or DAG accumulation. This finding indicates that the $G\alpha_{15}$ protein can effectively link the $A_{2B}AR$ to downstream signaling, which was previously also demonstrated in calcium mobilization assays [44]. However, the $G\alpha_q$ protein also weakly mobilized intracellular calcium via the $A_{2B}AR$, which was not detected by the PKC or DAG biosensors in the present study, possibly due to a lower sensitivity of the employed BRET assays and less amplification along the signaling cascade. Gβγ overexpression had no effect on the BRET ratio shift or on the potency of the ligands in any of the tested conditions.

Lastly, a biosensor pair between an RLucII-tagged Gγ5 protein and GFP10-tagged GRK2 protein was used to detect activation of Gα proteins by the $A_{2B}AR$ [197]. The biosensors were co-transfected with the receptor, $G\beta_1$, and a selected Gα subunit (100 ng each). GRK2 can bind free Gβγ dimers, and therefore the BRET ratio increases upon Gα protein activation by a receptor ligand, because the Gα protein separates from its previously associated Gβγ dimer (**Figure 21 A**). When co-transfecting any Gα protein subunit with $G\beta_1\gamma_5$-RLucII and GRK2-GFP10, the basal BRET ratio between Gγ5-RLucII and GRK2-GFP10 decreases, because the Gα protein subunits capture the free Gγ5-RLucII proteins, thereby preventing their interaction with GRK2-GFP10. Upon receptor-induced dissociation of heterotrimeric G proteins, the BRET ratio increases due to increased co-localization of the free Gβγ dimers with GRK2. If no Gα protein subunit is recombinantly overexpressed, this assay can detect the activation of endogenously expressed Gα protein subunits.

Using 100 µM of adenosine, we detected minor activation of endogenous G proteins by the $A_{2B}AR$ in HEK cells and discovered strong activation of the positive control, the Gαq Y67C mutant, a promiscuous Gα protein, the $G\alpha_{15}$, $G\alpha_z$, and also the $G\alpha_{12/13}$ proteins (**Figure 21 B**). Weak activation of $G\alpha_q$, $G\alpha_{i1}$, and $G\alpha_{oA/B}$ were observed. Overall, data from Gγ-GRK co-localization assays were consistent with data obtained by EMTA assays well. Activation of some Gα proteins, which occurred only at high Gα cDNA amounts used for transfections in GEMTA assays or in TRUPATH BRET2 assays [44], e.g. to $G\alpha_{11}$ and $G\alpha_{i2\text{-}3}$, were not detected in the Gγ-GRK co-localization assay. It is of note that this assay does not work reliably with $G\alpha_s$ proteins, presumably due to their irregular behavior at the cell membrane, i.e. dissociation of the activated $G\alpha_s$ protein from the membrane (see decreasing BRET ratios upon $G\alpha_s$ activation in ebBRET assays).

Additionally, this assay offers the possibility to investigate the influence of individual Gβγ subunits on Gα protein activation when transfecting different individual Gβ- or Gγ-RLucII subunits, which has not been investigated so far.

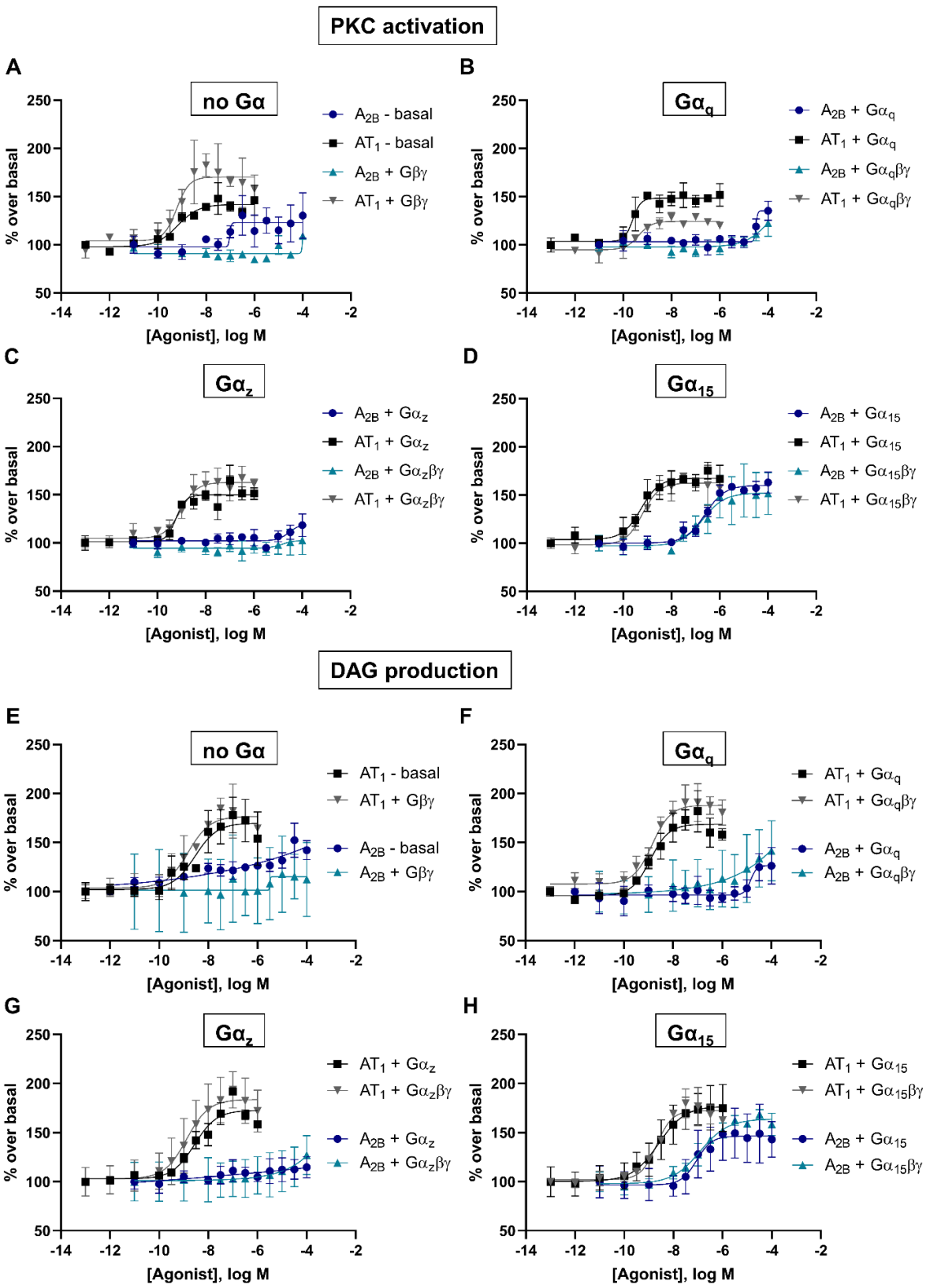

Figure 20. Normalized (% over basal) BRET ratio shifts of the angiotensin II-activated AT_1R and the adenosine-activated $A_{2B}AR$ in PKC activation (**A-D**) and DAG production (**E-G**) assays. Curves were recorded either in absence of heterologously expressed Gα subunits (**A,E**), or in presence the of the $G\alpha_q$ (**B, F**), $G\alpha_z$ (**C, G**), or $G\alpha_{15}$ proteins (**D, H**) and in the presence or absence of additional $G\beta_1\gamma_1$ subunits. Data points were obtained from three individual experiments performed in duplicate.

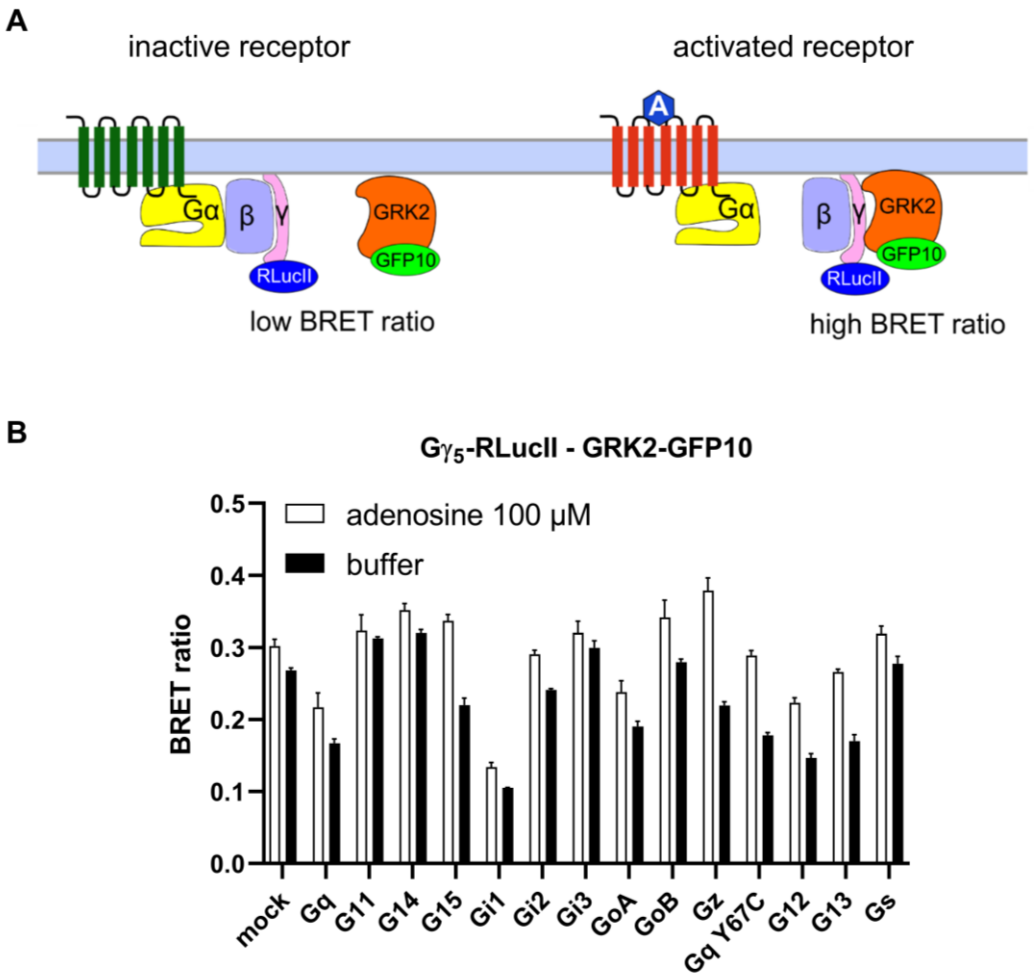

Figure 21: GRK-Gγ co-localization assays. **A**. Visualization of the GRK-G co-localization assay principle. **B**. BRET ratios of the adenosine-activated (white) or non-stimulated (black) $A_{2B}AR$ to Gα proteins measured in the Gγ5-RLucII–GRK2-GFP10 co-localization BRET assay. Shown data points are preliminary obtained in one experiment performed in triplicate.

Findings obtained in the laboratory of Prof. Bouvier confirm the promiscuity of the adenosine-activated $A_{2B}AR$, which can activate a broad range of Gα proteins with varying degrees of efficacy. Additionally, we observed that certain Gα protein subunits, such as the $G\alpha_{12}$, $G\alpha_{13}$, and $G\alpha_{o}$ proteins, require high expression levels for an efficacious activation by the adenosine-activated $A_{2B}AR$. Gα protein subunits such as the $G\alpha_{15}$, $G\alpha_{s}$, and $G\alpha_{z}$ proteins, which were efficaciously activated by the $A_{2B}AR$ under default assay conditions, only required very low Gα protein cDNA amounts for transfection in order to be activated by the $A_{2B}AR$ in an efficacious manner. Subunits such as $G\alpha_{q}$ and $G\alpha_{i1\text{-}3}$ proteins are activated with low efficacy, even at high Gα protein concentrations (see **Figure 18** and **Figure 19**).

Assays detecting PKC activation and DAG production demonstrate that the $G\alpha_{15}$ protein is the preferred $A_{2B}AR$ effector from the $G\alpha_{q/11}$ protein family. In calcium assays, we previously observed weak activation of the $G\alpha_q$ protein as well (see section 13.3), which did not result in a signal in the present study. Only heterologous expression of the $G\alpha_{15}$ subunit resulted in a strong PKC/DAG response upon $A_{2B}AR$ activation. This highlights a putative key role of the $G\alpha_{15}$ protein for the signal transduction of the $A_{2B}AR$ in the hematopoietic system, where the $G\alpha_{15}$ protein is exclusively expressed [172].

8.2 Methods

Mixture of cDNA for transfection. Each BRET requires a certain combination of cDNA plasmids for transfection; the following cDNA amounts were used for the transfection of 1 ml cell suspension at a cell density of $3.5*10^5$ cells per ml. For ebBRET assays monitoring $G\alpha_s$ protein activation: 200 ng receptor, 10 ng $G\alpha_s$67-RLucII, 100 ng $G\beta_1$, 100 ng $G\gamma_1$, 500 ng rGFP-CAAX. ebBRET assays monitoring β-arrestin recruitment: 200 ng receptor, 5 ng β-arr1/2-RLucII, 100 ng GRK2, 500 ng rGFP-CAAX. EMTA assays for $G\alpha_{q/11/14}$: 200 ng receptor, 64 ng $G\alpha_{q/11/14}$, 10 ng p63-RLucII, 500 ng rGFP-CAAX. EMTA assays for $G\alpha_{15}$: 200 ng receptor, 16 ng $G\alpha_{15}$, 10 ng p63-RLucII, 500 ng rGFP-CAAX. EMTA assays for $G\alpha_{12/13}$ proteins with p115 biosensor: 200 ng receptor (100 ng in case of TPα receptor), 40 ng $G\alpha_{12/13}$, 25 ng p115-RLucII, 500 ng rGFP-CAAX. EMTA assays for $G\alpha_{12/13}$ proteins with PDZ biosensor: 200 ng receptor (100 ng in case of TPα receptor), 40 ng $G\alpha_{12/13}$, 10 ng PDZ-RLucII, 500 ng rGFP-CAAX. EMTA assays for $G\alpha_{i/o}$ proteins with the exception of $G\alpha_z$: 200 ng receptor, 20 ng $G\alpha_{i/o}$, 5 ng Rap1GAP-RLucII, 500 ng rGFP-CAAX. EMTA assays for $G\alpha_z$ proteins: 200 ng receptor, 10 ng $G\alpha_z$, 10 ng Rap1GAP-RLucII, 500 ng rGFP-CAAX. PKC activation assays: 200 ng receptor, 20 ng PKC biosensor; with or without the indicated Gα, Gβ, and Gγ subunits (100 ng per 3.5×10^5 cells each). DAG production assays: 200 ng receptor, 20 ng cbI-RLucII, 500 ng rGFP-CAAX; with or without each 100 ng of the indicated Gα, Gβ, and Gγ subunits. GRK-Gγ co-localization assays: 250 ng receptor, 100 ng $G\beta_1$, 100 ng Gα, 20 ng $G\gamma_5$-RLucII, 600 ng GRK2-GFP10. DNA concentrations were adjusted to 1 µg/ml with salmon sperm DNA and diluted to 50 µl with phosphate-buffered saline (PBS).

Transfection of cells. All BRET assays were performed in a similar manner, which differed mostly in the plasmids used for transfection. HEK293 cells are seeded and transfected 48h before measurement. For transfection, a mixture of plasmids is prepared at a DNA concentration of 1 µg per 50 µl in PBS for 1 ml of cell solution. The DNA mixture is incubated in a 1:1 volume ratio of a 60 µg/ml polyethylenimine (PEI) solution, dissolved in PBS, for 30 min before addition of the cells to the mixture. HEK293 cells were washed with PBS twice and detached by brief incubation with a trypsin-EDTA solution. Cell density was adjusted to $3.5*10^5$ cells per ml, diluted in Dulbecco's

modified eagle medium (DMEM) + 10% newborn calf serum (NCS) + penicillin (100 U/ml) and streptomycin (0.1 mg/ml). Afterwards, cells were mixed with the DNA-PEI mixture and directly transferred to 96-well white-bottom plates (100 µl per well, respectively 35,000 cells).

BRET assays. Cell culture medium was aspired from 96-well plates and cells were washed briefly with PBS before adding 80 µl of Tyrode assay buffer (137 mM NaCl, 0.9 mM KCl, 1 mM $MgCl_2$, 11.9 mM $NaHCO_3$, 3.6 mM NaH_2PO_4, 25 mM HEPES, 5.5. mM glucose, 1 mM $CaCl_2$, pH adjusted to 7.4 with NaOH). Plates were incubated at 37°C for 15 min before addition of 10 µl of agonist solution. Following a 5 min incubation period, luciferase substrate (10 µl; final concentrations: 1 µM in case of Prolume Purple or 5 µM in case of Deep Blue C (both from NanoLight Technologies; Pinetop, AZ, USA)) was added and incubated for 5 min before measurement with a Spark® plate reader (TECAN, Männedorf, Switzerland) at 37°C. Luminescence was measured at 395 nm and fluorescence was measured at 510 nm. When detecting DAG production, substrate was added first; agonist was added after 5 min and the plate was measured instantly as DAG production is transient.

9. Summary

This thesis presents research results from two related projects, focusing on signal transduction via G protein-coupled receptors (GPCR) and heterotrimeric guanine nucleotide-binding proteins (G proteins). The first research objective deals with the inhibition mechanism of macrocyclic $G\alpha_{q/11}$ protein inhibitors, and the second research project focuses on the G protein coupling of the adenosine A_{2B} receptor ($A_{2B}AR$). This section contains a detailed summary and discussion of obtained data and provides an outlook towards future experiments.

9.1. Studies on binding mechanism and binding kinetics of macrocyclic $G\alpha_{q/11}$ protein inhibitors

As part of the Deutsche Forschungsgemeinschaft (DFG)-funded research unit FOR2372, a part of the work presented in this thesis focused on the elucidation of the binding mechanism of macrocyclic $G\alpha_{q/11}$ protein inhibitors and sought to provide a rationale for the distinct binding kinetics of YM25480 (YM)- and FR900359 (FR)-derived radioligands in a combined mutagenesis and computational study (section 4). Competition-association experiments were employed to quantify the residence times of derivatives and analogs of YM and FR (section 5). The radioligands were further employed to image the $G\alpha_{q/11}$ protein distribution in mouse organs, including acute asthmatic lung tissue, via autoradiography experiments (section 6). Additionally, we published a review article, containing a detailed overview of small molecules and peptides interacting with Gα proteins and a perspective on pharmacological mechanisms of Gα protein modulation (section 3).

Radiolabeled derivatives of YM ([^{3}H]PSB-16254-YM) and FR ([^{3}H]PSB-15900-FR) had previously been obtained by catalytic tritiation and a radioligand binding assay had been established [151]. Both radioligands (see **Figure 22 A** for molecular structures) selectively bound to $G\alpha_{q/11}$ proteins with nanomolar affinities [151]. In kinetic binding experiments, however, we found that the FR-derived radioligand [^{3}H]PSB-15900-FR displayed an approx. 20-fold longer dissociation half-life compared to the [^{3}H]PSB-16254-YM ($t_{1/2}$ [^{3}H]PSB-15900-FR FR = 92 min, $t_{1/2}$ [^{3}H]PSB-16254-YM = 3.8 min; determined at human platelet membrane preparations, 37° C), despite their similar association rate and near-identical affinities determined in saturation binding assays (**Figure 22 B,C**) [151]. This finding was unexpected due to the nearly identical structures of [^{3}H]PSB-15900-FR and [^{3}H]PSB-16254-YM. [^{3}H]PSB-15900-FR contains two larger lipophilic groups as compared to [^{3}H]PSB-16254-YM, which we termed "anchor 1" (ethyl residue in FR and its derived radioligand, methyl residue in YM and its derived radioligand) and "anchor 2" (isopropyl side chain in FR and its derived radioligand, methyl group in YM and its derived radioligand, see **Figure 22 A**).

The identification of residue-ligand interactions that contribute to the long-lasting interaction between the $G\alpha_q$ protein and [^{3}H]PSB-15900-FR is important to delineate the molecular mechanism behind the long residence time. Therefore, we conducted a mutagenesis study of the $G\alpha_q$ protein inhibitor binding pocket around the interaction sites of FR's anchors 1 and 2. Mutations were selected based on the co-crystal structure of the $G\alpha_{i/q}\beta_1\gamma_2$ protein in complex with YM and GDP [132], and the docked pose of FR in the respective protein complex. The selected mutations were introduced to the mouse *Gnaq* gene (identical to the human *GNAQ* gene except for an A171S amino acid exchange from human to mouse) by site-directed mutagenesis; the mutant *Gnaq* genes were cloned into retroviral expression vectors, and stably transfected into HEK293 cells, which were depleted of *GNAQ/GNA11* genes by CRISPR-Cas9 gene editing (HEK293 $\Delta G\alpha_{q/11}$). Membrane preparations of recombinant HEK293 cells were obtained, and $G\alpha_q$ protein expression was confirmed by Western blotting. The binding affinity and inhibitory potency of YM and FR at mutant $G\alpha_q$ proteins was determined by radioligand binding assays and calcium mobilization assays, respectively. Mutations of key residues, e.g. F75K and I190F/W, abolished high-affinity binding of the radioligand and were accompanied by a significant reduction of the inhibitory potency of YM and FR as observed in calcium mobilization assays. Nonetheless, most $G\alpha_q$ mutants displayed high-affinity binding of both radioligands and a virtually identical binding affinity for YM (determined by pseudo-homologous competition binding experiments between YM and [^{3}H]PSB-16254-YM). The inhibitory potency of YM and FR was similar between most of the mutant $G\alpha_q$ proteins and the wt $G\alpha_q$ protein in calcium mobilization assays.

In kinetic experiments, we determined similar association rates of both radioligands at most mutant $G\alpha_q$ proteins compared to the wt $G\alpha_q$ protein, however, all mutations significantly accelerated the dissociation of the radioligands from the $G\alpha_q$ protein. The residence time of the slowly dissociating [^{3}H]PSB-15900-FR was shortened by up to a 100-fold compared to the wt $G\alpha_q$ protein. Results from kinetic studies are displayed in **Figure 22 D,E**. In summary, we found that the hydrophobic environment around the anchors 1 and 2 was crucial for the long residence time of [^{3}H]PSB-15900-FR; even mutations at the fringe regions of the binding site significantly accelerated radioligand dissociation.

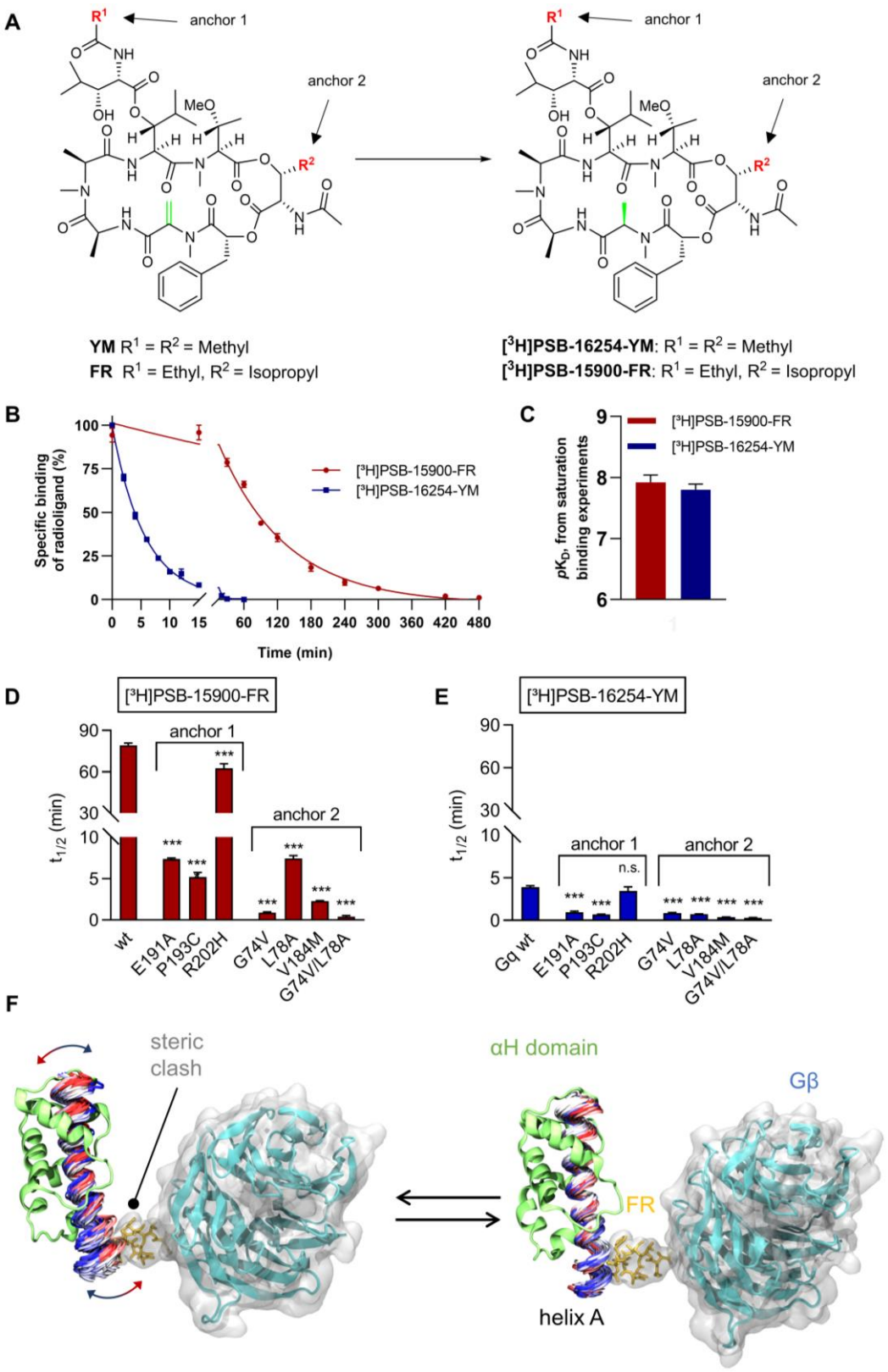

Figure 22: Elucidating the binding mechanism of macrocyclic $G\alpha_{q/11}$ protein inhibitors. **A**. Structure of YM, FR, and the derived radiotracers [^{3}H]PSB-16254-YM and [^{3}H]PSB-15900-FR. **B**. Dissociation kinetics of both radioligands determined at 37°C. **C**. Affinity values obtained from saturation binding experiments (3h incubation at 37°C). **D**, **E**. Dissociation half-lives of (**D**) [^{3}H]PSB-15900-FR and (**E**) [^{3}H]PSB-16254-YM from wt and mutant $G\alpha_q$ proteins. **F**. Schematic depiction of the mechanism explaining the conformational selection (movement of the helix A in the αH domain) as suggested by molecular dynamics simulations.

As mentioned above, binding affinity and inhibitory potency of the macrocyclic $G\alpha_{q/11}$ protein inhibitors were not significantly affected by the introduced mutations. However, an accelerated dissociation rate combined with an unaltered association rate should in theory result in a decreased binding affinity under the assumption of a one-step "key and lock" binding model. Therefore, we closely investigated the binding mode of both radioligands and detected an exponential decay of the observed association rate, k_{obs}, with increasing radioligand concentrations. This finding strongly indicating inhibitor binding via a conformational selection mechanism and was supported by molecular dynamics simulations, which suggested that a conformational change in the $G\alpha_q$ αA helix may precede inhibitor binding (see **Figure 22 F**).

To complement the mutagenesis study, we characterized the binding kinetics of available YM and FR analogues – either obtained by total synthesis [131, 153] or isolated from the plant *Ardisia crenata* or from recombinant bacterial culture [127, 156] – to establish a structure-kinetics relationship of macrocyclic $G\alpha_{q/11}$ protein inhibitors. To this end, we established a radioligand competition-association binding assay by the method of Motulsky & Mahan [158], which had previously been used to characterize the binding kinetics of non-radiolabeled ligands for various target proteins [160, 198–200]. The structure-kinetics relationship clearly showed that the isopropyl group of FR and its derivatives ("anchor 2") is essential for a long residence time at the $G\alpha_q$ protein. Importantly, YM and FR displayed a significantly longer residence time than their respective hydrogenated analogues employed as radioligands (residence time FR = 466 min, [^{3}H]PSB-15900-FR = 131 min , YM = 57 min, [^{3}H]PSB-16254-YM = 6 min). Several other minor structural changes to the original YM and FR molecules resulted in a significant reduction of affinity and residence time. Modifications were best-tolerated in the two alanine residues, which are part of the macrocyclic core. The substituents of these residues are predicted to point towards the aqueous phase and do not participate in the complex interaction between the inhibitors and the $G\alpha_q$ protein.

In another series of experiments, both the YM- and FR-derived radioligands were employed for autoradiography studies of mouse tissues (section 6). In this study, we aimed to quantify the expression levels and image the distribution of $G\alpha_{q/11}$ proteins in healthy and diseased tissues. The expression level of $G\alpha_{q/11}$ proteins is ranked in the order kidney > liver > brain > pancreas > lung > spleen >> heart in cryosections of healthy CD1 mice. In brain slices, we additionally observed a sharp contrast between different brain regions, showing the region-specific expression of $G\alpha_{q/11}$ proteins. Both radioligands displayed virtually identical binding patterns and only very low non-specific binding to the tissues. Comparison of $G\alpha_{q/11}$ protein expression between lung slices of healthy mice and mice with induced *asthma bronchiale*, showed no difference in radioligand binding. It is therefore concluded that the acute asthma does not involve $G\alpha_{q/11}$ overexpression, but rather receptor-mediated $G\alpha_{q/11}$ hyperactivation. Because of the low

background signal of both radioligands, the sharp contrasts between areas of high and low $G\alpha_{q/11}$ protein expression, the long residence time of FR, and its high affinity, future development of a diagnostic, [^{18}F]-labeled FR-derivative is promising to detect diseases with altered $G\alpha_{q/11}$ protein expression. In the near future, we will analyze human tumor samples, e.g. from melanoma, lung, liver, breast, and colorectal cancer, and compare the $G\alpha_{q/11}$ protein expression with that of healthy tissues.

In summary, the work performed within this thesis has greatly improved the understanding of the molecular binding mechanism of macrocyclic $G\alpha_{q/11}$ protein inhibitors. The complex pharmacophore of these compounds is of great interest due to the scarcity of potent and selective Gα protein inhibitors [4]. Since minor modifications of the compounds result in major reduction in affinity, we consider it challenging to develop potent and selective Gα protein inhibitors based on the FR/YM-scaffold for different Gα protein subtypes. Macrocyclic $G\alpha_{q/11}$ protein inhibitors have been investigated for the treatment of complex diseases, e.g. *asthma bronchiale*, pain, and hypertension, delivering promising results [136, 140, 146]. Further research by our group demonstrated that FR accumulates in the lung and leads to long-lasting airway relaxation [141]. Targeted drug delivery to the bronchi may reduce systemic side effects in the future [141, 142]. In autoradiography studies, the radiolabeled derivatives displayed nearly undetectable non-specific binding, which is in agreement with another study that ruled out off-target effects of FR [133]. Moreover, our work provides a molecular basis for future (semi-)synthetic or biotechnological modifications of $G\alpha_{q/11}$ inhibitors; especially the derivative FR-1 appears to be a promising starting point for conjugate reactions due to its solvent-exposed free hydroxyl group.

9.2. Gα protein activation profile of the adenosine A_{2B} receptor

The second part of this thesis describes a detailed investigation of the A_{2B}AR's Gα protein coupling, focusing on the following research questions:

- Which Gα protein subunits can be activated by the A_{2B}AR?
- Do structurally diverse A_{2B}AR agonists activate distinct Gα proteins with different potencies and efficacies?
- What role do A_{2B}AR agonist potency and receptor efficacy at distinct Gα proteins play for second messenger formation on a cellular level?
- How dependent is the observed coupling and signaling on receptor and/or Gα protein expression?

The A_{2B}AR is of great interest as a drug target in immuno-oncology . It is overexpressed on immune cells and on many cancer cells, where it mediates immunosuppression, increased cancer cell proliferation, angiogenesis, and metastasis [201, 202]. The receptor has been known to activate $G\alpha_s$ and $G\alpha_{q/11}$ family proteins depending on the cellular background [49, 188]; single reports of $G\alpha_{i/o}$ protein activation have been published as well [189, 190]. However, the exact Gα protein subtypes involved in A_{2B}AR signaling had remained unknown. Recently, assay techniques have become available to study activation of most of the 16 Gα protein subunits separately [8, 43, 87, 203]. One of these assays, the TRUPATH assay [87], employs renilla luciferase 8-tagged Gα subunits (Gα-RLuc8) and green fluorescent protein 2-tagged Gγ subunits (Gγ-GFP2). The Gα-RLuc8 protein dissociates from the GFP2-tagged Gβγ dimer upon GPCR activation, resulting in a decreasing BRET ratio.

In our study, we stimulated the A_{2B}AR with three structurally diverse agonists (adenosine, the metabolically more stable 5'-*N*-ethylcarboxamidoadenosine (NECA), and the non-nucleosidic partial agonist BAY-60-6583) and measured (i) calcium mobilization in CRISPR-Cas9-edited HEK293 cells selectively overexpressing members of the $G\alpha_{q/11}$ protein family, and (ii) direct G protein activation with the TRUPATH assay (see section 7) [87].

Adenosine and NECA efficaciously led to calcium mobilization via the $G\alpha_q$ and $G\alpha_{15}$ proteins, being more potent at the HEK-$G\alpha_{15}$ cells. Both compounds failed to fully activate the $G\alpha_{11}$ and $G\alpha_{14}$ proteins at concentrations of up to 100 µM. We conclude that the A_{2B}AR preferentially induces calcium mobilization via $G\alpha_{15}$ proteins, and it can also signal via the ubiquitously expressed $G\alpha_q$ protein. When overexpressing the A_{2B}AR in HEK-$G\alpha_{15}$ cells, the efficacy and potency of adenosine and NECA increased depending on the receptor expression level. At high receptor expression levels, BAY 60-6583 displayed typical partial agonistic behavior, while it failed to induce a calcium signal in HEK cells with native A_{2B}AR expression levels.

In TRUPATH BRET^2 assays, the A_{2B}AR was observed to be a highly promiscuous receptor. The endogenous agonist adenosine activated all investigated Gα proteins ($G\alpha_s$, $G\alpha_q$, $G\alpha_{11}$, $G\alpha_{15}$, $G\alpha_{i1}$, $G\alpha_{i2}$, $G\alpha_{i3}$, $G\alpha_{oA}$, $G\alpha_{oB}$; $G\alpha_z$, $G\alpha_{12}$, $G\alpha_{13}$) with similar potency, with exception of the sensory $G\alpha_{gust}$ subunit, which was not activated by the A_{2B}AR. The structurally related agonist NECA could activate all Gα proteins as well, but displayed a higher potency at the $G\alpha_s$, $G\alpha_{15}$, and $G\alpha_{i1\text{-}3}$ proteins. The partial agonist BAY 60-6583 exclusively activated $G\alpha_s$, $G\alpha_{15}$, and $G\alpha_{12}$ protein subunits with high potency and displayed no Gα protein activation at the other subunits.

To determine efficacies, we compared the observed efficacy of an agonist-A_{2B}AR-Gα protein combination with the maximum efficacy observed for a prototypical agonist/receptor combination at each Gα subunit [87] and normalized our data accordingly. The adenosine-activated A_{2B}AR most efficaciously activated $G\alpha_s$, $G\alpha_{15}$, and $G\alpha_{12}$ proteins and activated all other Gα protein subunits with lower efficacies. Consistently, $G\alpha_s$, $G\alpha_{15}$, and $G\alpha_{12}$ were the only Gα protein subunits activated by the partial agonist BAY 60-6583. BAY60-6583 activated the $G\alpha_{15}$ protein with and efficacy higher than that of adenosine and NECA, but displayed a very low efficacy at the $G\alpha_s$ and $G\alpha_{12}$ proteins. Efficacies of the NECA-activated A_{2B}AR were mostly similar to the adenosine-activated A_{2B}AR, with two exceptions: the $G\alpha_{i2}$ subunit was activated with a high efficacy by NECA, but not by adenosine, while the $G\alpha_s$ protein was activated with lower efficacy by NECA as compared to adenosine. At other Gα proteins, the adenosine/NECA-activated A_{2B}AR induced Gα protein activation with submaximal efficacy (less than 50% efficacy compared to the respective control receptor). Potency and affinity data from calcium mobilization assays and TRUPATH BRET^2 assays are summarized in **Figure 23**.

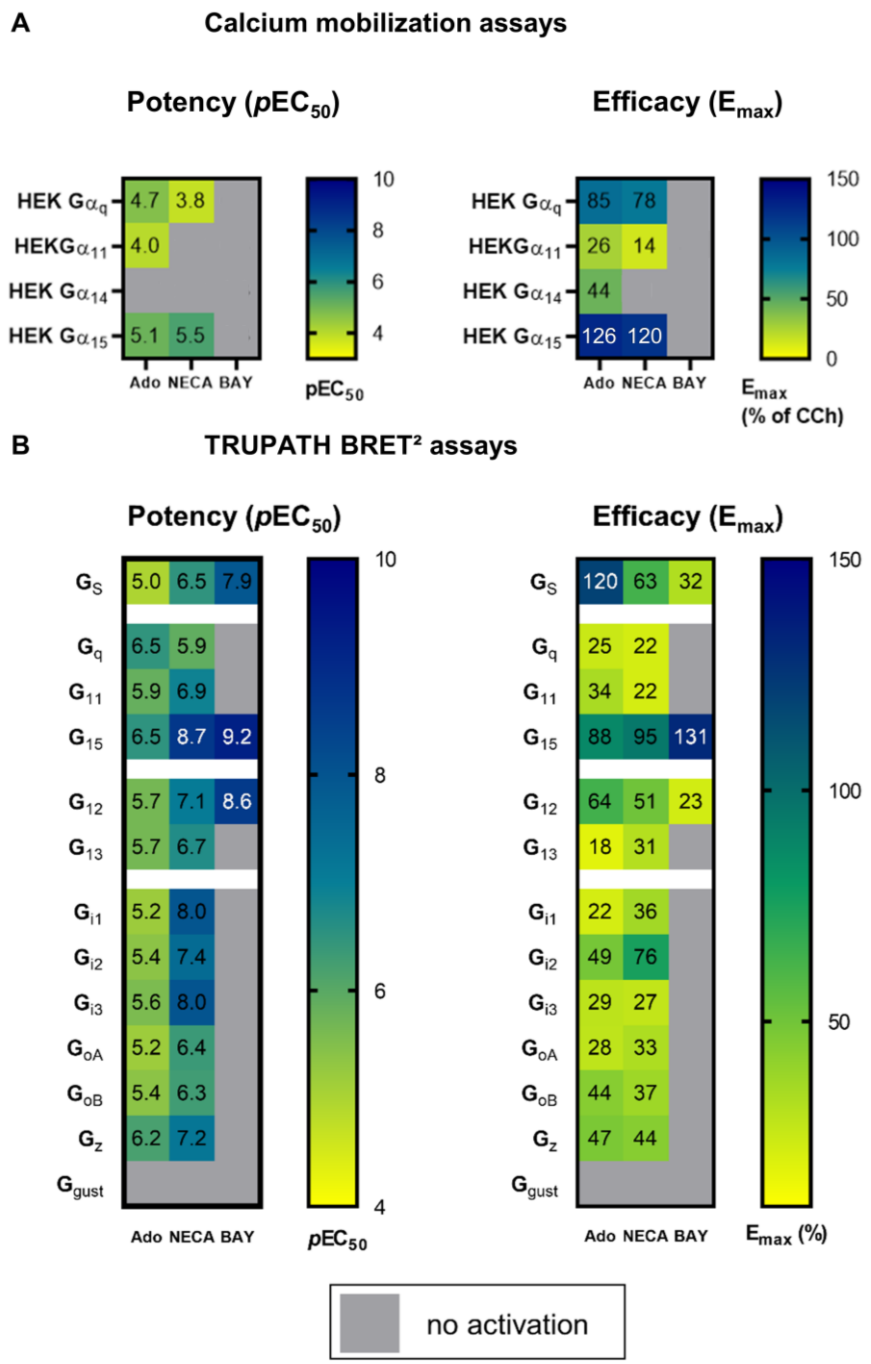

Figure 23: Heatmaps of (**A**) calcium mobilization assays and (**B**) TRUPATH BRET^2 assays, displaying potency (pEC_{50}) and efficacy (E_{max}, % of maximum control receptor activation; calcium assays: carbachol-activated muscarinic M_3 receptor in all calcium assays; TRUPATH assays: $G\alpha_s$ protein, isoprotenerol-activated β_2 adrenoceptor; $G\alpha_{i/o}$ family, DAMGO-activated μ-opioid receptor; $G\alpha_{q/11}$ and $G\alpha_{12/13}$ families, neurotensin-activated neurotensin 1 receptor) of the agonist-activated $A_{2B}AR$ at diverse Gα protein subunits.

Our data suggest that each agonist stabilizes a distinct receptor certain conformation, which displays different Gα activation patterns. The agonist concentration required for the effective activation of distinct Gα protein subunits can vary, e.g. NECA activates the $G\alpha_{15}$ protein more potently than the $G\alpha_q$ protein. Most importantly, the agonist-activated $A_{2B}AR$ only activates a subset of Gα proteins with high efficacy ($G\alpha_s$, $G\alpha_{15}$, $G\alpha_{12}$) and acts analogously to a weak partial

agonist at other Gα subunits. This provides an explanation for the observation that A_{2B}AR activation results in a $G\alpha_s$-mediated cAMP increase and only a weak $G\alpha_{q/11}$-mediated calcium signal in many cells ($G\alpha_{15}$ is barely expressed outside of the hematopoietic system [172, 173]), and e.g. not in a $G\alpha_{i/o}$-mediated cAMP decrease, despite the promiscuous coupling behavior of the receptor. Possible interactions between receptor and Gα protein, which do not result in the dissociation of the G protein heterotrimer, can, however, not be detected by the TRUPATH $BRET^2$ assay.

Further experiments with various novel BRET assay probes (section 8) indicated that not only the expression levels of the receptor, but also of the expression level of the Gα proteins determine, which Gα proteins are activated by the A_{2B}AR: Under most conditions, the adenosine-activated A_{2B}AR exclusively activates $G\alpha_s$, $G\alpha_{15}$, and $G\alpha_z$ proteins. Only when the Gα protein expression was increased, coupling to $G\alpha_{12/13}$ and $G\alpha_{i/o}$ proteins was observed. This finding was confirmed by GRK2-Gγ co-localization assays, in which A_{2B}AR coupling to $G\alpha_{12/13}$, $G\alpha_{15}$, $G\alpha_{oA/B}$, and $G\alpha_z$ proteins was observed at high Gα protein expression levels. As high levels of both receptor and Gα expression were required in this case, the affinity of the adenosine-activated A_{2B}AR to these subunits may be low, despite efficacious recruitment of RLucII-tagged effector proteins to the cell membrane in our experiments.

Monitoring of PKC activation and DAG production revealed that endogenous G protein levels in HEK293 cells are not sufficient for detectable $G\alpha_{q/11}$ signaling. Overexpression of the $G\alpha_{15}$ protein, but not of the $G\alpha_q$ protein, led to PKC activation and DAG production in these experiments, further emphasizing the strong coupling of the A_{2B}AR to $G\alpha_{15}$ proteins; $G\alpha_q$ proteins, on the other hand, appear to be moderate signal transducers for the A_{2B}AR.

In summary, the A_{2B}AR is a promiscuous receptor, which can couple to Gα protein subunits of all Gα protein families. Whether effective coupling occurs, is dictated both by the employed agonist and by the expression levels of both receptor and Gα protein. A systemic evaluation of A_{2B}AR-mediated Gα activation across several assay systems with multiple, clearly defined expression levels of the receptor and of Gα proteins will be useful to identify and characterize all variables of the interactions between the A_{2B}AR and Gα proteins. It is of great interest to investigate how the A_{2B}AR transmits its signals *in vivo* in health and disease, however, there is currently no selective full A_{2B}AR agonist available, which mimics adenosine actions, hindering a better understanding of the A_{2B}AR's (patho)physiological effects. The activation of the $G\alpha_{15}$ protein, an effective transmitter of A_{2B}AR signaling by adenosine, deserves special attention in an immuno-oncological context according to our data and warrants future studies.

10. References

1. Fredriksson, R.; Lagerström, M. C.; Lundin, L.-G.; Schiöth, H. B. The G-protein-coupled receptors in the human genome form five main families. Phylogenetic analysis, paralogon groups, and fingerprints. *Mol. Pharmacol.* **2003**, 63 (6), 1256–1272. DOI: 10.1124/mol.63.6.1256.

2. Tang, X.; Wang, Y.; Li, D.; Luo, J.; Liu, M. Orphan G protein-coupled receptors (GPCRs): biological functions and potential drug targets. *Acta Pharmacol. Sin.* **2012**, 33 (3), 363–371. DOI: 10.1038/aps.2011.210.

3. Garland, S. L. Are GPCRs still a source of new targets? *J. Biomol. Screen.* **2013**, 18 (9), 947–966. DOI: 10.1177/1087057113498418.

4. Voss, J. H.; Müller, C. E. Heterotrimeric G protein α subunits - structures, peptide-derived inhibitors, and mechanisms. *Curr. Med. Chem.* **2022**, Epub ahead of print. DOI: 10.2174/0929867329666220308112424.

5. Stevens, R. C.; Cherezov, V.; Katritch, V.; Abagyan, R.; Kuhn, P.; Rosen, H.; Wüthrich, K. The GPCR Network: A large-scale collaboration to determine human GPCR structure and function. *Nat. Rev. Drug Discov.* **2013**, 12 (1), 25–34. DOI: 10.1038/nrd3859.

6. Young, J. M.; Trask, B. J. The sense of smell: genomics of vertebrate odorant receptors. *Hum. Mol. Genet.* **2002**, 11 (10), 1153–1160. DOI: 10.1093/hmg/11.10.1153.

7. Chen, X.; Wang, L.; Cui, Q.; Ding, Z.; Han, L.; Kou, Y.; Zhang, W.; Wang, H.; Jia, X.; Dai, M.; Shi, Z.; Li, Y.; Li, X.; Geng, Y. Structural insights into the activation of human calcium-sensing receptor. *eLife* **2021**, 10. DOI: 10.7554/eLife.68578.

8. Inoue, A.; Raimondi, F.; Kadji, F. M. N.; Singh, G.; Kishi, T.; Uwamizu, A.; Ono, Y.; Shinjo, Y.; Ishida, S.; Arang, N.; Kawakami, K.; Gutkind, J. S.; Aoki, J.; Russell, R. B. Illuminating G protein-coupling selectivity of GPCRs. *Cell* **2019**, 177 (7), 1933-1947.e25. DOI: 10.1016/j.cell.2019.04.044.

9. Ballesteros, J. A.; Weinstein, H. [19] Integrated methods for the construction of three-dimensional models and computational probing of structure-function relations in G protein-coupled receptors. *In Methods in Neurosciences: Receptor Molecular Biology*; Sealfon, S. C., Ed.; Academic Press, **1995**, pp 366–428. DOI: 10.1016/S1043-9471(05)80049-7.

10. Katritch, V.; Cherezov, V.; Stevens, R. C. Structure-function of the G protein-coupled receptor superfamily. *Annu. Rev. Pharmacol. Toxicol.* **2013**, 53, 531–556. DOI: 10.1146/annurev-pharmtox-032112-135923.

11. Rasmussen, S. G. F.; DeVree, B. T.; Zou, Y.; Kruse, A. C.; Chung, K. Y.; Kobilka, T. S.; Thian, F. S.; Chae, P. S.; Pardon, E.; Calinski, D.; Mathiesen, J. M.; Shah, S. T. A.; Lyons, J. A.; Caffrey, M.; Gellman, S. H.; Steyaert, J.; Skiniotis, G.; Weis, W. I.; Sunahara, R. K.; Kobilka, B. K. Crystal structure of the β_2 adrenergic receptor-G_s protein complex. *Nature* **2011**, 477 (7366), 549–555. DOI: 10.1038/nature10361.

12. Rosenbaum, D. M.; Cherezov, V.; Hanson, M. A.; Rasmussen, S. G. F.; Thian, F. S.; Kobilka, T. S.; Choi, H.-J.; Yao, X.-J.; Weis, W. I.; Stevens, R. C.; Kobilka, B. K. GPCR engineering yields high-resolution structural insights into β_2-adrenergic receptor function. *Science* **2007**, 318 (5854), 1266–1273. DOI: 10.1126/science.1150609.

13. García-Nafría, J.; Tate, C. G. Structure determination of GPCRs: cryo-EM compared with X-ray crystallography. *Biochem. Soc. Trans.* **2021**, 49 (5), 2345–2355. DOI: 10.1042/BST20210431.

14. García-Nafría, J.; Tate, C. G. Cryo-EM structures of GPCRs coupled to G_s, G_i and G_o. *Mol. Cell. Endocrinol.* **2019**, 488, 1–13. DOI: 10.1016/j.mce.2019.02.006.

15. Hilger, D. The role of structural dynamics in GPCR-mediated signaling. *FEBS J.* **2021**, 288 (8), 2461–2489. DOI: 10.1111/febs.15841.

16. Kooistra, A. J.; Mordalski, S.; Pándy-Szekeres, G.; Esguerra, M.; Mamyrbekov, A.; Munk, C.; Keserű, G. M.; Gloriam, D. E. GPCRdb in 2021: integrating GPCR sequence, structure and function. *Nucleic Acids Res.* **2021**, 49 (D1), D335-D343. DOI: 10.1093/nar/gkaa1080.

17. Pándy-Szekeres, G.; Esguerra, M.; Hauser, A. S.; Caroli, J.; Munk, C.; Pilger, S.; Keserű, G. M.; Kooistra, A. J.; Gloriam, D. E. The G protein database, GproteinDb. *Nucleic Acids Res.* **2022**, 50 (D1), D518-D525. DOI: 10.1093/nar/gkab852.

18. Katritch, V.; Cherezov, V.; Stevens, R. C. Diversity and modularity of G protein-coupled receptor structures. *Trends Pharmacol. Sci.* **2012**, 33 (1), 17–27. DOI: 10.1016/j.tips.2011.09.003.

19. Cherezov, V.; Rosenbaum, D. M.; Hanson, M. A.; Rasmussen, S. G. F.; Thian, F. S.; Kobilka, T. S.; Choi, H.-J.; Kuhn, P.; Weis, W. I.; Kobilka, B. K.; Stevens, R. C. High-resolution crystal structure of an engineered human β_2-adrenergic G protein-coupled receptor. *Science* **2007**, 318 (5854), 1258–1265. DOI: 10.1126/science.1150577.

20. Liu, W.; Chun, E.; Thompson, A. A.; Chubukov, P.; Xu, F.; Katritch, V.; Han, G. W.; Roth, C. B.; Heitman, L. H.; IJzerman, A. P.; Cherezov, V.; Stevens, R. C. Structural basis for allosteric regulation of GPCRs by sodium ions. *Science* **2012**, 337 (6091), 232–236. DOI: 10.1126/science.1219218.

21. Wu, B.; Chien, E. Y. T.; Mol, C. D.; Fenalti, G.; Liu, W.; Katritch, V.; Abagyan, R.; Brooun, A.; Wells, P.; Bi, F. C.; Hamel, D. J.; Kuhn, P.; Handel, T. M.; Cherezov, V.; Stevens, R. C. Structures of the CXCR4 chemokine GPCR with small-molecule and cyclic peptide antagonists. *Science* **2010**, 330 (6007), 1066–1071. DOI: 10.1126/science.1194396.

22. Warne, T.; Serrano-Vega, M. J.; Baker, J. G.; Moukhametzianov, R.; Edwards, P. C.; Henderson, R.; Leslie, A. G. W.; Tate, C. G.; Schertler, G. F. X. Structure of a β_1-adrenergic G-protein-coupled receptor. *Nature* **2008**, 454 (7203), 486–491. DOI: 10.1038/nature07101.

23. Zhou, Q.; Yang, D.; Wu, M.; Guo, Y.; Guo, W.; Zhong, L.; Cai, X.; Dai, A.; Jang, W.; Shakhnovich, E. I.; Liu, Z.-J.; Stevens, R. C.; Lambert, N. A.; Babu, M. M.; Wang, M.-W.; Zhao, S. Common activation mechanism of class A GPCRs. *eLife* **2019**, 8. DOI: 10.7554/eLife.50279.

24. García-Nafría, J.; Lee, Y.; Bai, X.; Carpenter, B.; Tate, C. G. Cryo-EM structure of the adenosine A_{2A} receptor coupled to an engineered heterotrimeric G protein. *eLife* **2018**, 7. DOI: 10.7554/eLife.35946.

25. Lebon, G.; Warne, T.; Edwards, P. C.; Bennett, K.; Langmead, C. J.; Leslie, A. G. W.; Tate, C. G. Agonist-bound adenosine A_{2A} receptor structures reveal common features of GPCR activation. *Nature* **2011**, 474 (7352), 521–525. DOI: 10.1038/nature10136.

26. Filipek, S. Molecular switches in GPCRs. *Curr. Opin. Struct. Biol.* **2019**, 55, 114–120. DOI: 10.1016/j.sbi.2019.03.017.

27. Katritch, V.; Fenalti, G.; Abola, E. E.; Roth, B. L.; Cherezov, V.; Stevens, R. C. Allosteric sodium in class A GPCR signaling. *Trends Biochem. Sci.* **2014**, 39 (5), 233–244. DOI: 10.1016/j.tibs.2014.03.002.

28. Huang, P.; Zheng, S.; Wierbowski, B. M.; Kim, Y.; Nedelcu, D.; Aravena, L.; Liu, J.; Kruse, A. C.; Salic, A. Structural basis of Smoothened activation in Hedgehog signaling. *Cell* **2018**, 174 (2), 312-324.e16. DOI: 10.1016/j.cell.2018.04.029.

29. Okashah, N.; Wan, Q.; Ghosh, S.; Sandhu, M.; Inoue, A.; Vaidehi, N.; Lambert, N. A. Variable G protein determinants of GPCR coupling selectivity. *Proc. Natl. Acad. Sci. U. S. A.* **2019**, 116 (24), 12054–12059. DOI: 10.1073/pnas.1905993116.

30. Edward Zhou, X.; Melcher, K.; Eric Xu, H. Structural biology of G protein-coupled receptor signaling complexes. *Protein Sci.* **2019**, 28 (3), 487–501. DOI: 10.1002/pro.3526.

31. Qiao, A.; Han, S.; Li, X.; Li, Z.; Zhao, P.; Dai, A.; Chang, R.; Tai, L.; Tan, Q.; Chu, X.; Ma, L.; Thorsen, T. S.; Reedtz-Runge, S.; Yang, D.; Wang, M.-W.; Sexton, P. M.; Wootten, D.; Sun, F.; Zhao, Q.; Wu, B. Structural basis of G_s and G_i recognition by the human glucagon receptor. *Science* **2020**, 367 (6484), 1346–1352. DOI: 10.1126/science.aaz5346.

32. Mobbs, J. I.; Belousoff, M. J.; Harikumar, K. G.; Piper, S. J.; Xu, X.; Furness, S. G. B.; Venugopal, H.; Christopoulos, A.; Danev, R.; Wootten, D.; Thal, D. M.; Miller, L. J.; Sexton, P. M. Structures of the human cholecystokinin 1 (CCK1) receptor bound to G_s and G_q mimetic proteins provide insight into mechanisms of G protein selectivity. *PLoS Biol.* **2021**, 19 (6), e3001295. DOI: 10.1371/journal.pbio.3001295.

33. Jang, W.; Adams, C. E.; Liu, H.; Zhang, C.; Levy, F. O.; Andressen, K. W.; Lambert, N. A. An inactive receptor-G protein complex maintains the dynamic range of agonist-induced signaling. *Proc. Natl. Acad. Sci. U. S. A.* **2020**, 117 (48), 30755–30762. DOI: 10.1073/pnas.2010801117.

34. Huang, W.; Masureel, M.; Qu, Q.; Janetzko, J.; Inoue, A.; Kato, H. E.; Robertson, M. J.; Nguyen, K. C.; Glenn, J. S.; Skiniotis, G.; Kobilka, B. K. Structure of the neurotensin receptor 1 in complex with β-arrestin 1. *Nature* **2020**, 579 (7798), 303–308. DOI: 10.1038/s41586-020-1953-1.

35. Lee, Y.; Warne, T.; Nehmé, R.; Pandey, S.; Dwivedi-Agnihotri, H.; Chaturvedi, M.; Edwards, P. C.; García-Nafría, J.; Leslie, A. G. W.; Shukla, A. K.; Tate, C. G. Molecular basis of β-arrestin coupling to formoterol-bound β1-adrenoceptor. *Nature* **2020**, 583 (7818), 862–866. DOI: 10.1038/s41586-020-2419-1.

36. Zhou, X. E.; He, Y.; Waal, P. W. de; Gao, X.; Kang, Y.; van Eps, N.; Yin, Y.; Pal, K.; Goswami, D.; White, T. A.; Barty, A.; Latorraca, N. R.; Chapman, H. N.; Hubbell, W. L.; Dror, R. O.; Stevens, R. C.; Cherezov, V.; Gurevich, V. V.; Griffin, P. R.; Ernst, O. P.; Melcher, K.; Xu, H. E. Identification of phosphorylation codes for arrestin recruitment by G protein coupled receptors. *Cell* **2017**, 170 (3), 457-469.e13. DOI: 10.1016/j.cell.2017.07.002.

37. Yin, W.; Li, Z.; Jin, M.; Yin, Y.-L.; Waal, P. W. de; Pal, K.; Yin, Y.; Gao, X.; He, Y.; Gao, J.; Wang, X.; Zhang, Y.; Zhou, H.; Melcher, K.; Jiang, Y.; Cong, Y.; Edward Zhou, X.; Yu, X.; Eric Xu, H. A complex structure of arrestin-2 bound to a G protein-coupled receptor. *Cell Res.* **2019**, 29 (12), 971–983. DOI: 10.1038/s41422-019-0256-2.

38. Nguyen, A. H.; Thomsen, A. R. B.; Cahill, T. J.; Huang, R.; Huang, L.-Y.; Marcink, T.; Clarke, O. B.; Heissel, S.; Masoudi, A.; Ben-Hail, D.; Samaan, F.; Dandey, V. P.; Tan, Y. Z.; Hong, C.; Mahoney, J. P.; Triest, S.; Little, J.; Chen, X.; Sunahara, R.; Steyaert, J.; Molina, H.; Yu, Z.; Des Georges, A.; Lefkowitz, R. J. Structure of an endosomal signaling GPCR-G protein-β-arrestin megacomplex. *Nature Struct. Mol. Biol.* **2019**, 26 (12), 1123–1131. DOI: 10.1038/s41594-019-0330-y.

39. Thomsen, A. R. B.; Plouffe, B.; Cahill, T. J.; Shukla, A. K.; Tarrasch, J. T.; Dosey, A. M.; Kahsai, A. W.; Strachan, R. T.; Pani, B.; Mahoney, J. P.; Huang, L.; Breton, B.; Heydenreich, F. M.; Sunahara, R. K.; Skiniotis, G.; Bouvier, M.; Lefkowitz, R. J. GPCR-G Protein-β-Arrestin Super-Complex Mediates Sustained G Protein Signaling. *Cell* **2016**, 166 (4), 907–919. DOI: 10.1016/j.cell.2016.07.004.

40. Jeong, E.; Kim, Y.; Jeong, J.; Cho, Y. Structure of the class C orphan GPCR GPR158 in complex with RGS7-Gβ5. *Nat. Commun.* **2021**, 12 (1), 6805. DOI: 10.1038/s41467-021-27147-1.

41. Wingler, L. M.; Skiba, M. A.; McMahon, C.; Staus, D. P.; Kleinhenz, A. L. W.; Suomivuori, C.-M.; Latorraca, N. R.; Dror, R. O.; Lefkowitz, R. J.; Kruse, A. C. Angiotensin and biased analogs induce structurally distinct active conformations within a GPCR. *Science* **2020**, 367 (6480), 888–892. DOI: 10.1126/science.aay9813.

42. Smith, J. S.; Lefkowitz, R. J.; Rajagopal, S. Biased signalling: from simple switches to allosteric microprocessors. *Nat. Rev. Drug Discov.* **2018**, 17 (4), 243–260. DOI: 10.1038/nrd.2017.229.

43. Avet, C.; Mancini, A.; Breton, B.; Le Gouill, C.; Hauser, A. S.; Normand, C.; Kobayashi, H.; Gross, F.; Hogue, M.; Lukasheva, V.; St-Onge, S.; Carrier, M.; Héroux, M.; Morissette, S.; Fauman, E. B.; Fortin, J.-P.; Schann, S.; Leroy, X.; Gloriam, D. E.; Bouvier, M. Effector membrane translocation biosensors reveal G protein and βarrestin coupling profiles of 100 therapeutically relevant GPCRs. *eLife* **2022**, 11. DOI: 10.7554/eLife.74101.

44. Voss, J. H.; Mahardhika, A. B.; Inoue, A.; Müller, C. E. Agonist-dependent coupling of the promiscuous adenosine A_{2B} receptor to Gα protein subunits. *ACS Pharmacol. Transl. Sci.* **2022**. DOI: 10.1021/acsptsci.2c00020.

45. Hinz, S.; Navarro, G.; Borroto-Escuela, D.; Seibt, B. F.; Ammon, Y.-C.; Filippo, E. de; Danish, A.; Lacher, S. K.; Červinková, B.; Rafehi, M.; Fuxe, K.; Schiedel, A. C.; Franco, R.; Müller, C. E. Adenosine A_{2A} receptor ligand recognition and signaling is blocked by A_{2B} receptors. *Oncotarget* **2018**, 9 (17), 13593–13611. DOI: 10.18632/oncotarget.24423.

46. Lohse, M. J. Dimerization in GPCR mobility and signaling. *Curr. Opin. Pharmacol.* **2010**, 10 (1), 53–58. DOI: 10.1016/j.coph.2009.10.007.

47. Calebiro, D.; Koszegi, Z. The subcellular dynamics of GPCR signaling. *Mol. Cell. Endocrinol.* **2019**, 483, 24–30. DOI: 10.1016/j.mce.2018.12.020.

48. Sungkaworn, T.; Jobin, M.-L.; Burnecki, K.; Weron, A.; Lohse, M. J.; Calebiro, D. Single-molecule imaging reveals receptor-G protein interactions at cell surface hot spots. *Nature* **2017**, 550 (7677), 543–547. DOI: 10.1038/nature24264.

49. Gao, Z.-G.; Inoue, A.; Jacobson, K. A. On the G protein-coupling selectivity of the native A_{2B} adenosine receptor. *Biochem. Pharmacol.* **2018**, 151, 201–213. DOI: 10.1016/j.bcp.2017.12.003.

50. Simon, M. I.; Strathmann, M. P.; Gautam, N. Diversity of G proteins in signal transduction. *Science* **1991**, 252 (5007), 802–808.

51. Khan, S. M.; Sleno, R.; Gora, S.; Zylbergold, P.; Laverdure, J.-P.; Labbé, J.-C.; Miller, G. J.; Hébert, T. E. The expanding roles of Gβγ subunits in G protein-coupled receptor signaling and drug action. *Pharmacol. Rev.* **2013**, 65 (2), 545–577. DOI: 10.1124/pr.111.005603.

52. Pfeil, E. M.; Brands, J.; Merten, N.; Vögtle, T.; Vescovo, M.; Rick, U.; Albrecht, I.-M.; Heycke, N.; Kawakami, K.; Ono, Y.; Ngako Kadji, F. M.; Hiratsuka, S.; Aoki, J.; Häberlein, F.; Matthey, M.; Garg, J.; Hennen, S.; Jobin, M.-L.; Seier, K.; Calebiro, D.; Pfeifer, A.; Heinemann, A.; Wenzel, D.; König, G. M.; Nieswandt, B.; Fleischmann, B. K.; Inoue, A.; Simon, K.; Kostenis, E. Heterotrimeric G protein subunit $G\alpha_q$ is a master switch for Gβγ-mediated calcium mobilization by G_i-coupled GPCRs. *Mol. Cell.* **2020**, 80 (6), 940-954.e6. DOI: 10.1016/j.molcel.2020.10.027.

53. Masuho, I.; Balaji, S.; Muntean, B. S.; Skamangas, N. K.; Chavali, S.; Tesmer, J. J. G.; Babu, M. M.; Martemyanov, K. A. A global map of G protein signaling regulation by RGS proteins. *Cell* **2020**, 183 (2), 503-521.e19. DOI: 10.1016/j.cell.2020.08.052.

54. Flock, T.; Ravarani, C. N. J.; Sun, D.; Venkatakrishnan, A. J.; Kayikci, M.; Tate, C. G.; Veprintsev, D. B.; Babu, M. M. Universal allosteric mechanism for Gα activation by GPCRs. *Nature* **2015**, 524 (7564), 173–179. DOI: 10.1038/nature14663.

55. Sun, D.; Flock, T.; Deupi, X.; Maeda, S.; Matkovic, M.; Mendieta, S.; Mayer, D.; Dawson, R.; Schertler, G. F. X.; Madan Babu, M.; Veprintsev, D. B. Probing $G\alpha_{i1}$ protein activation at single-amino acid resolution. *Nat. Struct. Mol. Biol.* **2015**, 22 (9), 686–694. DOI: 10.1038/nsmb.3070.

56. Sprang, S. R. G protein mechanisms: Insights from structural analysis. *Annu. Rev. Biochem.* **1997**, 66, 639–678. DOI: 10.1146/annurev.biochem.66.1.639.

57. Qi, C.; Sorrentino, S.; Medalia, O.; Korkhov, V. M. The structure of a membrane adenylyl cyclase bound to an activated stimulatory G protein. *Science* **2019**, 364 (6438), 389–394. DOI: 10.1126/science.aav0778.

58. Taylor, S. J.; Chae, H. Z.; Rhee, S. G.; Exton, J. H. Activation of the β1 isozyme of phospholipase C by alpha subunits of the G_q class of G proteins. *Nature* **1991**, 350 (6318), 516–518. DOI: 10.1038/350516a0.

59. Suzuki, N.; Hajicek, N.; Kozasa, T. Regulation and physiological functions of $G_{12/13}$-mediated signaling pathways. *Neurosignals* **2009**, 17 (1), 55–70. DOI: 10.1159/000186690.

60. Chen, Z.; Singer, W. D.; Sternweis, P. C.; Sprang, S. R. Structure of the p115RhoGEF rgRGS domain-Galpha13/i1 chimera complex suggests convergent evolution of a GTPase activator. *Nat. Struct. Mol. Biol.* **2005**, 12 (2), 191–197. DOI: 10.1038/nsmb888.

61. Hauser, A. S.; Avet, C.; Normand, C.; Mancini, A.; Inoue, A.; Bouvier, M.; Gloriam, D. E. Common coupling map advances GPCR-G protein selectivity. *eLife* **2022**, 11. DOI: 10.7554/eLife.74107.

62. Lu, J. J.; Polgar, W. E.; Mann, A.; Dasgupta, P.; Schulz, S.; Zaveri, N. T. Differential In vitro Pharmacological Profiles of Structurally Diverse Nociceptin Receptor Agonists in Activating G-protein and Beta-arrestin Signaling at the Human Nociceptin Opioid Receptor. *Mol. Pharmacol.* **2021**, MOLPHARM-AR-2020-000076. DOI: 10.1124/molpharm.120.000076.

63. Barnett, M. E.; Knapp, B. I.; Bidlack, J. M. Unique Pharmacological Properties of the Kappa Opioid Receptor Signaling Through Gαz as Shown with BRET. *Mol. Pharmacol.* **2020**, mol.120.119404. DOI: 10.1124/mol.120.119404.

64. Gurevich, V. V.; Gurevich, E. V. GPCR Signaling Regulation: The Role of GRKs and Arrestins. *Front. Pharmacol.* **2019**, 10, 125. DOI: 10.3389/fphar.2019.00125.

65. Eichel, K.; von Zastrow, M. Subcellular Organization of GPCR Signaling. *Trends Pharmacol. Sci.* **2018**, 39 (2), 200–208. DOI: 10.1016/j.tips.2017.11.009.

66. Caron, M. G.; Barak, L. S. A Brief History of the β-Arrestins. *Methods Mol. Biol.* **2019**, 1957, 3–8. DOI: 10.1007/978-1-4939-9158-7_1.

67. Wright, S. C.; Lukasheva, V.; Le Gouill, C.; Kobayashi, H.; Breton, B.; Mailhot-Larouche, S.; Blondel-Tepaz, É.; Antunes Vieira, N.; Costa-Neto, C.; Héroux, M.; Lambert, N. A.; Parreiras-

E-Silva, L. T.; Bouvier, M. BRET-based effector membrane translocation assay monitors GPCR-promoted and endocytosis-mediated G_q activation at early endosomes. *Proc. Natl. Acad. Sci. U. S. A.* **2021**, 118 (20). DOI: 10.1073/pnas.2025846118.

68. Gurevich, V. V.; Gurevich, E. V. Arrestin-mediated signaling: Is there a controversy? *World J. Biol. Chem.* **2018**, 9 (3), 25–35. DOI: 10.4331/wjbc.v9.i3.25.

69. Grundmann, M.; Merten, N.; Malfacini, D.; Inoue, A.; Preis, P.; Simon, K.; Rüttiger, N.; Ziegler, N.; Benkel, T.; Schmitt, N. K.; Ishida, S.; Müller, I.; Reher, R.; Kawakami, K.; Inoue, A.; Rick, U.; Kühl, T.; Imhof, D.; Aoki, J.; König, G. M.; Hoffmann, C.; Gomeza, J.; Wess, J.; Kostenis, E. Lack of β-arrestin signaling in the absence of active G proteins. *Nat. Commun.* **2018**, 9 (1), 341. DOI: 10.1038/s41467-017-02661-3.

70. Gutkind, J. S.; Kostenis, E. Arrestins as rheostats of GPCR signalling. *Nat. Rev. Mol. Cell. Biol.* **2018**, 19 (10), 615–616. DOI: 10.1038/s41580-018-0041-y.

71. Eichel, K.; Jullié, D.; Barsi-Rhyne, B.; Latorraca, N. R.; Masureel, M.; Sibarita, J.-B.; Dror, R. O.; Zastrow, M. von. Catalytic activation of β-arrestin by GPCRs. *Nature* **2018**, 557 (7705), 381–386. DOI: 10.1038/s41586-018-0079-1.

72. Jean-Charles, P.-Y.; Kaur, S.; Shenoy, S. K. G protein-coupled receptor signaling through β-arrestin-dependent mechanisms. *J. Cardiovasc. Pharmacol.* **2017**, 70 (3), 142–158. DOI: 10.1097/FJC.0000000000000482.

73. Oligny-Longpré, G.; Corbani, M.; Zhou, J.; Hogue, M.; Guillon, G.; Bouvier, M. Engagement of β-arrestin by transactivated insulin-like growth factor receptor is needed for V2 vasopressin receptor-stimulated ERK1/2 activation. *Proc. Natl. Acad. Sci. U. S. A.* **2012**, 109 (17), E1028-37. DOI: 10.1073/pnas.1112422109.

74. Pandey, S.; Kumari, P.; Baidya, M.; Kise, R.; Cao, Y.; Dwivedi-Agnihotri, H.; Banerjee, R.; Li, X. X.; Cui, C. S.; Lee, J. D.; Kawakami, K.; Maharana, J.; Ranjan, A.; Chaturvedi, M.; Jhingan, G. D.; Laporte, S. A.; Woodruff, T. M.; Inoue, A.; Shukla, A. K. Intrinsic bias at non-canonical, β-arrestin-coupled seven transmembrane receptors. *Mol. Cell.* **2021**, 81 (22), 4605-4621.e11. DOI: 10.1016/j.molcel.2021.09.007.

75. Kenakin, T.; Strachan, R. T. PAM-Antagonists: A better way to block pathological receptor signaling? *Trends Pharmacol. Sci.* **2018**, 39 (8), 748–765. DOI: 10.1016/j.tips.2018.05.001.

76. Pedersen, M. F.; Wróbel, T. M.; Märcher-Rørsted, E.; Pedersen, D. S.; Møller, T. C.; Gabriele, F.; Pedersen, H.; Matosiuk, D.; Foster, S. R.; Bouvier, M.; Bräuner-Osborne, H. Biased agonism of clinically approved μ-opioid receptor agonists and TRV130 is not controlled by

binding and signaling kinetics. *Neuropharmacology* **2020**, 166, 107718. DOI: 10.1016/j.neuropharm.2019.107718.

77. Miyano, K.; Manabe, S.; Komatsu, A.; Fujii, Y.; Mizobuchi, Y.; Uezono, E.; Ohshima, K.; Nonaka, M.; Kuroda, Y.; Narita, M.; Uezono, Y. The G protein signal-biased compound trv130; structures, its site of action and clinical studies. *Curr. Top. Med. Chem.* **2020**, 20 (31), 2822–2829. DOI: 10.2174/1568026620999201027224229.

78. Che, T.; Dwivedi-Agnihotri, H.; Shukla, A. K.; Roth, B. L. Biased ligands at opioid receptors: Current status and future directions. *Sci. Signal.* **2021**, 14 (677). DOI: 10.1126/scisignal.aav0320.

79. Mores, K. L.; Cummins, B. R.; Cassell, R. J.; van Rijn, R. M. A review of the therapeutic developed G protein-biased kappa agonists. *Front. Pharmacol.* **2019**, 10, 407. DOI: 10.3389/fphar.2019.00407.

80. Pang, P. S.; Butler, J.; Collins, S. P.; Cotter, G.; Davison, B. A.; Ezekowitz, J. A.; Filippatos, G.; M.; Ponikowski, P.; Teerlink, J. R.; Voors, A. A.; Bharucha, D.; Goin, K.; Soergel, D. G.; Felker, G. M. Biased ligand of the angiotensin II type 1 receptor in patients with acute heart failure: a randomized, double-blind, placebo-controlled, phase IIB, dose ranging trial (BLAST-AHF). *Eur. Heart J.* **2017**, 38 (30), 2364–2373. DOI: 10.1093/eurheartj/ehx196.

81. Hulme, E. C.; Trevethick, M. A. Ligand binding assays at equilibrium: Validation and interpretation. *Br. J. Pharmacol.* **2010**, 161 (6), 1219–1237. DOI: 10.1111/j.1476-5381.2009.00604.x.

82. Lin, K.; Wu, G. Isothermal titration calorimetry assays to measure binding affinities in vitro. *Methods Mol. Biol.* **2019**, 1893, 257–272. DOI: 10.1007/978-1-4939-8910-2_19.

83. Olaru, A.; Bala, C.; Jaffrezic-Renault, N.; Aboul-Enein, H. Y. Surface plasmon resonance (SPR) biosensors in pharmaceutical analysis. *Crit. Rev. Anal. Chem.* **2015**, 45 (2), 97–105. DOI: 10.1080/10408347.2014.881250.

84. Auguet, M.; Delaflotte, S.; Chabrier, P.-E.; Pirotzky, E.; Clostre, F.; Braquet, P. Endothelin and Ca++ agonist bay K 8644: Different vasoconstrictive properties. *Biochem. Biophys. Res. Commun.* **1988,** 156 (1), 186–192. DOI: 10.1016/S0006-291X(88)80822-2.

85. Eguchi, S.; Hirata, Y.; Imai, T.; Marumo, F. Endothelin receptor subtypes are coupled to adenylate cyclase via different guanyl nucleotide-binding proteins in vasculature. *Endocrinology* **1993**, 132 (2), 524–529. DOI: 10.1210/endo.132.2.7678793.

86. Wright, S. C.; Bouvier, M. Illuminating the complexity of GPCR pathway selectivity - advances in biosensor development. *Curr. Opin. Struct. Biol.* **2021**, 69, 142–149. DOI: 10.1016/j.sbi.2021.04.006.

87. Olsen, R. H. J.; DiBerto, J. F.; English, J. G.; Glaudin, A. M.; Krumm, B. E.; Slocum, S. T.; Che, T.; Gavin, A. C.; McCorvy, J. D.; Roth, B. L.; Strachan, R. T. TRUPATH, an open-source biosensor platform for interrogating the GPCR transducerome. *Nat. Chem. Biol.* **2020**. DOI: 10.1038/s41589-020-0535-8.

88. Galés, C.; Rebois, R. V.; Hogue, M.; Trieu, P.; Breit, A.; Hébert, T. E.; Bouvier, M. Real-time monitoring of receptor and G-protein interactions in living cells. *Nat. Methods* **2005**, 2 (3), 177–184. DOI: 10.1038/nmeth743.

89. Galés, C.; van Durm, J. J. J.; Schaak, S.; Pontier, S.; Percherancier, Y.; Audet, M.; Paris, H.; Bouvier, M. Probing the activation-promoted structural rearrangements in preassembled receptor-G protein complexes. *Nat. Struct. Mol. Biol.* **2006**, 13 (9), 778–786. DOI: 10.1038/nsmb1134.

90. Inoue, A.; Ishiguro, J.; Kitamura, H.; Arima, N.; Okutani, M.; Shuto, A.; Higashiyama, S.; Ohwada, T.; Arai, H.; Makide, K.; Aoki, J. TGFα shedding assay: an accurate and versatile method for detecting GPCR activation. *Nat. Methods* **2012**, 9 (10), 1021–1029. DOI: 10.1038/nmeth.2172.

91. Ren, X.-R.; Reiter, E.; Ahn, S.; Kim, J.; Chen, W.; Lefkowitz, R. J. Different G protein-coupled receptor kinases govern G protein and beta-arrestin-mediated signaling of V2 vasopressin receptor. *Proc. Natl. Acad. Sci. U. S. A.* **2005**, 102 (5), 1448–1453. DOI: 10.1073/pnas.0409534102.

92. Yin, H.; Chu, A.; Li, W.; Wang, B.; Shelton, F.; Otero, F.; Nguyen, D. G.; Caldwell, J. S.; Chen, Y. A. Lipid G protein-coupled receptor ligand identification using beta-arrestin PathHunter assay. *J. Biol. Chem.* **2009**, 284 (18), 12328–12338. DOI: 10.1074/jbc.M806516200.

93. Quoyer, J.; Janz, J. M.; Luo, J.; Ren, Y.; Armando, S.; Lukashova, V.; Benovic, J. L.; Carlson, K. E.; Hunt, S. W.; Bouvier, M. Pepducin targeting the C-X-C chemokine receptor type 4 acts as a biased agonist favoring activation of the inhibitory G protein. *Proc. Natl. Acad. Sci. U. S. A.* **2013**, 110 (52), E5088-97. DOI: 10.1073/pnas.1312515110.

94. Namkung, Y.; Le Gouill, C.; Lukashova, V.; Kobayashi, H.; Hogue, M.; Khoury, E.; Song, M.; Bouvier, M.; Laporte, S. A. Monitoring G protein-coupled receptor and β-arrestin trafficking in live cells using enhanced bystander BRET. *Nat. Commun.* **2016**, 7, 12178. DOI: 10.1038/ncomms12178.

95. Dixon, A. S.; Schwinn, M. K.; Hall, M. P.; Zimmerman, K.; Otto, P.; Lubben, T. H.; Butler, B. L.; Binkowski, B. F.; Machleidt, T.; Kirkland, T. A.; Wood, M. G.; Eggers, C. T.; Encell, L. P.; Wood, K. V. NanoLuc complementation reporter optimized for accurate measurement of protein interactions in cells. *ACS Chem. Biol.* **2016**, 11 (2), 400–408. DOI: 10.1021/acschembio.5b00753.

96. Hauge Pedersen, M.; Pham, J.; Mancebo, H.; Inoue, A.; Asher, W. B.; Javitch, J. A. A novel luminescence-based β-arrestin recruitment assay for unmodified receptors. *J. Biol. Chem.* **2021**, 296, 100503. DOI: 10.1016/j.jbc.2021.100503.

97. Kroeze, W. K.; Sassano, M. F.; Huang, X.-P.; Lansu, K.; McCorvy, J. D.; Giguère, P. M.; Sciaky, N.; Roth, B. L. PRESTO-Tango as an open-source resource for interrogation of the druggable human GPCRome. *Nat. Struct. Mol. Biol.* **2015**, 22 (5), 362–369. DOI: 10.1038/nsmb.3014.

98. Wedegaertner, P. B.; Wilson, P. T.; Bourne, H. R. Lipid modifications of trimeric G proteins. *J. Biol. Chem.* **1995**, 270 (2), 503–506. DOI: 10.1074/jbc.270.2.503.

99. Masuho, I.; Skamangas, N. K.; Muntean, B. S.; Martemyanov, K. A. Diversity of the Gβγ complexes defines spatial and temporal bias of GPCR signaling. *Cell Syst.* **2021**, 12 (4), 324-337.e5. DOI: 10.1016/j.cels.2021.02.001.

100. Mukhopadhyay, S.; Ross, E. M. Rapid GTP binding and hydrolysis by Gq promoted by receptor and GTPase-activating proteins. *Proc. Natl. Acad. Sci. U. S. A.* **1999**, 96 (17), 9539–9544. DOI: 10.1073/pnas.96.17.9539.

101. Mignery, G. A.; Südhof, T. C. The ligand binding site and transduction mechanism in the inositol-1,4,5-triphosphate receptor. *EMBO J.* **1990**, 9 (12), 3893–3898. DOI: 10.1002/j.1460-2075.1990.tb07609.x.

102. Santulli, G.; Marks, A. R.. Essential roles of intracellular calcium release channels in muscle, brain, metabolism, and aging. *Curr. Mol. Pharmacol.*, 8 (2), 206–222. DOI: 10.2174/1874467208666150507105105.

103. Huang, K.-P. The mechanism of protein kinase C activation. *Trends Neurosci.* **1989**, 12 (11), 425–432. DOI: 10.1016/0166-2236(89)90091-X.

104. Park, D.; Jhon, D. Y.; Lee, C. W.; Lee, K. H.; Rhee, S. G. Activation of phospholipase C isozymes by G protein beta gamma subunits. *J. Biol. Chem.* **1993**, 268 (7), 4573–4576.

105. Tesmer, V. M.; Kawano, T.; Shankaranarayanan, A.; Kozasa, T.; Tesmer, J. J. G. Snapshot of activated G proteins at the membrane: The Galphaq-GRK2-Gbetagamma complex. *Science* **2005**, 310 (5754), 1686–1690. DOI: 10.1126/science.1118890.

106. Lutz, S.; Shankaranarayanan, A.; Coco, C.; Ridilla, M.; Nance, M. R.; Vettel, C.; Baltus, D.; Evelyn, C. R.; Neubig, R. R.; Wieland, T.; Tesmer, J. J. G. Structure of Galphaq-p63RhoGEF-RhoA complex reveals a pathway for the activation of RhoA by GPCRs. *Science* **2007**, 318 (5858), 1923–1927. DOI: 10.1126/science.1147554.

107. Taylor, V. G.; Bommarito, P. A.; Tesmer, J. J. G. Structure of the regulator of G protein signaling 8 (RGS8)-$G\alpha_q$ complex: Molecular basis for Gα selectivity. *J. Biol. Chem.* **2016**, 291 (10), 5138–5145. DOI: 10.1074/jbc.M115.712075.

108. Kimple, A. J.; Soundararajan, M.; Hutsell, S. Q.; Roos, A. K.; Urban, D. J.; Setola, V.; Temple, B. R. S.; Roth, B. L.; Knapp, S.; Willard, F. S.; Siderovski, D. P. Structural determinants of G-protein alpha subunit selectivity by regulator of G-protein signaling 2 (RGS2). *J. Biol. Chem.* **2009**, 284 (29), 19402–19411. DOI: 10.1074/jbc.M109.024711.

109. Sánchez-Fernández, G.; Cabezudo, S.; García-Hoz, C.; Benincá, C.; Aragay, A. M.; Mayor, F.; Ribas, C. $G\alpha_q$ signalling: The new and the old. *Cell. Signal.* **2014**, 26 (5), 833–848. DOI: 10.1016/j.cellsig.2014.01.010.

110. Sprang, S. R. Invited review: Activation of G proteins by GTP and the mechanism of Gα-catalyzed GTP hydrolysis. *Biopolymers* **2016**, 105 (8), 449–462. DOI: 10.1002/bip.22836.

111. Chidiac, P.; Ross, E. M. Phospholipase C-β1 directly accelerates GTP hydrolysis by $G\alpha_q$ and acceleration is inhibited by Gβγ subunits. *J. Biol. Chem.* **1999**, 274 (28), 19639–19643.

112. Robertson, A. G.; Shih, J.; Yau, C.; Gibb, E. A.; Oba, J.; Mungall, K. L.; Hess, J. M.; Uzunangelov, V.; Walter, V.; Danilova, L.; Lichtenberg, T. M.; Kucherlapati, M.; Kimes, P. K.; Tang, M.; Penson, A.; Babur, O.; Akbani, R.; Bristow, C. A.; Hoadley, K. A.; Iype, L.; Chang, M. T.; Cherniack, A. D.; Benz, C.; Mills, G. B.; Verhaak, R. G. W.; Griewank, K. G.; Felau, I.; Zenklusen, J. C.; Gershenwald, J. E.; Schoenfield, L.; Lazar, A. J.; Abdel-Rahman, M. H.; Roman-Roman, S.; Stern, M.-H.; Cebulla, C. M.; Williams, M. D.; Jager, M. J.; Coupland, S. E.; Esmaeli, B.; Kandoth, C.; Woodman, S. E. Integrative analysis identifies four molecular and clinical subsets in uveal melanoma. *Cancer Cell* **2017**, 32 (2), 204-220.e15. DOI: 10.1016/j.ccell.2017.07.003.

113. van Raamsdonk, C. D.; Griewank, K. G.; Crosby, M. B.; Garrido, M. C.; Vemula, S.; Wiesner, T.; Obenauf, A. C.; Wackernagel, W.; Green, G.; Bouvier, N.; Sozen, M. M.; Baimukanova, G.; Roy, R.; Heguy, A.; Dolgalev, I.; Khanin, R.; Busam, K.; Speicher, M. R.; O'Brien, J.; Bastian, B. C. Mutations in GNA11 in uveal melanoma. *N. Engl. J. Med.* **2010**, 363 (23), 2191–2199. DOI: 10.1056/NEJMoa1000584.

114. Wright, S. J.; Inchausti, R.; Eaton, C. J.; Krystofova, S.; Borkovich, K. A. RIC8 is a guanine-nucleotide exchange factor for Gα subunits that regulates growth and development in Neurospora crassa. *Genetics* **2011**, 189 (1), 165–176. DOI: 10.1534/genetics.111.129270.

115. Chan, P.; Gabay, M.; Wright, F. A.; Tall, G. G. Ric-8B is a GTP-dependent G protein α_s guanine nucleotide exchange factor. *J. Biol. Chem.* **2011**, 286 (22), 19932–19942. DOI: 10.1074/jbc.M110.163675.

116. Tall, G. G.; Patel, B. R.; Chan, P. Ric-8 folding of G proteins better explains Ric-8 apparent amplification of G protein-coupled receptor signaling. *Proc. Natl. Acad. Sci. U. S. A.* **2013**, 110 (34), E3148. DOI: 10.1073/pnas.1307476110.

117. Gabay, M.; Pinter, M. E.; Wright, F. A.; Chan, P.; Murphy, A. J.; Valenzuela, D. M.; Yancopoulos, G. D.; Tall, G. G. Ric-8 proteins are molecular chaperones that direct nascent G protein α subunit membrane association. *Science signaling* **2011**, 4 (200), ra79. DOI: 10.1126/scisignal.2002223.

118. Chan, P.; Thomas, C. J.; Sprang, S. R.; Tall, G. G. Molecular chaperoning function of Ric-8 is to fold nascent heterotrimeric G protein α subunits. *Proc. Natl. Acad. Sci. U. S. A.* **2013**, 110 (10), 3794–3799. DOI: 10.1073/pnas.1220943110.

119. Seven, A. B.; Hilger, D.; Papasergi-Scott, M. M.; Zhang, L.; Qu, Q.; Kobilka, B. K.; Tall, G. G.; Skiniotis, G. Structures of Gα proteins in complex with their chaperone reveal quality control mechanisms. *Cell Rep.* **2020**. DOI: 10.1016/j.celrep.2020.02.086.

120. Chan, P.; Gabay, M.; Wright, F. A.; Kan, W.; Oner, S. S.; Lanier, S. M.; Smrcka, A. V.; Blumer, J. B.; Tall, G. G. Purification of heterotrimeric G protein alpha subunits by GST-Ric-8 association: primary characterization of purified $G\alpha_{olf}$. *J. Biol. Chem.* **2011**, 286 (4), 2625–2635. DOI: 10.1074/jbc.M110.178897.

121. Katada, T.; Tamura, M.; Ui, M. The A protomer of islet-activating protein, pertussis toxin, as an active peptide catalyzing ADP-ribosylation of a membrane protein. *Arch. Biochem. Biophys.* **1983**, 224 (1), 290–298. DOI: 10.1016/0003-9861(83)90212-6.

122. Zhang, H.; Nielsen, A. L.; Strømgaard, K. Recent achievements in developing selective Gq inhibitors. *Med. Res. Rev.* **2020**, 40 (1), 135–157. DOI: 10.1002/med.21598.

123. Hermes, C.; König, G. M.; Crüsemann, M. The chromodepsins - chemistry, biology and biosynthesis of a selective G_q inhibitor natural product family. *Nat. Prod. Rep.* **2021**. DOI: 10.1039/d1np00005e.

124. Kostenis, E.; Pfeil, E. M.; Annala, S. Heterotrimeric Gq proteins as therapeutic targets? *J. Biol. Chem.* **2020**. DOI: 10.1074/jbc.REV119.007061.

125. Fujioka, M.; Koda, S.; Morimoto, Y.; Biemann, K. Structure of FR900359, a cyclic depsipeptide from Ardisia crenata sims. *J. Org. Chem.* **1988**, 53 (12), 2820–2825. DOI: 10.1021/jo00247a030.

126. Schrage, R.; Schmitz, A.-L.; Gaffal, E.; Annala, S.; Kehraus, S.; Wenzel, D.; Büllesbach, K. M.; Bald, T.; Inoue, A.; Shinjo, Y.; Galandrin, S.; Shridhar, N.; Hesse, M.; Grundmann, M.; Merten, N.; Charpentier, T. H.; Martz, M.; Butcher, A. J.; Slodczyk, T.; Armando, S.; Effern, M.; Namkung, Y.; Jenkins, L.; Horn, V.; Stößel, A.; Dargatz, H.; Tietze, D.; Imhof, D.; Galés, C.; Drewke, C.; Müller, C. E.; Hölzel, M.; Milligan, G.; Tobin, A. B.; Gomeza, J.; Dohlman, H. G.; Sondek, J.; Harden, T. K.; Bouvier, M.; Laporte, S. A.; Aoki, J.; Fleischmann, B. K.; Mohr, K.; König, G. M.; Tüting, T.; Kostenis, E. The experimental power of FR900359 to study Gq-regulated biological processes. *Nat. Commun.* **2015**, 6, 10156. DOI: 10.1038/ncomms10156.

127. Hermes, C.; Richarz, R.; Wirtz, D. A.; Patt, J.; Hanke, W.; Kehraus, S.; Voss, J. H.; Küppers, J.; Ohbayashi, T.; Namasivayam, V.; Alenfelder, J.; Inoue, A.; Mergaert, P.; Gütschow, M.; Müller, C. E.; Kostenis, E.; König, G. M.; Crüsemann, M. Thioesterase-mediated side chain transesterification generates potent Gq signaling inhibitor FR900359. *Nat. Commun.* **2021**, 12 (1), 144. DOI: 10.1038/s41467-020-20418-3.

128. Carlier, A.; Fehr, L.; Pinto-Carbó, M.; Schäberle, T.; Reher, R.; Dessein, S.; König, G.; Eberl, L. The genome analysis of Candidatus Burkholderia crenata reveals that secondary metabolism may be a key function of the Ardisia crenata leaf nodule symbiosis. *Environ. Microbiol.* **2016**, 18 (8), 2507–2522. DOI: 10.1111/1462-2920.13184.

129. Taniguchi, M.; Nagai, K.; Arao, N.; Kawasaki, T.; Saito, T.; Moritani, Y.; Takasaki, J.; Hayashi, K.; Fujita, S.; Suzuki, K.; Tsukamoto, S. YM-254890, a novel platelet aggregation inhibitor produced by Chromobacterium sp. QS3666. *J. Antibiot.* **2003**, 56 (4), 358–363.

130. Taniguchi, M.; Suzumura, K.-I.; Nagai, K.; Kawasaki, T.; Takasaki, J.; Sekiguchi, M.; Moritani, Y.; Saito, T.; Hayashi, K.; Fujita, S.; Tsukamoto, S.; Suzuki, K. YM-254890 analogues, novel cyclic depsipeptides with $G\alpha_{q/11}$ inhibitory activity from Chromobacterium sp. QS3666. *Bioorg. Med. Chem.* **2004**, 12 (12), 3125–3133. DOI: 10.1016/j.bmc.2004.04.006.

131. Xiong, X.-F.; Zhang, H.; Underwood, C. R.; Harpsøe, K.; Gardella, T. J.; Wöldike, M. F.; Mannstadt, M.; Gloriam, D. E.; Bräuner-Osborne, H.; Strømgaard, K. Total synthesis and structure-activity relationship studies of a series of selective G protein inhibitors. *Nat. Chem.* **2016**, 8 (11), 1035–1041. DOI: 10.1038/nchem.2577.

132. Nishimura, A.; Kitano, K.; Takasaki, J.; Taniguchi, M.; Mizuno, N.; Tago, K.; Hakoshima, T.; Itoh, H. Structural basis for the specific inhibition of heterotrimeric G_q protein by a small

molecule. *Proc. Natl. Acad. Sci. U. S. A.* **2010**, 107 (31), 13666–13671. DOI: 10.1073/pnas.1003553107.

133. Patt, J.; Alenfelder, J.; Pfeil, E. M.; Voss, J. H.; Merten, N.; Eryilmaz, F.; Heycke, N.; Rick, U.; Inoue, A.; Kehraus, S.; Deupi, X.; Müller, C. E.; König, G. M.; Crüsemann, M.; Kostenis, E. An experimental strategy to probe Gq contribution to signal transduction in living cells. *J. Biol. Chem.* **2021**, 100472. DOI: 10.1016/j.jbc.2021.100472.

134. Kukkonen, J. P. G-protein inhibition profile of the reported $G_{q/11}$ inhibitor UBO-QIC. *Biochem. Biophys. Res. Commun.* **2016**, 469 (1), 101–107. DOI: 10.1016/j.bbrc.2015.11.078.

135. Klepac, K.; Kilić, A.; Gnad, T.; Brown, L. M.; Herrmann, B.; Wilderman, A.; Balkow, A.; Glöde, A.; Simon, K.; Lidell, M. E.; Betz, M. J.; Enerbäck, S.; Wess, J.; Freichel, M.; Blüher, M.; König, G.; Kostenis, E.; Insel, P. A.; Pfeifer, A. The G_q signalling pathway inhibits brown and beige adipose tissue. *Nat. Commun.* **2016**, 7, 10895. DOI: 10.1038/ncomms10895.

136. Marwari, S.; Kowalski, C.; Martemyanov, K. A. Exploring pharmacological inhibition of Gq/11 as an analgesic strategy. *Br. J. Pharmacol.* **2022**. DOI: 10.1111/bph.15935.

137. Onken, M. D.; Makepeace, C. M.; Kaltenbronn, K. M.; Kanai, S. M.; Todd, T. D.; Wang, S.; Broekelmann, T. J.; Rao, P. K.; Cooper, J. A.; Blumer, K. J. Targeting nucleotide exchange to inhibit constitutively active G protein α subunits in cancer cells. *Sci. Signal.* **2018**, 11 (546). DOI: 10.1126/scisignal.aao6852.

138. Lapadula, D.; Farias, E.; Randolph, C. E.; Purwin, T.; McGrath, D.; Charpentier, T.; Zhang, L.; Wu, S.; Terai, M.; Sato, T.; Tall, G. G.; Zhou, N.; Wedegaertner, P.; Aplin, A. E.; Aguirre-Ghiso, J.; Benovic, J. L. Effects of oncogenic $G\alpha_q$ and $G\alpha_{11}$ inhibition by FR900359 in uveal melanoma. *Mol. Cancer Res.* **2018**. DOI: 10.1158/1541-7786.MCR-18-0574.

139. Annala, S.; Feng, X.; Shridhar, N.; Eryilmaz, F.; Patt, J.; Yang, J.; Pfeil, E. M.; Cervantes-Villagrana, R. D.; Inoue, A.; Häberlein, F.; Slodczyk, T.; Reher, R.; Kehraus, S.; Monteleone, S.; Schrage, R.; Heycke, N.; Rick, U.; Engel, S.; Pfeifer, A.; Kolb, P.; König, G.; Bünemann, M.; Tüting, T.; Vázquez-Prado, J.; Gutkind, J. S.; Gaffal, E.; Kostenis, E. Direct targeting of $G\alpha_q$ and $G\alpha_{11}$ oncoproteins in cancer cells. *Sci. Signal.* **2019**, 12 (573). DOI: 10.1126/scisignal.aau5948.

140. Matthey, M.; Roberts, R.; Seidinger, A.; Simon, A.; Schröder, R.; Kuschak, M.; Annala, S.; König, G. M.; Müller, C. E.; Hall, I. P.; Kostenis, E.; Fleischmann, B. K.; Wenzel, D. Targeted inhibition of Gq signaling induces airway relaxation in mouse models of asthma. *Sci. Transl. Med.* **2017**, 9 (407). DOI: 10.1126/scitranslmed.aag2288.

141. Schlegel, J. G.; Tahoun, M.; Seidinger, A.; Voss, J. H.; Kuschak, M.; Kehraus, S.; Schneider, M.; Matthey, M.; Fleischmann, B. K.; König, G. M.; Wenzel, D.; Müller, C. E. Macrocyclic G_q Protein Inhibitors FR900359 and/or YM-254890–Fit for Translation? *ACS Pharmacol. Transl. Sci.* **2021**. DOI: 10.1021/acsptsci.1c00021.

142. Kuschak, M.; Schlegel, J. G.; Schneider, M.; Kehraus, S.; Voss, J. H.; Seidinger, A.; Matthey, M.; Wenzel, D.; Fleischmann, B. K.; König, G. M.; Müller, C. E. Sensitive LC-MS/MS Method for the Quantification of Macrocyclic $G\alpha_q$ Protein Inhibitors in Biological Samples. *Front. Chem.* **2020**, 8, 833. DOI: 10.3389/fchem.2020.00833.

143. Milligan, G.; Kostenis, E. Heterotrimeric G proteins: A short history. *Br. J. Pharmacol.* **2006**, 147 Suppl 1, S46-55. DOI: 10.1038/sj.bjp.0706405.

144. Oldham, W. M.; Hamm, H. E. Heterotrimeric G protein activation by G protein-coupled receptors. *Nat. Rev. Mol. Cell. Biol.* **2008**, 9 (1), 60–71. DOI: 10.1038/nrm2299.

145. Chua, V.; Lapadula, D.; Randolph, C.; Benovic, J. L.; Wedegaertner, P. B.; Aplin, A. E. Dysregulated GPCR Signaling and Therapeutic Options in Uveal Melanoma. *Mol. Cancer Res.* **2017**, 15 (5), 501–506. DOI: 10.1158/1541-7786.MCR-17-0007.

146. Meleka, M. M.; Edwards, A. J.; Xia, J.; Dahlen, S. A.; Mohanty, I.; Medcalf, M.; Aggarwal, S.; Moeller, K. D.; Mortensen, O. V.; Osei-Owusu, P. Anti-hypertensive mechanisms of cyclic depsipeptide inhibitor ligands for $G_{q/11}$ class G proteins. *Pharmacol. Res.* **2019**, 141, 264–275. DOI: 10.1016/j.phrs.2019.01.012.

147. White, A. D.; Jean-Alphonse, F. G.; Fang, F.; Peña, K. A.; Liu, S.; König, G. M.; Inoue, A.; Aslanoglou, D.; Gellman, S. H.; Kostenis, E.; Xiao, K.; Vilardaga, J.-P. $G_{q/11}$-dependent regulation of endosomal cAMP generation by parathyroid hormone class B GPCR. *Proc. Natl. Acad. Sci. U. S. A.* **2020**, 117 (13), 7455–7460. DOI: 10.1073/pnas.1918158117.

148. Pistorius, D.; Buntin, K.; Weber, E.; Richard, E.; Bouquet, C.; Wollbrett, S.; Regenass, H.; Peón, V.; Böhm, M.; Kessler, R.; Gempeler, T.; Haberkorn, A.; Wimmer, L.; Lanshoeft, C.; Davis, J.; Hainzl, D.; D'Alessio, J. A.; Manchado, E.; Petersen, F. Promoter-Driven Overexpression in *Chromobacterium vaccinii* facilitates access to FR900359 and yields novel low abundance analogs. *Chemistry* **2022**, 28 (8), e202103888. DOI: 10.1002/chem.202103888.

149. Offermanns, S.; Simon, M. I. $G\alpha_{15}$ and $G\alpha_{16}$ couple a wide variety of receptors to phospholipase C. *J. Biol. Chem.* **1995**, 270 (25), 15175–15180. DOI: 10.1074/jbc.270.25.15175.

150. Takasaki, J.; Saito, T.; Taniguchi, M.; Kawasaki, T.; Moritani, Y.; Hayashi, K.; Kobori, M. A novel $G\alpha_{q/11}$-selective inhibitor. *J. Biol. Chem.* **2004**, 279 (46), 47438–47445. DOI: 10.1074/jbc.M408846200.

151. Kuschak, M.; Namasivayam, V.; Rafehi, M.; Voss, J. H.; Garg, J.; Schlegel, J. G.; Abdelrahman, A.; Kehraus, S.; Reher, R.; Küppers, J.; Sylvester, K.; Hinz, S.; Matthey, M.; Wenzel, D.; Fleischmann, B. K.; Pfeifer, A.; Inoue, A.; Gütschow, M.; König, G. M.; Müller, C. E. Cell-permeable high-affinity tracers for G_q proteins provide structural insights, reveal distinct binding kinetics, and identify small molecule inhibitors. *Br. J. Pharmacol.* **2019**. DOI: 10.1111/bph.14960.

152. Copeland, R. A. The drug-target residence time model: A 10-year retrospective. *Nat. Rev. Drug Discov.* **2016**, 15 (2), 87–95. DOI: 10.1038/nrd.2015.18.

153. Zhang, H.; Xiong, X.-F.; Boesgaard, M. W.; Underwood, C. R.; Bräuner-Osborne, H.; Strømgaard, K. Structure-activity relationship studies of the cyclic depsipeptide natural product YM-254890, targeting the Gq protein. *ChemMedChem* **2017**, 12 (11), 830–834. DOI: 10.1002/cmdc.201700155.

154. Zhang, H.; Nielsen, A. L.; Boesgaard, M. W.; Harpsøe, K.; Daly, N. L.; Xiong, X.-F.; Underwood, C. R.; Haugaard-Kedström, L. M.; Bräuner-Osborne, H.; Gloriam, D. E.; Strømgaard, K. Structure-activity relationship and conformational studies of the natural product cyclic depsipeptides YM-254890 and FR900359. *Eur. J. Med. Chem.* **2018**, 156, 847–860. DOI: 10.1016/j.ejmech.2018.07.023.

155. Xiong, X.-F.; Zhang, H.; Boesgaard, M. W.; Underwood, C. R.; Bräuner-Osborne, H.; Strømgaard, K. Structure-activity relationship studies of the natural product Gq/11 protein inhibitor YM-254890. *ChemMedChem* **2019**. DOI: 10.1002/cmdc.201900018.

156. Reher, R.; Kuschak, M.; Heycke, N.; Annala, S.; Kehraus, S.; Dai, H.-F.; Müller, C. E.; Kostenis, E.; König, G. M.; Crüsemann, M. Applying molecular networking for the detection of natural sources and analogues of the selective G_q protein inhibitor FR900359. *J. Nat. Prod.* **2018**, 81 (7), 1628–1635. DOI: 10.1021/acs.jnatprod.8b00222.

157. Hanke, W.; Patt, J.; Alenfelder, J.; Voss, J. H.; Zdouc, M. M.; Kehraus, S.; Kim, J. B.; Grujičić, G. V.; Namasivayam, V.; Reher, R.; Müller, C. E.; Kostenis, E.; Crüsemann, M.; König, G. M. Feature-based molecular networking for the targeted identification of Gq-inhibiting FR900359 derivatives. *J. Nat. Prod.* **2021**, 84 (7), 1941–1953. DOI: 10.1021/acs.jnatprod.1c00194.

158. Motulsky, H. J.; Mahan, L. C. The kinetics of competitive radioligand binding predicted by the law of mass action. *Mol. Pharmacol.* **1984**, 25 (1), 1–9. DOI: not available.

159. Voss, J. H.; Nagel, J.; Rafehi, M.; Guixà-González, R.; Malfacini, D.; Patt, J.; Kehraus, S.; Inoue, A.; König, G. M.; Kostenis, E.; Deupi, X.; Namasivayam, V.; Müller, C. E. Unraveling binding mechanism and kinetics of macrocyclic $G\alpha_q$ protein inhibitors. *Pharmacol. Res.* **2021**, 173, 105880. DOI: 10.1016/j.phrs.2021.105880.

160. Dowling, M. R.; Charlton, S. J. Quantifying the association and dissociation rates of unlabeled antagonists at the muscarinic M3 receptor. *Br. J. Pharmacol.* **2006**, 148 (7), 927–937. DOI: 10.1038/sj.bjp.0706819.

161. Guo, D.; van Dorp, E. J. H.; Mulder-Krieger, T.; van Veldhoven, J. P. D.; Brussee, J.; IJzerman, A. P.; Heitman, L. H. Dual-point competition association assay: a fast and high-throughput kinetic screening method for assessing ligand-receptor binding kinetics. *J. Biol. Screen.* **2013**, 18 (3), 309–320. DOI: 10.1177/1087057112464776.

162. Reher, R.; Kühl, T.; Annala, S.; Benkel, T.; Kaufmann, D.; Nubbemeyer, B.; Odhiambo, J. P.; Heimer, P.; Bäuml, C. A.; Kehraus, S.; Crüsemann, M.; Kostenis, E.; Tietze, D.; König, G. M.; Imhof, D. Deciphering specificity determinants for FR900359-Derived Gq α inhibitors based on computational and structure-activity studies. *ChemMedChem* **2018**, 13 (16), 1634–1643. DOI: 10.1002/cmdc.201800304.

163. Tietze, D.; Kaufmann, D.; Tietze, A. A.; Voll, A.; Reher, R.; König, G.; Hausch, F. Structural and dynamical basis of G protein inhibition by YM-254890 and FR900359: an inhibitor in action. *J. Chem. Inf. Model.* **2019**, 59 (10), 4361–4373. DOI: 10.1021/acs.jcim.9b00433.

164. Vauquelin, G.; Charlton, S. J. Long-lasting target binding and rebinding as mechanisms to prolong in vivo drug action. *Br. J. Pharmacol.* **2010**, 161 (3), 488–508. DOI: 10.1111/j.1476-5381.2010.00936.x.

165. Malfacini, D.; Patt, J.; Annala, S.; Harpsøe, K.; Eryilmaz, F.; Reher, R.; Crüsemann, M.; Hanke, W.; Zhang, H.; Tietze, D.; Gloriam, D. E.; Bräuner-Osborne, H.; Strømgaard, K.; König, G. M.; Inoue, A.; Gomeza, J.; Kostenis, E. Rational design of a heterotrimeric G protein α subunit with artificial inhibitor sensitivity. *J. Biol. Chem.* **2019**. DOI: 10.1074/jbc.RA118.007250.

166. Boesgaard, M. W.; Harpsøe, K.; Malmberg, M.; Underwood, C. R.; Inoue, A.; Mathiesen, J. M.; König, G. M.; Kostenis, E.; Gloriam, D. E.; Bräuner-Osborne, H. Delineation of molecular determinants for FR900359 inhibition of $G_{q/11}$ unlocks inhibition of $G\alpha_s$. *J. Biol. Chem.* **2020**. DOI: 10.1074/jbc.RA120.013002.

167. Lowry, O. H.; Rosebrough, N. J.; Farr, A. L.; Randall, R. J. Protein measurement with the Folin phenol reagent. *J. Biol. Chem.* **1951**, 193 (1), 265–275. DOI: not available.

168. Ho, M. K.; Yung, L. Y.; Chan, J. S.; Chan, J. H.; Wong, C. S.; Wong, Y. H. Galpha(14) links a variety of G(i)- and G(s)-coupled receptors to the stimulation of phospholipase C. *Br. J. Pharmacol.* **2001**, 132 (7), 1431–1440. DOI: 10.1038/sj.bjp.0703933.

169. Uniprot Consortium. UniProt: The universal protein knowledgebase. *Nucleic Acids Res.* **2017**, 45 (D1), D158-D169. DOI: 10.1093/nar/gkw1099.

170. Needleman, S. B.; Wunsch, C. D. A general method applicable to the search for similarities in the amino acid sequence of two proteins. *J. Mol. Biol.* **1970**, 48 (3), 443–453. DOI: 10.1016/0022-2836(70)90057-4.

171. Uhlén, M.; Fagerberg, L.; Hallström, B. M.; Lindskog, C.; Oksvold, P.; Mardinoglu, A.; Sivertsson, Å.; Kampf, C.; Sjöstedt, E.; Asplund, A.; Olsson, I.; Edlund, K.; Lundberg, E.; Navani, S.; Szigyarto, C. A.-K.; Odeberg, J.; Djureinovic, D.; Takanen, J. O.; Hober, S.; Alm, T.; Edqvist, P.-H.; Berling, H.; Tegel, H.; Mulder, J.; Rockberg, J.; Nilsson, P.; Schwenk, J. M.; Hamsten, M.; Feilitzen, K. von; Forsberg, M.; Persson, L.; Johansson, F.; Zwahlen, M.; Heijne, G. von; Nielsen, J.; Pontén, F. Proteomics. Tissue-based map of the human proteome. *Science* **2015**, 347 (6220), 1260419. DOI: 10.1126/science.1260419.

172. Amatruda, T. T.; Steele, D. A.; Slepak, V. Z.; Simon, M. I. G alpha 16, a G protein alpha subunit specifically expressed in hematopoietic cells. *Proc. Natl. Acad. Sci. U. S. A.* **1991**, 88 (13), 5587–5591. DOI: 10.1073/pnas.88.13.5587.

173. Su, Y.; Ho, M. K. C.; Wong, Y. H. A hematopoietic perspective on the promiscuity and specificity of $G\alpha_{16}$ signaling. *Neurosignals* **2009**, 17 (1), 71–81. DOI: 10.1159/000186691.

174. Zhu, T.; Fang, L.; Xie, X. Development of a universal high-throughput calcium assay for G-protein- coupled receptors with promiscuous G-protein $G\alpha_{15/16}$. *Acta Pharmacol. Sin.* **2008**, 29 (4), 507–516. DOI: 10.1111/j.1745-7254.2008.00775.x.

175. Offermanns, S.; Zhao, L. P.; Gohla, A.; Sarosi, I.; Simon, M. I.; Wilkie, T. M. Embryonic cardiomyocyte hypoplasia and craniofacial defects in $G\alpha_q/G\alpha_{11}$-mutant mice. *EMBO J.* **1998**, 17 (15), 4304–4312. DOI: 10.1093/emboj/17.15.4304.

176. Viswanathan, G.; Mamazhakypov, A.; Schermuly, R. T.; Rajagopal, S. The role of G protein-coupled receptors in the right ventricle in pulmonary hypertension. *Front. Cardiovasc. Med.* **2018**, 5, 179. DOI: 10.3389/fcvm.2018.00179.

177. Wettschureck, N.; Rütten, H.; Zywietz, A.; Gehring, D.; Wilkie, T. M.; Chen, J.; Chien, K. R.; Offermanns, S. Absence of pressure overload induced myocardial hypertrophy after

conditional inactivation of $G\alpha_q/G\alpha_{11}$ in cardiomyocytes. *Nat. Med.* 2001, 7 (11), 1236–1240. DOI: 10.1038/nm1101-1236.

178. Hainmueller, T.; Bartos, M. Dentate gyrus circuits for encoding, retrieval and discrimination of episodic memories. *Nat. Rev. Neurosci.* **2020**, 21 (3), 153–168. DOI: 10.1038/s41583-019-0260-z.

179. Schüller, U.; Lamp, E. C.; Schilling, K. Developmental expression of heterotrimeric G proteins in the murine cerebellar cortex. *Histochem. Cell Biol.* **2001**, 116 (2), 149–159. DOI: 10.1007/s004180100303.

180. Hartmann, J.; Blum, R.; Kovalchuk, Y.; Adelsberger, H.; Kuner, R.; Durand, G. M.; Miyata, M.; Kano, M.; Offermanns, S.; Konnerth, A. Distinct roles of $G\alpha_q$ and $G\alpha_{11}$ for Purkinje cell signaling and motor behavior. *J. Neurosci.* **2004**, 24 (22), 5119–5130. DOI: 10.1523/JNEUROSCI.4193-03.2004.

181. Vignola, A. M.; Kips, J.; Bousquet, J. Tissue remodeling as a feature of persistent asthma. *J. Allergy Clin. Immunol.* **2000**, 105 (6 Pt 1), 1041–1053. DOI: 10.1067/mai.2000.107195.

182. Pahlavan, S.; Oberhofer, M.; Sauer, B.; Ruppenthal, S.; Tian, Q.; Scholz, A.; Kaestner, L.; Lipp, P. $G\alpha_q$ and $G\alpha_{11}$ contribute to the maintenance of cellular electrophysiology and Ca^{2+} handling in ventricular cardiomyocytes. *Cardiovasc. Res.* **2012**, 95 (1), 48–58. DOI: 10.1093/cvr/cvs162.

183. Baskin, D. G.; Filuk, P. E.; Stahl, W. L. Standardization of tritium-sensitive film for quantitative autoradiography. *J. Histochem. Cytochem.* **1989**, 37 (9), 1337–1344. DOI: 10.1177/37.9.2768806.

184. Caviness, V. S.; Barkley, D. S. Section thickness and grain count variation in tritium autoradiography. *Stain Technol.* **1971**, 46 (3), 131–135. DOI: 10.3109/10520297109067837.

185. Gao, Z.-G.; Jacobson, K. A. A_{2B} Adenosine Receptor and Cancer. *Int. J. Mol. Sci.* **2019**, 20 (20). DOI: 10.3390/ijms20205139.

186. Feoktistov, I.; Biaggioni, I. Role of adenosine A_{2B} receptors in inflammation. *Adv. Pharmacol.* **2011**, 61, 115–144. DOI: 10.1016/B978-0-12-385526-8.00005-9.

187. Koeppen, M.; Eckle, T.; Eltzschig, H. K. Interplay of hypoxia and A_{2B} adenosine receptors in tissue protection. *Adv. Pharmacol.* **2011**, 61, 145–186. DOI: 10.1016/B978-0-12-385526-8.00006-0.

188. Hinz, S.; Lacher, S. K.; Seibt, B. F.; Müller, C. E. BAY60-6583 acts as a partial agonist at adenosine A_{2B} receptors. *J. Pharmacol. Exp. Ther.* **2014**, 349 (3), 427–436. DOI: 10.1124/jpet.113.210849.

189. Cohen, M. V.; Yang, X.; Downey, J. M. A_{2B} adenosine receptors can change their spots. *Br. J. Pharmacol.* **2010**, 159 (8), 1595–1597. DOI: 10.1111/j.1476-5381.2010.00668.x.

190. Yang, X.; Xin, W.; Yang, X.-M.; Kuno, A.; Rich, T. C.; Cohen, M. V.; Downey, J. M. A_{2B} adenosine receptors inhibit superoxide production from mitochondrial complex I in rabbit cardiomyocytes via a mechanism sensitive to Pertussis toxin. *Br. J. Pharmacol.* **2011**, 163 (5), 995–1006. DOI: 10.1111/j.1476-5381.2011.01288.x.

191. Inoue, A.; Raimondi, F.; Kadji, F. M. N.; Singh, G.; Kishi, T.; Uwamizu, A.; Ono, Y.; Shinjo, Y.; Ishida, S.; Arang, N.; Kawakami, K.; Gutkind, J. S.; Aoki, J.; Russell, R. B. Illuminating G-Protein-Coupling Selectivity of GPCRs. *Cell* **2019**, 177 (7), 1933-1947.e25. DOI: 10.1016/j.cell.2019.04.044.

192. Gracia, E.; Farré, D.; Cortés, A.; Ferrer-Costa, C.; Orozco, M.; Mallol, J.; Lluís, C.; Canela, E. I.; McCormick, P. J.; Franco, R.; Fanelli, F.; Casadó, V. The catalytic site structural gate of adenosine deaminase allosterically modulates ligand binding to adenosine receptors. *FASEB J.* **2013**, 27 (3), 1048–1061. DOI: 10.1096/fj.12-212621.

193. Herrera, C.; Casadó, V.; Ciruela, F.; Schofield, P.; Mallol, J.; Lluis, C.; Franco, R. Adenosine A2B receptors behave as an alternative anchoring protein for cell surface adenosine deaminase in lymphocytes and cultured cells. *Mol. Pharmacol.* **2001**, 59 (1), 127–134.

194. Moreno, E.; Canet, J.; Gracia, E.; Lluís, C.; Mallol, J.; Canela, E. I.; Cortés, A.; Casadó, V. Molecular Evidence of Adenosine Deaminase Linking Adenosine A_{2A} Receptor and CD26 Proteins. *Front. Pharmacol.* **2018**, 9, 106. DOI: 10.3389/fphar.2018.00106.

195. Okashah, N.; Wright, S. C.; Kawakami, K.; Mathiasen, S.; Zhou, J.; Lu, S.; Javitch, J. A.; Inoue, A.; Bouvier, M.; Lambert, N. A. Agonist-induced formation of unproductive receptor-G12 complexes. *Proc. Natl. Acad. Sci. U. S. A.* **2020**, 117 (35), 21723–21730. DOI: 10.1073/pnas.2003787117.

196. Atwood, B. K.; Lopez, J.; Wager-Miller, J.; Mackie, K.; Straiker, A. Expression of G protein-coupled receptors and related proteins in HEK293, AtT20, BV2, and N18 cell lines as revealed by microarray analysis. *BMC Genomics* **2011**, 12, 14. DOI: 10.1186/1471-2164-12-14.

197. Mende, F.; Hundahl, C.; Plouffe, B.; Skov, L. J.; Sivertsen, B.; Madsen, A. N.; Lückmann, M.; Diep, T. A.; Offermanns, S.; Frimurer, T. M.; Bouvier, M.; Holst, B. Translating biased signaling in the ghrelin receptor system into differential in vivo functions. *Proc. Natl. Acad. Sci. U. S. A.* **2018**, 115 (43), E10255-E10264. DOI: 10.1073/pnas.1804003115.

198. Xia, L.; Burger, W. A. C.; van Veldhoven, J. P. D.; Kuiper, B. J.; van Duijl, T. T.; Lenselink, E. B.; Paasman, E.; Heitman, L. H.; IJzerman, A. P. Structure-affinity relationships and structure-kinetics relationships of pyrido2,1-fpurine-2,4-dione derivatives as human adenosine A3 receptor antagonists. *J. Med. Chem.* **2017**, 60 (17), 7555–7568. DOI: 10.1021/acs.jmedchem.7b00950.

199. Guo, D.; Xia, L.; van Veldhoven, J. P. D.; Hazeu, M.; Mocking, T.; Brussee, J.; IJzerman, A. P.; Heitman, L. H. Binding kinetics of ZM241385 derivatives at the human adenosine A_{2A} receptor. *ChemMedChem* **2014**, 9 (4), 752–761. DOI: 10.1002/cmdc.201300474.

200. Nederpelt, I.; Georgi, V.; Schiele, F.; Nowak-Reppel, K.; Fernández-Montalván, A. E.; IJzerman, A. P.; Heitman, L. H. Characterization of 12 GnRH peptide agonists - a kinetic perspective. *Br. J. Pharmacol.* **2016**, 173 (1), 128–141. DOI: 10.1111/bph.13342.

201. Müller, C. E.; Baqi, Y.; Hinz, S.; Namasivayam, V. Medicinal Chemistry of A_{2B} Adenosine Receptors. In The Adenosine Receptors; Borea, P. A., Varani, K., Gessi, S., Merighi, S., Vincenzi, F., Eds.; *The Receptors Vol. 34*; Springer International Publishing, **2018**, pp 137–168. DOI: 10.1007/978-3-319-90808-3_6.

202. Long, J. S.; Crighton, D.; O'Prey, J.; Mackay, G.; Zheng, L.; Palmer, T. M.; Gottlieb, E.; Ryan, K. M. Extracellular adenosine sensing-a metabolic cell death priming mechanism downstream of p53. *Mol. Cell* **2013**, 50 (3), 394–406. DOI: 10.1016/j.molcel.2013.03.016.

203. Maziarz, M.; Park, J.-C.; Leyme, A.; Marivin, A.; Garcia-Lopez, A.; Patel, P. P.; Garcia-Marcos, M. Revealing the activity of trimeric G proteins in live cells with a versatile biosensor design. *Cell* **2020**, 182 (3), 770-785.e16. DOI: 10.1016/j.cell.2020.06.020.

11. Acknowledgements

Die Liste der Leute, denen ich danken möchte, ist recht lang. An erster Stelle möchte ich meiner Doktormutter Prof. Dr. Christa E. Müller danken – dafür, dass sie mich als Doktoranden in ihrem Arbeitskreis aufgenommen hat, für zahlreiche Diskussionen, für die vielen Freiheiten, die sie mir im Rahmen meiner Forschung gelassen hat, die stets großzügige Ausstattung, Offenheit für neue Ideen und für alles, was ich in den letzten Jahren von ihr lernen konnte.

Ich danke den weiteren Mitgliedern meiner Prüfungskommission, Dr. Anke Schiedel, Prof. Dr. Evi Kostenis und Prof. Dr. Rainer Manthey für ihre Bereitschaft, meine Dissertation zu lesen und zu bewerten.

Ich möchte ohne besondere Reihenfolge all den Leuten danken, die meine Arbeit in den vergangenen Jahren nach vorne gebracht haben und mir dabei auf die eine oder andere Weise geholfen haben. Zuerst danke ich Dr. Muhammad Rafehi und Dr. Markus Kuschak sowie Dr. Vigneshwaran Namasivayam für die Einarbeitung zu Beginn der Promotion. Ich danke Jessica Nagel für die immense Hilfe, die sie mir im Rahmen ihrer Masterarbeit war. Ich danke Dr. Winnie Deuther-Conrad vom Helmholtz Zentrum Dresden-Rossendorf für ihre geduldige und sehr freundliche Betreuung der autoradiographischen Experimente. Des Weiteren danke ich allen weiteren Kollaborateueren in den hier beschriebenen und weiteren Projekten: Prof. Dr. Evi Kostenis, Dr. Xavier Deupi, Dr. Ramon Guixà, Dr. Julian Patt, Funda Eryilmaz, Dr. Max Crüsemann, Prof. Dr. Gabriele König, und Prof. Dr. Asuka Inoue.

Des Weiteren bin ich der Deutschen Forschungsgemeinschaft für die großzügige Förderung unseres Projektes im Rahmen der Forschergruppe 2372 meinen Dank schuldig, sowie auch dem Boehringer Ingelheim Funds für die Förderung meines Forschungsaufenthalts in Kanada und der Bonn International Graduate School of Drug Sciences (ganz persönlichen Dank an Dorothee Müssemeier!).

Besonderen Dank an Prof. Dr. Michel Bouvier von der Université de Montreal für die Bereitschaft, mich für zwei Monate in seinem Arbeitskreis willkommen zu heißen, für die Diskussionen und seine Ideen zum Projekt und dafür, etwas seiner Erfahrung mit mir zu teilen. Ich danke auch seinen Mitarbeiterinnen Dr. Monique Lagacé und Dr. Supriya A. Gaitonde für den organistorischen Aufwand, den sie mit mir hatten, und für die gute Betreuung im Labor.

Danke an das Team des besten Praktikums am Pharmazeutischen Institut, Instrumentelle Analytik, an die alten Kollegen Dr. Martin Schlesinger, Dr. Lukas Wendt und Dr. Georg Rolshoven. Und an die neuen Kollegen Dr. Ali El-Tayeb, Katrin Nekipelov, Irina Honin und Luca Svolacchia.

Ich danke allen Kollegen aus den biologischen Laboren des AK Müller für die stets freundliche Arbeitsatmosphäre, an dieser Stelle noch einen ganz besonderen Dank an die technischen

Assistentinnen Katharina Sylvester, Christin Vielmuth und Christiane Bous, die mit ihrer Engelsgeduld den Laborbetrieb oft auf ihren Schultern tragen. Ein expliziter Dank geht an das Kaffeepausen-Team Laura und Robin, wie an all jene, die nicht nur Kollegen geblieben sind, sondern im Laufe der vergangenen vier Jahre Freunde wurden.

Privat danke ich meiner Familie, hier insbesondere meinen Eltern und Großeltern, die mir immer eine ganz freie Wahl gelassen haben, was ich machen will, mich nie unter Druck setzten, aber immer mit hilfreichen Hinweisen zur Seite standen, wenn ich sie brauchte. Ich danke meinen Freunden, mit denen ich in den vergangenen Jahren viele schöne Stunden verbracht habe. Ich danke Johanna für alles, und dafür, mich ständig motiviert zu haben, wenn ich es von mir aus nicht war.

Zuletzt danke ich meiner Partnerin Areso. Für vieles, unter anderem dafür, dass du so für mich da bist, wie du es bist, dass du deine Zukunft mit mir verbringen möchtest und mir auf diese Art und Weise viel Mut gibst, die Zukunft auch wirklich anzupacken und mich darauf zu freuen.

Allen Beteiligten gebührt ihr jeweiliger Anteil daran, dass diese Zeit zur bisher Besten in meinem Leben wurde; eine Zeit, an die ich mich immer gerne erinnern werde.

12. List of abbreviations

$A_{2A}AR$	Adenosine A_{2A} receptor
$A_{2B}AR$	Adenosine A_{2B} receptor
ADA	adenosine deaminase
ANOVA	analysis of variance
AP	alkaline phosphatase
AT_1R	angiotensin II type 1 receptor
B_{max}	maximum binding capacity
β-arr	β-arrestin
β-Gal	β-galactosidase
β-HyLeu	β-hydroxyleucine
BRET	bioluminescence resonance energy transfer
BSA	bovine serum albumin
cAMP	3',5'-cyclic adenosine monophosphate
cpm	counts per minute
CRISPR	clustered regularly interspaced short palindromic repeats
cryo-EM	cryogenic electron microscopy
DAG	diacylglycerol
DMEM	Dulbecco's modified eagle medium
DMSO	dimethylsulfoxide
ECL	extracellular loop
ER	endoplasmic reticulum
ERK	extracellular signal-regulated kinase
ET	endothelin
FCS	fetal calf serum
FR	FR900359

G protein	Heterotrimeric gunanine-nucleotide binding protein
GAP	GTPase-activating protein
GDP	guanosine diphosphate
GEF	guanine-nucleotide exchange factor
GFP	green fluorescent protein
GPCR	G protein-coupled receptor
GRK	G protein-coupled receptor kinase
GTP	guanosine triphosphate
Gα	G protein α subunits
HBSS	Hank's balanced salt solution
HE	hematoxylin-eosin
HEK293	human embryonic kidney 293 cells
ICL	intracellular loop
IP_3	inositol trisphosphate
KRI	kinetic rate index
n.d.	not determined
n.s.	not significant
NCS	newborn calf serum
NECA	5′-*N*-ethylcarboxamide adenosine
PBS	phosphate buffered saline
PCR	polymerase chain reaction
PEI	polyethylenimine
PK	ProLink
PKC	protein kinase C
PLC-β	phospholipase C-β
rGFP	renilla green fluorescent protein

RGS	Regulator of G protein signaling
RLuc	renilla luciferase
SD	standard deviation
SEM	standard error of the mean
$t_{1/2}$	half-life
τ	residence time
TGF-α	transforming growth factor α
TM	transmembrane helix
wt	wild-type
YM	YM-254890

13. Appendix

This section includes the full-length papers, including the supporting information, published during the doctoral studies. The respective introductions to the papers are found within the sections 3, 4, and 7. In this appendix, the publications appear in the same order, starting with appendix A "Heterotrimeric G protein α-subunits - structures, peptide-derived inhibitors, and mechanisms", followed by appendix B "Unraveling binding mechanism and kinetics of macrocyclic $G\alpha_q$ protein inhibitors", and closing with appendix C "Agonist-dependent coupling of the promiscuous adenosine A_{2B} receptor to Gα protein subunits". The copyright of the papers belongs to the respective publishers of the journals, as indicated by copyright statements displayed before each paper.

13.1. Appendix A – Heterotrimeric G protein α-subunits - structures, peptide-derived inhibitors, and mechanisms

This section contains the accepted manuscript of the review article "Heterotrimeric G protein α-subunits - structures, peptide-derived inhibitors, and mechanisms". The manuscript has been accepted for publication in *Curr. Med. Chem.* by Bentham Science and is currently published online ahead of print. Reprinted from *Curr. Med. Chem.*, Online ahead of print, Voss JH and Müller CE, Heterotrimeric G protein α-subunits - structures, peptide-derived inhibitors, and mechanisms, Copyright (2022), with permission from Bentham.

Send Orders for Reprints to reprints@benthamscience.net

Current Medicinal Chemistry, XXXX, *XX*, 1-00 1

REVIEW ARTICLE

Heterotrimeric G Protein α-Subunits - Structures, Peptide-Derived Inhibitors, and Mechanisms[§]

Jan H. Voss[1] and Christa E. Müller[1,*]

[1]*PharmaCenter Bonn, Pharmaceutical Institute, Pharmaceutical & Medicinal Chemistry, University of Bonn, An der Immenburg 4, D-53121Bonn, Germany*

ARTICLE HISTORY

Received: October 06, 2021
Revised: December 24, 2021
Accepted: January 01, 2022

DOI: 10.2174/0929867329666220308112424

Abstract: G protein-coupled receptors are the largest protein family in the human body and represent the most important class of drug targets. They receive extracellular signals and transduce them into the cytosol. The guanine nucleotide-binding Gα proteins represent the main relays by which GPCRs induce intracellular effects. More than 800 different GPCRs interact with 16 Gα proteins belonging to 4 families, $G\alpha_i$, $G\alpha_s$, $G\alpha_q$, and $G\alpha_{12/13}$. The direct inhibition of Gα protein subunits rather than the modulation of GPCR subtypes has been proposed as a novel strategy for the treatment of complex diseases, including inflammation and cancer. This mini-review presents an introduction to G protein structure and function and describes achievements in the development of peptidic and peptide-derived Gα protein inhibitors. They have become indispensable pharmacological tools, and some of them exhibit significant potential as future drugs.

Keywords : Cyclo(depsi)peptide, FR900359, heterotrimeric G protein, Gα protein, G protein-coupled receptor, peptide, YM-254890, inhibitor.

1. INTRODUCTI

Heterotrimeric guanine nucleotide-binding proteins (G proteins) are ternary protein complexes located at the inner layer of the cellular membrane, where they transmit signals from activated G protein-coupled receptors (GPCRs) across the membrane into the cytoplasm [1]. They play a key role in nearly all physiological processes, such as vision, taste, smell, or hormonal responses, but can also be involved in the transduction and generation of pathological signals [2, 3]. G proteins consist of three subunits: the Gα subunit, which is the main interaction partner for both the receptor and the downstream effector(s), and the Gβ and Gγ subunits, which remain tightly associated with each other and partake in independent signaling events upon G protein activation [4, 5]. The exploration of various physiological functions induced or modulated by the different Gβ and Gγ subunits is still in its infancy [6]. In contrast, the interactions of activated GPCRs with Gα subunits have been intensively studied in the last decades and are already quite well-understood [7, 8].

The Gα protein subunits are encoded by 16 genes in the human species sharing a common protein architecture; they are grouped into four families based on sequence similarity, which correlates well with the main effector proteins for each family (Fig. **1A**; only the canonical effectors of the respective Gα protein family are depicted) [9]. For instance, $G\alpha_s$ family proteins increase intracellular levels of the second messenger cAMP by stimulation of adenylate cyclase (AC). In contrast, $G\alpha_{i/o}$ family proteins decrease cAMP levels through AC inhibition. $G\alpha_{q/11}$ proteins activate phospholipase C-β (PLC-β) leading to the release of inositol trisphosphate (IP_3) and diacylglycerol (DAG) [10, 11]. $G\alpha_{12/13}$ proteins recruit small guanosine triphosphate (GTP) hydrolases (GTPases) by interaction with their guanine exchange factors (RhoGEFs) leading to effects on the cytoskeleton [12, 13]. Activated Gα proteins may interact with a plentitude of further proteins [14], but the above-mentioned interactions are the best-characterized ones.

G proteins are intracellular switches for GPCR signal transduction, and their activation cycle is under

*Address correspondence to this author at the Pharmaceutical Institute, Pharmaceutical & Medicinal Chemistry, University of Bonn, An der Immenburg 4, D-53121 Bonn, Germany,
Tel: +49-(0)228-73-2301; Fax: +49-(0)228-73-2567;
E-mail: christa.mueller@uni-bonn.de.

§ Dedicated to the memory of Prof. Dr. Wolfgang Voelter, a visionary medicinal chemist and peptide scientist, a brilliant teacher and a dedicated mentor, and, above all, a great human being, who facilitated the careers of many talented scientists around the globe.

0929-8673/XX $65.00+.00

tight physiological control (see Fig. **1B**). In its basal, inactive state the Gα protein subunit is binding guanosine diphosphate (GDP) and is associated with the Gβγ dimer forming an inactive GDP-bound heterotrimeric α β γ-complex [15]. Upon interaction with the activated GPCR, the bound GDP is released from the Gα protein, which subsequently binds guanosine trisphosphate (GTP) instead [16] present in significantly higher concentration in the cell (estimated concentrations: > 300 µM GTP, ca. 30-40 µM (GDP) [17]. Upon receptor activation, conformational changes within the Gα subunit occur inducing an exchange of the nucleotide GDP for GTP. The underlying mechanism appears to be highly conserved in all Gα protein subunits [18, 19]. The GTP-bound Gα subunit dissociates from the Gβγ dimer and adopts an active conformation by changes in the so-called switch regions (SwI-III), thereby allowing recognition of and interaction with effector proteins [4, 20, 21]. Signaling is terminated by GTP hydrolysis *via* the Gα subunit's intrinsic GTPase activity, which can be enhanced and accelerated by effector proteins or regulators of G protein signaling (RGS) proteins [22-24].

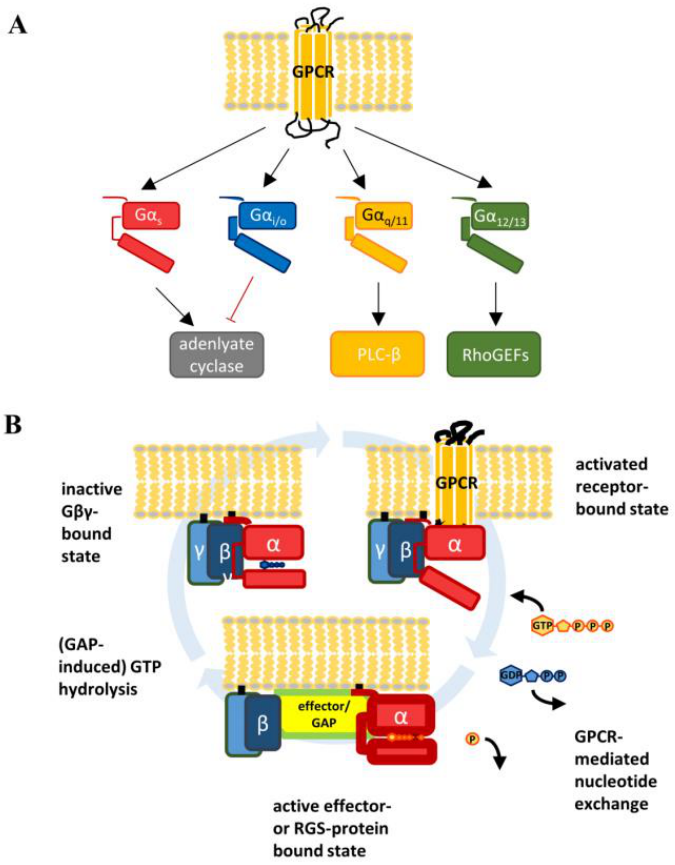

Fig. (1). Generic activation mechanism of G proteins. (**A**). Each GPCR-activated Gα protein family leads to distinct responses. The $G\alpha_s$ protein family activates adenylate cyclase, while the $G\alpha_{i/o}$ protein family inhibits the enzyme. $G\alpha_{q/11}$ proteins activate PLC-β, leading to the production of IP_3 and DAG. $G\alpha_{12/13}$ proteins interact with RhoGEFs and lead to cytoskeletal rearrangements. (**B**). Top left: Inactive Gαβγ-trimer with bound GDP (blue cartoon). Gα and Gγ proteins are anchored (black line) in the plasma membrane (yellow-gray color). **Top right**: Upon GPCR activation (yellow color), GDP release is facilitated by sequestering the Gα helical domain from its Ras-like domain. The GPCR acts as a guanine-nucleotide exchange factor (GEF). **Bottom**: After GTP association, the Gα subunit dissociates from the receptor and the βγ-dimer and binds to effector proteins. Signaling is terminated by GTP hydrolysis, which is facilitated by GTPase-activating proteins (GAPs). Subsequently, the G protein subunits re-associate forming the inactive Gαβγ-heterotrimer. (*A higher resolution / colour version of this figure is available in the electronic copy of the article*).

Drug development targeting GPCRs has been tremendously successful. Nowadays, roughly one-third of all marketed drugs mediate their effects by activation or inhibition of one or several of the more than 800 GPCRs encoded by the human genome [25]. However, direct modulation of heterotrimeric G proteins is not yet therapeutically applied. In recent years, structural information on several G protein subtypes in their active and inactive states has become available [15, 20, 26] which will likely promote the development of drugs directly targeting Gα proteins.

In this review article, we provide insights into the structure and function of G proteins and highlight the discovery of peptidic modulators for Gα proteins that are useful as tool compounds and have potential as lead structures for development as novel diagnostic and therapeutic drugs.

2. THE ARCHITECTURE OF Gα PROTEINS

Mammalian Gα protein subunits share a common architecture and consist of two domains, the GTPase domain (also called Ras-like domain due to its homology with small GTPases of the Ras superfamily) [27] and the α-helical domain (αH), which is unique for heterotrimeric G protein α-subunits (Fig. **2A**). In humans, 16 genes encode 16 distinct Gα proteins that are highly conserved within the different Gα protein subfamilies (see Fig. **2B**) and also between vertebrate orthologs. For example, the human $G\alpha_q$ protein is identical to the mouse $G\alpha_q$ protein except for a single residue. This high conservation emphasizes their important physiological role.

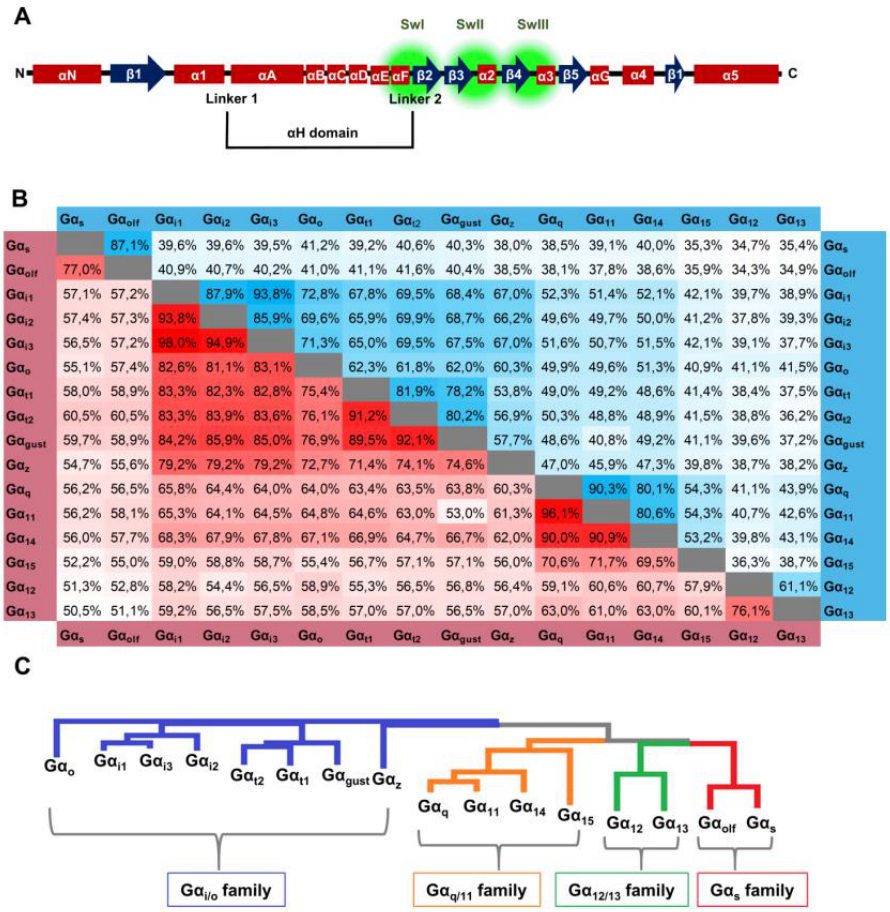

	Gαs	Gαolf	Gαi1	Gαi2	Gαi3	Gαo	Gαt1	Gαt2	Gαgust	Gαz	Gαq	Gα11	Gα14	Gα15	Gα12	Gα13	
Gαs		87,1%	39,6%	39,6%	39,5%	41,2%	39,2%	40,6%	40,3%	38,0%	38,5%	39,1%	40,0%	35,3%	34,7%	35,4%	Gαs
Gαolf	77,0%		40,9%	40,7%	40,2%	41,0%	41,1%	41,6%	40,4%	38,5%	38,1%	37,8%	38,6%	35,9%	34,3%	34,9%	Gαolf
Gαi1	57,1%	57,2%		87,9%	93,8%	72,8%	67,8%	69,5%	68,4%	67,0%	52,3%	51,4%	52,1%	42,1%	39,7%	38,9%	Gαi1
Gαi2	57,4%	57,3%	93,8%		85,9%	69,6%	65,9%	69,9%	68,7%	66,2%	49,6%	49,7%	50,0%	41,2%	37,8%	39,3%	Gαi2
Gαi3	56,5%	57,2%	98,0%	94,9%		71,3%	65,0%	69,5%	67,5%	67,0%	51,6%	50,7%	51,5%	42,1%	39,1%	37,7%	Gαi3
Gαo	55,1%	57,4%	82,6%	81,1%	83,1%		62,3%	61,8%	62,0%	60,3%	49,9%	49,6%	51,3%	40,9%	41,1%	41,5%	Gαo
Gαt1	58,0%	58,9%	83,3%	82,3%	82,8%	75,4%		81,9%	78,2%	53,8%	49,0%	49,2%	48,6%	41,4%	38,4%	37,5%	Gαt1
Gαt2	60,5%	60,5%	83,3%	83,9%	83,6%	76,1%	91,2%		80,2%	56,9%	50,3%	48,8%	48,9%	41,5%	38,8%	36,2%	Gαt2
Gαgust	59,7%	58,9%	84,2%	85,9%	85,0%	76,9%	89,5%	92,1%		57,7%	48,6%	40,8%	49,2%	41,1%	39,6%	37,2%	Gαgust
Gαz	54,7%	55,6%	79,2%	79,2%	79,2%	72,7%	71,4%	74,1%	74,6%		47,0%	45,9%	47,3%	39,8%	38,7%	38,2%	Gαz
Gαq	56,2%	56,5%	65,8%	64,4%	64,0%	64,0%	63,4%	63,5%	63,8%	60,3%		90,3%	80,1%	54,3%	41,1%	43,9%	Gαq
Gα11	56,2%	58,1%	65,3%	64,1%	64,5%	64,8%	64,6%	63,0%	53,0%	61,3%	96,1%		80,6%	54,3%	40,7%	42,6%	Gα11
Gα14	56,0%	57,7%	68,3%	67,9%	67,8%	67,1%	66,9%	64,7%	66,7%	62,0%	90,0%	90,9%		53,2%	39,8%	43,1%	Gα14
Gα15	52,2%	55,0%	59,0%	58,8%	58,7%	55,4%	56,7%	57,1%	57,1%	56,0%	70,6%	71,7%	69,5%		36,3%	38,7%	Gα15
Gα12	51,3%	52,8%	58,2%	54,4%	56,5%	58,9%	55,3%	56,5%	56,8%	56,4%	59,1%	60,6%	60,7%	57,9%		61,1%	Gα12
Gα13	50,5%	51,1%	59,2%	56,5%	57,5%	58,5%	57,0%	57,0%	56,5%	57,0%	63,0%	61,0%	63,0%	60,1%	76,1%		Gα13
	Gαs	Gαolf	Gαi1	Gαi2	Gαi3	Gαo	Gαt1	Gαt2	Gαgust	Gαz	Gαq	Gα11	Gα14	Gα15	Gα12	Gα13	

Fig. (2). Structure and phylogenetic relationships of Gα protein subunits. (**A**). Linear arrangement of a Gα protein showing secondary structural elements, namely linker regions, switch regions, and the αH domain. (**B**). Sequence identity (blue) and similarity (red) of the 16 human Gα protein subunits obtained by pairwise sequence alignments. (**C**). Phylogenic tree depicting the relative evolutionary distance between human Gα protein subunits. (*A higher resolution / colour version of this figure is available in the electronic copy of the article*).

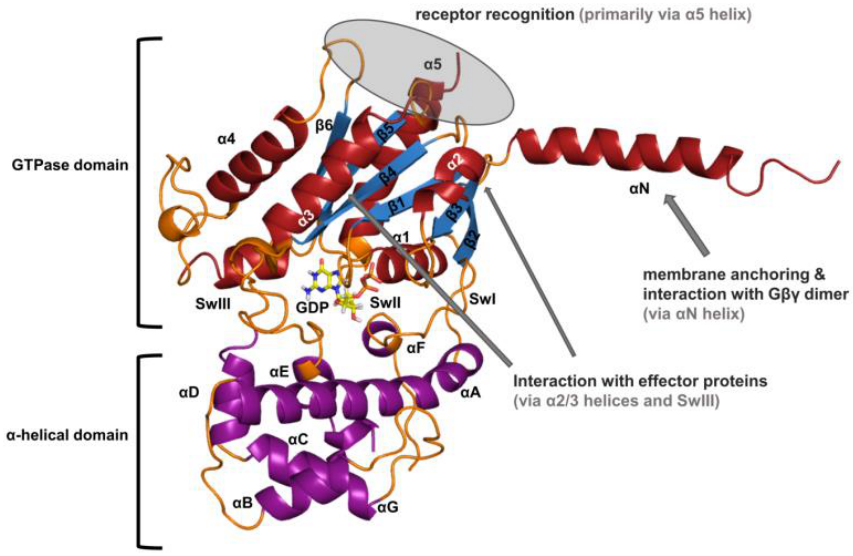

Fig. (3). The architecture of a Gα protein subunit, exemplified by the structure of the inactive, GDP-bound $G\alpha_q$ protein (protein data bank-identification (PDB-ID): 3AH8 [41]). α-Helices are depicted in red in the GTPase domain and purple in the αH domain, β-sheets are indicated in blue. The nucleotide GDP is depicted in yellow with nitrogen atoms in blue, oxygen atoms in red, and hydrogen atoms in white. Secondary structural elements are labeled. (*A higher resolution / colour version of this figure is available in the electronic copy of the article*).

Especially residues contributing to the key functions of the Gα protein, *i.e.* nucleotide exchange and GTP hydrolysis, are fully conserved between different human Gα proteins. The αH-domain, the αN-helix, effector-recognizing regions, and receptor-recognizing sequences (*e.g.* the α5 helix) are mostly conserved within Gα protein subfamilies. Clustering of Gα proteins by sequence similarity results in the well-known Gα protein subfamilies $G\alpha_{i/o}$, $G\alpha_s$, $G\alpha_{q/11}$, and $G\alpha_{12/13}$ (Fig. **2B** and **C**). Gα proteins within one subfamily are often activated by a similar range of receptors and often share sequence elements relevant for effector protein recognition [1, 26]. However, only recently, platforms for studying the interactions of GPCR subtypes with each of the Gα protein subunits have become available, and this has become a most intensively studied area in current pharmacological research [28-31].

Gα proteins consist of several domains as depicted in Fig. **2A**. The N-terminal helix (αN) is posttranslationally myristoylated and/or palmitoylated at glycine (*N*-acylation) and cysteine residues (forming thioesters), respectively, to anchor the Gα subunit in the plasma membrane [32-34]. The C-terminal part of the αN helix and the kink between the αN helix and the β1 sheet can contribute to receptor recognition [35]. The β1 sheet is followed by a short so-called P-loop, which is closely interacting with the guanine nucleotide and the α1 helix. A flexible linker connects the GTPase domain with the helical domain, which consists of the helices αA-αF (numbered in Roman letters, while secondary structural elements in the GTPase domain are numbered in Arabic numerals). The linker 2/switch 1 (Sw1) region re-aligns the sequence back into the GTP-ase domain, which consists of several α-helices and β-sheets forming a globular domain, that interacts with the bound guanine nucleotide, parts of the GPCR, and the effector protein. The C-terminal α5 helix inserts directly into a cavity at the intracellular surface of the active GPCR. It is considered to be a key element for GPCR recognition. According to the common paradigm, GPCRs recruit heterotrimeric G proteins upon receptor activation [36]. However, biochemical evidence exists for the pre-coupling of some GPCRs with G proteins in their basic, non-activated states [37, 38].

Whenever explicit residues of a Gα protein are mentioned, the residue numbering refers to the common Gα numbering (CGN) system developed by Flock *et al*. [18].

2.1. Guanine Nucleotide-binding Site of Gα Proteins

Since the protein sequences and secondary structural elements of all Gα proteins are very similar, their 3-dimensional structures are also comparable. Information about the 3-dimensional structure of heterotrimeric G proteins was first obtained in the 1990s by X-ray crystallography [39]. Till now, a significant number of human Gα subunits have been successfully crystallized. The solved X-ray structures represent the three major conformational states: (i) the inactive, GDP-

bound conformation in complex with the Gβγ-dimer, (ii) the active conformation binding GTP, a GTP-analog, or GDP + Mg^{2+} + AlF_4^- (tetrafluoroaluminate, which activates Gα proteins by imitating the γ-phosphate of GTP [40]), and (iii) the nucleotide-free open state in complex with a GPCR. An exemplary depiction of the inactive GDP-bound $G\alpha_q$ protein is presented in Fig. (**3**) [41], highlighting secodary and tertiary structure elements of a Gα protein.

The inactive Gαβγ trimer is depicted in Fig. (**4A**); the Gβγ dimer binds to the Gα protein *via* interactions with the αN helix and the GTPase domain. The inactive and active nucleotide-bound states of the Gα proteins look very similar at first glance: in both states, the αH domain and the GTPase domain are wrapped around the bound nucleotide and adopt a similar conformation in many parts of the protein, except for the three switch regions (SwI-III). These regions rearrange their conformation depending on the bound nucleotide (see Fig. **4B**). The SwI region, also termed linker 2, contains a catalytic arginine ($R^{G.hfs.2.2}$) residue that interacts closely with the bound GTP. In the absence of GTP, the SwI moves slightly away from the nucleotide. SwII is a small loop between the β3 sheet and the α2 helix, containing a conserved GGQ-motif. The glutamine $Q^{G.s3h2.3}$ interacts closely with GTP and is involved in the hydrolysis of the nucleotide; in the GDP-bound state, it rotates outward and forms polar contacts with the Gβ subunit [42]. Mutations of this residue result in constitutively active G proteins associated with diseases such as uveal melanoma [3, 43, 44]. SwIII is a long loop without a defined secondary structure, located between the β4 sheet and the α3 helix. It undergoes major conformational rearrangements depending on the bound nucleotide and is involved in effector protein interaction.

The third major conformational ensemble of heterotrimeric G proteins is the nucleotide-free open state, which involves rotation of the helical domain, allowing nucleotide release (see Fig. **4C** and **D**). This conformation has been observed in GPCR-G protein structures determined by X-ray crystallography and by cryo-electron microscopy (cryo-EM). Here, the Gβγ dimer is still bound to the Gα protein subunit. The GTP-ase domain of the Gα subunit interacts with the GPCR, and the αH domain rotates outward. The Gα protein conformation is stabilized by interaction with the Gβγ dimer as observed in a recent cryo-EM structure of the neurotensin 1 receptor in complex with $G\alpha_{i1}\beta_1\gamma_1$ reconstituted in lipid nanodiscs [45]. Independent of the bound GPCR or the Gα protein family, all structures resolved so far display very similar conformations of the open Gα protein state, indicating a highly conserved nucleotide exchange mechanism [18, 46].

2.2. Interaction Surfaces of Gα Proteins with Downstream Effector Proteins

All currently resolved interactions between Gα proteins and their downstream effector proteins occur on the surface of the GTPase domain [47, 48]. Table **1** lists the resolved structures of Gα proteins in complex with a downstream effector along with their respective interaction surface. The list does not contain structures of Gαβγ protein trimers or GPCR-G protein complexes but focuses on structures containing an active-state (GTP-bound) Gα protein. The binding site of the Gβγ dimer is well conserved at the SwII/α2 helix, both recognizing the inactive state of the G protein and blocking its interaction site with effector proteins. The GPCR binding site is dependent on the individual GPCR-Gα subunit but always includes the C-terminal α5 helix as a central interaction partner. Currently, the number of available structures of GPCR-G protein complexes is rapidly growing through the wide-spread use of cryo-EM techniques and would thus justify a comprehensive review on its own [46, 49, 50].

Interaction surfaces of canonical effector proteins such as phosphodiesterases (PDEs), AC, and PLC-β, center around the α2 and α3 helices of the Gα subunit (see Table **1**, Fig. **5A** and **B**). While the individual interaction patterns between a Gα protein and its effectors are different, the secondary structural elements of the Gα protein involved in effector protein binding are identical. Proteins with GAP function at Gα subunits can be divided into non-canonical RGS proteins (effector proteins that increase the GTP hydrolysis rate of Gα proteins) and canonical RGS proteins (members of the RGS protein family, *e.g.* RGS2 and RGS4), which differ from each other regarding their interactions with the Gα protein. Non-canonical RGS proteins (such as p113RhoGEF, Fig. **5C**) engage the Gα protein in an effector-like manner at the α2- and α3-helix and display additional contacts in a groove between the αA helix and SwI. In contrast, canonical RGS proteins engage Gα subunits *via* their switch domains and figuratively embrace the α2 helix (Fig. **5D**). RGS family proteins do not increase the GTP hydrolysis rate of Gα proteins by contributing catalytic residues but are discussed to stabilize the switch regions, allowing a more efficient GTP hydrolysis [51]. The GTP hydrolysis reaction catalyzed by heterotrimeric G proteins was extensively reviewed elsewhere [40]. Interactions of RGS domains with $G\alpha_{i/o}$- and $G\alpha_{q/11}$ family proteins have been captured by X-ray crystallography. These structures display a mostly similar binding pose, however, some Gα

protein-RGS interactions differ from each other, *e.g.* the $G\alpha_{i3}$-RGS10 interaction does not involve SwIII, and the $G\alpha_q$-RGS2 structure features several interactions between the αH domain of the Gα protein and the RGS protein that are not present in the $G\alpha_{i3}$-RGS2 structure. Additionally, structures of the $G\alpha_{13}$ protein with rgRGS domains of RhoGEF proteins are available. The binding mode of the p113RhoGEF rgRGS domain resembles the interaction mode of canonical effector proteins and not of RGS protein family members (Fig. **5A-D**) [52-54]. Furthermore, it is known that members of the RGS protein family do not increase the nucleotide hydrolysis rate of $G\alpha_s$ or $G\alpha_{12/13}$ family proteins [23], however non-canonical RGS proteins can nevertheless act as GAPs at these Gα proteins, *e.g.* p113RhoGEF at the $G\alpha_{13}$ protein (Fig. **5C**).

In the effector protein binding region of Gα proteins, the α2 helix is relatively conserved throughout all human Gα protein subunits, while the SwIII region and the α3 helix exhibit large differences between Gα subfamilies as shown by sequence alignment (Fig. **5E**) [55]. Thus, the SwIII/α3 helix structure appears to determine subunit specificity for effector protein recognition.

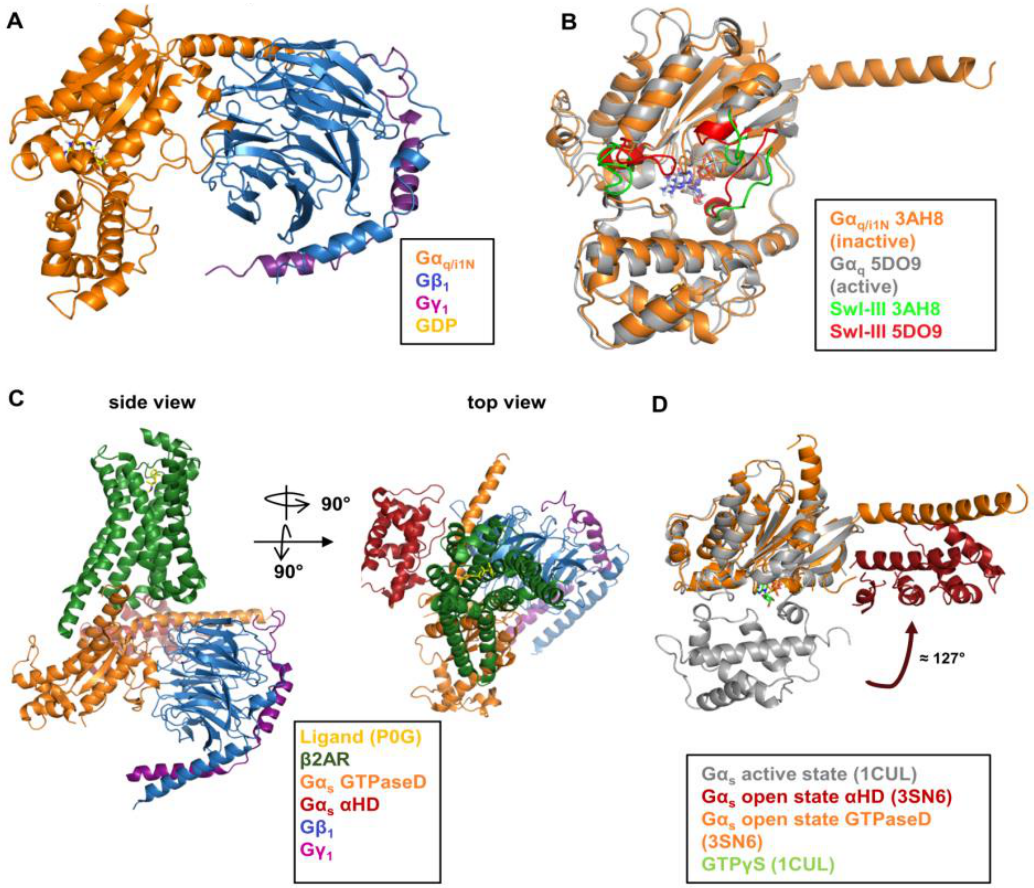

Fig. (4). Structures of heterotrimeric G proteins in guanine nucleotide-bound inactive, guanine nucleotide-bound active, and nucleotide-free states. (**A**). Structure of the inactive $G\alpha_{q/iN}\beta_1\gamma_2$ heterotrimer (PDB: 3AH8) [41] ($G\alpha_{q/iN}$ orange, $G\beta_1$ blue, $G\gamma_2$ purple, GDP yellow). (**B**). Alignment of active GDP + Mg^{2+} + AlF_4^--bound and inactive GDP-bound $G\alpha_q$ proteins, highlighting the switch regions (PDB: 3AH8 [41], 5DO9 [47]; inactive $G\alpha_{q/iN}$ orange, SwI-III green; active $G\alpha_q$ grey, SwI-III red). (**C**). β2 adrenoceptor (β_2AR)-bound nucleotide-free $G\alpha_s\beta_1\gamma_2$ heterotrimer in side view (left) and top view (right, PDB: 3SN6 [16]; β_2AR green, $G\alpha_s$ GTPase domain orange, $G\alpha_s$ αHD red, $G\beta_1$ blue, $G\gamma_2$ purple, ligand P0G yellow). (**D**). Alignment of the open state and the active state $G\alpha_s$ protein (PDB: 3SN6 [16], 1CUL [48]; open-state $G\alpha_s$ GTPase domain/αN orange, $G\alpha_s$ αHD red, active $G\alpha_s$ grey, GTPγS green), displaying a ~127° movement of the αH domain for the αN helix. (*A higher resolution / colour version of this figure is available in the electronic copy of the article*).

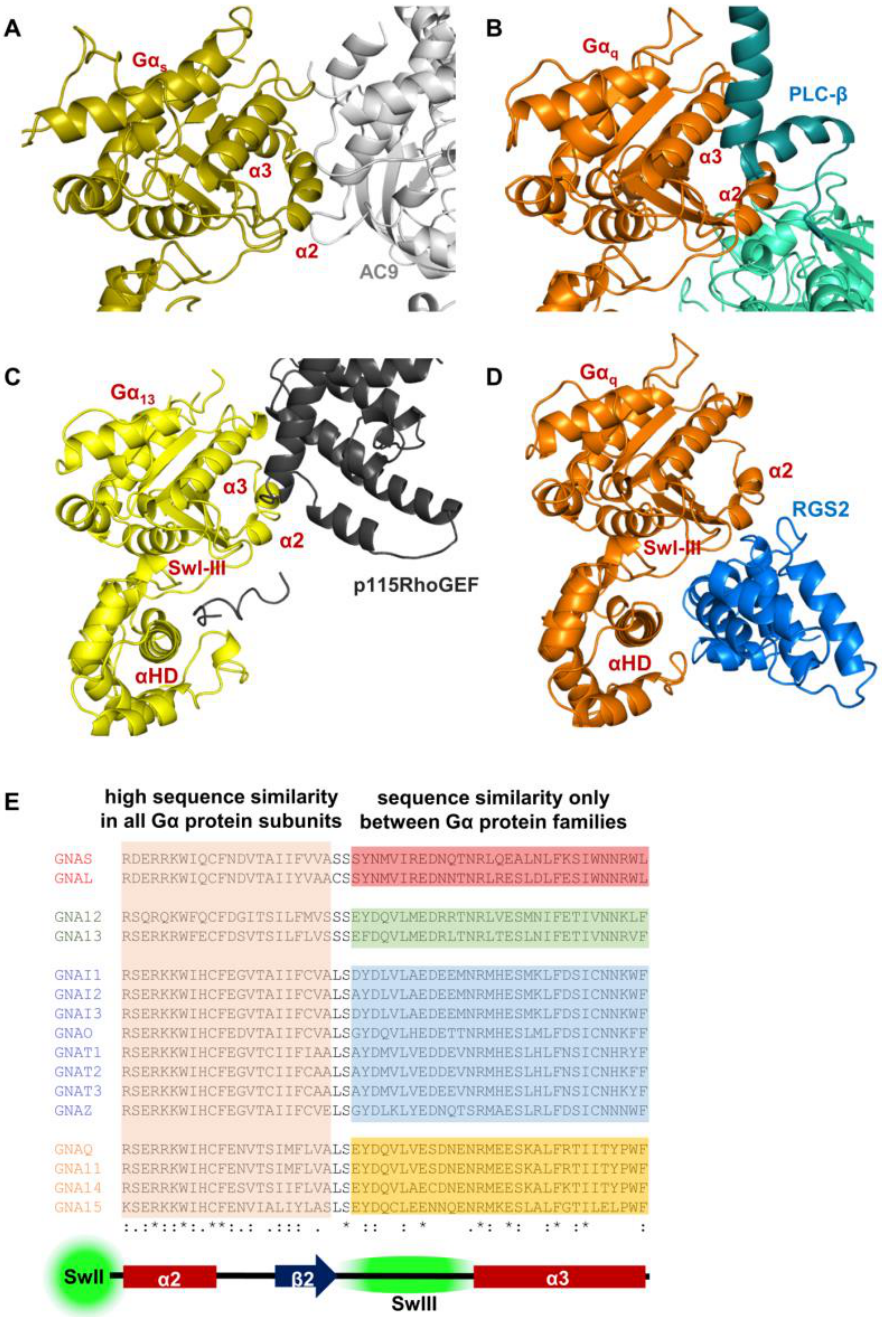

Fig. (5). Protein-protein interactions of Gα proteins with downstream interactions partners. (**A**) The active $G\alpha_s$ protein (gold) engages the AC9γ subunit (white) by interactions near the α2/3 helix in the GTPase domain of the Gα subunit (PDB: 6R3Q [52]). (**B**) The effector enzyme PLC-β (cyan) interacts with the active $G\alpha_q$ protein (orange) by insertion of a C-terminal helix--turn-helix motif (dark cyan) between the α2 and α3 helices (PDB: 4GNK [42]). (**C**) The $G\alpha_{13}$ protein (yellow) interacts with the rgRGS domain of the p115RhoGEF protein (black) at two sites: the canonical effector binding site in the α2/3 region, and a groove between the αA helix and SwI (PDB: 3AB3 [53]). (**D**) RGS proteins interact with active Gα proteins *via* a surface formed by the α2 helix, the SwI-III regions and the αA helix and the β2 sheet, as depicted in the exemplary interaction between the $G\alpha_q$ protein (orange) and the RGS2 protein (blue; PDB: 4EKD [54]). (**E**) Sequence alignment of the α2/β2/SwIII/α3 region of the human Gα protein subunits; this region is crucial for effector and RGS protein binding. Conserved residues are labeled with asterisks; residues with highly similar properties in all Gα proteins are labeled with colons; residues with moderately similar residues are labeled with dots. Human Gα protein sequences were obtained from UniProt [55]. (*A higher resolution / colour version of this figure is available in the electronic copy of the article*).

Table 1. List of published active-state (GTP- or GTP analog-bound) Gα protein structures interacting with downstream effector proteins providing information about structural elements of the Gα protein involved in effector recognition

Gα Protein	Interaction Partner	Interaction Surface	PDB-ID, Reference
$G\alpha_s$	AC9, ACII/V	α2/3 helices, α3β5 loop, SwI	6R3Q [52]; 6R4P [52]; 1CJU [56]; 1AZS [57]; 3C14 [58]; 1TL7 [59]
$G\alpha_o$	RGS16	αA helix, α2, β2, Sw I, SwII, SwIII	3C7K [60]
$G\alpha_{i1}$	RGS4	αA helix, αB/αC loop,α2 helix, β2 sheet, SwI, SwII, SwIII	1AGR [51]
	RGS1	β2 sheet, α2 helix, SwI, SwII, SwIII	2GTP [61]
	RGS16	β2 sheet, α2 helix, SwI, SwII, SwIII	2IK8 [61]
$G\alpha_{i3}$	RGS2	β2 sheet, α2 helix, SwI, SwII, SwIII	2V4Z [62]
	RGS10	αA helix, α2 helix, β2 sheet, SwI, SwII	2IHB [61]
	RGS8	αA helix, α2 helix, β2 sheet, SwI, SwII, SwIII	2ODE [61]
$G\alpha_{t1}$	PDE6	α2/α3 helices	7JSN [63]
	RGS9/PDE6 subunit γ	RGS9: αA/αB helices, α2 helix, β2 sheet, SwI, SwII, SwIII; PDE6: α2/α3 helices	1FQK/J [64]
$G\alpha_q$	PLC-β3	α2/3 helices, SwIII	4GNK [42]; 3OHM [65]; 4QJ3 [66]
	GRK2	α2/3 helices, Gβ	2BCJ [67]
	RGS2	αB/C loop, β2, α2, SwI, Sw II, SwIII	4EKC; 4EKD [54]
	RGS8	αB/C loop, β2, α2, SwI, Sw II, SwIII	5DO9 [47]
	p63RhoGEF	α2/3 helices	2RGN [68]
$G\alpha_{13}$	p115RhoGEF rgRGS domain, PDZRhoGEF rgRGS domain	α2/3 helices, αA helix, SwIII	3AB3 [53]; 1SHZ [13]; 3CX6-8 [69]

3. PHARMACOLOGICAL MODULATION OF HETEROTRIMERIC G PROTEINS

Activation of heterotrimeric G proteins is tightly regulated by their interaction partners and physiologically controlled in several ways. As hundreds of GPCRs converge on sixteen G proteins which then interact with a larger number of intracellular binding partners, pharmaceutical intervention on the G protein level appears promising for the treatment of multifactorial diseases. However, it would require selective targeting of certain subunits that play a role in specific tissues. Besides their potential as novel drugs, selective modulators are most valuable as pharmacological tool compounds. So far, only a few modulators of heterotrimeric G proteins are known, most of which are natural products, and none of which interacts with $G\alpha_{12/13}$ subunits [70, 71]. A straightforward pharmacological approach would be the development of guanine nucleotide-competitive inhibitors that could either stabilize an active or an inactive state of a certain G protein. A challenging obstacle for guanine nucleotide competitors is the high (nearly millimolar) concentration of free guanine nucleotides present in the cytoplasm [17], along with the high affinity of Gα proteins for guanine nucleotides (K_D for GTPγS at recombinant $G\alpha_s$ protein purified from *E. coli* ca. 100 nM; K_D < 1 nM at transducins in rod outer segment membranes [72, 73]). Therefore, extremely potent competitors would be required. During the development of ATP-competitive protein kinase inhibitors, a similar problem had to be overcome; however, the affinity of most protein kinases for their co-substrate ATP is only in the high micromolar to millimolar range compared to low millimolar intracellular ATP concentrations [74]. Moreover, most of the guanine nucleotide-binding residues of Gα proteins are highly conserved, which limits the possibility to achieve selectivity for a specific subunit [40]. Alternative approaches to modulate G protein activity target protein-protein interactions of the Gα protein subunit include, *e.g.,* (i) inhibiting interactions of G proteins with GPCRs, (ii) modulating nucleotide exchange, (iii) blocking interactions of G proteins with their effectors, and (iv) activating or inhibiting GTP hydrolysis. In the following sections, we highlight these four different pharmacological mechanisms for the modulation of Gα protein activation (for a list of discussed compounds see Table **2**; peptide sequences are listed in Table **3**, chemical structures of the small molecule are depicted in Fig. **6**).

3.1. Inhibition of GPCR-Gα Protein Recognition

Manipulation of GPCR-G protein interaction can be achieved by pertussis toxin (PTX), a bacterial exotoxin produced by *Bordetella pertussis*. It consists of two large subunits, A and B, the A component possessing enzymatic activity, and the B subunit being responsible for cell membrane receptor binding and cellular uptake. PTX is activated in the cells, possibly by glutathion or other reducing thiols, and catalyzes the ADP-ribosylation of a C-terminal cysteine ($C^{G.H5.23}$) residue of $G\alpha_{i/o}$ subfamily proteins (with the exception of the $G\alpha_z$ protein, where the cysteine is replaced by isoleucine). Thereby, it period and thereby irreversibly inhibits GPCR-G protein recognition arresting the $G_{i/o}$ proteins in an inactive state, resulting in *e.g.* elevated intracellular cAMP concentrations [75-77]. Since its discovery, PTX has been employed in countless studies as an inhibitor of $G_{i/o}$-activation. It proved to be extremely useful as a tool compound in pharmacological studies. Up to now, PTX is the best-established tool for the *in vitro* inhibition of heterotrimeric $G_{i/o}$ proteins.

Small molecules, such as suramin and its analogues (for structures see Fig. **6**), were described to block GPCR recognition as well, but they display low potency, interact with many other protein targets (suramin was originally developed for the treatment of African sleeping sickness), and the suramin binding site on G proteins has never been validated [78, 79]. Suramin derivatives contain multiple negative charges which hinder membrane permeation and therefore limit their utility as tool compounds. A more recent study claimed that suramin does not directly block GPCR-Gα interactions, but blocks the association of the Gα protein with the Gβγ dimer instead [80].

Peptides derived from the C-terminal part of various Gα protein subunits were used to stabilize active GPCR states. They were shown to affect GPCR-ligand binding affinity, and were found to compete with G proteins for their binding to the active conformation of GPCRs, thereby effectively blocking downstream signaling [81-85]. Conversely, the substance P analogues GPAnt-1-4 were found to block receptor activation-induced GTP hydrolysis in $G_{i/o}$ and G_s proteins by competing with the ligand-activated receptor at concentrations of 10 μM [86].

A well-known issue with peptidic inhibitors is their low membrane permeability and limited metabolic stability hindering their use in living cells or animal models. Most peptidic inhibitors were characterized using membrane preparations, permeabilized cells, or purified proteins, and they may facilitate further mechanistic studies in such systems. Technological advances, such as peptide lipidation in pepducins, have been applied to target intracellular sites of GPCRs and may also prove useful for targeting G proteins [87, 88].

3.2. Compounds Affecting Nucleotide Exchange

Activation of a GPCR typically results in nucleotide exchange from GDP to GTP, which constitutes the rate-limiting step in G protein activation [89, 90]. This process can be inhibited by natural products of the chromodepsin family, produced by bacteria. The most potent $G\alpha_q$ protein inhibitors from this class of compounds are the macrocylic depsipeptides YM-254890 (YM), isolated from *Chromobacterium sp. QS3666* [91, 92], and FR900359 (FR), produced by the plant endosymbiont *Cand. burkholderia crenata* [93, 94]. Both compounds are potent and selective nucleotide exchange inhibitors that are selective for the members of the $G\alpha_q$ subfamily, $G\alpha_q$, $G\alpha_{11}$, and $G\alpha_{14}$, but are much weaker or even inactive at $G\alpha_{15/16}$ and at the other Gα protein subfamilies. The cyclic compounds with a molecular mass of around 1000 g/mol bind to the SwI/linker 1 region of the Gα protein and thereby prevent domain separation, trapping the $G\alpha_q$ family proteins in an inactive, GDP-bound state [41]. Biosynthesis, ecological aspects, pharmacology, and applications were recently reviewed [70, 95]. In the last years, both $G\alpha_q$ protein inhibitors have sparked great interest and have been established as biochemical tools to probe $G\alpha_{q/11/14}$ activity [29, 96, 97]. Initial pharmacological studies suggested similar potencies and an identical mode of action [98]. However, FR displays a significantly longer residence time at the $G\alpha_q$ protein as compared to YM, which was shown to translate into a much longer lasting *in vivo* activity [99-101]. YM and its somewhat more lipophilic analog FR display different tissue distribution upon application in mice, and FR is metabolized faster than YM by liver microsomes, and is therefore metabolically less stable [100, 102]. To further allow biochemical studies with both compounds on insensitive Gα proteins, their binding site was transferred to $G\alpha_{15/16}$ and $G\alpha_s$ proteins [103, 104].

Total synthesis of both natural products as well as a series of derivatives and analogs was achieved, however, none of the synthetic compounds exceeded the potency of the parent drugs [105-107]. Analogs of FR have also been obtained by extraction from the plant *A. crenata* and some of them were found to be similarly potent as FR [108], while the intermediate product designated FR-core, which is lacking a crucial side-chain, was significantly less potent [93].

In a competition binding assay versus the radiolabeled FR derivative [^{3}H]PSB-15900, obtained by hydrogenation of FR with tritium gas, the small molecule Ebselen (see Fig. **6**), a cysteine-reactive drug, was identified as a screening hit; it was shown to inhibit G_q protein-mediated effects in recombinant cells as well as in native brown adipocytes [99].

The amphiphilic 26-residue peptide mellitin, a major component of bee venom, was suggested to inhibit GDP release during nucleotide turnover at $G\alpha_s$ proteins at concentrations exceeding 10 μM, however, it was also found to have a stimulatory effect on $G\alpha_{11}$ and $G\alpha_{i1}$ proteins [109, 110]. There are also indications of a direct stimulation of $G\alpha_q$ proteins by mellitin [111]. Besides mellitin and mastoparan (see section 3.4), no further peptides isolated from animal venoms have been described to affect heterotrimeric G proteins.

Nucleotide exchange can also be facilitated by non-receptor guanine nucleotide exchange factors (GEFs), promoting an active state of heterotrimeric G proteins: the GIV/Girdin-protein binds to the SwII region (the G protein binding motif was co-crystallized with the $G\alpha_{i3}$ protein; PDB-ID: 6MHF) of $G_{i/o}$ family proteins and destabilizes the high-affinity state for GDP binding of the SwII region, ultimately resulting in an allosteric destabilization of the hydrophobic core of the $G\alpha_i$ protein, and in GDP dissociation [112, 113]. Similarly, the heterotrimeric G_i protein can be "activated" by proteins bearing the GoLoco motif. This 19-amino acid motif inserts into the groove between the α2/α3 helices and additionally interacts with the αH domain leading to Gβγ dissociation in the absence of GPCR activation [114]. Ric8, another protein with observed GEF activity [115], was lately suggested to act as a chaperone for Gα proteins [116].

The small, peptide-derived heterocyclic molecules BIM-46174, a thiol derivative, and its oxidized, dimeric disulfide BIM-46187 (see Fig. **6**) were demonstrated to directly bind and functionally inhibit $G\alpha_q$ proteins [117, 118]. In contrast to YM and FR, both BIM compounds are predicted to trap the $G\alpha_q$ protein in a nucleotide-free state [119]. These compounds may react with free cysteine residues, putatively $C330^{G.s6h5.2}$. Relatively high concentrations (30-100 μM) of the compounds are required for inhibition of the $G\alpha_q$ protein in IP_1 accumulation assays. The BIM compounds do not compete with YM and FR for their binding site [99]. The synthesis of a series of BIM analogs revealed that a basic function (at the N-terminus of the cysteine residue), a redox-reactive thiol/disulfide substructure, a cyclohexyl-alanine moiety, and a bicyclic scaffold are required for G protein inhibition [120, 121]. Unfortunately, several compounds of the series displayed cytotoxicity affecting cytoskeletal dynamics independent of their effect on the $G\alpha_q$ protein [121].

3.3. Competition With Downstream Gα Protein Interaction Partners

A further approach towards G protein modulation is the blockade of specific G protein-effector interactions. Specific interactions between a Gα protein subunit and a particular effector are blocked resulting in a finely tuned pharmacological intervention. However, due to the shared effector and RGS protein binding sites (see Fig. **5A-D**), the effects may be less specific than expected. To date, only a few peptidic inhibitors have been developed using this approach.

A compound designated "27-mer", a peptide consisting of 27 amino acid residues, derived from the G protein-binding domain of PLC-β [122], blocks the interaction between the $G\alpha_q$ protein and PLC-β, and was shown to block $G\alpha_q$-mediated p63RhoGEF activation in recombinant cells and mouse brain slices.

Several peptides binding to the SwII/α3 region of $G\alpha_i$ and $G\alpha_s$ proteins were developed using a phage display approach. Some of these peptides, *e.g.* KB-1753, were co-crystallized with a GDP-AlF_4^--activated $G\alpha_{i1}$ protein (PDB-ID: 2G83) to determine their binding site. KB-1753 was found to compete with effector molecules, such as a phosphodiesterase γ-derived peptide at the $G\alpha_t$ protein [123].

Another inhibitor, designated GsIN-1, is a cell-permeable macrocyclic compound identified in a large library screening of cyclic peptides as an active state $G\alpha_s$ inhibitor, binding to a pocket located in the SwI-I/α2/α3 region, and thereby blocking AC binding to the $G\alpha_s$ protein with a potency of ca. 1 μM. A co-crystal structure of GsIN-1 and the $G\alpha_s$ protein is available (PDB-ID: 7BPH) [124].

3.4. Modulation of Intrinsic GTPase Activity

Another conceivable approach to affect heterotrimeric G protein function is the modulation of the GTP hydrolysis rate. The variety of natural RGS proteins and of effector proteins that increase the GTP hydrolysis rate of Gα proteins demonstrates that termination of G protein signaling is physiologically essential [23]. Besides RGS proteins, the wasp venom peptide mastoparan (and further cationic amphiphilic substances and lipoamines) were found to increase GTP hydrolysis rates and to additionally increase the dissociation rate of the formed GDP,

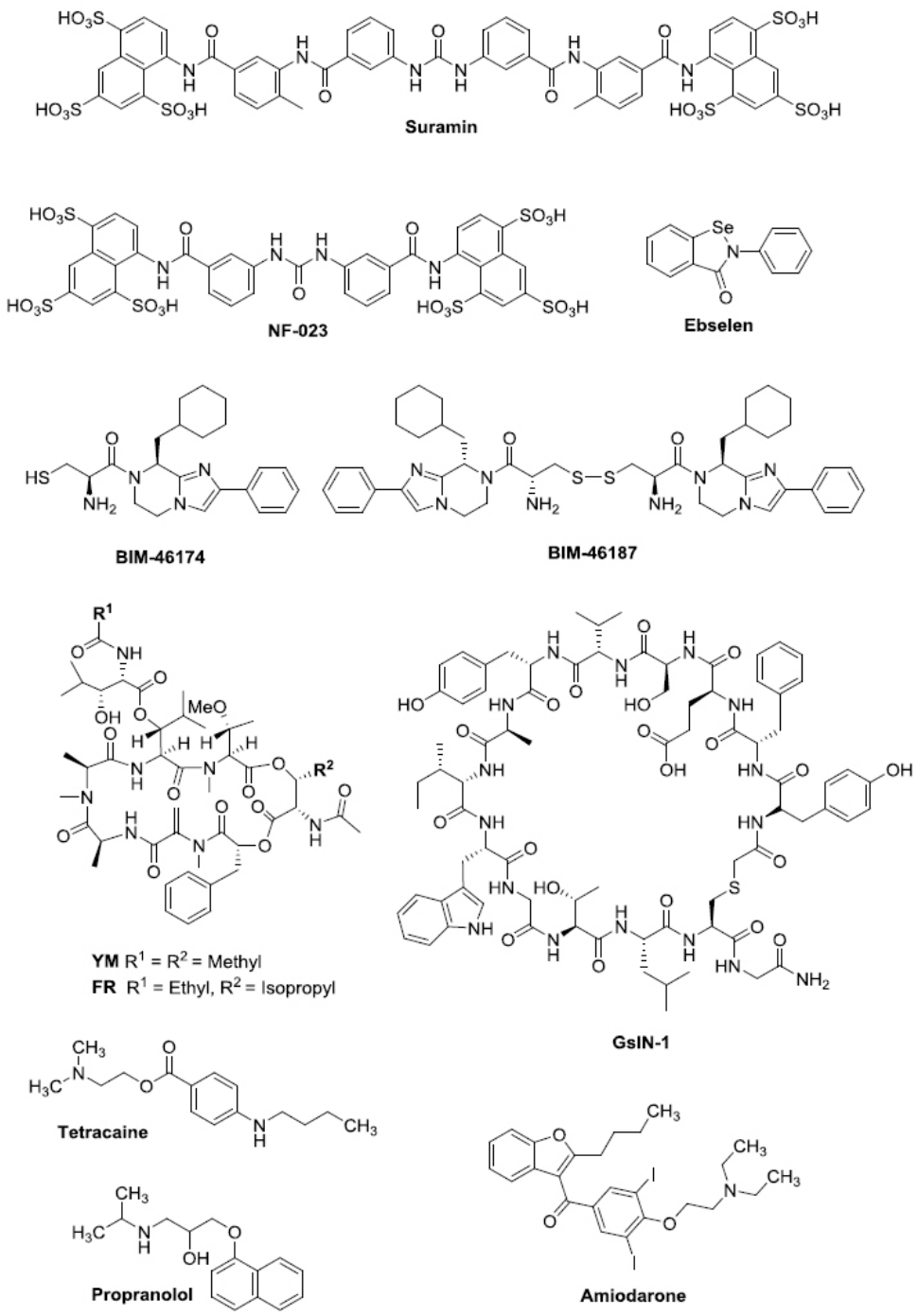

Fig. (6). Chemical structures of small molecule modulators of Gα proteins.

thereby effectively increasing GTP turnover [110, 125-127]. Some approved drugs, such as amiodarone, tetracaine, and other local anesthetics, as well as propranolol and other β-blockers, were found to directly stimulate GTPase activity of PTX-sensitive G proteins [128, 129]. However, none of these compounds were established as tool compounds for pharmacological research, probably due to their only low potency typically in the micromolar range, as well as their lacking selectivity.

A prominent modulator of Gα protein GTPase activity is the bacterial toxin cholera toxin (CTX). CTX spe-

cifically ADP-ribosylates an arginine residue ($R^{G.hfs.2.2}$) of the $G\alpha_s$ protein, but unlike PTX, it renders the $G\alpha_s$ subunit unable to hydrolyze GTP and therefore traps it in its active state. Similar to the $G\alpha_{i/o}$ protein inhibitor PTX, this results in an increasing intracellular cAMP concentration [130].

Currently, none of the listed compounds that increase or decrease GTP hydrolysis rate appear to be used as tool compounds probably due to their low potency and unknown selectivity. Nevertheless, this approach seems promising for selective Gα protein modulation, *e.g.* by developing a compound that exclusively blocks the RGS protein binding site of a certain Gα protein subunit. Similarly, efforts are made to develop selective RGS protein inhibitors to modulate signaling *via* certain Gα protein subunits. O'Brien *et al.* published a recent review on current RGS protein inhibitor development [131].

Table 2. List of peptidic compounds and small molecules directly modulating Gα protein activity, grouped by their target G protein. Established tool compounds are highlighted in blue.

Compound	Effect	Comments
	$G\alpha_{i/o}$	
PTX	Bacterial AB toxin catalyzing covalent ADP-ribosylation of a C-terminal cysteine residue of $G\alpha_{i/o}$-family proteins (exception: $G\alpha_z$), which blocks GPCR-G protein interactions [75, 132].	A well-established tool of historical importance for the characterization of G protein and GPCR function. It is however costly period. Assay protocols frequently require overnight incubation. Typical assay concentration: 100 ng/ml.
KB-1753	Peptide binding the SwII/α3 region of active $G\alpha_{i1}$ and $G\alpha_t$ proteins competing with effector molecules. KB-752, identified in a related study, displays specificity for the GDP-bound $G\alpha_t$ state [123, 133].	Crystal structures are available; in related studies, the authors synthesized a series of G protein-binding peptides.
Tetracain (and other local anesthetics)	Local anesthetic, which was found to directly activate GTP-ase activity [128].	The cationic amphiphilic structure apparently promotes direct GTP-ase stimulation. Low potency and debatable pharmacological relevance as local anesthetics target voltage-gated sodium channels.
Lipoamines	Direct stimulation of GTPase activity with low potency, possibly binding to a C-terminal region of the Gα protein [127].	The cationic amphiphilic structure apparently promotes direct GTP-ase stimulation.
Amiodarone	Approved antiarrhythmic drug, which directly activates GTPase activity [129].	The cationic amphiphilic structure apparently promotes direct GTP-ase stimulation. Low potency and debatable pharmacological relevance; amiodarone targets voltage-gated calcium and potassium channels.
Propranolol (and other β-blockers)	**B**-blocker, which was found to directly activa GTP-ase activity [128].	The cationic amphiphilic structure apparently promotes direct GTP-ase stimulation. Far more potent at β-adrenoceptors.
	$G\alpha_q$	
FR900359 (FR)	Macrocyclic depsipeptide, which acts as $G\alpha_{q/11/14}$-selective guanine nucleotide dissociation inhibitor, highly potent [98].	Selective and highly potent $G\alpha_q$ protein inhibitor employed in several pharmacological studies. A large body of work has been performed on its mechanism of action. Similar structure as YM and identical mechanism of action; long target residence time [99, 101], but more rapid metabolization [100].
YM-254890 (YM)	Macrocyclic depsipeptide, which acts as $G\alpha_{q/11/14}$-selective guanine nucleotide dissociation inhibitor, highly potent [91, 92].	Commercially available, selective, and potent $G\alpha_q$ protein inhibitor employed in several pharmacological studies. Co-crystal structure with the heterotrimeric $G\alpha_q$ protein available. Similar structure as FR and identical mechanism of action; short target residence time [99].
27mer	A 27-amino acid peptide derived from PLC-β; competes with other effector proteins for the $G\alpha_q$ binding site. Two mutations within the peptide sequence (Ile860Ala, Met869Nle (Nle = norleucine)) further increased the affinity by 10-fold (K_D of 0.4 nM) [122].	Potent *in vitro* tool to block $G\alpha_q$ downstream signaling without affecting nucleotide-binding/turnover of the $G\alpha_q$ protein.

(Table 2) contd....

Compound	Effect	Comments
BIM-46174 and BIM-46187	Small molecules with cysteine-reactive moieties predicted to trap $G\alpha_q$ proteins in a nucleotide-free state [119].	Commercially available; BIM and analogs display low potency (> 10 μM) and significant cytotoxicity.
Ebselen	Small cysteine-reactive molecule; blocks $G\alpha_q$ signaling in recombinant and native cells [99].	Irreversible binder displaces labeled FR and YM analogues from their binding site. Its binding site is still unknown. Not selective; interactions with several further proteins described.
$G\alpha_s$		
CTX	Bacterial AB toxin catalyzes covalent ADP-ribosylation of $G\alpha_s$ proteins, disabling their GTPase activity and thus keeping the protein in an active state [130].	Hyperactivation of $G\alpha_s$ protein leads to a similar phenotype as PTX- mediated $G\alpha_{i/o}$-inhibition: intracellular cAMP accumulation. Assay protocols often require overnight incubation.
GsIN-1	Cyclic peptide specifically blocks the interaction between the activated $G\alpha_s$ protein and its downstream effectors [124].	The utility of the inhibitor is still unclear; interesting lead for further optimization.
Multiple Gα proteins		
Mastoparan	Wasp venom peptide; increases nucleotide turnover by promoting GTP hydrolysis and GDP dissociation [111, 125].	Occasionally used in pharmacological studies as G protein activator
Mellitin	Bee venom peptide; suggested to inhibit GDP dissociation, but also found to stimulate $G\alpha_{i1}/G\alpha_{11}/G\alpha_q$ activity [109, 111].	Contradictory results have been published; not selective.
Substance P analogues (GPAnt-1-4)	Inhibit the G protein by competition with the receptor as demonstrated in reconstituted vesicles [86].	Rather low potency (applied concentration: 10 μM); only a single publication describes its use.
Suramin and analogues	Small molecules with multiple negative charges predicted to either block GPCR-Gα protein recognition or to block the association of Gα and βγ-subunits [78-80].	Some analogues display Gα subtype selectivity; the binding site is unknown, and mechanism of action is debated; non-selective since they are also acting on several other proteins.

Table 3. Primary sequences of peptidic G protein modulators (Nle = norleucine, pGlu= pyroglutamic acid).

Name	Sequence
27mer	His - Gln - Asp - Tyr - Ala - Glu - Ala - Leu - Ile - Asn - Pro - Ile - Lys - His - Val - Ser - Leu - Met - Asp - Gln - Arg - Ala - Arg - Gln - Leu - Ala - Ala
27mer (I860A)	His - Gln - Asp - Tyr - Ala - Glu - Ala - Leu - Ala - Asn - Pro - Ile - Lys - His - Val - Ser - Leu - Nle - Asp - Gln - Arg - Ala - Arg - Gln - Leu - Ala - Al
KB-752	Ser - Arg - Val - Thr - Trp - Tyr - Asp - Phe - Leu - Met - Glu - Asp - Thr - Lys - Ser - Arg
KB-1753	Ser - Ser - Arg - Gly - Tyr - Tyr - His - Gly - Ile - Trp - Val - Gly - Glu - Glu - Gly - Arg - Leu - Ser - Arg
Mastoparan	Ile - Asn - Leu - Lys - Ala - Leu - Ala - Ala - Leu - Ala - Lys - Lys - Ile - Leu - NH2
Mellitin	Gly - Ile - Gly - Ala - Val - Leu - Lys - Val - Leu - Thr - Thr - Gly - Leu - Pro - Ala - Leu - Ile - Ser - Trp - Ile - Lys - Arg - Lys - Arg - Gln - Gln
GPAnt-1	D-Pro - Gln - Gln - D-Trp - Phe - D-Trp - D-Trp - Met - NH_2
GPAnt-2	pGlu - Gln - D-Trp - Phe - D-Trp - D-Trp - Met - NH_2
GPAnt-3	Gln - Gln - D-Trp - Phe - D-Trp - D-Trp - Met - NH_2
GPAnt-4	Ac - Gln - Gln - D-Trp - Phe - D-Trp - D-Trp - Met - NH_2

CONCLUSION

GPCR signaling converges on the level of G proteins, which trigger intracellular signaling cascades upon activation. G proteins are largely conserved in structure and function, but the interactions with GPCRs and with downstream effector proteins vary between individual Gα protein subunits. The plentitude and specifici-

ty of interactions active Gα proteins highlight the physiological importance and careful regulation of G protein activation. However, only a few Gα protein modulators, namely PTX ($G\alpha_i$ inhibitor), CTX ($G\alpha_s$ activator), and FR and YM (both $G\alpha_q$ inhibitors) have become established tool compounds to study G protein function and GPCR signaling cascades, due to their high potency, G protein subtype selectivity, and applicability in cellular assays. Despite the development of novel assay techniques to investigate GPCR-G protein coupling [29, 30, 134], there is still a huge demand for tool compounds activating or inhibiting heterotrimeric G protein subunits, as demonstrated by the tremendous recent interest in the $G\alpha_q$ protein inhibitors FR and YM, and by their rapid establishment in pharmacological research. Novel tool compounds would allow the scientific community to further investigate coupling events and downstream signaling of individual G protein subunits, especially of understudied subunits, *e.g.* the $G\alpha_{15}$ or $G\alpha_{12/13}$ proteins. Besides peptides and peptidomimetics, macrocyclic compounds appear promising due to their often high membrane permeability enabling their use in living cells and animal models, and also due to their potential to block protein-protein interactions by being able to target shallow, lipophilic binding sites.

CONSENT FOR PUBLICATION

Not applicable.

FUNDING

The work was supported by a research grant from the Deutsche Forschungsgemeinschaft (DFG), grant number MU-1665/7-2.

CONFLICT OF INTEREST

The authors declare no conflict of interest, financial or otherwise.

ACKNOWLEDGEMENTS

Declared none.

REFERENCES

[1] Milligan, G.; Kostenis, E. Heterotrimeric G-proteins: A short history. *Br. J. Pharmacol.,* **2006**, *147*(Suppl. 1), S46-S55. http://dx.doi.org/10.1038/sj.bjp.0706405 PMID: 16402120

[2] Chua, V.; Lapadula, D.; Randolph, C.; Benovic, J.L.; Wedegaertner, P.B.; Aplin, A.E. Dysregulated GPCR signaling and therapeutic options in uveal melanoma. *Mol. Cancer Res.,* **2017**, *15*(5), 501-506. http://dx.doi.org/10.1158/1541-7786.MCR-17-0007 PMID: 28223438

[3] Robertson, A.G.; Shih, J.; Yau, C.; Gibb, E.A.; Oba, J.; Mungall, K.L.; Hess, J.M.; Uzunangelov, V.; Walter, V.; Danilova, L.; Lichtenberg, T.M.; Kucherlapati, M.; Kimes, P.K.; Tang, M.; Penson, A.; Babur, O.; Akbani, R.; Bristow, C.A.; Hoadley, K.A.; Iype, L.; Chang, M.T.; Cherniack, A.D.; Benz, C.; Mills, G.B.; Verhaak, R.G.W.; Griewank, K.G.; Felau, I.; Zenklusen, J.C.; Gershenwald, J.E.; Schoenfield, L.; Lazar, A.J.; Abdel-Rahman, M.H.; Roman-Roman, S.; Stern, M-H.; Cebulla, C.M.; Williams, M.D.; Jager, M.J.; Coupland, S.E.; Esmaeli, B.; Kandoth, C.; Woodman, S.E. Integrative analysis identifies four molecular and clinical subsets in uveal melanoma. *Cancer Cell,* **2017**, *32*(2), 204-220.e15. http://dx.doi.org/10.1016/j.ccell.2017.07.003 PMID: 28810145

[4] Oldham, W.M.; Hamm, H.E. Heterotrimeric G protein activation by G-protein-coupled receptors. *Nat. Rev. Mol. Cell Biol.,* **2008**, *9*(1), 60-71. http://dx.doi.org/10.1038/nrm2299 PMID: 18043707

[5] Pfeil, E.M.; Brands, J.; Merten, N.; Vögtle, T.; Vescovo, M.; Rick, U.; Albrecht, I-M.; Heycke, N.; Kawakami, K.; Ono, Y.; Ngako Kadji, F.M.; Hiratsuka, S.; Aoki, J.; Häberlein, F.; Matthey, M.; Garg, J.; Hennen, S.; Jobin, M-L.; Seier, K.; Calebiro, D.; Pfeifer, A.; Heinemann, A.; Wenzel, D.; König, G.M.; Nieswandt, B.; Fleischmann, B.K.; Inoue, A.; Simon, K.; Kostenis, E.; Heterotrimeric, G. Heterotrimeric G protein subunit Gαq is a master switch for Gβγ-mediated calcium mobilization by Gi-coupled GPCRs. *Mol. Cell,* **2020**, *80*(6), 940-954.e6. http://dx.doi.org/10.1016/j.molcel.2020.10.027 PMID: 33202251

[6] Masuho, I.; Skamangas, N.K.; Muntean, B.S.; Martemyanov, K.A. Diversity of the Gβγ complexes defines spatial and temporal bias of GPCR signaling. *Cell Syst.,* **2021**, *12*(4), 324-337.e5. http://dx.doi.org/10.1016/j.cels.2021.02.001 PMID: 33667409

[7] Latorraca, N.R.; Venkatakrishnan, A.J.; Dror, R.O. GPCR dynamics: Structures in motion. *Chem. Rev.,* **2017**, *117*(1), 139-155. http://dx.doi.org/10.1021/acs.chemrev.6b00177 PMID: 27622975

[8] Hilger, D.; Masureel, M.; Kobilka, B.K. Structure and dynamics of GPCR signaling complexes. *Nat. Struct. Mol. Biol.,* **2018**, *25*(1), 4-12. http://dx.doi.org/10.1038/s41594-017-0011-7 PMID: 29323277

[9] Simon, M.I.; Strathmann, M.P.; Gautam, N. Diversity of G proteins in signal transduction. *Science,* **1991**, *252*(5007), 802-808. http://dx.doi.org/10.1126/science.1902986 PMID: 1902986

[10] Offermanns, S.; Simon, M.I. G alpha 15 and G alpha 16 couple a wide variety of receptors to phospholipase C. *J. Biol. Chem.,* **1995**, *270*(25), 15175-15180. http://dx.doi.org/10.1074/jbc.270.25.15175 PMID: 7797501

[11] Taylor, S.J.; Chae, H.Z.; Rhee, S.G.; Exton, J.H. Activation of the beta 1 isozyme of phospholipase C by alpha subunits of the Gq class of G proteins. *Nature,* **1991**, *350*(6318), 516-518. http://dx.doi.org/10.1038/350516a0 PMID: 1707501

[12] Suzuki, N.; Hajicek, N.; Kozasa, T. Regulation and physiological functions of G12/13-mediated signaling pathways. *Neurosignals,* **2009**, *17*(1), 55-70.

http://dx.doi.org/10.1159/000186690 PMID: 19212140

[13] Chen, Z.; Singer, W.D.; Sternweis, P.C.; Sprang, S.R. Structure of the p115RhoGEF rgRGS domain-Galpha13/i1 chimera complex suggests convergent evolution of a GTPase activator. *Nat. Struct. Mol. Biol.,* **2005**, *12*(2), 191-197. http://dx.doi.org/10.1038/nsmb888 PMID: 15665872

[14] Sánchez-Fernández, G.; Cabezudo, S.; García-Hoz, C.; Benincá, C.; Aragay, A.M.; Mayor, F., Jr; Ribas, C. Gαq signalling: The new and the old. *Cell. Signal.,* **2014**, *26*(5), 833-848. http://dx.doi.org/10.1016/j.cellsig.2014.01.010 PMID: 24440667

[15] Wall, M.A.; Coleman, D.E.; Lee, E.; Iñiguez-Lluhi, J.A.; Posner, B.A.; Gilman, A.G.; Sprang, S.R. The structure of the G protein heterotrimer Gi alpha 1 beta 1 gamma 2. *Cell,* **1995**, *83*(6), 1047-1058. http://dx.doi.org/10.1016/0092-8674(95)90220-1 PMID: 8521505

[16] Rasmussen, S.G.F.; DeVree, B.T.; Zou, Y.; Kruse, A.C.; Chung, K.Y.; Kobilka, T.S.; Thian, F.S.; Chae, P.S.; Pardon, E.; Calinski, D.; Mathiesen, J.M.; Shah, S.T.A.; Lyons, J.A.; Caffrey, M.; Gellman, S.H.; Steyaert, J.; Skiniotis, G.; Weis, W.I.; Sunahara, R.K.; Kobilka, B.K. Crystal structure of the β2 adrenergic receptor-Gs protein complex. *Nature,* **2011**, *477*(7366), 549-555. http://dx.doi.org/10.1038/nature10361 PMID: 21772288

[17] Traut, T.W. Physiological concentrations of purines and pyrimidines. *Mol. Cell. Biochem.,* **1994**, *140*(1), 1-22. http://dx.doi.org/10.1007/BF00928361 PMID: 7877593

[18] Flock, T.; Ravarani, C.N.J.; Sun, D.; Venkatakrishnan, A.J.; Kayikci, M.; Tate, C.G.; Veprintsev, D.B.; Babu, M.M. Universal allosteric mechanism for Gα activation by GPCRs. *Nature,* **2015**, *524*(7564), 173-179. http://dx.doi.org/10.1038/nature14663 PMID: 26147082

[19] Yao, X-Q.; Malik, R.U.; Griggs, N.W.; Skjærven, L.; Traynor, J.R.; Sivaramakrishnan, S.; Grant, B.J. Dynamic coupling and allosteric networks in the α subunit of heterotrimeric G proteins. *J. Biol. Chem.,* **2016**, *291*(9), 4742-4753. http://dx.doi.org/10.1074/jbc.M115.702605 PMID: 26703464

[20] Lambright, D.G.; Noel, J.P.; Hamm, H.E.; Sigler, P.B. Structural determinants for activation of the alpha-subunit of a heterotrimeric G protein. *Nature,* **1994**, *369*(6482), 621-628. http://dx.doi.org/10.1038/369621a0 PMID: 8208289

[21] Vetter, I.R.; Wittinghofer, A. The guanine nucleotide-binding switch in three dimensions. *Science,* **2001**, *294*(5545), 1299-1304. http://dx.doi.org/10.1126/science.1062023 PMID: 11701921

[22] Mukhopadhyay, S.; Ross, E.M. Rapid GTP binding and hydrolysis by G(q) promoted by receptor and GTPase-activating proteins. *Proc. Natl. Acad. Sci. USA,* **1999**, *96*(17), 9539-9544. http://dx.doi.org/10.1073/pnas.96.17.9539 PMID: 10449728

[23] Masuho, I.; Balaji, S.; Muntean, B.S.; Skamangas, N.K.; Chavali, S.; Tesmer, J.J.G.; Babu, M.M.; Martemyanov, K.A. A global map of G protein signaling regulation by RGS proteins. *Cell,* **2020**, *183*(2), 503-521.e19. http://dx.doi.org/10.1016/j.cell.2020.08.052 PMID: 33007266

[24] Berstein, G.; Blank, J.L.; Jhon, D.Y.; Exton, J.H.; Rhee, S.G.; Ross, E.M. Phospholipase C-beta 1 is a GTPase-activating protein for Gq/11, its physiologic regulator. *Cell,* **1992**, *70*(3), 411-418. http://dx.doi.org/10.1016/0092-8674(92)90165-9 PMID: 1322796

[25] Hauser, A.S.; Attwood, M.M.; Rask-Andersen, M.; Schiöth, H.B.; Gloriam, D.E. Trends in GPCR drug discovery: new agents, targets and indications. *Nat. Rev. Drug Discov.,* **2017**, *16*(12), 829-842. http://dx.doi.org/10.1038/nrd.2017.178 PMID: 29075003

[26] Noel, J.P.; Hamm, H.E.; Sigler, P.B. The 2.2 A crystal structure of transducin-alpha complexed with GTP gamma S. *Nature,* **1993**, *366*(6456), 654-663. http://dx.doi.org/10.1038/366654a0 PMID: 8259210

[27] Holbrook, S.R.; Kim, S.H. Molecular model of the G protein alpha subunit based on the crystal structure of the HRAS protein. *Proc. Natl. Acad. Sci. USA,* **1989**, *86*(6), 1751-1755. http://dx.doi.org/10.1073/pnas.86.6.1751 PMID: 2494654

[28] Avet, C.; Mancini, A.; Breton, B.; Le Gouill, C.; Hauser, A.S.; Normand, C.; Kobayashi, H.; Gross, F.; Hogue, M.; Lukasheva, V.; Morissette, S.; Fauman, E.; Fortin, J-P.; Schann, S.; Leroy, X.; Gloriam, D.E.; Bouvier, M. Selectivity landscape of 100 therapeutically relevant GPCR profiled by an effector translocation-based BRET platform. *bioRxiv,* **2020**, *2020*, 2.

[29] Inoue, A.; Raimondi, F.; Kadji, F.M.N.; Singh, G.; Kishi, T.; Uwamizu, A.; Ono, Y.; Shinjo, Y.; Ishida, S.; Arang, N.; Kawakami, K.; Gutkind, J.S.; Aoki, J.; Russell, R.B. Illuminating G-protein-coupling selectivity of GPCRs. *Cell,* **2019**, *177*(7), 1933-1947.e25. http://dx.doi.org/10.1016/j.cell.2019.04.044 PMID: 31160049

[30] Olsen, R.H.J.; DiBerto, J.F.; English, J.G.; Glaudin, A.M.; Krumm, B.E.; Slocum, S.T.; Che, T.; Gavin, A.C.; McCorvy, J.D.; Roth, B.L.; Strachan, R.T. TRUPATH, an open-source biosensor platform for interrogating the GPCR transducerome. *Nat. Chem. Biol.,* **2020**, *16*(8), 841-849. http://dx.doi.org/10.1038/s41589-020-0535-8 PMID: 32367019

[31] Inoue, A.; Ishiguro, J.; Kitamura, H.; Arima, N.; Okutani, M.; Shuto, A.; Higashiyama, S.; Ohwada, T.; Arai, H.; Makide, K.; Aoki, J. TGFα shedding assay: An accurate and versatile method for detecting GPCR activation. *Nat. Methods,* **2012**, *9*(10), 1021-1029. http://dx.doi.org/10.1038/nmeth.2172 PMID: 22983457

[32] Milligan, G.; Grassie, M.A. How do G-proteins stay at the plasma membrane? *Essays Biochem.,* **1997**, *32*, 49-60. PMID: 9493010

[33] Lyon, A.M.; Taylor, V.G.; Tesmer, J.J.G. Strike a pose: Gαq complexes at the membrane. *Trends Pharmacol. Sci.,* **2014**, *35*(1), 23-30. http://dx.doi.org/10.1016/j.tips.2013.10.008 PMID: 24287282

[34] Wedegaertner, P.B.; Wilson, P.T.; Bourne, H.R. Lipid modifications of trimeric G proteins. *J. Biol. Chem.,* **1995**, *270*(2), 503-506. http://dx.doi.org/10.1074/jbc.270.2.503 PMID: 7822269

[35] Maeda, S.; Qu, Q.; Robertson, M.J.; Skiniotis, G.; Kobilka, B.K. Structures of the M1 and M2 muscarinic acetylcholine receptor/G-protein complexes. *Science,* **2019**, *364*(6440), 552-557. http://dx.doi.org/10.1126/science.aaw5188 PMID: 31073061

[36] Calebiro, D.; Koszegi, Z.; Lanoiselée, Y.; Miljus, T.; O'Brien, S. G protein-coupled receptor-G protein interactions: A single-molecule perspective. *Physiol. Rev.,* **2021**, *101*(3), 857-906. http://dx.doi.org/10.1152/physrev.00021.2020 PMID: 33331229

[37] Jang, W.; Adams, C.E.; Liu, H.; Zhang, C.; Levy, F.O.; Andressen, K.W.; Lambert, N.A. An inactive receptor-G protein complex maintains the dynamic range of agonist-induced signaling. *Proc. Natl. Acad. Sci. USA,* **2020**, *117*(48), 30755-30762. http://dx.doi.org/10.1073/pnas.2010801117 PMID: 33199589

[38] Nobles, M.; Benians, A.; Tinker, A. Heterotrimeric G proteins precouple with G protein-coupled receptors in living cells. *Proc. Natl. Acad. Sci. USA,* **2005**, *102*(51), 18706-18711. http://dx.doi.org/10.1073/pnas.0504778102 PMID: 16352729

[39] Coleman, D.E.; Berghuis, A.M.; Lee, E.; Linder, M.E.; Gilman, A.G.; Sprang, S.R. Structures of active conformations of Gi alpha 1 and the mechanism of GTP hydrolysis. *Science,* **1994**, *265*(5177), 1405-1412. http://dx.doi.org/10.1126/science.8073283 PMID: 8073283

[40] Sprang, S.R. Invited review: Activation of G proteins by GTP and the mechanism of Gα-catalyzed GTP hydrolysis. *Biopolymers,* **2016**, *105*(8), 449-462. http://dx.doi.org/10.1002/bip.22836 PMID: 26996924

[41] Nishimura, A.; Kitano, K.; Takasaki, J.; Taniguchi, M.; Mizuno, N.; Tago, K.; Hakoshima, T.; Itoh, H. Structural basis for the specific inhibition of heterotrimeric Gq protein by a small molecule. *Proc. Natl. Acad. Sci. USA,* **2010**, *107*(31), 13666-13671. http://dx.doi.org/10.1073/pnas.1003553107 PMID: 20639466

[42] Lyon, A.M.; Dutta, S.; Boguth, C.A.; Skiniotis, G.; Tesmer, J.J.G. Full-length Gα(q)-phospholipase C-β3 structure reveals interfaces of the C-terminal coiled-coil domain. *Nat. Struct. Mol. Biol.,* **2013**, *20*(3), 355-362. http://dx.doi.org/10.1038/nsmb.2497 PMID: 23377541

[43] Maziarz, M.; Leyme, A.; Marivin, A.; Luebbers, A.; Patel, P.P.; Chen, Z.; Sprang, S.R.; Garcia-Marcos, M. Atypical activation of the G protein $G\alpha_q$ by the oncogenic mutation Q209P. *J. Biol. Chem.,* **2018**, *293*(51), 19586-19599. http://dx.doi.org/10.1074/jbc.RA118.005291 PMID: 30352874

[44] Van Raamsdonk, C.D.; Griewank, K.G.; Crosby, M.B.; Garrido, M.C.; Vemula, S.; Wiesner, T.; Obenauf, A.C.; Wackernagel, W.; Green, G.; Bouvier, N.; Sozen, M.M.; Baimukanova, G.; Roy, R.; Heguy, A.; Dolgalev, I.; Khanin, R.; Busam, K.; Speicher, M.R.; O'Brien, J.; Bastian, B.C. Mutations in GNA11 in uveal melanoma. *N. Engl. J. Med.,* **2010**, *363*(23), 2191-2199. http://dx.doi.org/10.1056/NEJMoa1000584 PMID: 21083380

[45] Zhang, M.; Gui, M.; Wang, Z-F.; Gorgulla, C.; Yu, J.J.; Wu, H.; Sun, Z.J.; Klenk, C.; Merklinger, L.; Morstein, L.; Hagn, F.; Plückthun, A.; Brown, A.; Nasr, M.L.; Wagner, G. Cryo-EM structure of an activated GPCR-G protein complex in lipid nanodiscs. *Nat. Struct. Mol. Biol.,* **2021**, *28*(3), 258-267. http://dx.doi.org/10.1038/s41594-020-00554-6 PMID: 33633398

[46] García-Nafría, J.; Tate, C.G. Cryo-EM structures of GPCRs coupled to G_s, G_i and G_o. *Mol. Cell. Endocrinol.,* **2019**, *488*, 1-13. http://dx.doi.org/10.1016/j.mce.2019.02.006 PMID: 30930094

[47] Taylor, V.G.; Bommarito, P.A.; Tesmer, J.J.G. Structure of the regulator of G Protein Signaling 8 (RGS8)-Gαq Complex: Molecular basis for Gα selectivity. *J. Biol. Chem.,* **2016**, *291*(10), 5138-5145. http://dx.doi.org/10.1074/jbc.M115.712075 PMID: 26755720

[48] Tesmer, J.J.; Dessauer, C.W.; Sunahara, R.K.; Murray, L.D.; Johnson, R.A.; Gilman, A.G.; Sprang, S.R. Molecular basis for P-site inhibition of adenylyl cyclase. *Biochemistry,* **2000**, *39*(47), 14464-14471. http://dx.doi.org/10.1021/bi0015562 PMID: 11087399

[49] Edward Zhou, X.; Melcher, K.; Eric Xu, H. Structural biology of G protein-coupled receptor signaling complexes. *Protein Sci.,* **2019**, *28*(3), 487-501. PMID: 30311978

[50] Hilger, D. The role of structural dynamics in GPCR-mediated signaling. *FEBS J.,* **2021**, *288*(8), 2461-2489. http://dx.doi.org/10.1111/febs.15841 PMID: 33871923

[51] Tesmer, J.J.G.; Berman, D.M.; Gilman, A.G.; Sprang, S.R. Structure of RGS4 bound to AlF4-activated G(i α1): stabilization of the transition state for GTP hydrolysis. *Cell,* **1997**, *89*(2), 251-261. http://dx.doi.org/10.1016/S0092-8674(00)80204-4 PMID: 9108480

[52] Qi, C.; Sorrentino, S.; Medalia, O.; Korkhov, V.M. The structure of a membrane adenylyl cyclase bound to an activated stimulatory G protein. *Science,* **2019**, *364*(6438), 389-394. http://dx.doi.org/10.1126/science.aav0778 PMID: 31023924

[53] Hajicek, N.; Kukimoto-Niino, M.; Mishima-Tsumagari, C.; Chow, C.R.; Shirouzu, M.; Terada, T.; Patel, M.; Yokoyama, S.; Kozasa, T. Identification of critical residues in G(alpha)13 for stimulation of p115RhoGEF activity and the structure of the G(alpha)13-p115RhoGEF regulator of G protein signaling homology (RH) domain complex. *J. Biol. Chem.,* **2011**, *286*(23), 20625-20636. http://dx.doi.org/10.1074/jbc.M110.201392 PMID: 21507947

[54] Nance, M.R.; Kreutz, B.; Tesmer, V.M.; Sterne-Marr, R.; Kozasa, T.; Tesmer, J.J.G. Structural and functional analysis of the regulator of G protein signaling 2-gαq complex. *Structure,* **2013**, *21*(3), 438-448. http://dx.doi.org/10.1016/j.str.2012.12.016 PMID: 23434405

[55] Apweiler, R.; Bairoch, A.; Wu, C.H.; Barker, W.C.; Boeckmann, B.; Ferro, S.; Gasteiger, S.; Huang, H.; Lopez, R.; Magrane, M.; Martin, M.J.; Natale, D.A.; O'Donovan, C.; Redaschi, N.; Yeh, L.-S. L. UniProt: The universal protein knowledgebase. *Nucleic Acids Res.,* **2017**, *45*(D1), D158-D169. http://dx.doi.org/10.1093/nar/gkw1099 PMID: 27899622

[56] Tesmer, J.J.; Sunahara, R.K.; Johnson, R.A.; Gosselin, G.; Gilman, A.G.; Sprang, S.R. Two-metal-Ion catalysis in adenylyl cyclase. *Science,* **1999**, *285*(5428), 756-760. http://dx.doi.org/10.1126/science.285.5428.756 PMID: 10427002

[57] Tesmer, J.J.; Sunahara, R.K.; Gilman, A.G.; Sprang, S.R. Crystal structure of the catalytic domains of adenylyl cyclase in a complex with Gsalpha.GTPgammaS. *Science,* **1997**, *278*(5345), 1907-1916.

http://dx.doi.org/10.1126/science.278.5345.1907 PMID: 9417641

[58] Mou, T-C.; Masada, N.; Cooper, D.M.F.; Sprang, S.R. Structural basis for inhibition of mammalian adenylyl cyclase by calcium. *Biochemistry,* **2009**, *48*(15), 3387-3397. http://dx.doi.org/10.1021/bi802122k PMID: 19243146

[59] Mou, T-C.; Gille, A.; Fancy, D.A.; Seifert, R.; Sprang, S.R. Structural basis for the inhibition of mammalian membrane adenylyl cyclase by 2 '(3')-O-(N-Methylanthraniloyl)-guanosine 5 '-triphosphate. *J. Biol. Chem.,* **2005**, *280*(8), 7253-7261. http://dx.doi.org/10.1074/jbc.M409076200 PMID: 15591060

[60] Slep, K.C.; Kercher, M.A.; Wieland, T.; Chen, C-K.; Simon, M.I.; Sigler, P.B. Molecular architecture of Galphao and the structural basis for RGS16-mediated deactivation. *Proc. Natl. Acad. Sci. USA,* **2008**, *105*(17), 6243-6248. http://dx.doi.org/10.1073/pnas.0801569105 PMID: 18434540

[61] Soundararajan, M.; Willard, F.S.; Kimple, A.J.; Turnbull, A.P.; Ball, L.J.; Schoch, G.A.; Gileadi, C.; Fedorov, O.Y.; Dowler, E.F.; Higman, V.A.; Hutsell, S.Q.; Sundström, M.; Doyle, D.A.; Siderovski, D.P. Structural diversity in the RGS domain and its interaction with heterotrimeric G protein alpha-subunits. *Proc. Natl. Acad. Sci. USA,* **2008**, *105*(17), 6457-6462. http://dx.doi.org/10.1073/pnas.0801508105 PMID: 18434541

[62] Kimple, A.J.; Soundararajan, M.; Hutsell, S.Q.; Roos, A.K.; Urban, D.J.; Setola, V.; Temple, B.R.S.; Roth, B.L.; Knapp, S.; Willard, F.S.; Siderovski, D.P. Structural determinants of G-protein alpha subunit selectivity by regulator of G-protein signaling 2 (RGS2). *J. Biol. Chem.,* **2009**, *284*(29), 19402-19411. http://dx.doi.org/10.1074/jbc.M109.024711 PMID: 19478087

[63] Gao, Y.; Eskici, G.; Ramachandran, S.; Poitevin, F.; Seven, A.B.; Panova, O.; Skiniotis, G.; Cerione, R.A. Structure of the Visual Signaling Complex between Transducin and Phosphodiesterase 6. *Mol. Cell,* **2020**, *80*(2), 237-245.e4. http://dx.doi.org/10.1016/j.molcel.2020.09.013 PMID: 33007200

[64] Slep, K.C.; Kercher, M.A.; He, W.; Cowan, C.W.; Wensel, T.G.; Sigler, P.B. Structural determinants for regulation of phosphodiesterase by a G protein at 2.0 A. *Nature,* **2001**, *409*(6823), 1071-1077. http://dx.doi.org/10.1038/35059138 PMID: 11234020

[65] Waldo, G.L.; Ricks, T.K.; Hicks, S.N.; Cheever, M.L.; Kawano, T.; Tsuboi, K.; Wang, X.; Montell, C.; Kozasa, T.; Sondek, J.; Harden, T.K. Kinetic scaffolding mediated by a phospholipase C-beta and Gq signaling complex. *Science,* **2010**, *330*(6006), 974-980. http://dx.doi.org/10.1126/science.1193438 PMID: 20966218

[66] Lyon, A.M.; Begley, J.A.; Manett, T.D.; Tesmer, J.J.G. Molecular mechanisms of phospholipase C β3 autoinhibition. *Structure,* **2014**, *22*(12), 1844-1854. http://dx.doi.org/10.1016/j.str.2014.10.008 PMID: 25435326

[67] Tesmer, V.M.; Kawano, T.; Shankaranarayanan, A.; Kozasa, T.; Tesmer, J.J.G. Snapshot of activated G proteins at the membrane: the Galphaq-GRK2-Gbetagamma complex. *Science,* **2005**, *310*(5754), 1686-1690. http://dx.doi.org/10.1126/science.1118890 PMID: 16339447

[68] Lutz, S.; Shankaranarayanan, A.; Coco, C.; Ridilla, M.; Nance, M.R.; Vettel, C.; Baltus, D.; Evelyn, C.R.; Neubig, R.R.; Wieland, T.; Tesmer, J.J.G. Structure of Galphaq-p63RhoGEF-RhoA complex reveals a pathway for the activation of RhoA by GPCRs. *Science,* **2007**, *318*(5858), 1923-1927. http://dx.doi.org/10.1126/science.1147554 PMID: 18096806

[69] Chen, Z.; Singer, W.D.; Danesh, S.M.; Sternweis, P.C.; Sprang, S.R. Recognition of the activated states of Galpha13 by the rgRGS domain of PDZRhoGEF. *Structure,* **2008**, *16*(10), 1532-1543. http://dx.doi.org/10.1016/j.str.2008.07.009 PMID: 18940608

[70] Hermes, C.; König, G.M.; Crüsemann, M. The chromodepsins - chemistry, biology and biosynthesis of a selective Gq inhibitor natural product family. *Nat. Prod. Rep.,* **2021**, *38*(12), 2276-2292. http://dx.doi.org/10.1039/D1NP00005E PMID: 33998635

[71] Zhang, H.; Nielsen, A.L.; Strømgaard, K. Recent achievements in developing selective G_q inhibitors. *Med. Res. Rev.,* **2020**, *40*(1), 135-157. http://dx.doi.org/10.1002/med.21598 PMID: 31218731

[72] Graziano, M.P.; Freissmuth, M.; Gilman, A.G. Expression of Gs alpha in *Escherichia coli.* Purification and properties of two forms of the protein. *J. Biol. Chem.,* **1989**, *264*(1), 409-418. http://dx.doi.org/10.1016/S0021-9258(17)31273-5 PMID: 2491850

[73] Malinski, J.A.; Zera, E.M.; Angleson, J.K.; Wensel, T.G. High affinity interactions of GTPgammaS with the heterotrimeric G protein, transducin. Evidence at high and low protein concentrations. *J. Biol. Chem.,* **1996**, *271*(22), 12919-12924. http://dx.doi.org/10.1074/jbc.271.22.12919 PMID: 8662740

[74] Becher, I.; Savitski, M.M.; Savitski, M.F.; Hopf, C.; Bantscheff, M.; Drewes, G. Affinity profiling of the cellular kinome for the nucleotide cofactors ATP, ADP, and GTP. *ACS Chem. Biol.,* **2013**, *8*(3), 599-607. http://dx.doi.org/10.1021/cb3005879 PMID: 23215245

[75] Katada, T.; Tamura, M.; Ui, M. The A protomer of islet-activating protein, pertussis toxin, as an active peptide catalyzing ADP-ribosylation of a membrane protein. *Arch. Biochem. Biophys.,* **1983**, *224*(1), 290-298. http://dx.doi.org/10.1016/0003-9861(83)90212-6 PMID: 6683482

[76] Carbonetti, N.H. Pertussis toxin and adenylate cyclase toxin: Key virulence factors of Bordetella pertussis and cell biology tools. *Future Microbiol.,* **2010**, *5*(3), 455-469. http://dx.doi.org/10.2217/fmb.09.133 PMID: 20210554

[77] Moss, J.; Stanley, S.J.; Burns, D.L.; Hsia, J.A.; Yost, D.A.; Myers, G.A.; Hewlett, E.L. Activation by thiol of the latent NAD glycohydrolase and ADP-ribosyltransferase activities of *Bordetella pertussis* toxin (islet-activating protein). *J. Biol. Chem.,* **1983**, *258*(19), 11879-11882. http://dx.doi.org/10.1016/S0021-9258(17)44314-6 PMID: 6311827

[78] Beindl, W.; Mitterauer, T.; Hohenegger, M.; Ijzerman, A.P.; Nanoff, C.; Freissmuth, M. Inhibition of receptor/G protein coupling by suramin analogues. *Mol. Pharmacol.,* **1996**, *50*(2), 415-423. PMID: 8700151

[79] Freissmuth, M.; Boehm, S.; Beindl, W.; Nickel, P.; Ijzer-

man, A.P.; Hohenegger, M.; Nanoff, C. Suramin analogues as subtype-selective G protein inhibitors. *Mol. Pharmacol.,* **1996**, *49*(4), 602-611.
PMID: 8609887

[80] Chung, W-C.; Kermode, J.C. Suramin disrupts receptor-G protein coupling by blocking association of G protein alpha and betagamma subunits. *J. Pharmacol. Exp. Ther.,* **2005**, *313*(1), 191-198.
http://dx.doi.org/10.1124/jpet.104.078311 PMID: 15626724

[81] Mannes, M.; Martin, C.; Triest, S.; Pia Dimmito, M.; Mollica, A.; Laeremans, T.; Menet, C.J.; Ballet, S. Development of Generic G Protein Peptidomimetics able to stabilize active state G_s Protein-Coupled receptors for application in drug discovery. *Angew. Chem. Int. Ed. Engl.,* **2021**, *60*(18), 10247-10254.
http://dx.doi.org/10.1002/anie.202100180 PMID: 33596327

[82] Rasenick, M.M.; Watanabe, M.; Lazarevic, M.B.; Hatta, S.; Hamm, H.E. Synthetic peptides as probes for G protein function. Carboxyl-terminal G alpha s peptides mimic Gs and evoke high affinity agonist binding to beta-adrenergic receptors. *J. Biol. Chem.,* **1994**, *269*(34), 21519-21525.
http://dx.doi.org/10.1016/S0021-9258(17)31835-5 PMID: 8063788

[83] Scheerer, P.; Park, J.H.; Hildebrand, P.W.; Kim, Y.J.; Krauss, N.; Choe, H-W.; Hofmann, K.P.; Ernst, O.P. Crystal structure of opsin in its G-protein-interacting conformation. *Nature,* **2008**, *455*(7212), 497-502.
http://dx.doi.org/10.1038/nature07330 PMID: 18818650

[84] Herrmann, R.; Heck, M.; Henklein, P.; Kleuss, C.; Wray, V.; Hofmann, K.P.; Ernst, O.P. Rhodopsin-transducin coupling: role of the Galpha C-terminus in nucleotide exchange catalysis. *Vision Res.,* **2006**, *46*(27), 4582-4593.
http://dx.doi.org/10.1016/j.visres.2006.07.027 PMID: 17011013

[85] Feldman, D.S.; Zamah, A.M.; Pierce, K.L.; Miller, W.E.; Kelly, F.; Rapacciuolo, A.; Rockman, H.A.; Koch, W.J.; Luttrell, L.M. Selective inhibition of heterotrimeric Gs signaling. Targeting the receptor-G protein interface using a peptide minigene encoding the Galpha(s) carboxyl terminus. *J. Biol. Chem.,* **2002**, *277*(32), 28631-28640.
http://dx.doi.org/10.1074/jbc.M204753200 PMID: 12036966

[86] Mukai, H.; Munekata, E.; Higashijima, T. G protein antagonists. A novel hydrophobic peptide competes with receptor for G protein binding. *J. Biol. Chem.,* **1992**, *267*(23), 16237-16243.
http://dx.doi.org/10.1016/S0021-9258(18)41991-6 PMID: 1379592

[87] Covic, L.; Gresser, A.L.; Talavera, J.; Swift, S.; Kuliopulos, A. Activation and inhibition of G protein-coupled receptors by cell-penetrating membrane-tethered peptides. *Proc. Natl. Acad. Sci. USA,* **2002**, *99*(2), 643-648.
http://dx.doi.org/10.1073/pnas.022460899 PMID: 11805322

[88] Tressel, S.L.; Koukos, G.; Tchernychev, B.; Jacques, S.L.; Covic, L.; Kuliopulos, A. Pharmacology, biodistribution, and efficacy of GPCR-based pepducins in disease models. *Methods Mol. Biol.,* **2011**, *683*, 259-275.
http://dx.doi.org/10.1007/978-1-60761-919-2_19 PMID: 21053136

[89] Higashijima, T.; Ferguson, K.M.; Smigel, M.D.; Gilman, A.G. The effect of GTP and Mg2+ on the GTPase activity and the fluorescent properties of Go. *J. Biol. Chem.,* **1987**, *262*(2), 757-761.
http://dx.doi.org/10.1016/S0021-9258(19)75850-5 PMID: 3027067

[90] Higashijima, T.; Ferguson, K.M.; Sternweis, P.C.; Ross, E.M.; Smigel, M.D.; Gilman, A.G. The effect of activating ligands on the intrinsic fluorescence of guanine nucleotide-binding regulatory proteins. *J. Biol. Chem.,* **1987**, *262*(2), 752-756.
http://dx.doi.org/10.1016/S0021-9258(19)75849-9 PMID: 3100518

[91] Takasaki, J.; Saito, T.; Taniguchi, M.; Kawasaki, T.; Moritani, Y.; Hayashi, K.; Kobori, M. A novel Galphaq/11-selective inhibitor. *J. Biol. Chem.,* **2004**, *279*(46), 47438-47445.
http://dx.doi.org/10.1074/jbc.M408846200 PMID: 15339913

[92] Taniguchi, M.; Nagai, K.; Arao, N.; Kawasaki, T.; Saito, T.; Moritani, Y.; Takasaki, J.; Hayashi, K.; Fujita, S.; Suzuki, K.; Tsukamoto, S. YM-254890, a novel platelet aggregation inhibitor produced by Chromobacterium sp. QS3666. *J. Antibiot. (Tokyo),* **2003**, *56*(4), 358-363.
http://dx.doi.org/10.7164/antibiotics.56.358 PMID: 12817809

[93] Hermes, C.; Richarz, R.; Wirtz, D.A.; Patt, J.; Hanke, W.; Kehraus, S.; Voß, J.H.; Küppers, J.; Ohbayashi, T.; Namasivayam, V.; Alenfelder, J.; Inoue, A.; Mergaert, P.; Gütschow, M.; Müller, C.E.; Kostenis, E.; König, G.M.; Crüsemann, M. Thioesterase-mediated side chain transesterification generates potent Gq signaling inhibitor FR900359. *Nat. Commun.,* **2021**, *12*(1), 144.
http://dx.doi.org/10.1038/s41467-020-20418-3 PMID: 33420046

[94] Carlier, A.; Fehr, L.; Pinto-Carbó, M.; Schäberle, T.; Reher, R.; Dessein, S.; König, G.; Eberl, L. The genome analysis of *Candidatus burkholderia* Crenata reveals that secondary metabolism may be a key function of the Ardisia crenata leaf nodule symbiosis. *Environ. Microbiol.,* **2016**, *18*(8), 2507-2522.
http://dx.doi.org/10.1111/1462-2920.13184 PMID: 26663534

[95] Kostenis, E.; Pfeil, E.M.; Annala, S. Heterotrimeric G_q proteins as therapeutic targets? *J. Biol. Chem.,* **2020**, *295*(16), 5206-5215.
http://dx.doi.org/10.1074/jbc.REV119.007061 PMID: 32122969

[96] Matthey, M.; Roberts, R.; Seidinger, A.; Simon, A.; Schröder, R.; Kuschak, M.; Annala, S.; König, G.M.; Müller, C.E.; Hall, I.P.; Kostenis, E.; Fleischmann, B.K.; Wenzel, D. Targeted inhibition of G_q signaling induces airway relaxation in mouse models of asthma. *Sci. Transl. Med.,* **2017**, *9*(407), 9.
http://dx.doi.org/10.1126/scitranslmed.aag2288 PMID: 28904224

[97] White, A.D.; Jean-Alphonse, F.G.; Fang, F.; Peña, K.A.; Liu, S.; König, G.M.; Inoue, A.; Aslanoglou, D.; Gellman, S.H.; Kostenis, E.; Xiao, K.; Vilardaga, J-P. $G_{q/11}$-dependent regulation of endosomal cAMP generation by parathyroid hormone class B GPCR. *Proc. Natl. Acad. Sci. USA,* **2020**, *117*(13), 7455-7460.
http://dx.doi.org/10.1073/pnas.1918158117 PMID: 32184323

[98] Schrage, R.; Schmitz, A-L.; Gaffal, E.; Annala, S.; Kehraus, S.; Wenzel, D.; Büllesbach, K.M.; Bald, T.; Inoue, A.; Shinjo, Y.; Galandrin, S.; Shridhar, N.; Hesse, M.; Grundmann, M.; Merten, N.; Charpentier, T.H.; Martz, M.;

Butcher, A.J.; Slodczyk, T.; Armando, S.; Effern, M.; Namkung, Y.; Jenkins, L.; Horn, V.; Stößel, A.; Dargatz, H.; Tietze, D.; Imhof, D.; Galés, C.; Drewke, C.; Müller, C.E.; Hölzel, M.; Milligan, G.; Tobin, A.B.; Gomeza, J.; Dohlman, H.G.; Sondek, J.; Harden, T.K.; Bouvier, M.; Laporte, S.A.; Aoki, J.; Fleischmann, B.K.; Mohr, K.; König, G.M.; Tüting, T.; Kostenis, E. The experimental power of FR900359 to study Gq-regulated biological processes. *Nat. Commun.,* **2015**, *6*, 10156.
http://dx.doi.org/10.1038/ncomms10156 PMID: 26658454

[99] Kuschak, M.; Namasivayam, V.; Rafehi, M.; Voss, J.H.; Garg, J.; Schlegel, J.G.; Abdelrahman, A.; Kehraus, S.; Reher, R.; Küppers, J.; Sylvester, K.; Hinz, S.; Matthey, M.; Wenzel, D.; Fleischmann, B.K.; Pfeifer, A.; Inoue, A.; Gütschow, M.; König, G.M.; Müller, C.E. Cell-permeable high-affinity tracers for Gq proteins provide structural insights, reveal distinct binding kinetics, and identify small molecule inhibitors. *Br. J. Pharmacol.,* **2020**, *177*(8), 1898-1916.
PMID: 31881095

[100] Schlegel, J.G.; Tahoun, M.; Seidinger, A.; Voss, J.H.; Kuschak, M.; Kehraus, S.; Schneider, M.; Matthey, M.; Fleischmann, B.K.; König, G.M.; Wenzel, D.; Müller, C.E. Macrocyclic Gq protein inhibitors FR900359 and/or YM-254890-Fit for translation? *ACS Pharmacol. Transl. Sci.,* **2021**, *4*(2), 888-897.
http://dx.doi.org/10.1021/acsptsci.1c00021 PMID: 33860209

[101] Voss, J.H.; Nagel, J.; Rafehi, M.; Guixà-González, R.; Malfacini, D.; Patt, J.; Kehraus, S.; Inoue, A.; König, G.M.; Kostenis, E.; Deupi, X.; Namasivayam, V.; Müller, C.E. Unraveling binding mechanism and kinetics of macrocyclic $G\alpha_q$ protein inhibitors. *Pharmacol. Res.,* **2021**, *173*, 105880.
http://dx.doi.org/10.1016/j.phrs.2021.105880 PMID: 34506902

[102] Kuschak, M.; Schlegel, J.G.; Schneider, M.; Kehraus, S.; Voss, J.H.; Seidinger, A.; Matthey, M.; Wenzel, D.; Fleischmann, B.K.; König, G.M.; Müller, C.E. Sensitive LC-MS/MS method for the quantification of macrocyclic $G\alpha_q$ protein inhibitors in biological samples. *Front Chem.,* **2020**, *8*, 833.
http://dx.doi.org/10.3389/fchem.2020.00833 PMID: 33173765

[103] Malfacini, D.; Patt, J.; Annala, S.; Harpsøe, K.; Eryilmaz, F.; Reher, R.; Crüsemann, M.; Hanke, W.; Zhang, H.; Tietze, D.; Gloriam, D.E.; Bräuner-Osborne, H.; Strømgaard, K.; König, G.M.; Inoue, A.; Gomeza, J.; Kostenis, E. Rational design of a heterotrimeric G protein α subunit with artificial inhibitor sensitivity. *J. Biol. Chem.,* **2019**, *294*(15), 5747-5758.
http://dx.doi.org/10.1074/jbc.RA118.007250 PMID: 30745359

[104] Boesgaard, M.W.; Harpsøe, K.; Malmberg, M.; Underwood, C.R.; Inoue, A.; Mathiesen, J.M.; König, G.M.; Kostenis, E.; Gloriam, D.E.; Bräuner-Osborne, H. Delineation of molecular determinants for FR900359 inhibition of $G_{q/11}$ unlocks inhibition of $G\alpha_s$. *J. Biol. Chem.,* **2020**, *295*(40), 13850-13861.
http://dx.doi.org/10.1074/jbc.RA120.013002 PMID: 32753482

[105] Xiong, X-F.; Zhang, H.; Underwood, C.R.; Harpsøe, K.; Gardella, T.J.; Wöldike, M.F.; Mannstadt, M.; Gloriam, D.E.; Bräuner-Osborne, H.; Strømgaard, K. Total synthesis and structure-activity relationship studies of a series of selective G protein inhibitors. *Nat. Chem.,* **2016**, *8*(11), 1035-1041.
http://dx.doi.org/10.1038/nchem.2577 PMID: 27768111

[106] Zhang, H.; Nielsen, A.L.; Boesgaard, M.W.; Harpsøe, K.; Daly, N.L.; Xiong, X-F.; Underwood, C.R.; Haugaard-Kedström, L.M.; Bräuner-Osborne, H.; Gloriam, D.E.; Strømgaard, K. Structure-activity relationship and conformational studies of the natural product cyclic depsipeptides YM-254890 and FR900359. *Eur. J. Med. Chem.,* **2018**, *156*, 847-860.
http://dx.doi.org/10.1016/j.ejmech.2018.07.023 PMID: 30055466

[107] Reher, R.; Kühl, T.; Annala, S.; Benkel, T.; Kaufmann, D.; Nubbemeyer, B.; Odhiambo, J.P.; Heimer, P.; Bäuml, C.A.; Kehraus, S.; Crüsemann, M.; Kostenis, E.; Tietze, D.; König, G.M.; Imhof, D. Deciphering specificity determinants for FR900359-Derived G_q α inhibitors based on computational and structure-activity studies. *ChemMedChem,* **2018**, *13*(16), 1634-1643.
http://dx.doi.org/10.1002/cmdc.201800304 PMID: 29873888

[108] Reher, R.; Kuschak, M.; Heycke, N.; Annala, S.; Kehraus, S.; Dai, H-F.; Müller, C.E.; Kostenis, E.; König, G.M.; Crüsemann, M. Applying molecular networking for the detection of natural sources and analogues of the selective Gq protein inhibitor FR900359. *J. Nat. Prod.,* **2018**, *81*(7), 1628-1635.
http://dx.doi.org/10.1021/acs.jnatprod.8b00222 PMID: 29943987

[109] Fukushima, N.; Kohno, M.; Kato, T.; Kawamoto, S.; Okuda, K.; Misu, Y.; Ueda, H. Melittin, a metabostatic peptide inhibiting Gs activity. *Peptides,* **1998**, *19*(5), 811-819.
http://dx.doi.org/10.1016/S0196-9781(98)00027-8 PMID: 9663445

[110] Higashijima, T.; Burnier, J.; Ross, E.M. Regulation of Gi and Go by mastoparan, related amphiphilic peptides, and hydrophobic amines. Mechanism and structural determinants of activity. *J. Biol. Chem.,* **1990**, *265*(24), 14176-14186.
http://dx.doi.org/10.1016/S0021-9258(18)77284-0 PMID: 2117607

[111] Choi, O.H.; Padgett, W.L.; Daly, J.W. Effects of the amphiphilic peptides melittin and mastoparan on calcium influx, phosphoinositide breakdown and arachidonic acid release in rat pheochromocytoma PC12 cells. *J. Pharmacol. Exp. Ther.,* **1992**, *260*(1), 369-375.
PMID: 1309880

[112] DiGiacomo, V.; de Opakua, A.I.; Papakonstantinou, M.P.; Nguyen, L.T.; Merino, N.; Blanco-Canosa, J.B.; Blanco, F.J.; Garcia-Marcos, M. The Gαi-GIV binding interface is a druggable protein-protein interaction. *Sci. Rep.,* **2017**, *7*(1), 8575.
http://dx.doi.org/10.1038/s41598-017-08829-7 PMID: 28819150

[113] Kalogriopoulos, N.A.; Rees, S.D.; Ngo, T.; Kopcho, N.J.; Ilatovskiy, A.V.; Sun, N.; Komives, E.A.; Chang, G.; Ghosh, P.; Kufareva, I. Structural basis for GPCR-independent activation of heterotrimeric Gi proteins. *Proc. Natl. Acad. Sci. USA,* **2019**, *116*(33), 16394-16403.
http://dx.doi.org/10.1073/pnas.1906658116 PMID: 31363053

[114] Kimple, R.J.; Kimple, M.E.; Betts, L.; Sondek, J.; Siderovski, D.P. Structural determinants for GoLoco-induced inhibition of nucleotide release by Galpha subunits. *Nature,* **2002**, *416*(6883), 878-881.

http://dx.doi.org/10.1038/416878a PMID: 11976690

[115] Siderovski, D.P.; Willard, F.S. The GAPs, GEFs, and GDIs of heterotrimeric G-protein alpha subunits. *Int. J. Biol. Sci.,* **2005**, *1*(2), 51-66. http://dx.doi.org/10.7150/ijbs.1.51 PMID: 15951850

[116] Seven, A.B.; Hilger, D.; Papasergi-Scott, M.M.; Zhang, L.; Qu, Q.; Kobilka, B.K.; Tall, G.G.; Skiniotis, G. Structures of Gα proteins in complex with their chaperone reveal quality control mechanisms. *Cell Rep.,* **2020**, *30*(11), 3699-3709.e6. http://dx.doi.org/10.1016/j.celrep.2020.02.086 PMID: 32126208

[117] Ayoub, M.A.; Damian, M.; Gespach, C.; Ferrandis, E.; Lavergne, O.; De Wever, O.; Banères, J-L.; Pin, J-P.; Prévost, G.P. Inhibition of heterotrimeric G protein signaling by a small molecule acting on Galpha subunit. *J. Biol. Chem.,* **2009**, *284*(42), 29136-29145. http://dx.doi.org/10.1074/jbc.M109.042333 PMID: 19648112

[118] Prévost, G.P.; Lonchampt, M.O.; Holbeck, S.; Attoub, S.; Zaharevitz, D.; Alley, M.; Wright, J.; Brezak, M.C.; Coulomb, H.; Savola, A.; Huchet, M.; Chaumeron, S.; Nguyen, Q-D.; Forgez, P.; Bruyneel, E.; Bracke, M.; Ferrandis, E.; Roubert, P.; Demarquay, D.; Gespach, C.; Kasprzyk, P.G. Anticancer activity of BIM-46174, a new inhibitor of the heterotrimeric Galpha/Gbetagamma protein complex. *Cancer Res.,* **2006**, *66*(18), 9227-9234. http://dx.doi.org/10.1158/0008-5472.CAN-05-4205 PMID: 16982767

[119] Schmitz, A-L.; Schrage, R.; Gaffal, E.; Charpentier, T.H.; Wiest, J.; Hiltensperger, G.; Morschel, J.; Hennen, S.; Häußler, D.; Horn, V.; Wenzel, D.; Grundmann, M.; Büllesbach, K.M.; Schröder, R.; Brewitz, H.H.; Schmidt, J.; Gomeza, J.; Galés, C.; Fleischmann, B.K.; Tüting, T.; Imhof, D.; Tietze, D.; Gütschow, M.; Holzgrabe, U.; Sondek, J.; Harden, T.K.; Mohr, K.; Kostenis, E. A cell-permeable inhibitor to trap Gαq proteins in the empty pocket conformation. *Chem. Biol.,* **2014**, *21*(7), 890-902. http://dx.doi.org/10.1016/j.chembiol.2014.06.003 PMID: 25036778

[120] Küppers, J.; Benkel, T.; Annala, S.; Schnakenburg, G.; Kostenis, E.; Gütschow, M. BIM-46174 fragments as potential ligands of G proteins. *MedChemComm,* **2019**, *10*(10), 1838-1843. http://dx.doi.org/10.1039/C9MD00269C PMID: 32180917

[121] Gütschow, M.; Küppers, J.; Benkel, T.; Annala, S.; Kimura, K.; Reinelt, L.; Fleischmann, B.K.; Kostenis, E. Tetrahydroimidazo1,2-apyrazine derivatives: Synthesis and evaluation As Gαq-Protein Ligands. *Chemistry,* **2020**, *26*(55), 12615-12623.

[122] Charpentier, T.H.; Waldo, G.L.; Lowery-Gionta, E.G.; Krajewski, K.; Strahl, B.D.; Kash, T.L.; Harden, T.K.; Sondek, J. Potent and selective peptide-based inhibition of the G protein Gαq. *J. Biol. Chem.,* **2016**, *291*(49), 25608-25616. http://dx.doi.org/10.1074/jbc.M116.740407 PMID: 27742837

[123] Johnston, C.A.; Lobanova, E.S.; Shavkunov, A.S.; Low, J.; Ramer, J.K.; Blaesius, R.; Fredericks, Z.; Willard, F.S.; Kuhlman, B.; Arshavsky, V.Y.; Siderovski, D.P. Minimal determinants for binding activated G alpha from the structure of a G alpha(i1)-peptide dimer. *Biochemistry,* **2006**, *45*(38), 11390-11400. http://dx.doi.org/10.1021/bi0613832 PMID: 16981699

[124] Dai, S.A.; Hu, Q.; Gao, R.; Lazar, A.; Zhang, Z.; von Zastrow, M.; Suga, H.; Shokat, K.M. A GTP-state specific cyclic peptide inhibitor of the GTPase Gαs. *bioRxiv,* **2020**, *2020*, 054080. http://dx.doi.org/10.1101/2020.04.25.054080

[125] Higashijima, T.; Uzu, S.; Nakajima, T.; Ross, E.M. Mastoparan, a peptide toxin from wasp venom, mimics receptors by activating GTP-binding regulatory proteins (G proteins). *J. Biol. Chem.,* **1988**, *263*(14), 6491-6494. http://dx.doi.org/10.1016/S0021-9258(18)68669-7 PMID: 3129426

[126] Leschke, C.; Storm, R.; Breitweg-Lehmann, E.; Exner, T.; Nürnberg, B.; Schunack, W. Alkyl-substituted amino acid amides and analogous di- and triamines: new non-peptide G protein activators. *J. Med. Chem.,* **1997**, *40*(19), 3130-3139. http://dx.doi.org/10.1021/jm9703092 PMID: 9301677

[127] Breitweg-Lehmann, E.; Czupalla, C.; Storm, R.; Kudlacek, O.; Schunack, W.; Freissmuth, M.; Nürnberg, B. Activation and inhibition of G proteins by lipoamines. *Mol. Pharmacol.,* **2002**, *61*(3), 628-636. http://dx.doi.org/10.1124/mol.61.3.628 PMID: 11854444

[128] Hagelüken, A.; Grünbaum, L.; Nürnberg, B.; Harhammer, R.; Schunack, W.; Seifert, R. Lipophilic β-adrenoceptor antagonists and local anesthetics are effective direct activators of G-proteins. *Biochem. Pharmacol.,* **1994**, *47*(10), 1789-1795. http://dx.doi.org/10.1016/0006-2952(94)90307-7 PMID: 7911302

[129] Hagelüken, A.; Nürnberg, B.; Harhammer, R.; Grünbaum, L.; Schunack, W.; Seifert, R. The class III antiarrhythmic drug amiodarone directly activates pertussis toxin-sensitive G proteins. *Mol. Pharmacol.,* **1995**, *47*(2), 234-240. PMID: 7870030

[130] Sanchez, J.; Holmgren, J. Cholera toxin - a foe & a friend. *Indian J. Med. Res.,* **2011**, *133*, 153-163. PMID: 21415489

[131] O'Brien, J.B.; Wilkinson, J.C.; Roman, D.L. Regulator of G-protein signaling (RGS) proteins as drug targets: Progress and future potentials. *J. Biol. Chem.,* **2019**, *294*(49), 18571-18585. http://dx.doi.org/10.1074/jbc.REV119.007060 PMID: 31636120

[132] Mangmool, S.; Kurose, H. G(i/o) protein-dependent and -independent actions of Pertussis Toxin (PTX). *Toxins (Basel),* **2011**, *3*(7), 884-899. http://dx.doi.org/10.3390/toxins3070884 PMID: 22069745

[133] Johnston, C.A.; Willard, F.S.; Jezyk, M.R.; Fredericks, Z.; Bodor, E.T.; Jones, M.B.; Blaesius, R.; Watts, V.J.; Harden, T.K.; Sondek, J.; Ramer, J.K.; Siderovski, D.P. Structure of Galpha(i1) bound to a GDP-selective peptide provides insight into guanine nucleotide exchange. *Structure,* **2005**, *13*(7), 1069-1080. http://dx.doi.org/10.1016/j.str.2005.04.007 PMID: 16004878

[134] Galés, C.; Rebois, R.V.; Hogue, M.; Trieu, P.; Breit, A.; Hébert, T.E.; Bouvier, M. Real-time monitoring of receptor and G-protein interactions in living cells. *Nat. Methods,* **2005**, *2*(3), 177-184. http://dx.doi.org/10.1038/nmeth743 PMID: 15782186

13.2. Appendix B – Unraveling binding mechanism and kinetics of macrocyclic $G\alpha_q$ protein inhibitors

This section contains the article "Unraveling binding mechanism and kinetics of macrocyclic Gαq protein inhibitors" as it appears in the journal *Pharmacological Research* by Elsevier. As guaranteed by the author rights policy of the Elsevier publishing group, re-use of the article as a part of thesis or dissertation is allowed without permission or payment, as long as the thesis is not published commercially and with full acknowledgement of the original article. Both the main article and the supporting information are included in the next pages. The article is reprinted with permission from *Pharmacol. Res.* **2021**, 173, 105880

Pharmacological Research 173 (2021) 105880

Contents lists available at ScienceDirect

Pharmacological Research

journal homepage: www.elsevier.com/locate/yphrs

Unraveling binding mechanism and kinetics of macrocyclic $G\alpha_q$ protein inhibitors

Jan H. Voss [a], Jessica Nagel [a], Muhammad Rafehi [a], Ramon Guixà-González [b], Davide Malfacini [c], Julian Patt [c], Stefan Kehraus [c], Asuka Inoue [d], Gabriele M. König [c], Evi Kostenis [c], Xavier Deupi [b,e], Vigneshwaran Namasivayam [a], Christa E. Müller [a,*]

[a] PharmaCenter Bonn, Pharmaceutical Institute, Pharmaceutical & Medicinal Chemistry, University of Bonn, An der Immenburg 4, D-53121 Bonn, Germany
[b] Condensed Matter Theory Group, Paul Scherrer Institute (PSI), Forschungsstrasse 111, Villigen 5232, Switzerland
[c] Institute of Pharmaceutical Biology, University of Bonn, Nussallee 6, 53113 Bonn, Germany
[d] Tohoku University, Graduate School of Pharmaceutical Sciences, Sendai, Miyagi 980-8578 Japan
[e] Laboratory of Biomolecular Research, Paul Scherrer Institute (PSI), Forschungsstrasse 111, Villigen 5232, Switzerland

ARTICLE INFO

Keywords:
Conformational selection
FR900359
Gq protein
Molecular dynamics simulation
Residence time
YM-254890

ABSTRACT

G proteins represent intracellular switches that transduce signals relayed from G protein-coupled receptors. The structurally related macrocyclic depsipeptides FR900359 (FR) and YM-254890 (YM) are potent, selective inhibitors of the $G\alpha_q$ protein family. We recently discovered that radiolabeled FR and YM display strongly divergent residence times, which translates into significantly longer antiasthmatic effects of FR. The present study is aimed at investigating the molecular basis for this observed disparity. Based on docking studies, we mutated amino acid residues of the $G\alpha_q$ protein predicted to interact with FR or YM, and recombinantly expressed the mutated $G\alpha_q$ proteins in cells in which the native $G\alpha_q$ proteins had been knocked out by CRISPR-Cas9. Both radioligands showed similar association kinetics, and their binding followed a conformational selection mechanism, which was rationalized by molecular dynamics simulation studies. Several mutations of amino acid residues near the putative binding site of the "lipophilic anchors" of FR, especially those predicted to interact with the isopropyl group present in FR but not in YM, led to dramatically accelerated dissociation kinetics. Our data indicate that the long residence time of FR depends on lipophilic interactions within its binding site. The observed structure-kinetic relationships point to a complex binding mechanism of FR, which likely involves snap-lock- or dowel-like conformational changes of either ligand or protein, or both. These experimental data will be useful for the design of compounds with a desired residence time, a parameter that has now been recognized to be of utmost importance in drug development.

1. Introduction

Heterotrimeric guanine nucleotide binding proteins, G proteins, are crucial switches that transmit extracellular signals received by G protein-coupled receptors (GPCRs) across cellular membranes [1,2]. In the basal, inactive state, the GDP-bound Gα subunit is associated with the βγ-dimer [3]. Upon GPCR activation, the receptor couples to the G protein and triggers the exchange of GDP for GTP [4]. This leads to a separation of the Gα protein from the βγ-dimer thereby allowing the subunits to interact with their respective effector proteins [5]. Gα proteins are subdivided into four families according to their protein sequence: $G\alpha_s$, $G\alpha_i$, $G\alpha_{12/13}$ and $G\alpha_q$ [6,7]. The $G\alpha_q$ family comprises

List of Abbreviations: BSA, bovine serum albumin; CDK8/CycC, cyclin dependent kinase 8/Cyclin C; cpm, counts per minute; DMEM, Dulbecco's modified Eagle medium; DMSO, dimethyl sulfoxide; EDTA, ethylenediaminetetraacetic acid; FBS, fetal bovine serum; FR, FR900359; GDP, guanosine diphosphate; GPCR, G protein-coupled receptor; GTP, guanosine triphosphate; HA, hemagglutinin; HBSS, Hank's balanced salt solution; HEK, human embryonic kidney; HRP, horseradish peroxidase; IP_3, inositol trisphosphate; KO, knockout; PBS, phosphate buffered saline; PBS-T, phosphate buffered saline + 0.1% Tween 20; PCR, polymerase chain reaction; PLC-β, phospholipase C-β; RasD, Ras-like domain; SDS, sodium dodecyl sulfate; VSV-G, vesicular stomatitis virus G; wt, wild-type; YM, YM-254890; αH, α-helical domain.

* Correspondence to: Pharmaceutical Institute, Pharmaceutical & Medicinal Chemistry, University of Bonn, An der Immenburg 4, D-53121 Bonn, Germany.
E-mail address: christa.mueller@uni-bonn.de (C.E. Müller).

https://doi.org/10.1016/j.phrs.2021.105880
Received 31 May 2021; Received in revised form 23 August 2021; Accepted 5 September 2021
Available online 8 September 2021

four subclasses ($G\alpha_q$, $G\alpha_{11}$, $G\alpha_{14}$, and $G\alpha_{15/16}$), all of which activate phospholipase C-β (PLC-β) [8] resulting in the intracellular formation of diacylglycerol and inositol trisphosphate (IP_3) and subsequent Ca^{2+} mobilization. Further $G\alpha_q$-activated effector proteins have been described, including p63RhoGEF [9], and protein kinase C zeta [10].

Despite the important role of G proteins in signal transduction, only few potent and selective pharmacological modulators are known. These include the proteins pertussis toxin (irreversible $G\alpha_i$ inhibitor) and cholera toxin (irreversible $G\alpha_s$ activator) [11,12], and the macrocyclic depsipeptides YM-254890 (YM, PubChem SID: 315495489) and FR900359 (FR, PubChem CID: 14101198), natural products that act as reversible $G\alpha_q$ protein inhibitors (Fig. 1A) [13–15]. The $G\alpha_q$ inhibitor FR has been proposed for the treatment of asthma [16,17] and of cancers that show upregulation of G_q protein expression or mutations (e. g. uveal melanoma, a malignant disease driven by constitutively active $G\alpha_q$ proteins [18–21]). Further disease conditions that might benefit from $G\alpha_q$ blockade include metabolic disorders [22], cardiac hypertrophy [23], inflammation [24], and pulmonary hypertension [25,26].

FR was first reported in 1988, isolated from the leaves of the plant *Ardisia crenata* where it is synthesized by the endosymbiotic bacteria *Cand. burkholderia crenata* [29,30]. YM was discovered in 2003 as a bioactive natural product synthesized by the bacterial strain *Chromobacterium sp. QS3666* [31,32]. Both compounds showed inhibition of platelet aggregation and were later found to act as selective $G\alpha_q$ protein inhibitors [29,31]. FR and YM differ only in two substituents (Fig. 1A): FR contains a propionyl for R^1 instead of the acetyl present in YM, and an isopropyl instead of a methyl group for R^2. This results in an increased lipophilicity of FR as compared to YM [17]. A co-crystal structure revealed a wide pocket of the $G\alpha_q$ switch 1/hinge region near the Gα/β interface as the binding site of YM [27]. Docking of FR to this site suggested a virtually identical binding pose as that of YM (RMSD = 0.51 Å, measured in the carbon atoms of the depsipeptide ring; 15 atoms)

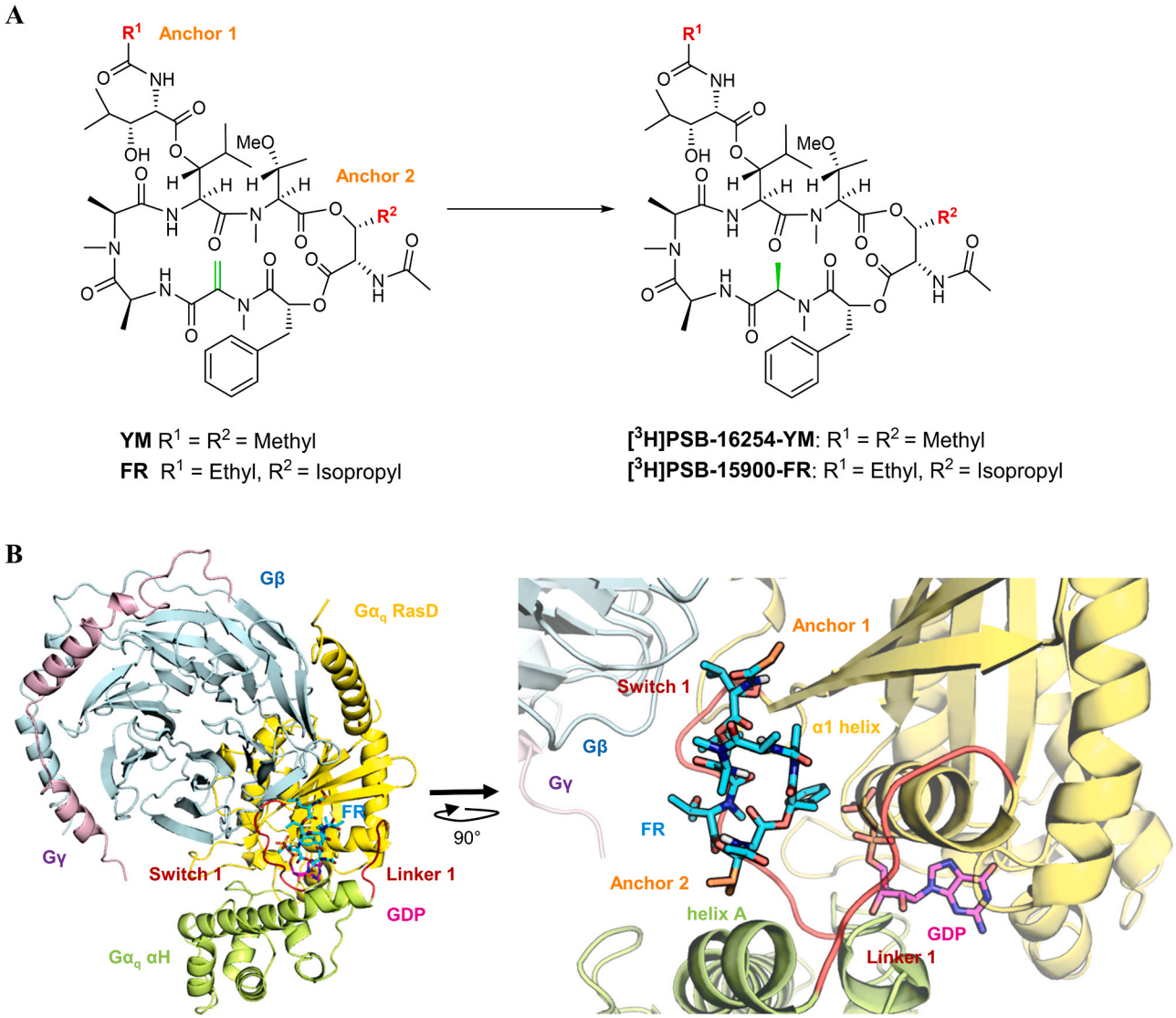

Fig. 1. Chemical structures and binding poses of the macrocyclic $G\alpha_q$ inhibitors. (**A**) Chemical structures of the $G\alpha_q$ inhibitors YM and FR and their tritiated derivatives [^{3}H]PSB-16254-YM and [^{3}H]PSB-15900-FR obtained by catalytic hydrogenation of the exocyclic double bond (green) with tritium gas. The residues that differ between YM and FR and their respective radioligands are shown in red (R^1, R^2), also designated "anchor 1″ and "anchor 2″. (**B**) Left: Model of the $G\alpha_{q/i1N}\beta_1\gamma_2$ heterotrimer bound to GDP and FR (based on the X-ray structure of a chimeric $G\alpha_q$ protein whose N-terminal helix was substituted from the $G\alpha_{i1}$ protein ($G\alpha_{q/i1N}\beta_1\gamma_2$ heterotrimer bound to YM; PDB-ID: 3AH8) [27,28]. The docked FR is shown as cyan sticks, the $G\alpha_q$ RasD is depicted in yellow, the αH domain in green, and linker 1 and switch 1 are highlighted in red. $G\beta_1$ is depicted in light blue, $G\gamma_2$ in pink, and GDP in magenta. Right: Close-up view of the YM/FR binding site in the $G\alpha_q$ subunit bound to FR. The inhibitor binding site is located between the α1 helix and helix A, and the linker 1 and switch 1 regions (in red) of the $G\alpha_q$ protein. GDP bound to its binding site is also shown. Anchors 1 and 2 of FR are highlighted in orange. Nitrogen atoms are shown in blue, oxygen in red, and phosphorus atoms in yellow.

(Fig. 1B) [28]. Both compounds, FR and YM, act as guanine nucleotide dissociation inhibitors, preventing the separation of the $G\alpha_q$ helical domain (αH) from its Ras-like domain (RasD) thereby trapping the $G\alpha_q$ subunit in its inactive GDP-bound state [13,27]. Molecular docking studies, radioligand binding experiments, and mutational analyses suggested a virtually identical mechanism of action and very similar potency of YM and FR [13,28,33,34] leading to the suggestion that both inhibitors may be interchangeable [35]. However, we recently discovered a remarkable difference in the dissociation kinetics of an FR- (as compared to a YM-) derived tritium-labeled radioligand (Fig. 1A) that translates into significantly different residence times ($1/k_{off}$ or τ) [28]. While [^{3}H]PSB-16254-YM, obtained by catalytic tritiation of the exocyclic double bond of YM, displayed a residence time of only about 5 min, determined at 37 °C, the corresponding FR-derived radiotracer [^{3}H]PSB-15900-FR showed a more than 20-fold longer residence time of 133 min [28]. This large difference is surprising, given the very similar structure of both inhibitors (Fig. 1A). Importantly, the increased residence time translates into a significantly longer duration of pharmacological effects of FR as compared to YM, as recently demonstrated in a mouse model of asthma [17].

Classical drug development has typically focused on improving the binding affinity of a drug, i.e., the strength of the protein-ligand interaction. More recently, dissociation rates, often expressed as residence times, have emerged as another, perhaps even more important drug property [36–38]. There is increasing evidence that the unbinding kinetics of drugs may be better correlated with drug efficacy than binding affinity since the pharmacological effect of a slowly dissociating drug may still be observed after the drug has disappeared from blood circulation [39]. However, the structural determinants of residence time are largely unknown, and only a limited number of studies has been published so far [40,41]. The development of computational methods to predict drug binding kinetics is currently hampered by the general lack of experimental data [42].

The binding mechanism of a ligand to its target is another determinant of drug action [37]. Classical pharmacological equations commonly employ a one step-binding model, where a target acts as a lock and the ligand as a key (Fig. 2, top). However, for most protein-ligand interactions, a more complex two-step binding model is assumed, requiring a conformational change of the protein, either prior to ligand binding (conformational selection; Fig. 2, bottom left) or after initial ligand binding (induced fit; Fig. 2, top right), to yield a high-affinity protein-ligand complex [43–45]. Some protein-ligand interactions are better described by a more complex combination of both features, e.g. selection of an initial binding conformation followed by a conformational change of the protein-ligand complex [46].

The present study aimed at elucidating the binding mechanism and the molecular basis for the strongly divergent dissociation kinetics of the macrocyclic $G\alpha_q$ inhibitors FR and YM. To this end, we introduced mutations based on molecular modeling and expressed the resulting $G\alpha_q$ protein mutants in human embryonic kidney (HEK) 293 cells in which the native $G\alpha_q$ proteins had been knocked out by CRISPR-Cas9. As previously observed for native platelet membranes, [^{3}H]PSB-15900-FR dissociated very slowly from the recombinant $G\alpha_q$ subunit expressed in HEK cells, while [^{3}H]PSB-16254-YM displayed fast dissociation. While most of the investigated $G\alpha_q$ protein mutants retained high potency and affinity, dissociation kinetics of the inhibitors, in particular those of the FR-radioligand, were strongly accelerated. Especially mutations around the binding site of the isopropyl residue of FR (R^2, anchor 2) led to rapid dissociation of the inhibitor-protein complex and thus to a strongly reduced residence time. Our results emphasize the importance of investigating the binding kinetics of protein-drug interactions.

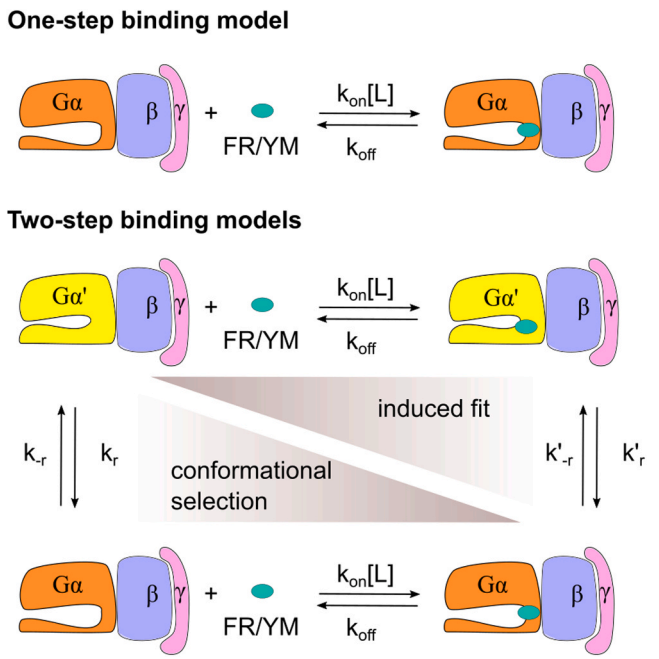

Fig. 2. Models of ligand binding to a heterotrimeric G protein. (**Top**) Schematic depiction of a lock-and-key binding mechanism: The ligand FR or YM binds to the G protein with a concentration-dependent association rate k_{on}[L] and unbinds with a concentration-independent rate k_{off}. No crucial conformational changes of the protein are required. (**Bottom**) Two-step binding models for ligand binding to heterotrimeric G proteins: In the induced-fit binding model (top right), the ligand FR or YM binds to the protein conformation Gα' to form a metastable low-affinity complex Gα'L driven by the concentration-dependent association rate k_{on}[L], similar to the one-step binding model. The complex dissociates with the concentration-independent rate k_{off}. However, Gα'L can be transformed to the high-affinity complex GαL by a conformational change of the protein, occurring with a rate constant k'_r. The conformational change can be reversed with the rate constant k'_{-r}. Conversely, in conformational selection (bottom left), the protein Gα' undergoes a conformational change towards the ligand-binding conformation Gα prior to ligand binding. Gα is formed from Gα' at the rate constant k_r, Gα' is formed from Gα at the rate constant k_{-r}. The ligand L binds in a concentration-dependent manner only to Gα, but not to Gα', at the rate of k_{on}[L]. The complex GαL dissociates with the concentration-independent rate k_{off}.

2. Materials and methods

2.1. Bioactive compounds

FR was isolated and purified from *A. crenata* leaves in the laboratory of G. M. König as previously described [13]. YM was purchased from Wako Chemicals (Neuss, Germany). The radioligands [^{3}H]PSB-15900-FR (FR-derived, specific activity: 1036 GBq*mmol^{-1}/28 Ci*mmol^{-1}) and [^{3}H]PSB-16254-YM (YM-derived, specific activity: 1147 GBq*mmol^{-1}/31 Ci*mmol^{-1}) were synthesized by catalytic hydrogenation of FR and YM, respectively, with tritium gas (Pharmaron, Cardiff, UK) as previously described [28].

2.2. Docking studies

The docked pose of FR in complex with the trimeric $G\alpha_q\beta_1\gamma_2$ protein was obtained as previously described [28]. In short, the protein structure (PDB-ID: 3AH8) [27] was prepared in MOE 2016.08 (Chemical Computing Group, Montreal, Canada). AutoDock 4.2 was used to dock FR into the inhibitor binding site [47]. Atomic partial charges were calculated by AutoDock Tools [47]. Based on the position of the co-crystallized ligand YM in the X-ray structure, three-dimensional energy scoring grids of 60 × 60×60 points were computed with a spacing

of 0.375 Å. During docking, which was performed by the *var*CPSO-ls algorithm from PSO@Autodock implemented in AutoDock 4.2 [48], FR was fully flexible, while the G protein remained rigid. We performed 50 independent docking calculations, terminated after 500,000 evaluation steps. The cognitive and social coefficients c1 and c2 of the *var*CPSO-ls algorithm were set at 6.05 with a swarm size of 60 individual particles; all other parameters remained at default. The depicted pose was selected based on lowest binding energy and visual inspection of the inhibitor-protein interactions. All docking images were created with PyMOL (Schrodinger, New York, USA).

2.3. Site-directed mutagenesis

The coding sequence of murine *Gnaq* (see UniProt ID P21279 for protein sequence) was obtained in pcDNA3.1(+), in which we performed site-directed mutagenesis. The sequence was modified to contain a partial internal HA-tag (DVPDYA; required mutations: E125D, N126V, Y128D, V129Y, and D130A) between residues 125–130. Single amino acid exchanges were induced by whole-plasmid polymerase chain reaction (PCR; 150 ng template DNA, 0.25 mM dNTP mixture, 0.25 µl DMSO, 5 µl GC-buffer, 125 nM each forward- and reverse primer, 0.5 µl Phusion polymerase (New England Biolabs, Ipswitch, MA, USA); thermocycling protocol: 30 s 98 °C, 20 cycles of 10 s 98 °C, 30 s 58 °C, 5 min 72 °C, 10 min final elongation at 72 °C) using a set of specific primers, listed in Supp. Table 1. Subsequently, competent DH5α *E. coli* were transformed with DpnI-digested (New England Biolabs; 90 min, 37 °C) PCR product and added onto Ampicillin-containing agar plates. The next day, cDNA was isolated from individual clones and the DNA sequence was confirmed by sequencing (Eurofins Genomics, Ebersberg, Germany). cDNA was amplified and cloned into the retroviral expression vector pQCXIN.

2.4. Cell culture

HEK293 cells (human, female), whose *GNAQ/GNA11* genes were previously removed via CRISPR/Cas9 (HEK293 $G\alpha_{q/11}$-KO; obtained from A. Inoue) [13,49], were cultured at 37 °C, 5% CO_2 in Dulbecco's modified Eagle medium (DMEM), supplemented with 10% fetal bovine serum (FBS), and a penicillin/streptomycin mixture (PenStrep; final concentrations: penicillin = 100 U*ml^{-1}, streptomycin = 0.1 mg*ml^{-1}). Medium for HEK293 $G\alpha_{q/11}$-KO cells recombinantly expressing $G\alpha_q$ protein was additionally supplemented with G418 (0.2 mg*ml^{-1}). When cells were about 70–80% confluent, the medium was discarded and the cell monolayer was rinsed with phosphate-buffered saline (PBS; 137 mM NaCl, 2.7 mM KCl, 4.3 mM Na_2HPO_4, 1.47 mM KH_2PO_4). Subsequently, cells were incubated in a trypsin-ethylenediaminetetraacetic acid (EDTA) solution at room temperature, detached from the cell culture flask, and diluted into new cell culture flasks. Cell lines were routinely checked for mycoplasma contamination by PCR; cell lines used for membrane preparations and calcium mobilization assays were passaged less than 10 times after retroviral transfection.

2.5. Retroviral transfection

HEK293 $G\alpha_{q/11}$-KO cells were stably transfected with the coding sequence for either wild-type (wt) or mutant murine *Gnaq* as previously described for the $P2Y_2$ receptor [50]: On the first day, 1.5 × 106 GP^+envAM12 packaging cells were seeded and transiently transfected with the *Gnaq* cDNA (in the pQCXIN vector, 6.25 µg) and vesicular stomatitis virus G (VSV-G, in pcDNA3.1, 3.75 µg) protein cDNA on day 2, utilizing lipofectamine 2000 (25 µl). After 16 h, production of viral vectors was induced by the addition of 3 ml DMEM containing 10% FBS, PenStrep and 5 mM sodium butyrate, followed by a 48 h incubation at 32 °C. Viral vectors were harvested, filtered (0.2 µm pore diameter), and added to HEK293 $G\alpha_{q/11}$-KO cells. Polybrene solution (6 µl, 4 mg*ml^{-1} in water, sterile filtered) was added. After 2.5 h, the virus solution was discarded and the cells were supplemented with fresh DMEM + 10% FCS + PenStrep. Selection for geneticin resistance was induced 72 h later by the addition of 0.2 mg/ml G418 to the media.

2.6. Cell membrane preparations

Recombinant HEK293 cells were cultured as described above and kept in an exponential growth phase. To obtain membrane preparations, HEK293 cells were seeded into cell culture dishes. When the cell monolayer became confluent, the medium was discarded, and the dishes were frozen at − 20 °C overnight. After defrosting, cells were detached with a rubber scraper while adding 5 mM Tris + 2 mM EDTA, pH 7.4. The cell suspension was homogenized with an UltraTurrax® (IKA Labortechnik, Staufen, Germany) for 1 min at level 4. The homogenate was centrifuged for 10 min at 1000 *g*, 4 °C; the pellet (P1) was discarded and the supernatant (S1) was then centrifuged for 1 h at 48,400 *g*, 4 °C. The supernatant (S2) was discarded, the pellet (P2) was resuspended in 5 mM Tris + 2 mM EDTA, pH 7.4, and centrifuged for another hour at 48,400 *g*, 4 °C. Again, the supernatant was discarded, the pellet resuspended in 50 mM Tris-HCl, pH 7.4, and aliquots were stored at − 80 °C until use.

2.7. Protein concentration determination

Protein concentration was determined by the Lowry method [51]: 2% (w/v) $NaHCO_3$ were dissolved in NaOH; this solution was mixed 50:1 with an aqueous 0.5% (w/v) Cu_2SO_4 + 1% (w/v) sodium tartrate solution. Of this mixture, 1 ml was added to 200 µl of sample solution (diluted 1:20 in Tris buffer) in 50 mM Tris buffer, pH 7.4. After incubation for 20 min at room temperature, 100 µl Folin phenol reagent solution (18 ml Folin reagent in 90 ml distilled water) were added to the mixture, which was then vortexed thoroughly. After another 30 min of incubation at room temperature, absorption was measured at 500 nm. A bovine serum albumin (BSA) calibration curve from 0.1 to 0.5 mg BSA/ml served for calibration.

2.8. SDS-PAGE and western blotting

HEK293 cell membrane preparation (20 µg of protein) was mixed with 4x sodium dodecyl sulfate (SDS) loading buffer, and the mixture was diluted with H_2O to a final volume of 20 µl. Samples were heated at 95 °C for 5 min and loaded onto a 10% acrylamide Tris-glycine gel. Proteins were separated by applying a constant voltage of 200 V for approximately 1 h and then transferred to a nitrocellulose membrane by tank blotting (75 V constant voltage, 90 min, in 200 mM glycine + 20 mM Tris + 20% MeOH on ice). Successful protein transfer was confirmed by an in-between Ponceau S staining of the nitrocellulose membrane; afterwards non-specific binding sites were blocked with PBS + 0.1% Tween 20 (PBS-T) + 5% milk powder (blocking buffer). Prestained PageRuler™ protein ladder (6 µl; ThermoFisher, Waltham, MA, USA) served as a protein standard. Recombinant expression of the $G\alpha_q$ protein was detected by its internal HA-tag. A primary murine antibody against the HA-epitope (BioLegend, Cat. Nr. 901502) was diluted in blocking buffer and the membrane was incubated at 4 °C overnight. The next day, the primary antibody solution was discarded, and the membrane was rinsed and washed with blocking buffer 4 times every 5 min. A secondary horseradish peroxidase (HRP)-coupled goat anti-mouse antibody (Jackson ImmunoResearch, 115–035–003, Lot No.: 146779; 1:4000 in blocking buffer) was incubated with the membrane for 90 min at room temperature. After washing the membrane five times for 5 min each step with PBS-T, it was covered with a luminol-peroxide detection reagent (ThermoFisher, Waltham, MA, USA). Chemiluminescence was detected by a multi-purpose imager (BioRad ChemiDoc, BioRad, Wien, Austria).

2.9. Determination of specific binding and competition binding assays

Radioligand binding assays were performed in 50 mM Tris-HCl, pH 7.4, in a final assay volume of 200 µl as previously described [28]. Wt or mutant HEK293 membrane preparations (50 µg of protein if not indicated otherwise) were co-incubated with ~5 nM of the respective radioligand for 90 min at 37 °C with gentle shaking. Total binding of the radioligand was determined in the presence of 5 µl dimethyl sulfoxide (DMSO) and non-specific binding was determined in the presence of FR or YM, respectively, dissolved in 5 µl DMSO (final concentration: 5 µM). In competition binding assays, different concentrations of unlabeled FR or YM, dissolved in DMSO, were added to the mixture.

Incubation was terminated by rapid filtration through GF/C glass-fiber filters using a Brandel 24-well harvester. Assay tubes were rinsed thrice with cold Tris-HCl + 0.1% BSA + 0.1% Tween20. Filters were dried, punched out, and transferred to scintillation vials. Luma Safe® scintillation cocktail (2.5 ml) were added and the filters were incubated for at least 9 h prior to measurement in a liquid scintillation counter (53–55% counting efficiency). Non-specific binding was subtracted from total binding to determine specific binding. Results are depicted in pmol bound radioligand per mg protein.

2.10. Calcium mobilization assays

Inhibition of G_q-mediated calcium mobilization by FR and YM in recombinant HEK293 cells was determined in analogy to described procedure [50,52]. One day prior to testing, HEK293 cells were detached from their cell culture flasks and seeded into black clear-bottom 96-well plates (Corning 3340) at a density of 45,000 cells per well. The following day, the medium was discarded and cells were incubated for 1 h with a mixture of fluo-4-acetoxymethyl ester (final concentration: 3 µM) and Pluronic F-127 (final concentration: 0.075% (w/v)), both dissolved in DMSO (final DMSO concentration at this step: 0.6%) in Hank's balanced salt solution (HBSS). All incubation steps were performed at 25 °C with gentle shaking of the plates. After removing excess dye, 178 µl HBSS + 2 µl FR/YM solution in DMSO were added to the cells, which were then incubated for 30 min. For activation, 20 µl of a solution of a GPCR agonist (ATP corresponding to an EC_{80} concentration if not mentioned otherwise), dissolved in HBSS, was pipetted into each well and fluorescence at $\lambda = 525$ nm was measured by a NovoStar microplate reader (BMG Labtech, Offenburg, Germany). As a positive control, cells were incubated with pure DMSO solution in the last step; in negative controls, cells were co-incubated with pure DMSO and stimulated with HBSS only.

2.11. Binding kinetics

Assays were performed in 50 mM Tris-HCl, pH 7.4, in a final assay volume of 200 µl. For association, HEK293 membrane preparation (50 µg of protein) was mixed with 95 µl of buffer and 5 µl of DMSO. Non-specific binding was determined in the presence of 5 µl YM or FR (final concentration: 5 µM) in DMSO. The mixture was incubated at 37 °C in a water bath upon gentle shaking. At given time points, 50 µl of radioligand solution was added to the mixture. Further assay handling was done as described above for the determination of specific binding. Specific binding of the radiotracers was determined, results were normalized to 0 cpm = 0% and specific binding at time 0 = 100%. Association half-life was calculated by the "one phase - association"-equation, implemented in GraphPad Prism 7.0 (GraphPad, San Diego, CA): $Y=Ymax^* [1-\exp(-k_{obs}^*X)]$, with $t_{1/2} = \ln(2)/k_{obs}$ (Y, specific binding; Ymax, maximum specific binding; X, time (min); k_{obs}, observed association rate). Observed association rates were not corrected for dissociation.

For dissociation experiments, 95 µl of buffer, 50 µl of HEK cell membrane suspension (50 µg of protein) and 50 µl of radioligand (final concentration: 5 nM) were pre-incubated for 60 min at 37 °C to reach equilibrium. Dissociation was initiated at given time points by adding 5 µl of YM or FR in DMSO (final concentration: 5 µM). The subsequent assay procedure was the same as described above. Specific binding was calculated and normalized as described above for association. Normalized data were fit with the "one phase exponential decay"-equation ($Y=(Y0-NS)^*\exp(-k_{off}^*X)$) in GraphPad Prism 7.0 and the dissociation $t_{1/2}$ was calculated ($t_{1/2} = \ln(2)/k_{off}$) (Y, specific binding, Y0, specific binding at X = 0, NS, non-specific binding, koff, dissociation rate).

2.12. Molecular dynamics simulations

VMD1.9.4 [53] was used to preprocess the crystal structure of the $G\alpha_{q/i1N}\beta1\gamma2$ protein in complex with YM-254890 (PDB-ID:3AH8). Any co-crystallization atoms different than water or GDP molecules closer than 5 Å to the protein were removed. One magnesium ion was modelled by homology (PDB-ID: 6EG8) next to the terminal phosphate group of GDP. Missing Gα N- and C-terminal residues 2–6 and 355–359 were modelled ab initio using MODELLER (version 10.1) [54]. MODELLER was also employed to model via homology modelling both the Gβ N-terminal residues 2–10, and the Gγ N- and C-terminal residues 2–10 and 61–67. The FR-bound structure was generated by superposing FR onto YM, and subsequently removing the latter. This initial pose of FR is very similar to the docked posed in Kuschak et al. [28] (RMSD = 0.60 Å; measured in the carbon atoms of the depsipeptide ring; 15 atoms). The inhibitor-free structure was generated by simply removing YM from the binding pocket. Each inhibitor-bound and the inhibitor-free structure was then placed into a 124 × 124×124 Å water box made of explicit TIP3 water molecules, the global electrostatic charge was neutralized and the ionic strength was adjusted with 0.15 M NaCl using the CHARMM-GUI builder [55]. All titratable residues of the protein were left in their dominant protonation state at pH 7.0, and all histidine residues were protonated at Nδ (the CHARMM-GUI default). Bond lengths involving hydrogen atoms were constrained using the LINCS algorithm. The solvated system was first geometry-optimized by 5000 steps of energy minimization using the steepest descent method. Subsequently, the systems were relaxed by applying harmonic positional restraints to all Cα atoms of the protein that were gradually released throughout the equilibration. The first step of the equilibration phase was run in the NVT ensemble (Berendsen thermostat; time constant: 0.5 ps; reference temperature: 310 K) for 0.125 ns, the second step was run in the NPT ensemble (Berendsen barostat; type: isotropic; time constant: 5 ps; reference pressure: 1.013 bar) for 5 ns. Three independent trajectories were spawned from the last snapshot of the equilibrated system using a random seed. Production simulations for each replica were run in the NVT ensemble (Nose-Hoover thermostat; time constant: 1 ps; reference temperature: 310 K) for 500 ns. The production simulations of this study yielded an aggregated time of 4.5 µs (3 systems x 3 replicas x 500 ns). All simulations were run using GROMACS v2020.4 [56] in combination with the CHARMM36m force field [57]. YM and FR parameters were generated with the CHARMM General Force Field [58]. Figures from simulations were rendered using the Tachyon renderer [59].

The Jensen-Shannon distance [60] was used to compare structural ensembles from the simulations via the relative entropy analysis module of the PENSA library [61].

The ligand-protein contact frequency analysis was performed using the mdciao library [62]. A cutoff distance of 4 Å between residue atoms was used to define contacts.

Angles between helices were calculated using the AngleBetweenHelices PyMOL module (https://github.com/Pymol-Scripts/Pymol-script-repo/blob/master/anglebetweenhelices.py).

2.13. Quantification and statistical analysis

For each data point, at least three individual experiments ($n \geq 3$) were performed, each in duplicate. The exact number of replicate

experiments can be found in figure and table legends. Unless otherwise stated, data are expressed as mean ± SEM.

Statistical analysis was carried out by using GraphPad Prism v. 7.0. To assess a mean difference between two groups, an unpaired t-test was employed when data displayed normality and variance homogeneity. When data showed variance inhomogeneity, Welch's t-test was used instead. Normality and variance homogeneity were assessed with Shapiro-Wilk's test and F-test, respectively. To determine significant differences of a mean in a series of three or more experimental conditions, a one-way analysis of variance (ANOVA) was carried out. If the difference among means was significant ($p < 0.05$), the mean of each column was compared with the mean of the reference condition and corrected for multiple comparisons using Dunnett's *post-hoc* test. To compare the difference between two groups (YM and FR) under multiple different conditions (several $G\alpha_q$ mutants), multiple unpaired t-tests were used and corrected for multiple comparisons according to the Holm-Sidak-method. P-values of < 0.05 were considered to be statistically significant (*), $p < 0.01$ was considered to be very statistically significant (**) and $p < 0.001$ was considered to be highly statistically significant (***).

2.14. Data and material availability statement

All data sets obtained in this study, retrovirally transfected HEK293 cell lines, mutated and wild-type *Gnaq* coding sequence in pcDNA3.1(+) and pQCXIN are available upon reasonable request by a qualified researcher. Radiolabeled compounds can only be made available to

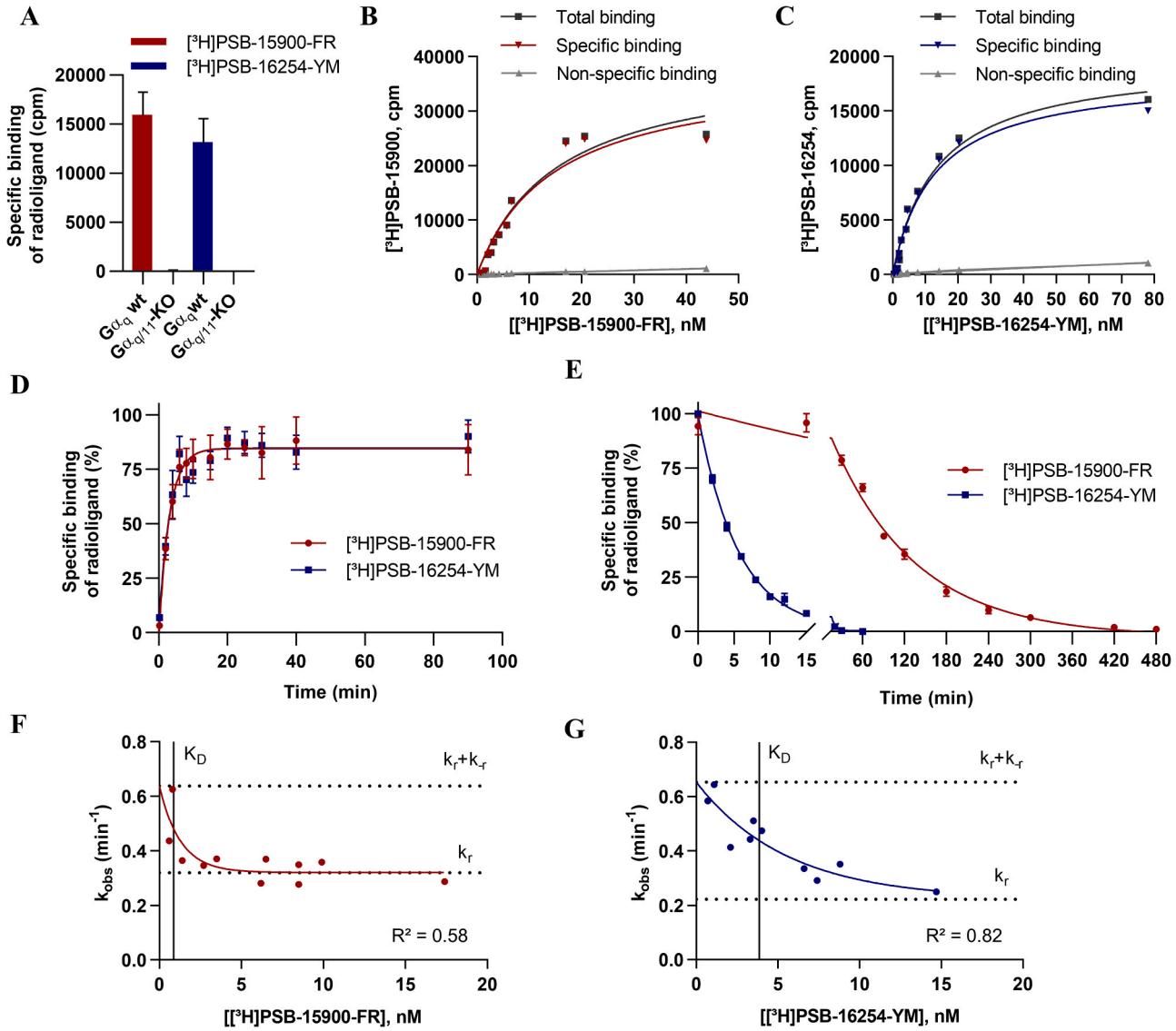

Fig. 3. Binding of FR-derived radioligand [^{3}H]PSB-15900-FR and YM-derived radioligand [^{3}H]PSB-16254-YM to HEK cell membrane preparations recombinantly expressing the wt $G\alpha_q$ protein. (**A**) Specific binding of [^{3}H]PSB-15900-FR and [^{3}H]PSB-16254-YM (5 nM each) to HEK293 $G\alpha_{q/11}$-KO membrane preparations (50 µg of protein) in the presence or absence of recombinantly expressed $G\alpha_q$ protein. Incubation was performed for 90 min at 37 °C. (**B**, **C**) Saturation binding curves of [^{3}H]PSB-15900-FR (**B**) and [^{3}H]PSB-16254-YM (**C**) to HEK293 membrane preparations (25 µg of protein) recombinantly expressing wt $G\alpha_q$ protein, incubated at 37 °C for 90 min (**D**) Association of [^{3}H]PSB-15900-FR or [^{3}H]PSB-16254-YM (5 nM each) to HEK293 cell membrane preparations recombinantly expressing wt $G\alpha_q$ protein (50 µg of protein) at 37 °C. (**E**) Dissociation of [^{3}H]PSB-15900-FR and [^{3}H]PSB-16254-YM (5 nM each) from wt $G\alpha_q$ protein-expressing HEK293 membrane preparations (50 µg of protein) at 37 °C. Dissociation was induced by the addition of 5 µM of FR, or YM, respectively, after a 60 min of pre-incubation with the radioligand. (**F**, **G**) Plots of k_{obs} (min^{-1}) versus [L] (nM) for [^{3}H]PSB-15900-FR (**F**) and [^{3}H]PSB-16254-YM binding (**G**). Association experiments were performed at 37 °C with wt $G\alpha_q$ HEK293 cell membrane preparations (10 µg of protein). Y-axis intercept (labeled as $k_r + k_{-r}$) and plateau levels (labeled as k_r) are indicated by dashed lines. Data points represent mean ± SEM of at least three independent experiments performed in duplicates (**A**, **D-F**). In panels **B** and **C**, a representative trace out of three individual experiments performed in duplicate is depicted; in panels **G** and **H**, each data point represents an individual experiment.

researchers with an appropriate handling license, and the access to those compounds may be limited due to radioligand batch size.

3. Results

3.1. Expression and characterization of the wildtype $G\alpha_q$ protein

As a first step, we expressed and comprehensively characterized the wt $G\alpha_q$ protein expressed in HEK293 cells whose *GNAQ/GNA11* genes had been knocked out by CRISPR-Cas9. To confirm recombinant expression of the $G\alpha_q$ protein, we determined binding of [^{3}H]PSB-15900-FR and [^{3}H]PSB-16254-YM to wt $G\alpha_q$-expressing HEK293 cell membrane preparations (Fig. 3A). HEK293 $G_{q/11}$-KO cells were selected for this study because they allow recombinant expression of (mutant) $G\alpha_q$ proteins without any background of endogenously expressed wt $G\alpha_q$ protein. In CRISPR-Cas9 knockout cells transfected with the wt $G\alpha_q$ protein we observed high specific binding of both radioligands, while no specific binding was detected in KO cells lacking $G\alpha_q$ proteins. To estimate $G\alpha_q$ protein expression levels and apparent dissociation constants (K_D values), saturation experiments were performed (Fig. 3B for [^{3}H]PSB-15900-FR, Fig. 3C for [^{3}H]PSB-16254-YM). Binding was saturable, and the following values were determined: [^{3}H]PSB-15900-FR, $pK_D = 7.92 \pm 0.12$, $B_{max} = 19.8 \pm 2.9$ pmol/mg protein; [^{3}H]PSB-16254-YM, $pK_D = 7.80 \pm 0.09$, $B_{max} = 21.8 \pm 4.7$ pmol/mg protein. There was no significant difference between apparent pK_D and B_{max} values obtained with either radioligand, [^{3}H]PSB-15900-FR or [^{3}H]PSB-16254-YM, confirming previous results on human platelet membranes [28].

Next, we studied binding kinetics. Association of both radioligands was rapid showing almost identical association kinetics ([^{3}H]PSB-15900-FR: association $t_{1/2} = 2.18 \pm 0.21$ min; [^{3}H]PSB-16254-YM: association $t_{1/2} = 2.47 \pm 0.57$ min; see Fig. 3D). However, dramatic differences in dissociation kinetics and thus in residence times of both radioligands were observed in recombinantly expressed wt $G\alpha_q$ proteins, consistent with those previously determined in native human blood platelet membranes [28]. In wt $G\alpha_q$ proteins, [^{3}H]PSB-15900-FR displayed a long dissociation half-life of 79.2 ± 1.54 min determined at 37 °C, while [^{3}H]PSB-16254-YM showed a substantially shorter half-life of only 3.89 ± 0.16 min (Fig. 3E). The calculation of kinetic K_D values (k_{off}/k_{on}) performed under the assumption of a one-step binding model (using the equation $k_{obs} = k_{on}[L]+k_{off}$; $k_{obs} = \ln(2)/\text{association } t_{1/2}$; [L] radioligand concentration, $k_{off} = \ln(2)/\text{dissociation } t_{1/2}$) resulted in kinetic pK_D values of 9.85 for [^{3}H]PSB-15900-FR and of 8.06 for [^{3}H]PSB-16254-YM.

Next, we examined the dependence of k_{obs} on ligand concentration, [L], by performing association experiments with varying concentrations of [^{3}H]PSB-15900-FR (Fig. 3F) and [^{3}H]PSB-16254-YM (Fig. 3G). Assuming a one-step binding model, k_{obs} would linearly increase with increasing ligand concentration [L]. The obtained data, however, fitted best to an exponentially decaying curve resulting in a Y-axis intercept of 0.64 min^{-1} and a plateau of 0.32 min^{-1} for [^{3}H]PSB-15900-FR, and a Y-axis intercept of 0.65 min^{-1} and a plateau of 0.22 min^{-1} for [^{3}H]PSB-16254-YM. This indicates a binding mechanism that is based on conformational selection (described in Fig. 2).

3.2. Site-directed mutagenesis study to reveal molecular determinants for the long residence time of FR

As a next step, we set out to study the molecular basis for the large difference in residence time between both radiotracers. The substituents R^1 and R^2 (Fig. 1) represent the only differences between FR and YM (and their radiolabelled derivatives) and must therefore be ultimately responsible for the large difference in dissociation kinetics. We hypothesized that the larger and more lipophilic substituents –ethyl (R^1) and isopropyl (R^2) in FR and its radioligand [^{3}H]PSB-15900-FR– may form stronger hydrophobic interactions with the $G\alpha_q$ protein than the methyl groups in the corresponding positions of YM and its radioligand [^{3}H]PSB-16254-YM. These residues in FR might act as anchors locking the inhibitor in its binding site [28]. To analyze the molecular basis for the differences in residence time, we modified the inhibitor binding site [27,28] in the $G\alpha_q$ protein by site-directed mutagenesis. We focused on residues presumed to interact with "anchor 1″ (R^1), and "anchor 2″ (R^2), respectively (see Fig. 1B and Fig. 4).

Anchor 1 of FR is proposed to bind to a rather wide interface [28] between Gβ and the β2/β3 strands of $G\alpha_q$ (residues I190$^{G.S02.02}$, E191$^{G.S02.03}$, P193$^{G.S02.05}$ and R202$^{G.S03.04}$, Fig. 1B and Fig. 4; residues are labeled according to the CGN numbering system for heterotrimeric G proteins [4]). The predicted binding mode potentially allows for significant conformational flexibility of anchor 1. We generated a series of point mutations in this region of the $G\alpha_q$ protein. Mutants I190F and I190W are expected to disrupt a small hydrophobic cluster that likely forms crucial hydrophobic interactions with FR [15]. Mutant E191A disrupts a salt bridge with R202$^{G.S03.04}$ that stabilizes the β2/β3 sheet (see Fig. 4). The R202H mutant preserves the charge of the side chain but alters its size introducing steric hindrance. Finally, mutant P193C (inspired by the YM/FR-resistant $G\alpha_{15/16}$ [33], which harbors the same amino acid exchange) was designed to alter the structure of the β2 strand. We expected that these alterations of the YM/FR binding pocket near anchor 1 would provide information on the molecular determinants of their binding interactions.

In anchor 2, the lipophilic isopropyl group of FR is predicted to contact residues in helix A of the αH Gα domain (G74$^{H.HA.06}$, F75$^{H.HA.07}$, L78$^{H.HA.10}$, see Fig. 4). In this region, we generated a series of mutants meant to directly disrupt these interactions. The small G74$^{H.HA.06}$ was replaced by a bulky valine residue (G74V), whose side chain may clash with the isopropyl moiety of FR. F75$^{H.HA.07}$ was exchanged to alanine (F75 A) to disrupt its predicted interaction with FR, and to lysine (F75K), respectively, to further disrupt the hydrophobic cluster between linker 1 and switch 1 [15], which was expected to perturb inhibitor binding. L78 $^{H.HA.10}$ was mutated to alanine (L78A) to eliminate another potential hydrophobic interaction partner for FR (see Fig. 4). In addition, we prepared the double mutant G74V/L78A, since both mutations were expected to affect the interaction of the isopropyl group in FR with the Gq protein. Finally, the exchange of V184$^{G.hfs2.03}$ (in switch 1) to methionine (V184M) was again inspired by the YM/FR-resistant $G\alpha_{15/16}$ mutant [33]. Although methionine is also lipophilic, its higher flexibility may affect ligand binding. All rationales for $G\alpha_q$ protein mutagenesis are summarized in Supp. Table 2.

3.3. Characterization of mutant $G\alpha_q$ proteins confirms binding of inhibitors

Mutations to the *Gnaq* gene were introduced by site-directed mutagenesis into the pcDNA3.1(+) vector. Cloning and expression were performed as described for the wt $G\alpha_q$ protein (see Sections 2.3, 2.5, and 3.1) to obtain membrane preparations of recombinant HEK293 $G\alpha_{q/11}$-KO cells expressing the designed mutants. All mutated proteins were found to be expressed in similar quantity with the exception of the E191A and I190W mutants, which showed lower expression levels (Fig. 5A; see Supp. Fig. 1 for full blots). We were unable to stably express the F 75 A mutant in HEK293 cells despite multiple attempts of retroviral transfection.

Next, we measured specific binding of both radioligands to HEK cell membrane preparations recombinantly expressing the mutant $G\alpha_q$ proteins (Fig. 5A). Membrane preparations expressing the $G\alpha_q$ mutants F75K, I190F, and I190W could not be labeled by the radioligands indicating that they had lost high affinity binding. In contrast, mutants E191A, P193C, R202H, G74V, L78A, V184M, and G74V/L78A all bound [^{3}H]PSB-15900-FR and [^{3}H]PSB-16254-YM with high affinity, although specific binding was notably lower than at the wt G_q protein, ranging between 10% and 54% ([^{3}H]PSB-15900-FR) and 4–33% ([^{3}H]PSB-16254-YM) (Fig. 5A). Both radioligands displayed only low specific binding at the G74V/L78A G_q protein mutant. Overall, [^{3}H]PSB-16254-

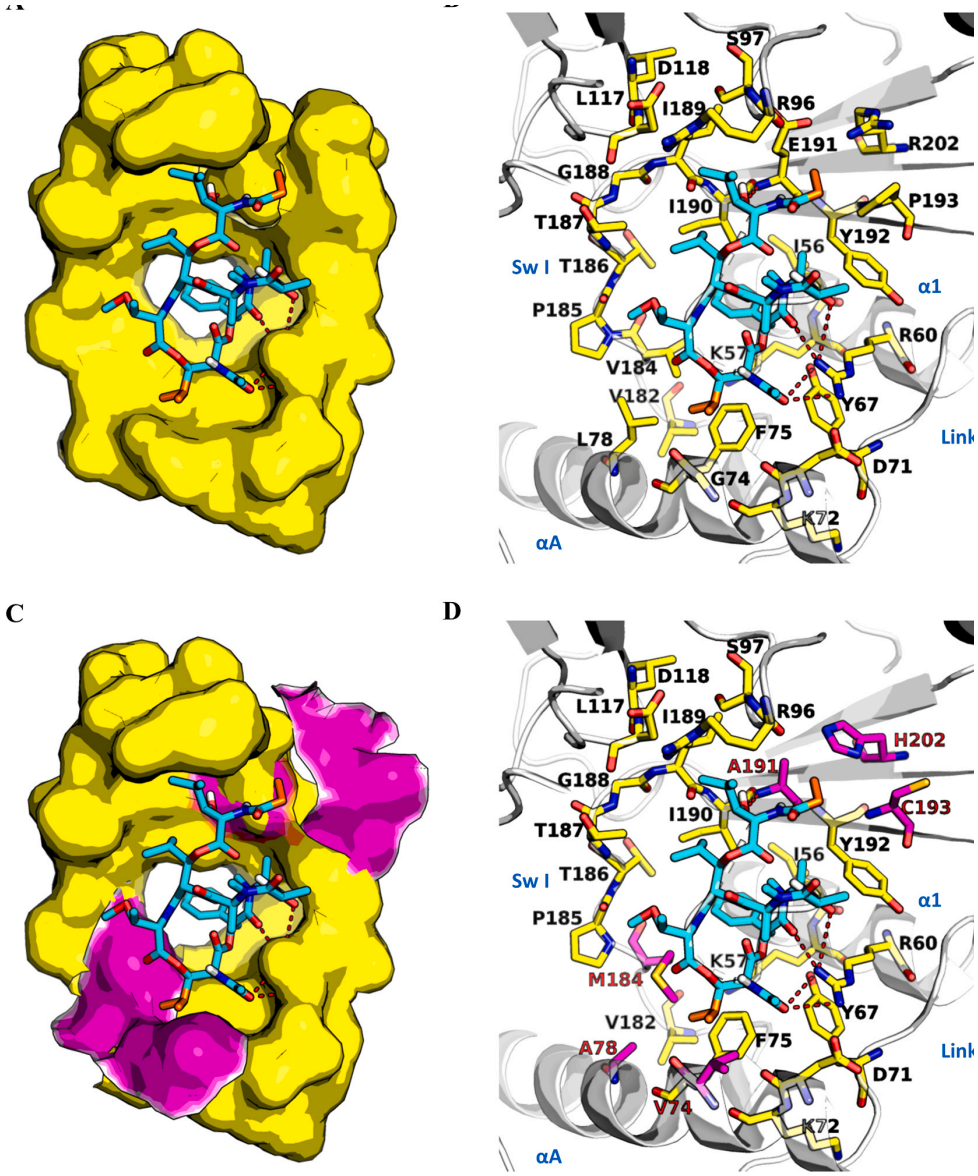

Fig. 4. Visualization of the residue exchanges near anchor 1 and anchor 2. (A) Surface representation and (B) stick model of the wt $G\alpha_q$ inhibitor binding site residues (yellow sticks) in complex with the docked pose of FR (cyan, anchors 1 (ethyl residue, top) and 2 (isopropyl residue, bottom) are highlighted in orange). A cartoon representation of the protein is shown in white. (C, D) Visualization of all mutations evaluated in binding assays at the $G\alpha_q$ binding site, highlighted in magenta. Residues are labeled in black, mutated residues shown in panel D, which were investigated in kinetic binding assays, are labeled in magenta. Secondary structure elements (white) involved in inhibitor binding are labeled in blue. The protein structure is based on the co-crystal structure of the heterotrimeric $G\alpha_q\beta_1\gamma_2$ protein in complex with GDP and YM; PDB-ID: 3AH8 [27].

YM showed somewhat lower specific binding at the mutant $G\alpha_q$ proteins than [^{3}H]PSB-15900-FR (Fig. 5A) determined under the same conditions.

Subsequently, the $G\alpha_q$ mutants were characterized in competition binding and functional assays to determine their affinity for FR and YM, their functionality, and the compounds' inhibitory potency. The pseudo-pK_D values of the mutants were determined using a competition binding assay of YM versus [^{3}H]PSB-16254-YM. We selected this radioligand due to its faster dissociation kinetics in wt $G\alpha_q$ proteins; therefore, it was easier to handle and did not require ultra-long incubation times to reach equilibrium. In the wt $G\alpha_q$ protein, the pseudo-pK_D value determined for YM was 8.19; all mutant $G\alpha_q$ subunits that could be investigated in binding studies showed similar values not significantly different from wt (i.e., all pseudo-pK_D values were around 8, see Supp. Table 4 and Fig. 5B).

Next, the inhibitory potencies of YM and FR were determined by GPCR-induced calcium mobilization assays in HEK293 cells expressing either the wt or a mutant $G\alpha_q$ protein. In preliminary experiments, we tested the potency and efficacy of several agonists of G_q protein-coupled GPCRs that are natively expressed in HEK cells. The nucleotides UDP, UTP, ADP, and ATP, and the acetylcholine analog carbachol all led to calcium mobilization in cells transfected with the wt $G\alpha_q$ protein (Supp.

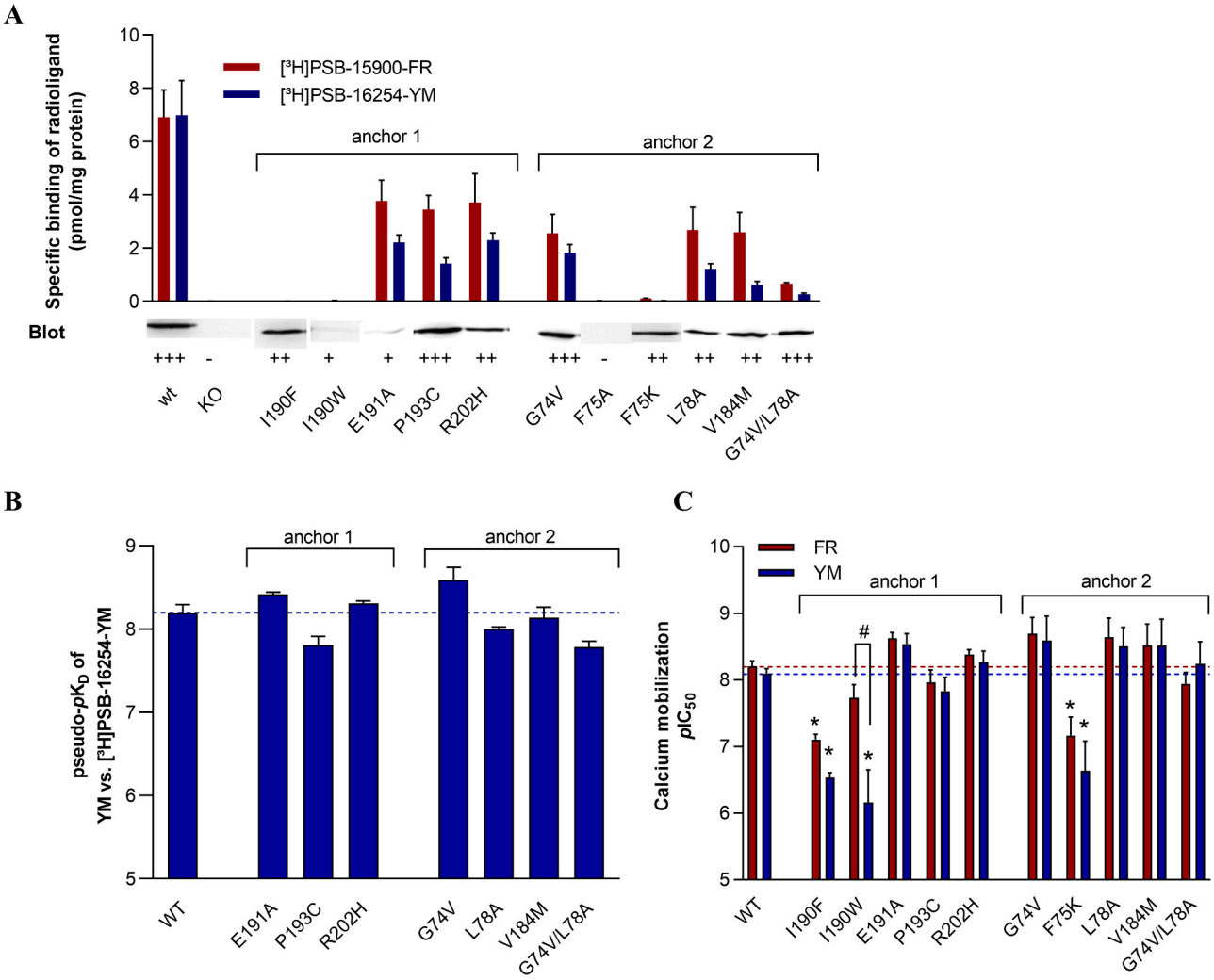

Fig. 5. Characterization of mutant $G\alpha_q$ proteins recombinantly expressed in HEK293 $G\alpha_{q/11}$-KO cells. (A) Top: Specific binding (% of wt) of [^{3}H]PSB-15900-FR (5 nM) to HEK293 cell membrane preparations recombinantly expressing $G\alpha_q$ subunits (50 µg of protein) after 90 min of incubation at 37 °C. Bottom: Western blot images of HEK293 $G\alpha_{q/11}$-KO cell membranes recombinantly expressing $G\alpha_q$ proteins (20 µg protein per lane). A primary antibody against the HA-tag was used to detect recombinant $G\alpha_q$ proteins; HEK293 $G\alpha_{q/11}$-KO cell membrane preparations served as a negative control. The expression level is indicated as follows: (−) no expression, (+) low expression, (++) moderate expression, (+++) high expression. Full Western blots are depicted in Supp. Fig. 1. (B) Pseudo-pK_D values [28] calculated by pseudo-homologous competition binding assays of YM versus [^{3}H]PSB-16254-YM. (C) Potency (pIC_{50}) of FR (red) and YM (blue) in HEK293 cells expressing mutated $G\alpha_q$ protein subunits compared to the wt $G\alpha_q$ protein. Calcium mobilization was induced by an EC_{80} concentration of ATP. Multiple t-tests were employed to compare the means between YM and FR of individual mutants; significant differences are indicated (#). The potency of YM and FR at all $G\alpha_q$ mutants was tested for significant differences from wt $G\alpha_q$ protein with a one-way ANOVA, followed by Dunnett's post-hoc test; significant differences ($p < 0.05$) are indicated with asterisks. All data represent means ± SEM of at least three separate experiments performed in duplicates.

Fig. 2A), while $G\alpha_{q/11}$-KO cells did not respond to any of these agonists (Supp. Fig. 2B). For subsequent experiments, we selected ATP, presumably acting via the $P2Y_{11}$ receptor endogenously expressed in HEK293 cells [63], because it provided the largest signal window. All mutants were found to be fully responsive to ATP (comparable to wt $G\alpha_q$ HEK293 cells) and displaying quantitatively similar calcium mobilization (see Supp. Fig. 2C). Both YM and FR (1 µM) were able to completely block ATP-induced calcium mobilization in the cell line expressing the wt $G\alpha_q$ protein as well as in most of the cell lines expressing mutant $G\alpha_q$ proteins. YM and FR had very similar potencies at the wt $G\alpha_q$ protein ($pIC_{50\ (FR)} = 8.20$, $pIC_{50\ (YM)} = 8.09$) and most of the mutant $G\alpha_q$ proteins (Fig. 4C). Exceptions were the $G\alpha_q$ mutants F75K, I190F, and I190W, which also had not shown high affinity binding in radioassays. For these mutants, higher concentrations of YM and FR were required to inhibit ATP-induced calcium mobilization. YM and FR did not display significant differences in potency at each individual $G\alpha_q$ mutant, with the exception of the I190W mutant, where YM was less potent than FR ($pIC_{50} = 7.73$ for FR and 6.16 for YM; all pIC_{50} values are summarized in Supp. Table 3).

3.4. Kinetic studies reveal drastically reduced residence times of FR at Gq protein mutants

As a next step, we measured the binding kinetics of both radioligands and all the mutants displaying sufficiently high radioligand binding. Association and dissociation rates of the radioligands (5 nM) at the recombinant HEK293 cell membrane preparations were determined at 37 °C and observed association half-lives ($t_{1/2} = \ln(2)/k_{obs}$) were calculated. In most cases, both radiotracers displayed fast association to the mutant $G\alpha_q$ subunits (Fig. 6A, B), similar as to wt $G\alpha_q$ protein ($t_{1/2}$ [^{3}H]PSB-15900-FR = 2.18 min; $t_{1/2}$ [^{3}H]PSB-16254-YM = 2.47 min; see also Fig. 3D). One exception was the E191A mutant, that exhibited a significantly slower association half-life of 7.71 min for [^{3}H]PSB-16254-YM, but not for [^{3}H]PSB-15900-FR (3.22 min)). Moreover, [^{3}H]PSB-

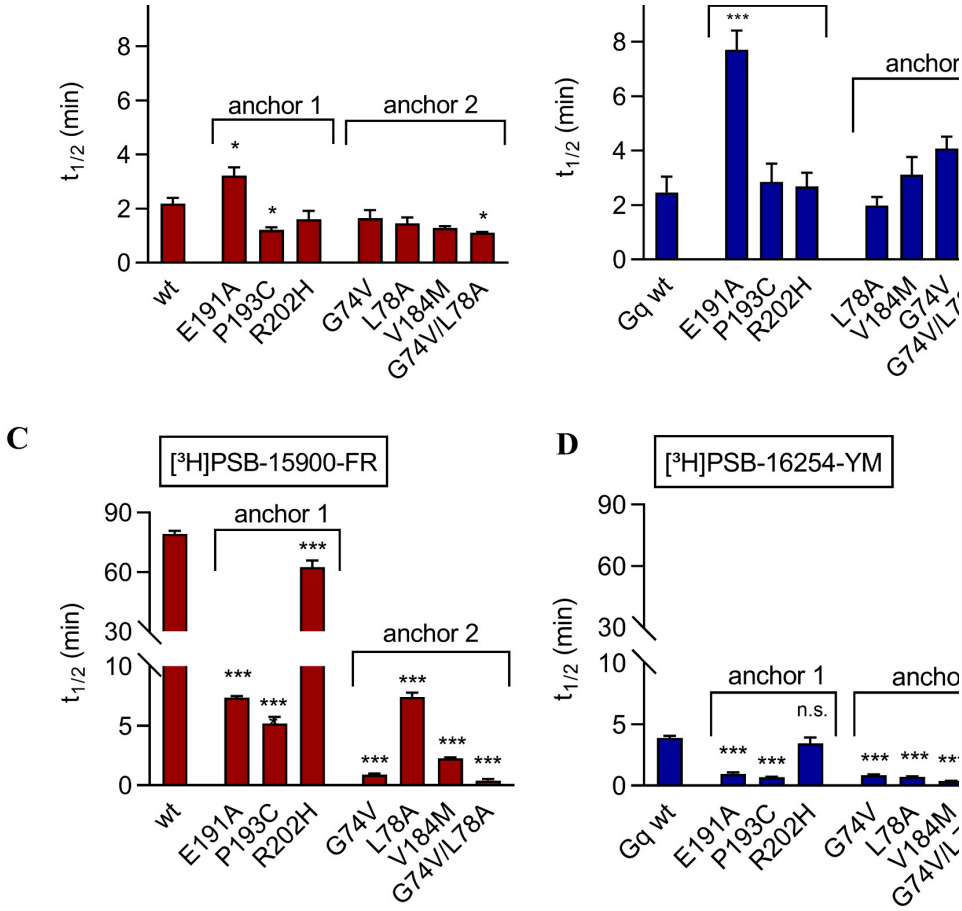

Fig. 6. Binding kinetics of $G\alpha_q$ radiotracers at HEK293 $G\alpha_{q/11}$-KO cells recombinantly expressing mutant $G\alpha_q$ proteins. (A) Association half-lives ($\ln(2)/k_{obs}$) of [^{3}H]PSB-15900-FR, (B) association half-lives of [^{3}H]PSB-16254-YM, (C) dissociation half-lives ($\ln(2)/k_{off}$) of [^{3}H]PSB-15900-FR, (D) dissociation half-lives of [^{3}H]PSB-16254-YM. All experiments were conducted with 5 nM of radioligand and 50 µg of protein at 37 °C. Data are presented as means ± SEM of three or four independent experiments each performed in duplicate (A-D).

15900-FR bound to the P193C and to the G74V/L78A double mutant somewhat faster than to the wt $G\alpha_q$ protein ($t_{1/2} = 1.21$ min for P193C and 1.11 min for G74V/L78A vs. 2.18 min for wt $G\alpha_q$ protein, see Supp. Table 5). All other determined association half-lives of both radioligands at the mutant $G\alpha_q$ proteins were not significantly different from those observed for the wt $G\alpha_q$ protein.

In contrast to the fast association, dissociation, in particular that of the slowly dissociating FR-derived radioligand, was strongly affected by the mutations in the binding sites (Fig. 6C,D, see Supp. Figs. 3 and 4 for dissociation curves and Supp. Table 6 for calculated values). For reference, in wt $G\alpha_q$-expressing cell membranes [^{3}H]PSB-15900-FR dissociated with a half-life of ~80 min at 37 °C, while [^{3}H]PSB-16254-YM dissociated about 20-fold faster, with a half-life of only ~4 min. All mutations in our study led to significantly accelerated dissociation of [^{3}H]PSB-15900-FR. The R202H mutant showed the smallest effect, with a decrease of the dissociation half-life from 80 to 60 min. All other mutations led to greatly reduced dissociation half-lives of below 10 min; the "anchor 2-mutants" G74V and G74V/L78A even caused [^{3}H]PSB-15900-FR to dissociate with a half-life of less than 1 min, accelerating the dissociation by 88- and 198-fold, respectively. The effects of the mutants on the dissociation rate of [^{3}H]PSB-16254-YM were qualitatively similar, but much less dramatic, since its dissociation determined at the wt $G\alpha_q$ protein was already fast ($t_{1/2} \sim 4$ min). [^{3}H]PSB-16254-YM displayed a dissociation half-life of only ~1 min at the E191A, P193C, G74V, and L78A mutants, which is approximately 4–5 times faster compared to that at the wt $G\alpha_q$ protein. The mutants V184M and G74V/L78A, located near "anchor 2", showed the fastest dissociation rate for [^{3}H]PSB-16254-YM resulting in half-lives of 0.37 and 0.30 min, respectively, which is more than 10 times faster than their dissociation from wt $G\alpha_q$ protein.

With the assumption of a one-step binding model, pK_D values for the rapidly dissociating mutants ($k_{off} > k_{obs}$) could not be calculated with the exception of the following radioligand – $G\alpha_q$ mutant combinations: [^{3}H]PSB-15900-FR binding to $G\alpha_q$ L78A ($pK_D = 8.92$), V184M (7.84), P193C (8.82), and R202H (9.88) and [^{3}H]PSB-16254-YM binding to $G\alpha_q$ R202H (7.77).

3.5. Molecular dynamics simulations support a conformational selection mechanism

In the past decade, advanced computational approaches have emerged to predict binding kinetics of ligand-target interactions

[64–67]. Some of these approaches are based on enhanced molecular dynamics methods that simulate the process of ligand binding/unbinding at the atomic level [67–70]. However, due to the potential conformational heterogeneity of the macrocyclic depsipeptides and of the $G\alpha_q$ binding site (which includes the flexible linker 1 and switch 1 regions), a very thorough sampling of the conformational landscape during the binding/unbinding process is required to predict binding kinetics of these inhibitors with accuracy. In this study, to gain insights into the inhibitor-G_q interactions at the atomic level, we settled to perform unbiased molecular dynamics simulations of the inhibitor-free G_q protein and of the G_q-FR and G_q-YM complexes (i.e., the start and end of the binding reaction) to search for clues of the origin of the conformational selection mechanism. We observed stable conformations of the Gαq subunit along the simulations, with only small fluctuations (below 2 Å RMSD) in some replicas (Supp. Fig. S5 and Supp. Fig. S6). We also observed stable binding poses for both inhibitors, although in some replicas they undergo slight rearrangements of ~2 Å to achieve new stable poses (Supp. Fig. S7). The base of helix A in the αH domain ($D69^{H.HA.01}$ - $L78^{H.HA.10}$) of $G\alpha_q$ shapes the inhibitor binding site, stabilizing several key hydrophobic interactions with anchor 1 of FR. Our simulations of the inhibitor-free G_q allowed us to explore the local structure around this region of the binding site (Fig. 7A). While helix A is relatively stable in the simulations (Supp. Fig. S8), we observed that, in the absence of an inhibitor, helix A can swing by ~12° between two extreme conformations. A population of this ensemble (red ribbons in Fig. 7A, left panel) results in a wider binding site suitable for inhibitor high-affinity binding (Fig. 7A, right panel). While the molecular mechanism of G_q inhibition by YM/FR is certainly more complex, we speculate that relocation of helix A in the αH domain of $G\alpha_q$ observed in our simulations is part of the conformational selection mechanism of these inhibitors (Fig. 7B).

In our simulations, we observed stable binding poses for both inhibitors, which establish persistent interactions with surrounding residues in the binding pocket (see Fig. 4). To find structural differences associated to the presence of the bound inhibitors, we compared conformational ensembles of apo versus inhibitor-bound simulations by measuring the relative entropy of the Jensen-Shannon distance (see Methods) of three structural metrics: backbone and sidechain torsion angles (Supp. Fig. 9) and distance between Cα atoms (Supp. Fig. 10). The analysis of the backbone torsion angles showed that YM- and FR-bound Gαq have similar differences in relative entropy with respect to the apo form (Supp. Fig. 9A + B). The residues with the highest difference for both inhibitor complexes are $E119^{H.hbhc.01}$ and $K120^{H.hbhc.02}$, which are exclusive of the Gαq family. Binding of the inhibitors significantly changes the mobility of this loop, which could be related to the stabilizing effect of the inhibitors that prevents the separation between the αH and RasD domains of Gαq. Interestingly, the region around switch II (s3h2 loop) also shows high entropy differences. The relative entropy analysis of sidechain torsion angles also revealed similarities between YM- and FR-bound Gαq with respect to the apo form (Supp. Fig. 9 C-D). While residue $S53^{G.H1.02}$ is most different between the apo and inhibitor-bound ensembles, residue $T54^{G.H1.03}$ is the second top-ranked residue only when FR is bound to the protein. Both $S53^{G.H1.02}$ and $T54^{G.H1.03}$ are conserved in all G protein families and lie at the nucleotide phosphate-binding P loop next to the GDP molecule, in direct contact with its terminal phosphate group, suggesting that the presence of the inhibitors may have a direct effect in the local structure of the nucleotide binding site. Finally, we also observe similarities in the relative entropies of Cα-Cα distances between YM- and FR-bound Gαq and the apo form, although the values are higher for the YM complex. The global heatmap (Supp. Fig. 10A+B) shows that the largest differences are around residues 180–210, which include linker 2/switch I, the S2/S3 beta strands, and switch II. Analysis of individual residues (Supp. Fig. 10C+D) revealed that most of the top-ranked relative entropies involve residues mutated in this study (Supp. Table 2). Most of the largest relative entropies correspond to residues around anchor 1 for both FR- and YM-bound Gαq. Remarkably, $G74^{H.HA.06}$ (whose mutation results in the largest reduction of the dissociation half-life of FR) is the only top-ranked residue around anchor 2, but only in the simulations of FR-bound Gαq. Also, the top-ranked relative entropies include $I190^{G.S02.02}$ – whose mutation to F/W result in loss of inhibitor binding – and $E191^{G.S02.03}$ – which exhibited a significantly slower association half-life for YM, but not for FR. $E191^{G.S02.03}$ is also the only residue among the 12 top-ranked residues interacting with the inhibitors that contacts FR but not YM (Supp. Fig. 11). Conversely, $V184^{G.hfs2.03}$, located near anchor 2 of the inhibitors, is the only residue in this list that contacts YM but not FR; its mutation showed the fastest dissociation rate for YM – more than 10 times faster than the wt.

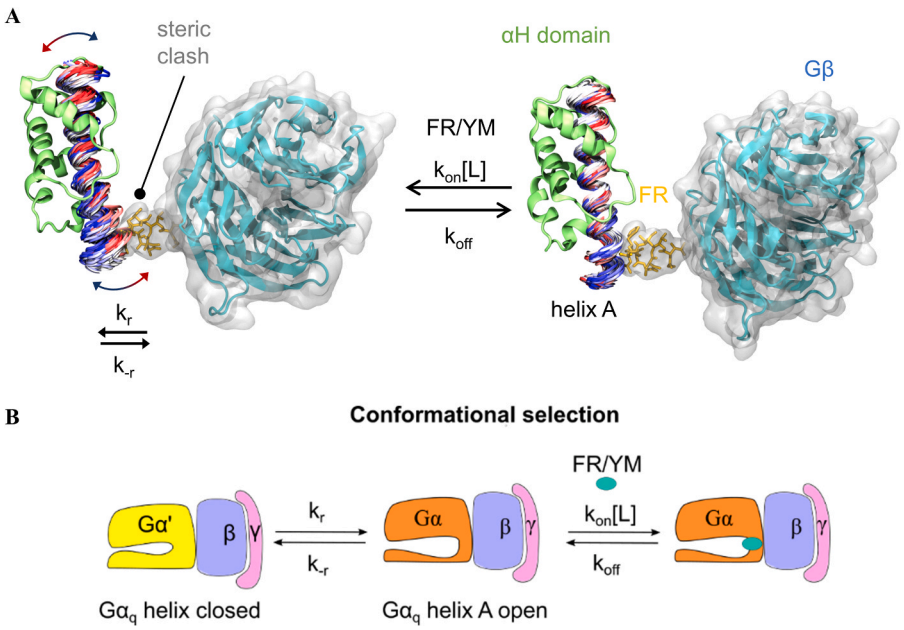

Fig. 7. Effect of FR/YM binding on the conformational dynamics of helix A in the αH domain of $G\alpha_q$. (A) The αH domain is shown as green cartoons, with time evolution across the simulation depicted on helix A (ribbons) in a blue-to-red gradient (blue – beginning of the simulation; red – end of the simulation) that colors 40 frames evenly distributed across the complete trajectory of a representative replica. The Gβ subunit is shown as blue cartoons and a translucent molecular surface. Except for helix A, only the first frame of the simulation is shown. In the absence of the inhibitor (left), the base of helix A can tilt towards the Gβ subunit thereby significantly obstructing the entrance route to the binding pocket (red ribbons); in this 'closed' conformation, residues at the base of helix A would clash with the inhibitor binding pose (docked pose (left) or initial frame of the simulations (right), shown as a translucent surface and orange sticks for reference). Inhibitors may select the open state of helix A (blue in the left panel) to bind with high affinity (right), thus preventing the inward tilt of helix A. (B) Proposed binding mechanism of YM and FR to the $G\alpha_q$ protein via a conformational selection mechanism. After a tilt of the helix A in the αH domain ($G\alpha_q$ helix A closed → $G\alpha_q$ helix A open), macrocyclic $G\alpha_q$ inhibitors can now bind to their binding site.

4. Discussion

The structurally similar cyclodepsipeptides FR and YM represent the only known non-protein entities inhibiting heterotrimeric G proteins with nanomolar potency, displaying selectivity for the $G\alpha_{q/11/14}$ subunits [13,15,28,35]. Because of the high impact of these tool compounds on pharmacological research, detailed information about their binding properties and interactions with the target is essential. In the present study, we aimed at elucidating the details of the binding mechanism and at investigating the molecular determinants for the long residence time of the macrocyclic $G\alpha_q$ protein inhibitor FR in comparison to its close analog YM. To this end, we expressed the wt and a series of mutant $G\alpha_q$ proteins in HEK293 $G\alpha_{q/11}$-KO cells [13,71]. As previously observed in native platelets (24-fold difference in residence time at 37 °C) [28], also in the recombinant system both radioligands showed a similarly large (20-fold) difference in dissociation kinetics and thus in residence time ($1/k_{off}$): 5.61 min for the YM-derived radioligand and 114 min for the FR-derived radioligand determined at 37 °C (Fig. 3E). Association of both compounds, however, was comparably fast (2.47 and 2.18 min, respectively) (Fig. 3D). In saturation binding assays, both radiotracers displayed nearly identical apparent pK_D values of around 8 (see Fig. 3B, C). These results were in agreement with data previously determined at platelet membrane preparations, and in accordance with pK_D values from pseudo-homologous competition binding studies (YM vs. [^{3}H]PSB-16254-YM, and FR vs. [^{3}H]PSB-15900-YM), in which both radioligands displayed virtually identical affinity at wt $G\alpha_q$ proteins expressed in HEK293 cells [28].

Whereas the calculated kinetic pK_D value of 9.5 obtained from association and dissociation experiments predicted a much higher affinity for [^{3}H]PSB-15900-FR, the kinetic pK_D value of [^{3}H]PSB-16254-YM was in good agreement with the apparent pK_D determined in the saturation binding studies. However, both the calculation of the apparent pK_D values from saturation binding and that of the kinetic pK_D value assume a one-step binding model and do not account for possible conformational transitions in the protein during binding or unbinding of the ligand. By performing concentration-dependent kinetic measurements (see Fig. 3F,G), we now provide evidence for a more complex binding mechanism predominantly characterized by initial conformational selection. Both, a one-step binding model, and an induced-fit model would necessarily result in an increase in k_{obs} with increasing ligand concentration, [L] [44]. However, we observed an exponential decrease. Therefore, conventional calculations must lead to invalid kinetic pK_D values, as the true on-rate k_{on} cannot be correctly estimated. Relevant kinetic parameters to describe a protein-ligand-interaction by a conformational selection model are the protein interconversion rates k_r and k_{-r}, which can be extracted from the Y-axis intercept (corresponding to the sum of $k_r + k_{-r}$) and the plateau (corresponding to k_r) of a plot of k_{obs} versus [L]. k_r describes the forward isomerization rate from a non-binding conformational ensemble of the protein towards a conformational ensemble that binds the ligand; conversely, k_{-r} describes the reverse isomerization rate. In the absence of a ligand, these protein states (labeled as Gα and Gα' in Fig. 2) are at equilibrium, but with increasing concentrations of ligand (FR or YM), the concentration of free Gα decreases and the formation of Gα from Gα' (k_r) becomes the rate-limiting step for ligand-protein complex formation. Analysis of the plots (Fig. 3F,G) yields similar interconversion rates of the wt $G\alpha_q$ protein with respect to both radioligands: forward isomerization of a non-binding conformation (Gα') towards a conformation capable of binding [^{3}H]PSB-15900-FR (Gα) occurs with a rate of $k_r = 0.32\ min^{-1}$ ($0.22\ min^{-1}$ for [^{3}H]PSB-16254-YM). The respective reverse isomerization rate for the [^{3}H]PSB-15900-FR-binding conformation is $k_{-r} = 0.32\ min^{-1}$ (0.43 for [^{3}H]PSB-16254-YM). A kinetic K_D value can be determined graphically from the plots as illustrated in Fig. 3 F,G, i.e. the concentration, at which k_{obs} equals the mean between the Y-axis intercept and the plateau. The kinetic K_D values determined by this method are 0.89 nM ($pK_D = 9.05$) for [^{3}H]PSB-15900-FR, and 3.86 nM ($pK_D = 8.41$) for [^{3}H]PSB-16254-YM, thus predicting a significantly higher affinity, especially for [^{3}H]PSB-15900-FR, than the determined apparent K_D values obtained by saturation experiments. These kinetic pK_D values are likely to be more accurate estimates of the compounds' affinities, correlating better with the very different k_{off} values of both radioligands, and taking their complex binding mechanism into account. We conclude that forward isomerization is the rate-limiting step in the association of [^{3}H]PSB-15900-FR and [^{3}H]PSB-16254-YM to the wt $G\alpha_q$ protein, which explains why determination of kinetic K_D values was not possible by equations designed for a one-step binding model.

Several reports on multi-step ligand binding to proteins have been published, either via induced fit or by conformational selection [45, 72–74]. In the present study we show that the $G\alpha_q$ protein inhibitors FR and YM bind through conformational selection. Taking into consideration the complex structure and the flexibility of the ligand, the major differences in residence time of both inhibitors, and the structural dynamics of Gα proteins [75–77], the entire binding mechanism may involve even further steps. Initial conformational selection is likely followed by induced-fit binding, possibly mediated by the hydrophobic anchors of FR, which act like "dowels" helping to retain the molecule in its binding pocket. Similar to a dowel or a snap-lock, FR and its radioligand are then presumably fixed by their lipophilic anchor residues, in particular by anchor 2. This mechanism explains the long residence time of FR in contrast to YM and its much higher kinetic pK_D value. Thus, the apparent pK_D value calculated for [^{3}H]PSB-15900-FR from saturation binding assays is markedly underestimated. It can be assumed that both inhibitors show an at least 4-fold difference in affinity as evidenced by their more accurate kinetic pK_D values derived from the two-step binding model.

In order to provide a structural explanation for the large differences in residence time, we mutated amino acid residues in $G\alpha_q$ protein around anchors 1 and 2 of bound FR. These residues were chosen based on molecular modeling and docking studies (Fig. 1, mutations are visualized in Fig. 4); our rationale is detailed in Supp. Table 2. Only the F75A mutant could not be expressed in our hands, while the F75K mutant lost high affinity binding and showed decreased potency for both FR and YM (Fig. 5). $F75^{H.HA.07}$ forms part of a small cluster of hydrophobic/aromatic amino acids ($Y67^{G.h1ha.04}$, $F75^{H.HA.07}$, $V184^{G.hfs2.03}$) joining linker 1 and switch 1, which link RasD and the αH domains of the Gα subunit. Our results show that disruption of this cluster leads to severely impaired inhibitor binding.

Most of the designed $G\alpha_q$ mutants exhibited high specific binding of both radioligands with similar affinity to the wt $G\alpha_q$ protein as determined in competition binding (Fig. 5B) and calcium mobilization studies (Fig. 5C). However, the I190F and I190W mutations led to a loss of high-affinity binding and reduced potency (Fig. 5, also see [78]). $I190^{G.S02.02}$ interacts with adjacent residues likely stabilizing switch 1 and is the top-ranked residue in relative entropies of Cα-Cα distances, i.e., there are pronounced differences in its position between apo and inhibitor-bound Gαq. The bulkier Phe and Trp side chains possibly perturb the local structure of the binding site near anchor 1. Interestingly, the reduction in potency appeared to be more pronounced for YM as compared to FR, especially in case of the I190W mutant (Fig. 5B) possibly because FR can compensate the unfavorable binding in the structurally altered mutants by its tighter binding due to its lipophilic anchors.

However, major differences among the studied mutants were observed in the kinetic studies. All mutations around anchors 1 and 2 dramatically accelerated the dissociation of the radiotracers, especially that of the slowly dissociating radioligand [^{3}H]PSB-15900-FR. This result is complementary to the structure-activity relationships observed for analogs of YM and FR [1,34,79] and a molecular networking analysis [80], which led to the conclusion that nearly every part of the inhibitor molecule contributes to its pharmacophore. The $G\alpha_q$ protein mutations accelerated the dissociation to variable extents. Kinetic data displayed the following rank order regarding the impact of the $G\alpha_q$ protein mutations on the dissociation of [^{3}H]PSB-15900-FR: G74V > V184M

> P193C > E191A, L78A > R202H.

The isopropyl residue (anchor 2) appears to play a key role for the long residence time of FR (Fig. 6C) since mutations around this region had even larger negative effects on the residence time of FR than those around anchor 1. The binding site near anchor 2 is likely tighter and features hydrophobic interactions with nearby residues including F75$^{H.HA.07}$, L78$^{H.HA.10}$, and V184$^{G.hfs2.03}$. Remarkably, the two most impactful single mutations analyzed are located around anchor 2. The G74V and G74V/L78A mutants are of particular interest since they dramatically reduced the dissociation half-life of [^{3}H]PSB-15900-FR by 88-fold and 198-fold, respectively, whereas the already low dissociation half-life of [^{3}H]PSB-16254-YM was reduced by 5- and 13-fold, respectively, resulting in virtually identical, very short residence times for both radioligands (0.53 and 0.43 min respectively). Residue G74$^{H.HA.06}$ is the only top-ranked one in relative entropy of Cα-Cα distances that can interact with anchor 2 of the inhibitors. This difference in the residue position (with respect to the apo Gαq protein) appears in the FR-bound simulations – but not in YM – suggesting that this change in mobility of helix A (possibly related to the conformational selection mechanism) is more substantial in case of FR binding. In the G74V mutant, the bulky side chain of the valine group likely clashes with the isopropyl moiety (anchor 2) of [^{3}H]PSB-15900-FR, resulting in a less stable binding pose with a faster off-rate. Conversely, exchange of L78$^{H.HA.10}$ for alanine might remove a favorable hydrophobic interaction partner for anchor 2 leading to a strongly reduced residence time of [^{3}H]PSB-15900-FR [28]. Alternatively, the observed effect of the L78A mutation on inhibitor dissociation might be caused by an impact on the structure/dynamics of helix A (where L78$^{H.HA.10}$ is located) that, in turn, alters the shape of the binding site, as this residue does not appear in the 15 most frequent inhibitor/protein contacts (Supp. Fig. 11). A similar mechanism could be associated to the V184M mutation in FR-bound Gαq, as this residue – located in switch II – is in contact with L78$^{H.HA.10}$ in helix A but does not frequently contact FR (Supp. Fig. 11).

In comparison, the binding pocket near anchor 1 is wider, allowing for flexible movements of the β-hydroxyleucine side chain of FR [28]. In this region, the only predicted interaction partner for anchor 1 is P193$^{G.S02.05}$. The P193C and V184M mutants were inspired by the FR-insensitive $G\alpha_{15/16}$ subunit, which is the closest $G\alpha_q$ paralog that does not bind the macrocylic inhibitors with high affinity. These $G\alpha_q$ mutants were previously found to be fully sensitive to YM and FR in functional assays [33], which is in good agreement with our data from calcium assays. However, we could now show that these single amino acid exchanges were sufficient to accelerate radioligand dissociation significantly. Also around anchor 1, the E191A mutation removes a salt bridge to the nearby R202$^{G.S03.04}$, which slowed down the association and accelerated the dissociation of the radiotracers. However, the more conservative R202H mutation, which maintains the positive charge, had no effect on association and a considerably lower impact on dissociation kinetics. These results show that the salt bridge between E191$^{G.S02.03}$ and R202$^{G.S03.04}$ (or H202 in the mutant) stabilizes a conformation of the β2/β3 sheet in the $G\alpha_q$ protein that favors binding of the inhibitors. Accordingly, E191$^{G.S02.03}$ is also among the top-ranked residues in relative entropy of Cα-Cα distances between apo and inhibitor-bound Gαq. Mutations around both anchors affected the dissociation half-life of the long-binding [^{3}H]PSB-15900-FR to a far greater extent than that of the short-binding [^{3}H]PSB-16254-YM (see Fig. 6 C + D and Supp. Table 6). For [^{3}H]PSB-15900-FR, minor changes of the protein binding site caused unexpectedly large changes in its dissociation. Mutagenesis studies with a focus on the study of ligand binding kinetics are scarce; only a limited number of structure-kinetic relationship studies have been performed, e.g. for the β_2-adrenoceptor [81], the cannabinoid CB_2 receptor [82], and cyclic dependent kinase 8/cyclin C (CDK8/CycC) [83]. However, no commonalities have been established for long-lasting ligand-protein complexes so far, and the interactions required for long-duration binding appear to be case-specific. These may include deep-pocket binding (CDK8/CycC inhibitors) [83], or – like in the present study – lipophilic interactions [82]. Moreover, there have been reports on compounds displaying a similar equilibrium K_i value at their target receptor despite large differences in their k_{off} values [84]. Residence time does not always correlate with the duration of action as shown e.g. for β_2 adrenoceptor agonists [81], but in other cases, a correlation has been observed, e.g. for adenosine A_{2A} receptor agonists [85]. In one of the few available in vivo studies of $G\alpha_q$ inhibitors, FR indeed inhibited metacholine-induced bronchoconstriction significantly longer than YM, and was pharmacologically active even 96 h after administration while the same dose of YM had lost all of its effect already after 48 h [17]. This report indicates that a long residence time leading to a long-lasting inhibition of $G\alpha_q$ is preferable, at least in the treatment of asthma bronchiale.

5. Conclusion

The previous development of radioligands obtained by ^{3}H-labeling of the potent and selective macrocyclic $G\alpha_q$ protein inhibitors FR and YM allowed us to perform structure-kinetics relationship studies at the $G\alpha_q$ inhibitor binding site. Mutation of selected amino acids revealed key interactions responsible for the long residence time of FR as compared to YM. Some of these residues form hydrophobic interactions with the isopropyl anchor 2 of FR (residues L78$^{H.HA.10}$ and V184$^{G.hfs2.03}$), providing a molecular basis for its long residence time. Surprisingly, binding affinity of FR and YM, inhibitory potency, and association kinetics in most of the investigated $G\alpha_q$ protein mutants appeared to be not significantly different to those of the wt $G\alpha_q$ protein, while dissociation was found to be dramatically accelerated, especially for the FR-radioligand.

A detailed investigation of the binding mode revealed that the observed association rate k_{obs} exponentially declines with increasing radioligand concentration, strongly suggesting that the radioligands bind to the wt $G\alpha_q$ protein via conformational selection. This finding is partially supported by molecular dynamics simulations that, despite not being able to describe the actual conformational selection mechanism, provide hints on its possible origin. Specifically, they allowed us to suggest that the binding mechanism of macrocyclic $G\alpha_q$ inhibitors, in particular that of the slowly dissociating FR, may involve yet further conformational changes, e.g., a "snap-lock"-like conformational rearrangement of the binding site around helix A in the αH domain of $G\alpha_q$ partially mediated by the anchors of FR, which is disrupted in the mutants. This mechanism provides an explanation for the much slower dissociation of FR as compared to YM. Furthermore, our data clearly demonstrate that an in-depth investigation of binding kinetics is crucial for the characterization of protein-ligand interactions. The present data are of general importance since residence time is increasingly recognized as a crucial parameter in drug development.

Funding Information

This work was supported by the Deutsche Forschungsgemeinschaft (DFG) (FOR2372, MU-1665/7-2) and by the Swiss National Science Foundation (SNF; grant number 192780) to XD.

CRediT authorship contribution statement

JHV and JN conducted and analyzed pharmacological experiments; JHV, MR, JP, DM, and EK contributed to molecular biology; SK and GMK isolated, purified, analyzed, and provided FR900359; AI prepared and provided HEK293 $G\alpha_{q/11}$-KO cells; VN, RG, and XD performed and supervised the computational studies; VN, JHV, and CEM selected mutants; CEM conceived, coordinated and supervised the project; JHV and CEM wrote the manuscript with contributions from all coauthors.

Declaration of Competing Interest

The authors declare that they have no known competing financial interests or personal relationships that could have appeared to influence the work reported in this paper.

Acknowledgements

The authors would like to thank Prof. Francesco Gervasio and his group for helpful suggestions regarding molecular dynamics simulations.

Appendix A. Supporting information

Supplementary data associated with this article can be found in the online version at doi:10.1016/j.phrs.2021.105880.

References

[1] H. Zhang, A.L. Nielsen, M.W. Boesgaard, K. Harpsøe, N.L. Daly, X.-F. Xiong, C. R. Underwood, L.M. Haugaard-Kedström, H. Bräuner-Osborne, D.E. Gloriam, K. Strømgaard, Structure-activity relationship and conformational studies of the natural product cyclic depsipeptides YM-254890 and FR900359, Eur. J. Med. Chem. 156 (2018) 847–860, https://doi.org/10.1016/j.ejmech.2018.07.023.

[2] W.M. Oldham, H.E. Hamm, Heterotrimeric G protein activation by G-protein-coupled receptors, Nat. Rev. Mol. Cell Biol. 9 (2008) 60–71, https://doi.org/10.1038/nrm2299.

[3] C.J. Schmidt, T.C. Thomas, M.A. Levine, E.J. Neer, Specificity of G protein beta and gamma subunit interactions, J. Biol. Chem. 267 (1992) 13807–13810.

[4] T. Flock, C.N.J. Ravarani, D. Sun, A.J. Venkatakrishnan, M. Kayikci, C.G. Tate, D. B. Veprintsev, M.M. Babu, Universal allosteric mechanism for Gα activation by GPCRs, Nature 524 (2015) 173–179, https://doi.org/10.1038/nature14663.

[5] K. Kristiansen, Molecular mechanisms of ligand binding, signaling, and regulation within the superfamily of G-protein-coupled receptors: molecular modeling and mutagenesis approaches to receptor structure and function, Pharmacol. Ther. 103 (2004) 21–80, https://doi.org/10.1016/j.pharmthera.2004.05.002.

[6] G.B. Downes, N. Gautam, The G protein subunit gene families, Genomics 62 (1999) 544–552, https://doi.org/10.1006/geno.1999.5992.

[7] D. Kamato, P. Mitra, F. Davis, N. Osman, R. Chaplin, P.J. Cabot, R. Afroz, W. Thomas, W. Zheng, H. Kaur, M. Brimble, P.J. Little, Gaq proteins: molecular pharmacology and therapeutic potential, Cell. Mol. Life Sci. 74 (2017) 1379–1390, https://doi.org/10.1007/s00018-016-2405-9.

[8] S.J. Taylor, H.Z. Chae, S.G. Rhee, J.H. Exton, Activation of the beta 1 isozyme of phospholipase C by alpha subunits of the Gq class of G proteins, Nature 350 (1991) 516–518, https://doi.org/10.1038/350516a0.

[9] S. Lutz, A. Shankaranarayanan, C. Coco, M. Ridilla, M.R. Nance, C. Vettel, D. Baltus, C.R. Evelyn, R.R. Neubig, T. Wieland, J.J.G. Tesmer, Structure of Galphaq-p63RhoGEF-RhoA complex reveals a pathway for the activation of RhoA by GPCRs, Science 318 (2007) 1923–1927, https://doi.org/10.1126/science.1147554.

[10] C. García-Hoz, G. Sánchez-Fernández, M.T. Díaz-Meco, J. Moscat, F. Mayor, C. Ribas, G alpha(q) acts as an adaptor protein in protein kinase C zeta (PKCzeta)-mediated ERK5 activation by G protein-coupled receptors (GPCR), J. Biol. Chem. 285 (2010) 13480–13489, https://doi.org/10.1074/jbc.M109.098699.

[11] S. Mangmool, H. Kurose, G(i/o) protein-dependent and -independent actions of Pertussis Toxin (PTX), Toxins (Basel) 3 (2011) 884–899, https://doi.org/10.3390/toxins3070884.

[12] J. Sanchez, J. Holmgren, Cholera toxin - a foe & a friend, Indian J. Med. Res. 133 (2011) 153–163.

[13] R. Schrage, A.-L. Schmitz, E. Gaffal, S. Annala, S. Kehraus, D. Wenzel, K. M. Büllesbach, T. Bald, A. Inoue, Y. Shinjo, S. Galandrin, N. Shridhar, M. Hesse, M. Grundmann, N. Merten, T.H. Charpentier, M. Martz, A.J. Butcher, T. Slodczyk, S. Armando, M. Effern, Y. Namkung, L. Jenkins, V. Horn, A. Stößel, H. Dargatz, D. Tietze, D. Imhof, C. Galés, C. Drewke, C.E. Müller, M. Hölzel, G. Milligan, A. B. Tobin, J. Gomeza, H.G. Dohlman, J. Sondek, T.K. Harden, M. Bouvier, S. A. Laporte, J. Aoki, B.K. Fleischmann, K. Mohr, G.M. König, T. Tüting, E. Kostenis, The experimental power of FR900359 to study Gq-regulated biological processes, Nat. Commun. 6 (2015) 10156, https://doi.org/10.1038/ncomms10156.

[14] J. Takasaki, T. Saito, M. Taniguchi, T. Kawasaki, Y. Moritani, K. Hayashi, M. Kobori, A novel Galphaq/11-selective inhibitor, J. Biol. Chem. 279 (2004) 47438–47445, https://doi.org/10.1074/jbc.M408846200.

[15] J. Patt, J. Alenfelder, E.M. Pfeil, J.H. Voss, N. Merten, F. Eryilmaz, N. Heycke, U. Rick, A. Inoue, S. Kehraus, X. Deupi, C.E. Müller, G.M. König, M. Crüsemann, E. Kostenis, An experimental strategy to probe Gq contribution to signal transduction in living cells, J. Biol. Chem. 296 (2021), 100472, https://doi.org/10.1016/j.jbc.2021.100472.

[16] M. Matthey, R. Roberts, A. Seidinger, A. Simon, R. Schröder, M. Kuschak, S. Annala, G.M. König, C.E. Müller, I.P. Hall, E. Kostenis, B.K. Fleischmann, D. Wenzel, Targeted inhibition of Gq signaling induces airway relaxation in mouse models of asthma, Sci. Transl. Med. 9 (2017), https://doi.org/10.1126/scitranslmed.aag2288.

[17] J.G. Schlegel, M. Tahoun, A. Seidinger, J.H. Voss, M. Kuschak, S. Kehraus, M. Schneider, M. Matthey, B.K. Fleischmann, G.M. König, D. Wenzel, C.E. Müller, Macrocyclic Gq Protein Inhibitors FR900359 and/or YM-254890–Fit for Translation? ACS Pharmacol. Transl. Sci. 4 (2021) 888–897, https://doi.org/10.1021/acsptsci.1c00021.

[18] S. Annala, X. Feng, N. Shridhar, F. Eryilmaz, J. Patt, J. Yang, E.M. Pfeil, R. D. Cervantes-Villagrana, A. Inoue, F. Häberlein, T. Slodczyk, R. Reher, S. Kehraus, S. Monteleone, R. Schrage, N. Heycke, U. Rick, S. Engel, A. Pfeifer, P. Kolb, G. König, M. Bünemann, T. Tüting, J. Vázquez-Prado, J.S. Gutkind, E. Gaffal, E. Kostenis, Direct targeting of Gαq and Gα11 oncoproteins in cancer cells, Sci. Signal. 12 (2019), https://doi.org/10.1126/scisignal.aau5948.

[19] M.D. Onken, C.M. Makepeace, K.M. Kaltenbronn, S.M. Kanai, T.D. Todd, S. Wang, T.J. Broekelmann, P.K. Rao, J.A. Cooper, K.J. Blumer, Targeting nucleotide exchange to inhibit constitutively active G protein α subunits in cancer cells, Sci. Signal. 11 (2018), https://doi.org/10.1126/scisignal.aao6852.

[20] M.M. Meleka, A.J. Edwards, J. Xia, S.A. Dahlen, I. Mohanty, M. Medcalf, S. Aggarwal, K.D. Moeller, O.V. Mortensen, P. Osei-Owusu, Anti-hypertensive mechanisms of cyclic depsipeptide inhibitor ligands for Gq/11 class G proteins, Pharmacol. Res. 141 (2019) 264–275, https://doi.org/10.1016/j.phrs.2019.01.012.

[21] E. Kostenis, E.M. Pfeil, S. Annala, Heterotrimeric Gq proteins as therapeutic targets? J. Biol. Chem. 295 (2020) 5206–5215, https://doi.org/10.1074/jbc.REV119.007061.

[22] K. Klepac, A. Kilić, T. Gnad, L.M. Brown, B. Herrmann, A. Wilderman, A. Balkow, A. Glöde, K. Simon, M.E. Lidell, M.J. Betz, S. Enerbäck, J. Wess, M. Freichel, M. Blüher, G. König, E. Kostenis, P.A. Insel, A. Pfeifer, The Gq signalling pathway inhibits brown and beige adipose tissue, Nat. Commun. 7 (2016) 10895, https://doi.org/10.1038/ncomms10895.

[23] G. Sánchez-Fernández, S. Cabezudo, C. García-Hoz, C. Benincá, A.M. Aragay, F. Mayor, C. Ribas, Gαq signalling: the new and the old, Cell. Signal. 26 (2014) 833–848, https://doi.org/10.1016/j.cellsig.2014.01.010.

[24] P.M. Grace, X. Wang, K.A. Strand, M.V. Baratta, Y. Zhang, E.L. Galer, H. Yin, S. F. Maier, L.R. Watkins, DREADDed microglia in pain: implications for spinal inflammatory signaling in male rats, Exp. Neurol. 304 (2018) 125–131, https://doi.org/10.1016/j.expneurol.2018.03.005.

[25] D. Strassheim, V. Karoor, K. Stenmark, A. Verin, E. Gerasimovskaya, A current view of G protein-coupled receptor - mediated signaling in pulmonary hypertension: finding opportunities for therapeutic intervention, Vessel 2 (2018), https://doi.org/10.20517/2574-1209.2018.44.

[26] G. Viswanathan, A. Mamazhakypov, R.T. Schermuly, S. Rajagopal, The role of g protein-coupled receptors in the right ventricle in pulmonary hypertension, Front. Cardiovasc. Med. 5 (2018) 179, https://doi.org/10.3389/fcvm.2018.00179.

[27] A. Nishimura, K. Kitano, J. Takasaki, M. Taniguchi, N. Mizuno, K. Tago, T. Hakoshima, H. Itoh, Structural basis for the specific inhibition of heterotrimeric Gq protein by a small molecule, Proc. Natl. Acad. Sci. U. S. A. 107 (2010) 13666–13671, https://doi.org/10.1073/pnas.1003553107.

[28] M. Kuschak, V. Namasivayam, M. Rafehi, J.H. Voss, J. Garg, J.G. Schlegel, A. Abdelrahman, S. Kehraus, R. Reher, J. Küppers, K. Sylvester, S. Hinz, M. Matthey, D. Wenzel, B.K. Fleischmann, A. Pfeifer, A. Inoue, M. Gütschow, G. M. König, C.E. Müller, Cell-permeable high-affinity tracers for Gq proteins provide structural insights, reveal distinct binding kinetics, and identify small molecule inhibitors, Br. J. Pharmacol. (2019), https://doi.org/10.1111/bph.14960.

[29] M. Fujioka, S. Koda, Y. Morimoto, K. Biemann, Structure of FR900359, a cyclic depsipeptide from Ardisia crenata sims, J. Org. Chem. 53 (1988) 2820–2825, https://doi.org/10.1021/jo00247a030.

[30] A. Carlier, L. Fehr, M. Pinto-Carbó, T. Schäberle, R. Reher, S. Dessein, G. König, L. Eberl, The genome analysis of Candidatus Burkholderia crenata reveals that secondary metabolism may be a key function of the Ardisia crenata leaf nodule symbiosis, Environ. Microbiol. 18 (2016) 2507–2522, https://doi.org/10.1111/1462-2920.13184.

[31] M. Taniguchi, K. Nagai, N. Arao, T. Kawasaki, T. Saito, Y. Moritani, J. Takasaki, K. Hayashi, S. Fujita, K.-i Suzuki, S.-i Tsukamoto, YM-254890, a novel platelet aggregation inhibitor produced by Chromobacterium sp, QS3666, J. Antibiot. 56 (2003) 358–363.

[32] C. Hermes, G.M. König, M. Crüsemann, The chromodepsins - chemistry, biology and biosynthesis of a selective Gq inhibitor natural product family, Nat. Prod. Rep. (2021), https://doi.org/10.1039/d1np00005e.

[33] D. Malfacini, J. Patt, S. Annala, K. Harpsøe, F. Eryilmaz, R. Reher, M. Crüsemann, W. Hanke, H. Zhang, D. Tietze, D.E. Gloriam, H. Bräuner-Osborne, K. Strømgaard, G.M. König, A. Inoue, J. Gomeza, E. Kostenis, Rational design of a heterotrimeric G protein α subunit with artificial inhibitor sensitivity, J. Biol. Chem. 294 (2019) 5747–5758, https://doi.org/10.1074/jbc.RA118.007250.

[34] X.-F. Xiong, H. Zhang, C.R. Underwood, K. Harpsøe, T.J. Gardella, M.F. Wöldike, M. Mannstadt, D.E. Gloriam, H. Bräuner-Osborne, K. Strømgaard, Total synthesis and structure-activity relationship studies of a series of selective G protein inhibitors, Nat. Chem. 8 (2016) 1035–1041, https://doi.org/10.1038/nchem.2577.

[35] H. Zhang, A.L. Nielsen, K. Strømgaard, Recent achievements in developing selective Gq inhibitors, Med. Res. Rev. 40 (2020) 135–157, https://doi.org/10.1002/med.21598.

[36] R.A. Copeland, The drug-target residence time model: a 10-year retrospective, Nat. Rev. Drug Discov. 15 (2016) 87–95, https://doi.org/10.1038/nrd.2015.18.

[37] P.J. Tonge, Drug–target kinetics in drug discovery, ACS Chem. Neurosci. 9 (2018) 29–39, https://doi.org/10.1021/acschemneuro.7b00185.

Declaration of Competing Interest

The authors declare that they have no known competing financial interests or personal relationships that could have appeared to influence the work reported in this paper.

Acknowledgements

The authors would like to thank Prof. Francesco Gervasio and his group for helpful suggestions regarding molecular dynamics simulations.

Appendix A. Supporting information

Supplementary data associated with this article can be found in the online version at doi:10.1016/j.phrs.2021.105880.

References

[1] H. Zhang, A.L. Nielsen, M.W. Boesgaard, K. Harpsøe, N.L. Daly, X.-F. Xiong, C. R. Underwood, L.M. Haugaard-Kedström, H. Bräuner-Osborne, D.E. Gloriam, K. Strømgaard, Structure-activity relationship and conformational studies of the natural product cyclic depsipeptides YM-254890 and FR900359, Eur. J. Med. Chem. 156 (2018) 847–860, https://doi.org/10.1016/j.ejmech.2018.07.023.

[2] W.M. Oldham, H.E. Hamm, Heterotrimeric G protein activation by G-protein-coupled receptors, Nat. Rev. Mol. Cell Biol. 9 (2008) 60–71, https://doi.org/10.1038/nrm2299.

[3] C.J. Schmidt, T.C. Thomas, M.A. Levine, E.J. Neer, Specificity of G protein beta and gamma subunit interactions, J. Biol. Chem. 267 (1992) 13807–13810.

[4] T. Flock, C.N.J. Ravarani, D. Sun, A.J. Venkatakrishnan, M. Kayikci, C.G. Tate, D. B. Veprintsev, M.M. Babu, Universal allosteric mechanism for Gα activation by GPCRs, Nature 524 (2015) 173–179, https://doi.org/10.1038/nature14663.

[5] K. Kristiansen, Molecular mechanisms of ligand binding, signaling, and regulation within the superfamily of G-protein-coupled receptors: molecular modeling and mutagenesis approaches to receptor structure and function, Pharmacol. Ther. 103 (2004) 21–80, https://doi.org/10.1016/j.pharmthera.2004.05.002.

[6] G.B. Downes, N. Gautam, The G protein subunit gene families, Genomics 62 (1999) 544–552, https://doi.org/10.1006/geno.1999.5992.

[7] D. Kamato, P. Mitra, F. Davis, N. Osman, R. Chaplin, P.J. Cabot, R. Afroz, W. Thomas, W. Zheng, H. Kaur, M. Brimble, P.J. Little, Gaq proteins: molecular pharmacology and therapeutic potential, Cell. Mol. Life Sci. 74 (2017) 1379–1390, https://doi.org/10.1007/s00018-016-2405-9.

[8] S.J. Taylor, H.Z. Chae, S.G. Rhee, J.H. Exton, Activation of the beta 1 isozyme of phospholipase C by alpha subunits of the Gq class of G proteins, Nature 350 (1991) 516–518, https://doi.org/10.1038/350516a0.

[9] S. Lutz, A. Shankaranarayanan, C. Coco, M. Ridilla, M.R. Nance, C. Vettel, D. Baltus, C.R. Evelyn, R.R. Neubig, T. Wieland, J.J.G. Tesmer, Structure of Galphaq-p63RhoGEF-RhoA complex reveals a pathway for the activation of RhoA by GPCRs, Science 318 (2007) 1923–1927, https://doi.org/10.1126/science.1147554.

[10] C. García-Hoz, G. Sánchez-Fernández, M.T. Díaz-Meco, J. Moscat, F. Mayor, C. Ribas, G alpha(q) acts as an adaptor protein in protein kinase C zeta (PKCzeta)-mediated ERK5 activation by G protein-coupled receptors (GPCR), J. Biol. Chem. 285 (2010) 13480–13489, https://doi.org/10.1074/jbc.M109.098699.

[11] S. Mangmool, H. Kurose, G(i/o) protein-dependent and -independent actions of Pertussis Toxin (PTX), Toxins (Basel) 3 (2011) 884–899, https://doi.org/10.3390/toxins3070884.

[12] J. Sanchez, J. Holmgren, Cholera toxin - a foe & a friend, Indian J. Med. Res. 133 (2011) 153–163.

[13] R. Schrage, A.-L. Schmitz, E. Gaffal, S. Annala, S. Kehraus, D. Wenzel, K. M. Büllesbach, T. Bald, A. Inoue, Y. Shinjo, S. Galandrin, N. Shridhar, M. Hesse, M. Grundmann, N. Merten, T.H. Charpentier, M. Martz, A.J. Butcher, T. Slodczyk, S. Armando, M. Effern, Y. Namkung, L. Jenkins, V. Horn, A. Stößel, H. Dargatz, D. Tietze, D. Imhof, C. Galés, C. Drewke, C.E. Müller, M. Hölzel, G. Milligan, A. B. Tobin, J. Gomeza, H.G. Dohlman, J. Sondek, T.K. Harden, M. Bouvier, S. A. Laporte, J. Aoki, B.K. Fleischmann, K. Mohr, G.M. König, T. Tüting, E. Kostenis, The experimental power of FR900359 to study Gq-regulated biological processes, Nat. Commun. 6 (2015) 10156, https://doi.org/10.1038/ncomms10156.

[14] J. Takasaki, T. Saito, M. Taniguchi, T. Kawasaki, Y. Moritani, K. Hayashi, M. Kobori, A novel Galphaq/11-selective inhibitor, J. Biol. Chem. 279 (2004) 47438–47445, https://doi.org/10.1074/jbc.M408846200.

[15] J. Patt, J. Alenfelder, E.M. Pfeil, J.H. Voss, N. Merten, F. Eryilmaz, N. Heycke, U. Rick, A. Inoue, S. Kehraus, X. Deupi, C.E. Müller, G.M. König, M. Crüsemann, E. Kostenis, An experimental strategy to probe Gq contribution to signal transduction in living cells, J. Biol. Chem. 296 (2021), 100472, https://doi.org/10.1016/j.jbc.2021.100472.

[16] M. Matthey, R. Roberts, A. Seidinger, A. Simon, R. Schröder, M. Kuschak, S. Annala, G.M. König, C.E. Müller, I.P. Hall, E. Kostenis, B.K. Fleischmann, D. Wenzel, Targeted inhibition of Gq signaling induces airway relaxation in mouse models of asthma, Sci. Transl. Med. 9 (2017), https://doi.org/10.1126/scitranslmed.aag2288.

[17] J.G. Schlegel, M. Tahoun, A. Seidinger, J.H. Voss, M. Kuschak, S. Kehraus, M. Schneider, M. Matthey, B.K. Fleischmann, G.M. König, D. Wenzel, C.E. Müller, Macrocyclic Gq Protein Inhibitors FR900359 and/or YM-254890–Fit for Translation? ACS Pharmacol. Transl. Sci. 4 (2021) 888–897, https://doi.org/10.1021/acsptsci.1c00021.

[18] S. Annala, X. Feng, N. Shridhar, F. Eryilmaz, J. Patt, J. Yang, E.M. Pfeil, R. D. Cervantes-Villagrana, A. Inoue, F. Häberlein, T. Slodczyk, R. Reher, S. Kehraus, S. Monteleone, R. Schrage, N. Heycke, U. Rick, S. Engel, A. Pfeifer, P. Kolb, G. König, M. Bünemann, T. Tüting, J. Vázquez-Prado, J.S. Gutkind, E. Gaffal, E. Kostenis, Direct targeting of Gαq and Gα11 oncoproteins in cancer cells, Sci. Signal. 12 (2019), https://doi.org/10.1126/scisignal.aau5948.

[19] M.D. Onken, C.M. Makepeace, K.M. Kaltenbronn, S.M. Kanai, T.D. Todd, S. Wang, T.J. Broekelmann, P.K. Rao, J.A. Cooper, K.J. Blumer, Targeting nucleotide exchange to inhibit constitutively active G protein α subunits in cancer cells, Sci. Signal. 11 (2018), https://doi.org/10.1126/scisignal.aao6852.

[20] M.M. Meleka, A.J. Edwards, J. Xia, S.A. Dahlen, I. Mohanty, M. Medcalf, S. Aggarwal, K.D. Moeller, O.V. Mortensen, P. Osei-Owusu, Anti-hypertensive mechanisms of cyclic depsipeptide inhibitor ligands for Gq/11 class G proteins, Pharmacol. Res. 141 (2019) 264–275, https://doi.org/10.1016/j.phrs.2019.01.012.

[21] E. Kostenis, E.M. Pfeil, S. Annala, Heterotrimeric Gq proteins as therapeutic targets? J. Biol. Chem. 295 (2020) 5206–5215, https://doi.org/10.1074/jbc.REV119.007061.

[22] K. Klepac, A. Kilić, T. Gnad, L.M. Brown, B. Herrmann, A. Wilderman, A. Balkow, A. Glöde, K. Simon, M.E. Lidell, M.J. Betz, S. Enerbäck, J. Wess, M. Freichel, M. Blüher, G. König, E. Kostenis, P.A. Insel, A. Pfeifer, The Gq signalling pathway inhibits brown and beige adipose tissue, Nat. Commun. 7 (2016) 10895, https://doi.org/10.1038/ncomms10895.

[23] G. Sánchez-Fernández, S. Cabezudo, C. García-Hoz, C. Benincá, A.M. Aragay, F. Mayor, C. Ribas, Gαq signalling: the new and the old, Cell. Signal. 26 (2014) 833–848, https://doi.org/10.1016/j.cellsig.2014.01.010.

[24] P.M. Grace, X. Wang, K.A. Strand, M.V. Baratta, Y. Zhang, E.L. Galer, H. Yin, S. F. Maier, L.R. Watkins, DREADDed microglia in pain: implications for spinal inflammatory signaling in male rats, Exp. Neurol. 304 (2018) 125–131, https://doi.org/10.1016/j.expneurol.2018.03.005.

[25] D. Strassheim, V. Karoor, K. Stenmark, A. Verin, E. Gerasimovskaya, A current view of G protein-coupled receptor - mediated signaling in pulmonary hypertension: finding opportunities for therapeutic intervention, Vessel 2 (2018), https://doi.org/10.20517/2574-1209.2018.44.

[26] G. Viswanathan, A. Mamazhakypov, R.T. Schermuly, S. Rajagopal, The role of g protein-coupled receptors in the right ventricle in pulmonary hypertension, Front. Cardiovasc. Med. 5 (2018) 179, https://doi.org/10.3389/fcvm.2018.00179.

[27] A. Nishimura, K. Kitano, J. Takasaki, M. Taniguchi, N. Mizuno, K. Tago, T. Hakoshima, H. Itoh, Structural basis for the specific inhibition of heterotrimeric Gq protein by a small molecule, Proc. Natl. Acad. Sci. U. S. A. 107 (2010) 13666–13671, https://doi.org/10.1073/pnas.1003553107.

[28] M. Kuschak, V. Namasivayam, M. Rafehi, J.H. Voss, J. Garg, J.G. Schlegel, A. Abdelrahman, S. Kehraus, R. Reher, J. Küppers, K. Sylvester, S. Hinz, M. Matthey, D. Wenzel, B.K. Fleischmann, A. Pfeifer, A. Inoue, M. Gütschow, G. M. König, C.E. Müller, Cell-permeable high-affinity tracers for Gq proteins provide structural insights, reveal distinct binding kinetics, and identify small molecule inhibitors, Br. J. Pharmacol. (2019), https://doi.org/10.1111/bph.14960.

[29] M. Fujioka, S. Koda, Y. Morimoto, K. Biemann, Structure of FR900359, a cyclic depsipeptide from Ardisia crenata sims, J. Org. Chem. 53 (1988) 2820–2825, https://doi.org/10.1021/jo00247a030.

[30] A. Carlier, L. Fehr, M. Pinto-Carbó, T. Schäberle, R. Reher, S. Dessein, G. König, L. Eberl, The genome analysis of Candidatus Burkholderia crenata reveals that secondary metabolism may be a key function of the Ardisia crenata leaf nodule symbiosis, Environ. Microbiol. 18 (2016) 2507–2522, https://doi.org/10.1111/1462-2920.13184.

[31] M. Taniguchi, K. Nagai, N. Arao, T. Kawasaki, T. Saito, Y. Moritani, J. Takasaki, K. Hayashi, S. Fujita, K.-i Suzuki, S.-i Tsukamoto, YM-254890, a novel platelet aggregation inhibitor produced by Chromobacterium sp, QS3666, J. Antibiot. 56 (2003) 358–363.

[32] C. Hermes, G.M. König, M. Crüsemann, The chromodepsins - chemistry, biology and biosynthesis of a selective Gq inhibitor natural product family, Nat. Prod. Rep. (2021), https://doi.org/10.1039/d1np00005e.

[33] D. Malfacini, J. Patt, S. Annala, K. Harpsøe, F. Eryilmaz, R. Reher, M. Crüsemann, W. Hanke, H. Zhang, D. Tietze, D.E. Gloriam, H. Bräuner-Osborne, K. Strømgaard, G.M. König, A. Inoue, J. Gomeza, E. Kostenis, Rational design of a heterotrimeric G protein α subunit with artificial inhibitor sensitivity, J. Biol. Chem. 294 (2019) 5747–5758, https://doi.org/10.1074/jbc.RA118.007250.

[34] X.-F. Xiong, H. Zhang, C.R. Underwood, K. Harpsøe, T.J. Gardella, M.F. Wöldike, M. Mannstadt, D.E. Gloriam, H. Bräuner-Osborne, K. Strømgaard, Total synthesis and structure-activity relationship studies of a series of selective G protein inhibitors, Nat. Chem. 8 (2016) 1035–1041, https://doi.org/10.1038/nchem.2577.

[35] H. Zhang, A.L. Nielsen, K. Strømgaard, Recent achievements in developing selective Gq inhibitors, Med. Res. Rev. 40 (2020) 135–157, https://doi.org/10.1002/med.21598.

[36] R.A. Copeland, The drug-target residence time model: a 10-year retrospective, Nat. Rev. Drug Discov. 15 (2016) 87–95, https://doi.org/10.1038/nrd.2015.18.

[37] P.J. Tonge, Drug–target kinetics in drug discovery, ACS Chem. Neurosci. 9 (2018) 29–39, https://doi.org/10.1021/acschemneuro.7b00185.

[82] M. Soethoudt, M.W.H. Hoorens, W. Doelman, A. Martella, M. van der Stelt, L. H. Heitman, Structure-kinetic relationship studies of cannabinoid CB2 receptor agonists reveal substituent-specific lipophilic effects on residence time, Biochem. Pharmacol. 152 (2018) 129–142, https://doi.org/10.1016/j.bcp.2018.03.018.

[83] E.V. Schneider, J. Böttcher, R. Huber, K. Maskos, L. Neumann, Structure-kinetic relationship study of CDK8/CycC specific compounds, Proc. Natl. Acad. Sci. U. S. A. 110 (2013) 8081–8086, https://doi.org/10.1073/pnas.1305378110.

[84] L. Xia, W.A.C. Burger, J.P.D. van Veldhoven, B.J. Kuiper, T.T. van Duijl, E. B. Lenselink, E. Paasman, L.H. Heitman, A.P. IJzerman, Structure-affinity relationships and structure-kinetics relationships of Pyrido2,1-fpurine-2,4-dione derivatives as human adenosine A3 receptor antagonists, J. Med. Chem. 60 (2017) 7555–7568, https://doi.org/10.1021/acs.jmedchem.7b00950.

[85] D. Guo, T. Mulder-Krieger, A.P. IJzerman, L.H. Heitman, Functional efficacy of adenosine A_2A receptor agonists is positively correlated to their receptor residence time, Br. J. Pharmacol. 166 (2012) 1846–1859, https://doi.org/10.1111/j.1476-5381.2012.01897.x.

Supporting Information

Unraveling binding mechanism

and kinetics of macrocyclic $G\alpha_q$ protein inhibitors

Pharmacol. Res., 2021

Pharmacol. Res.

Unraveling binding mechanism and kinetics of macrocyclic $G\alpha_q$ protein inhibitors

Jan H. Voss[1], Jessica Nagel[1], Muhammad Rafehi[1], Ramon Guixà-González[2], Davide Malfacini[3], Julian Patt[3], Stefan Kehraus[3], Asuka Inoue[4], Gabriele M. König[3], Evi Kostenis[3], Xavier Deupi[2,5], Vigneshwaran Namasivayam[1], and Christa E. Müller[1]*

[1]PharmaCenter Bonn, Pharmaceutical Institute, Pharmaceutical & Medicinal Chemistry, University of Bonn, An der Immenburg 4, D-53121 Bonn, Germany

[2]Condensed Matter Theory Group, Paul Scherrer Institute, Forschungsstrasse 111, 5232 Villigen PSI, Switzerland

[3]Institute of Pharmaceutical Biology, University of Bonn, Nussallee 6, 53113 Bonn, Germany

[4]Tohoku University, Graduate School of Pharmaceutical Sciences, Sendai, Miyagi, 980-8578 Japan

[5]Laboratory of Biomolecular Research, Paul Scherrer Institute, Forschungsstrasse 111, 5232 Villigen PSI, Switzerland

Keywords: binding kinetics, FR900359, Gq protein, conformational selection, residence time, YM-254890

[*]To whom correspondence should be addressed: Prof. Dr. Christa E. Müller, Pharmaceutical Institute, Pharmaceutical & Medicinal Chemistry, University of Bonn, An der Immenburg 4, D-53121 Bonn, Germany, Phone: +49-(0)228-73-2301; Fax: +49-(0)228-73-2567; e-mail: christa.mueller@uni-bonn.de

Table of contents

Supporting Figure 1: Full Western Blot images as obtained from the luminescence reader.. 4

Supporting Figure 2: GPCR agonist-induced calcium mobilization is transduced via wt and mutant $G\alpha_q$ proteins. 5

Supporting Figure 3: Dissociation kinetics of [^{3}H]PSB-15900-FR from membrane preparations of HEK293 $G\alpha_{q/11}$-KO cell membranes. 6

Supporting Figure 4: Dissociation kinetics of [^{3}H]PSB-16254-YM (5 nM) from membrane preparations of HEK293 $G\alpha_{q/11}$-KO cells recombinantly expressing $G\alpha_q$ proteins. 7

Supporting Figure 5: Root-mean-square deviation (RMSD) of the $G\alpha_q$ subunit (Cα atoms only) in the three simulation replicas. 8

Supporting Figure 6: Root-mean-square fluctuation (RMSF) across the $G\alpha_q$ subunit (Cα atoms only) in the three aggregated simulation replicas. 9

Supporting Figure 7: Root-mean-square deviation (RMSD) of the FR and YM inhibitors (heavy atoms only) in the three simulation replicas. 10

Supporting Figure 8: Root-mean-square deviation (RMSD) of helix A ($D69^{H.HA.01}$ – $L97^{H.HA.29}$) in the αH domain of $G\alpha_q$ (Cα atoms only) in the three simulation replicas. 11

Supporting Figure 9: Differences in backbone and sidechain torsion angles across the trajectories of apo versus inhibitor-bound MD simulations. 12

Supporting Figure 10: Differences in Cα distances across protein ensembles in apo versus inhibitor-bound MD simulations.. 14

Supporting Figure 11: Characterization of protein-ligand interactions across MD simulations.. 16

Supporting Table 1: Nucleotide sequences (5'→3') of primers used for mutagenesis and cloning. 17

Supporting Table 2: Rationale for $G\alpha_q$ protein mutagenesis of the FR/YM binding site near anchor 1 and anchor 2 of the inhibitors. 18

Supporting Table 3: pIC_{50}- and ΔpIC_{50}-values (means ± SEM, number of independent experiments) for FR and YM in ATP-mediated calcium mobilization experiments performed in HEK293 cells expressing recombinant $G\alpha_q$ proteins 19

Supporting Table 4: Pseudo-pKD values (mean ± SEM) obtained from pseudo-homologous competition experiments 20

Supporting Table 5: Association half-life of [^{3}H]PSB-15900-FR at wt and mutant Gq proteins. 21

Supporting Table 6: Dissociation half-life of [^{3}H]PSB-15900-FR at wt and mutant Gq proteins. 22

Supporting Information

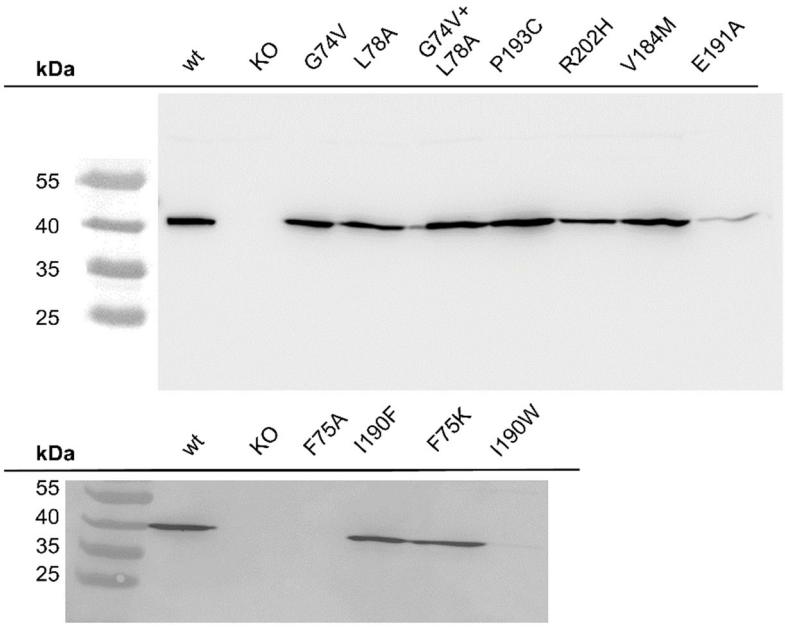

Supporting Figure 1: Full Western Blot images as obtained from the luminescence reader. Membrane preparation (20 µg of protein per lane) expressing the indicated $G\alpha_q$ mutant was applied. Proteins were detected via an internal HA-tag (see section 2.6 for reagent details); one representative experiment out of three replicate experiments is depicted.

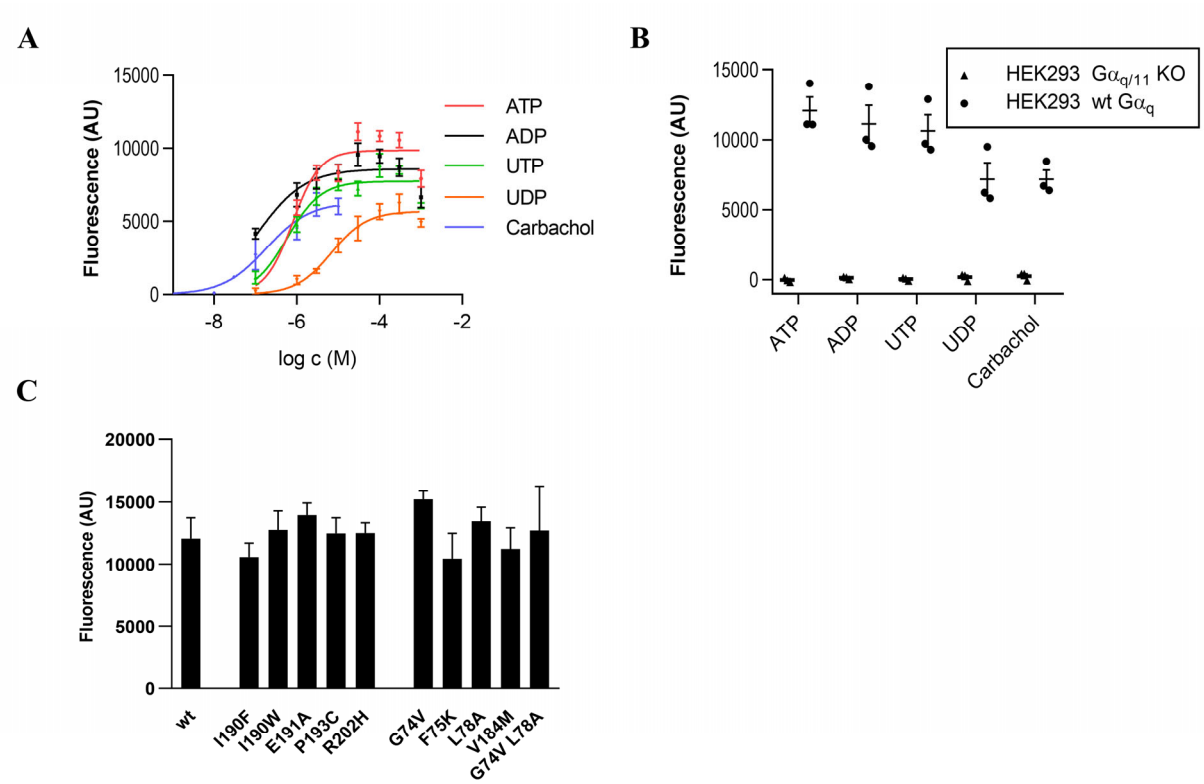

Supporting Figure 2: GPCR agonist-induced calcium mobilization is transduced via wt and mutant $G\alpha_q$ proteins. **(A)** GPCR-activated calcium mobilization by ADP, ATP, UDP, UTP, and carbachol in HEK293 cells expressing the wt $G\alpha_q$ protein. **(B)** $G\alpha_q$ protein expression is required for GPCR agonist-mediated calcium mobilization in HEK293 cells. Fluorescence was measured in HEK293 $G\alpha_{q/11}$-KO cells and HEK293 cells recombinantly expressing wt $G\alpha_q$ protein after receptor activation with an agonist concentration corresponding to the determined EC_{80} value (see **A**). **(C)** HEK293 $G\alpha_{q/11}$-KO cells expressing mutant $G\alpha_q$ proteins were activated by an EC_{80} concentration of ATP. Maximum signals were observed in all mutant HEK293 cells after ATP-induced calcium moblization in the presence of 1% DMSO and in the absence of YM or FR. Results are presented as arbitrary units (AU) of fluorescence as measured by the plate reader.

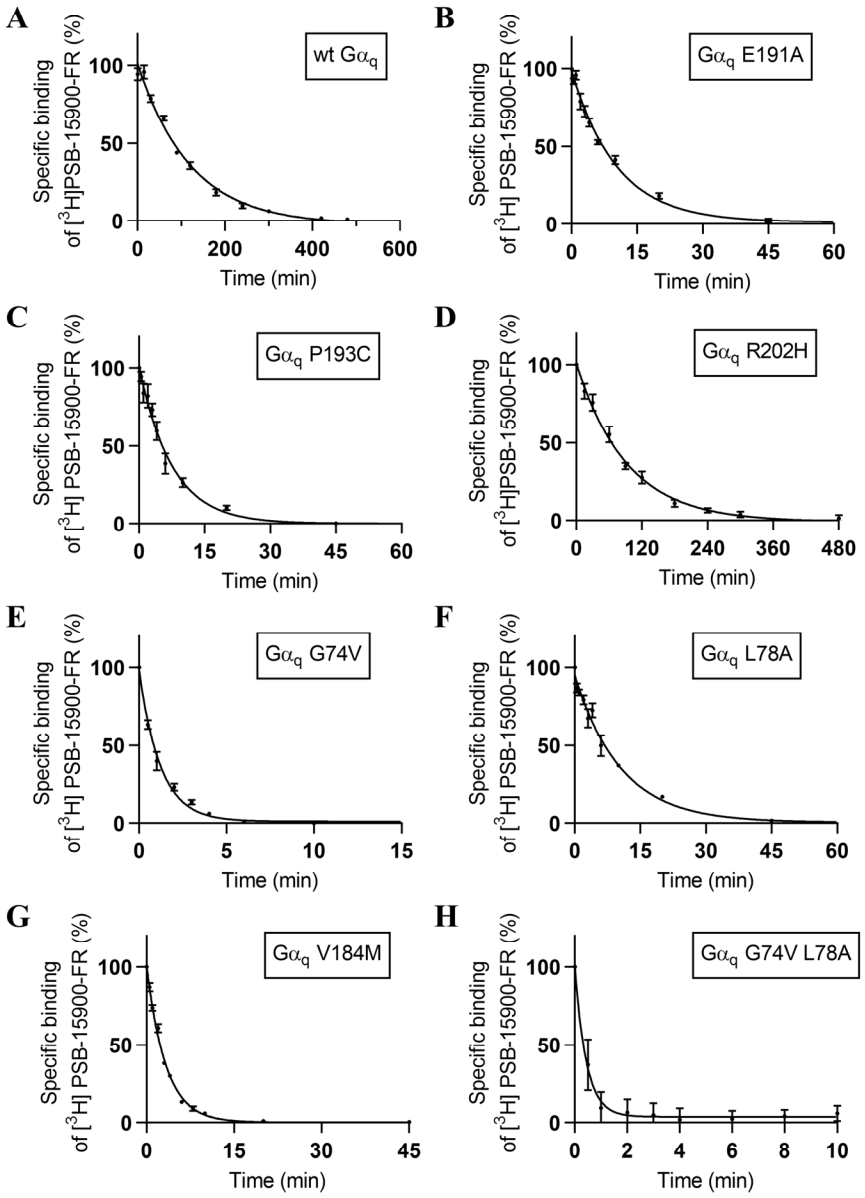

Supporting Figure 3: Dissociation kinetics of [³H]PSB-15900-FR (5 nM) from membrane preparations of HEK293 $G\alpha_{q/11}$-KO cells (50 µg of protein) recombinantly expressing $G\alpha_q$ protein, (**A**) wt, (**B**) E191A, (**C**) P193C, (**D**) R202H, (**E**) G74V, (**F**) L78A, (**G**) V184M, and (**H**) G74V/ 78A. Dissociation was induced by the addition of 5 µM FR at the indicated time points. Data are means ± SEM from three independent experiments, each performed with two technical replicates.

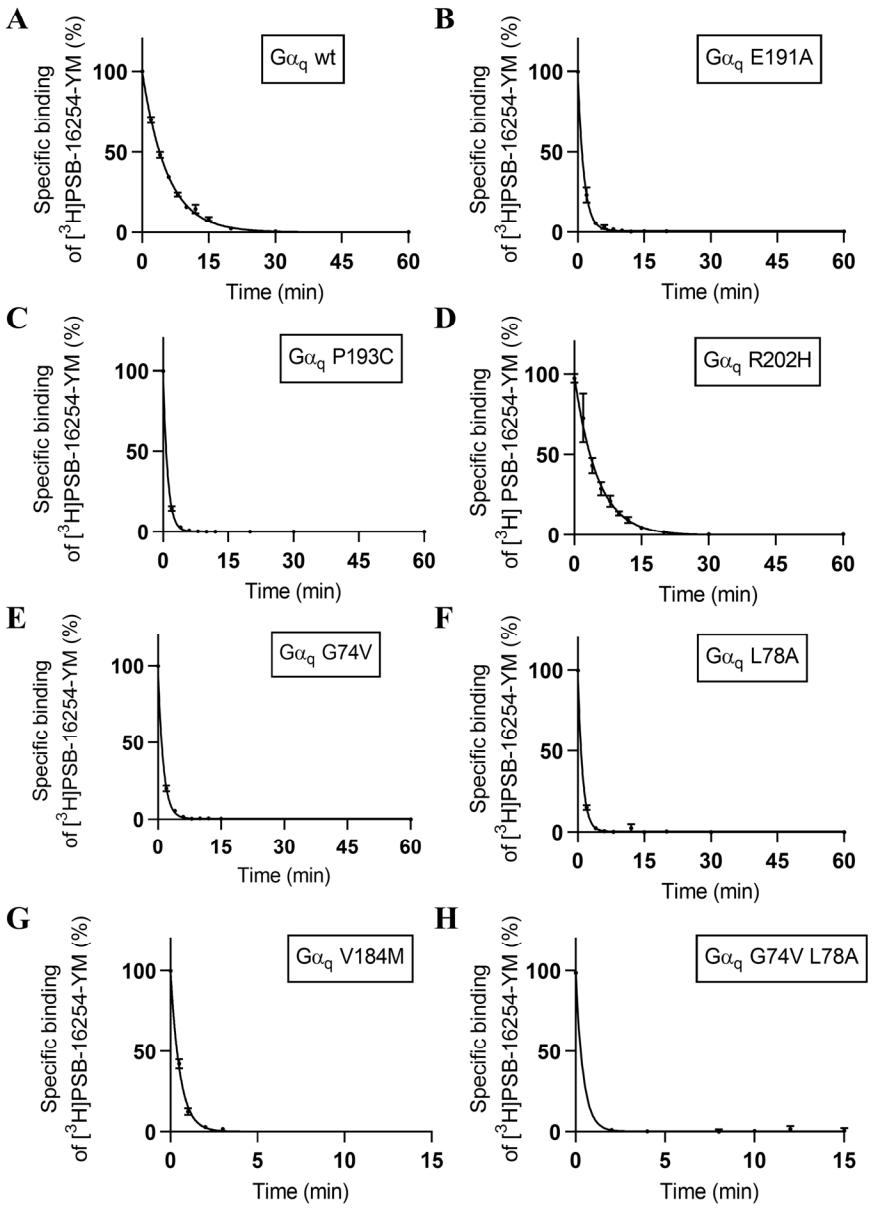

Supporting Figure 4: Dissociation kinetics of [³H]PSB-16254-YM (5 nM) from membrane preparations of HEK293 $G\alpha_{q/11}$-KO cells (50 µg of protein) recombinantly expressing $G\alpha_q$ (**A**) wt, (**B**) E191A, (**C**) P193C, (**D**) R202H, (**E**) G74V, (**F**) L78A, (**G**) V184M, and (**H**) G74V/L78A proteins. Dissociation was induced by the addition of 5 µM YM at indicated time points. Data are means ± SEM from three independent experiments, each performed with two technical replicates.

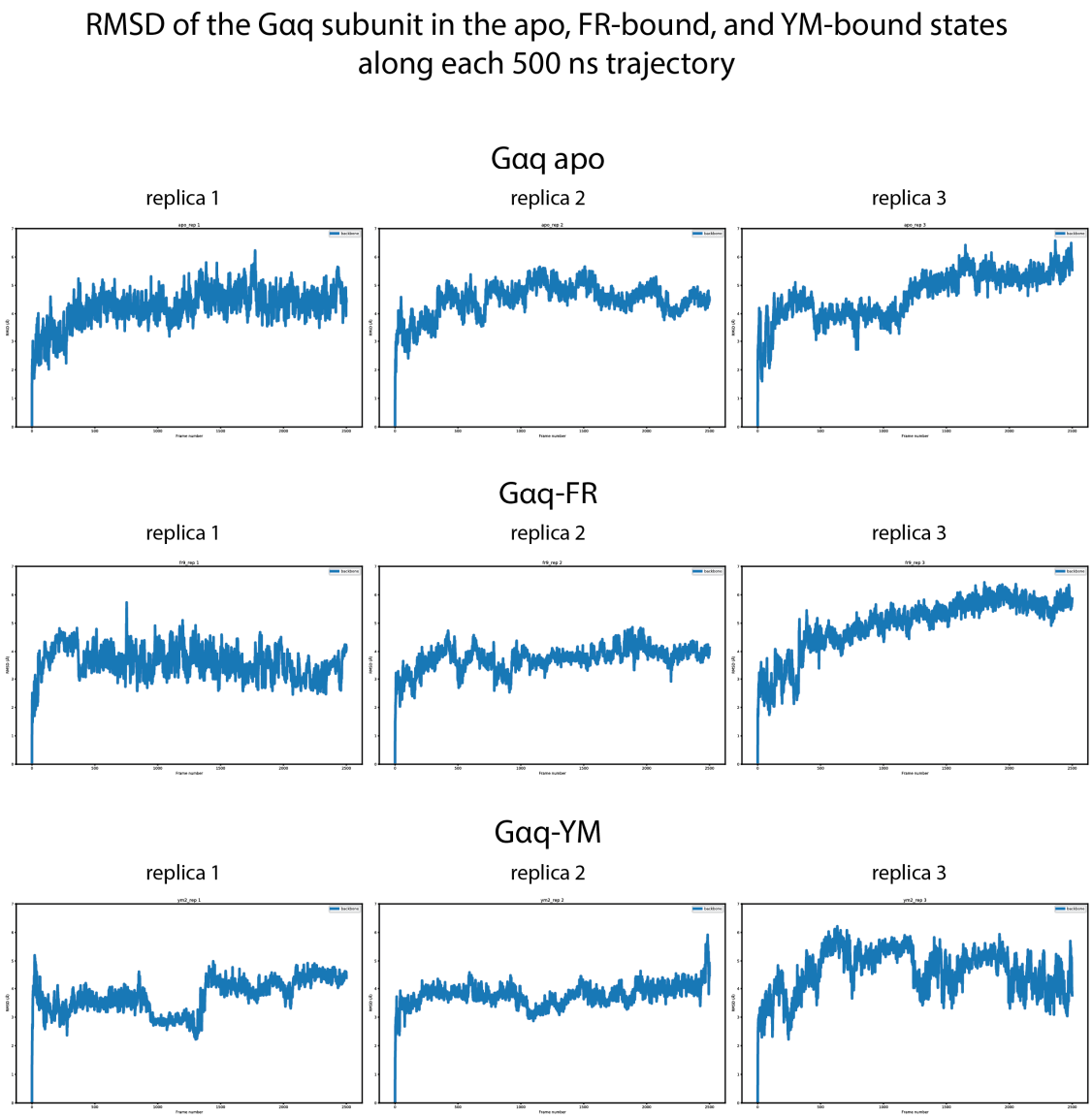

Supporting Figure 5: Root-mean-square deviation (RMSD) of the $G\alpha_q$ subunit (Cα atoms only) in the three simulation replicas.

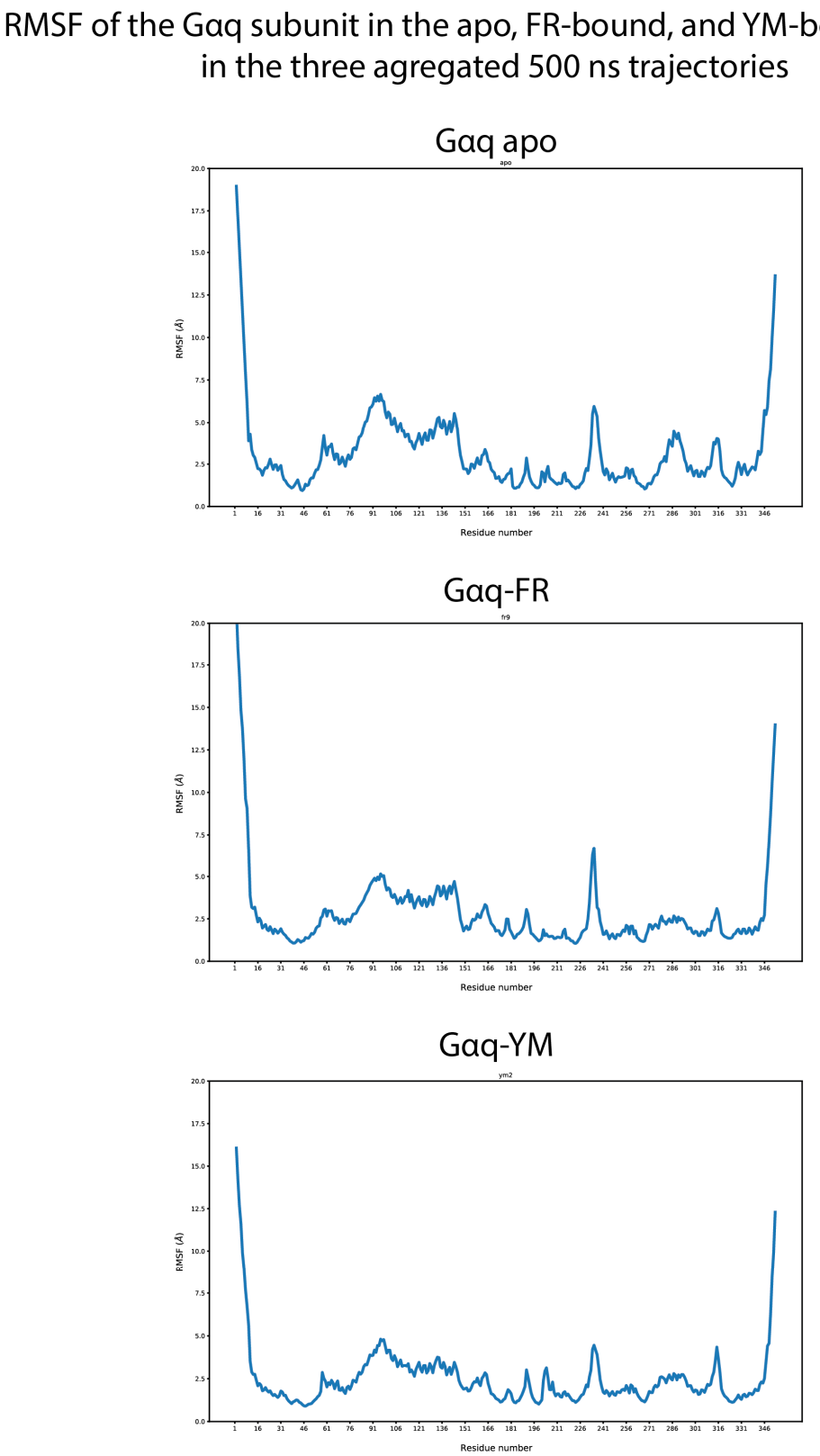

Supporting Figure 6: Root-mean-square fluctuation (RMSF) across the $G\alpha_q$ subunit (Cα atoms only) in the three aggregated simulation replicas.

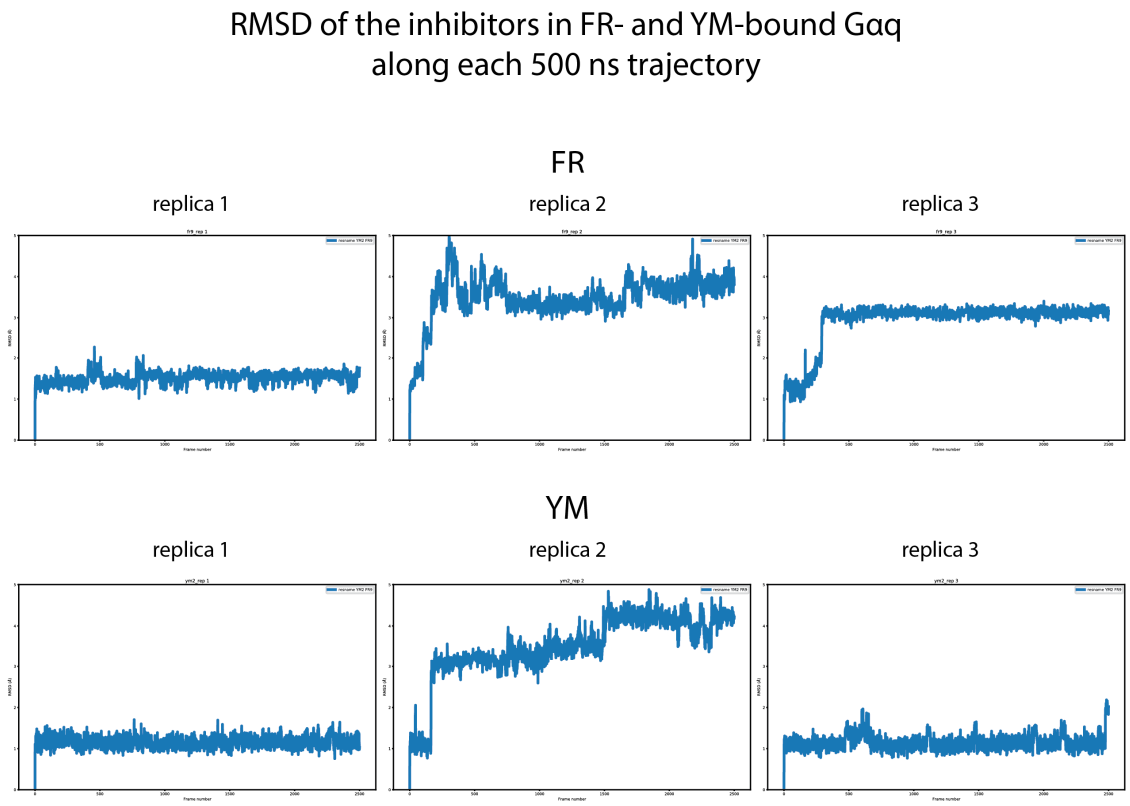

Supporting Figure 7: Root-mean-square deviation (RMSD) of the FR and YM inhibitors (heavy atoms only) in the three simulation replicas.

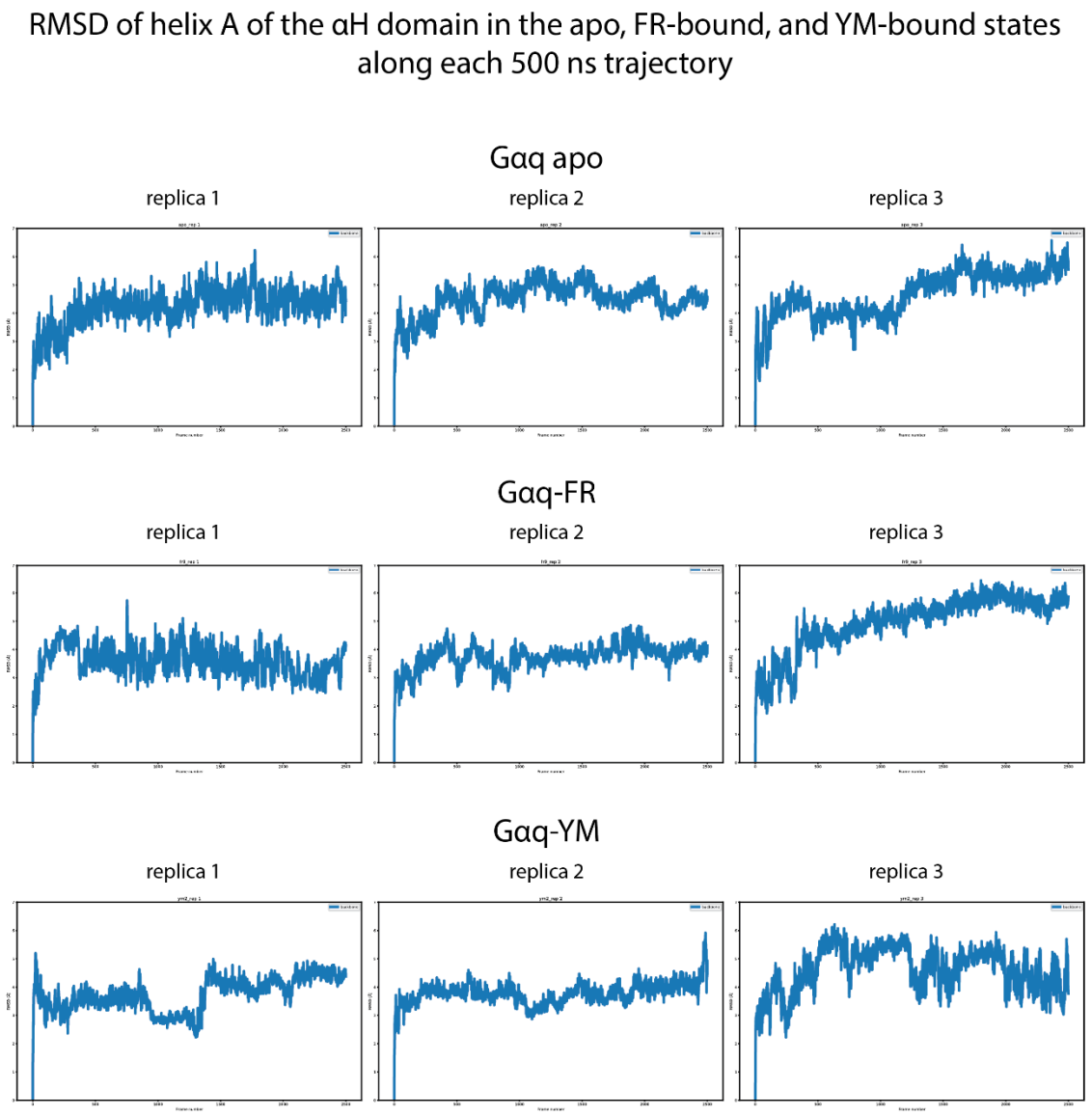

Supporting Figure 8: Root-mean-square deviation (RMSD) of helix A ($D69^{H.HA.01}$ – $L97^{H.HA.29}$) in the αH domain of $G\alpha_q$ (Cα atoms only) in the three simulation replicas.

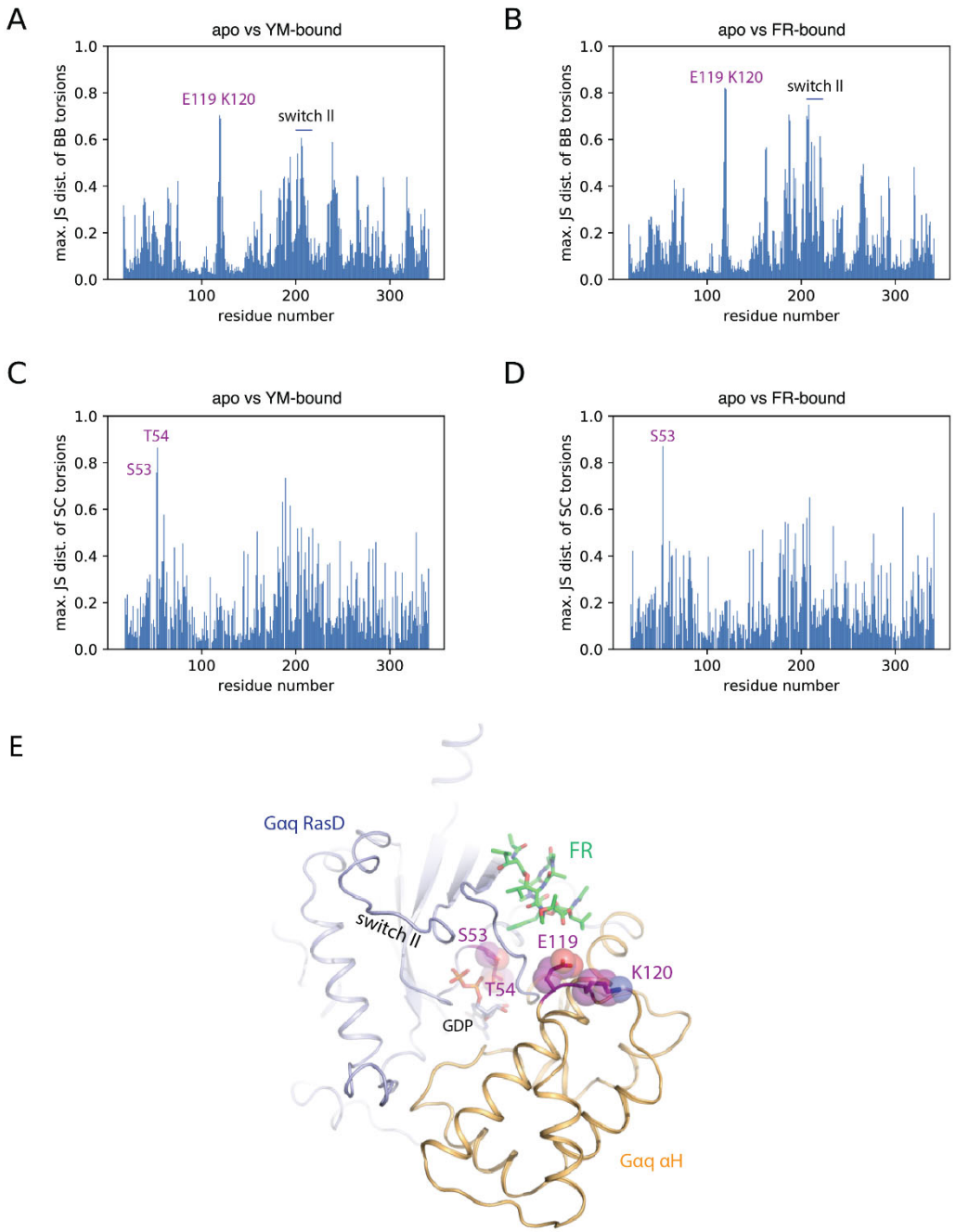

Supporting Figure 9: Differences in backbone and sidechain torsion angles across the trajectories of apo versus inhibitor-bound MD simulations. Plots show the relative entropy of protein residues along the sequence between inhibitor-free (apo) versus YM- (**A, C**) and FR-bound (**B, D**) simulations, measured by the Jensen-Shannon distance of their backbone (**A, B**) and sidechain (**C, D**) torsions. The residues/regions highlighted in A-D are shown in the structure of Gαq bound to FR (**E**); GPD and FR are shown as sticks, and highlighted residues are shown as sticks and translucent spheres.

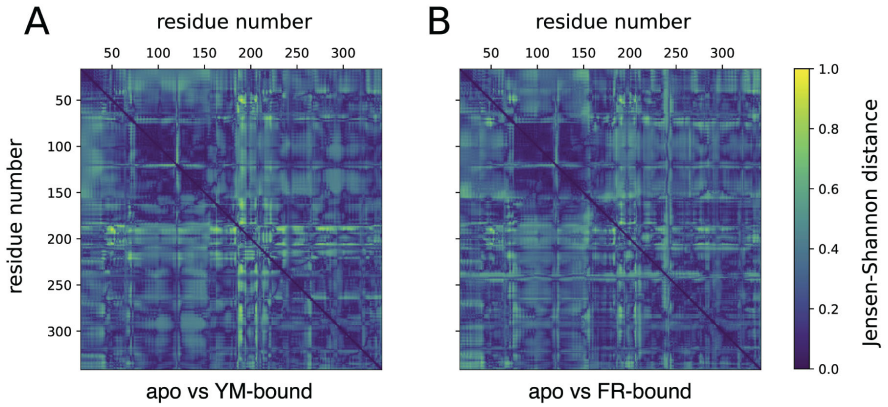
A
residue number
residue number
apo vs YM-bound
B
residue number
apo vs FR-bound
Jensen-Shannon distance

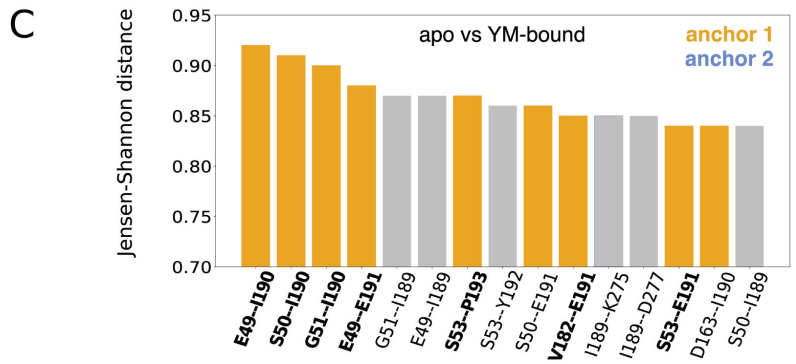
C
Jensen-Shannon distance
apo vs YM-bound
anchor 1
anchor 2
E49--I190
S50--I190
G51--I190
E49--E191
G51--I189
E49--I189
S53--P193
S53--Y192
S50--E191
V182--E191
I189--K275
I189--D277
S53--E191
D163--I190
S50--I189

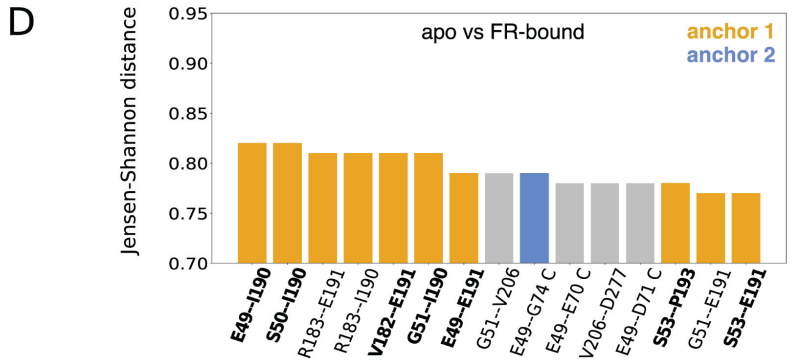
D
Jensen-Shannon distance
apo vs FR-bound
anchor 1
anchor 2
E49--I190
S50--I190
R183--E191
R183--I190
V182--E191
G51--I190
E49--E191
G51--V206
E49--G74 C
E49--E70 C
V206--D277
E49--D71 C
S53--P193
G51--E191
S53--E191

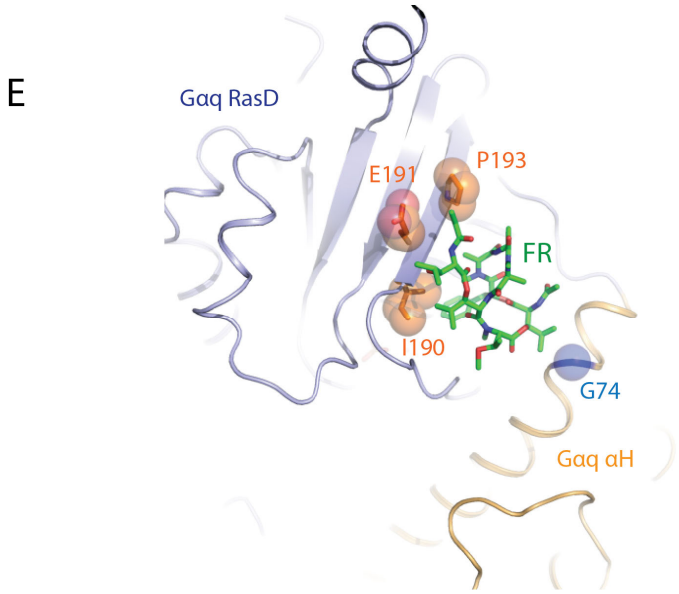
E
Gαq RasD
E191
P193
FR
I190
G74
Gαq αH

Supporting Figure 10: Differences in Cα distances across protein ensembles in apo versus inhibitor-bound MD simulations. A, B: Heatmaps of the relative entropy between inhibitor-free (apo) versus YM- (**A**) and FR-bound **B**) simulations, measured by the Jensen-Shannon distance of every Cα-Cα distance within the Gα subunit. (**C, D**): Bar plot of the top 15 most different Calpha-Calpha distances (i.e highest Jensen-Shannon distance) between the inhibitor-free (apo) vs YM- (**C**) and FR-bound (**D**) simulations. Distances involving residues around anchor 1 and 2 are colored in blue and orange, respectively. Common distances in both systems are highlighted in bold. The residues around anchor 1 ($I190^{G.S02.02}$, $E191^{G.S02.03}$, $P193^{G.S02.05}$; orange sticks/spheres) and anchor 2 ($G74^{H.HA.06}$; blue sphere) that appear in the top 15 lists and have been mutated in this work are shown in the structure of Gαq bound to FR (**E**). FR is shown as green sticks.

A

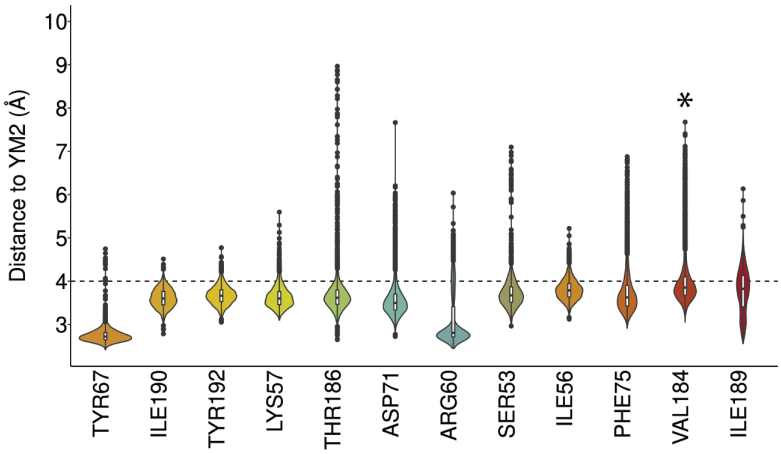
Distance to YM2 (Å)
10
9
8
7
6
5
4
3
*
TYR67
ILE190
TYR192
LYS57
THR186
ASP71
ARG60
SER53
ILE56
PHE75
VAL184
ILE189

B

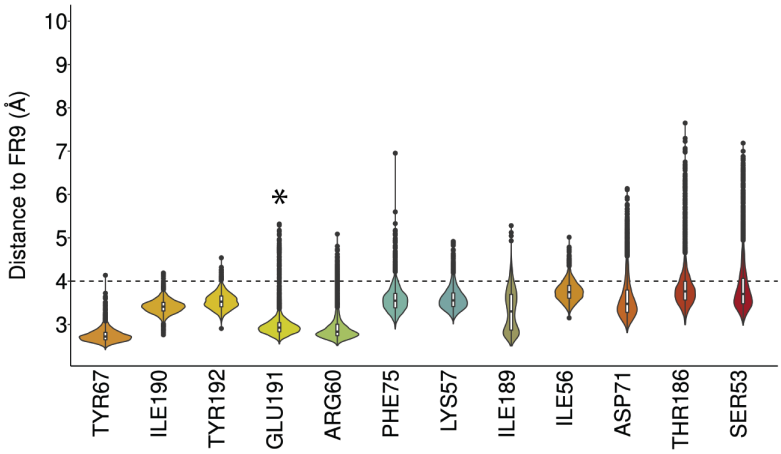
Distance to FR9 (Å)
10
9
8
7
6
5
4
3
*
TYR67
ILE190
TYR192
GLU191
ARG60
PHE75
LYS57
ILE189
ILE56
ASP71
THR186
SER53

C

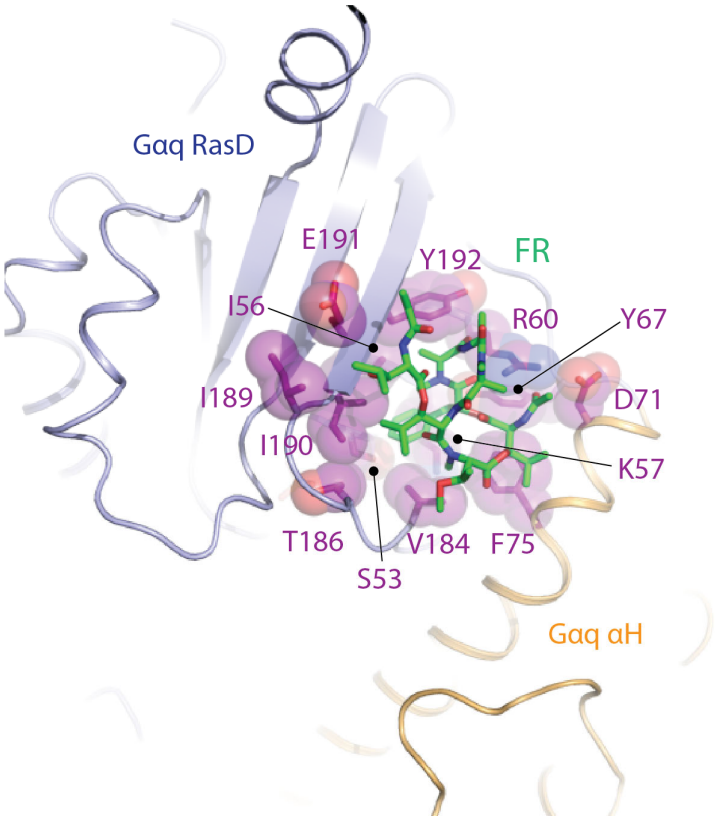
Gαq RasD
E191
Y192
FR
I56
R60
Y67
I189
D71
I190
K57
T186
V184
F75
S53
Gαq αH

15

Supporting Figure 11: Characterization of protein-ligand interactions across MD simulations. The figure shows a violin plot for each distribution of distances between YM (A) or FR (B) and the 12 top-ranked protein residues in terms of contact frequency. The complete protein-YM2/FR9 ensemble was used in the analysis.

Supporting Table 1: Nucleotide sequences (5'→3') of primers used for mutagenesis and cloning.

Primer	Nucleotide sequence (5'→3')
Gnaq G74V – fwd	GATACACCAGCTTGGTGAAGACGCGCTTG
Gnaq G74V – rev	CAAGCGCGTCTTCACCAAGCTGGTGTATC
Gnaq F75A – fwd	GCGCGGCGCCACCAAGCTGGTGTATCAG
Gnaq F75A – rev	CTGATACACCAGCTTGGTGGCGCCGCGC
Gnaq F75K – fwd	GCGCGGCAAAACCAAGCTGGTGTATCAG
Gnaq F75K – rev	CTGATACACCAGCTTGGTTTTGCCGCGC
Gnaq L78A – fwd	GCGGCTTCACCAAGGCGGTGTATCAGAAC
Gnaq L78A – rev	GTTCTGATACACCGCCTTGGTGAAGCCGC
Gnaq V184M – fwd	GCTTAGAGTTCGAATGCCCACTACAGGGATC
Gnaq V184M – rev	GATCCCTGTAGTGGGCATTCGAACTCTAAGC
Gnaq I190F – fwd	CAGGGATCTTCGAATACCCCTTTGACTTAC
Gnaq I190F – rev	GTAAGTCAAAGGGGTATTCGAAGATCCCTG
Gnaq I190W – fwd	CAGGGATCTGGGAATACCCCTTTGACTTAC
Gnaq I190W – rev	GTAAGTCAAAGGGGTATTCCCAGATCCCTG
Gnaq E191A – fwd	CTACAGGGATCATCGCATACCCCTTTGACTTAC
Gnaq E191A – rev	GTAAGCAAAGGGGTATGCGATGATCCCTGTAG
Gnaq P193C – fwd	CATCGAATACTGCTTTGACTTACAAAGTGTC
Gnaq P193C – rev	CACTTTGTAAGTCAAAGCAGTATTCGATG
Gnaq L78A/G74V – fwd	GCGTCTTCACCAAGGCGGTGTATCAGAAC
Gnaq L78A/G74V – rev	GTTCTGATACACCGCCTTGGTGAAGACGC
Gnaq-NotI-ATG – fwd	GTGACAGCGGCCGCATGACTCTGGAGTCCATCATG
Gnaq-BamHI-TGA –rev	CTTACTAGGATCCTTAGACCAGATTGTACTCCTTC

Supporting Table 2: Rationale for $G\alpha_q$ protein mutagenesis of the FR/YM binding site near anchor 1 and anchor 2 of the inhibitors.

Anchor 1 mutants	
I190F	Exchange of I190 for a bulky aromatic residue; constrains the rotational freedom of the YM and FR branched side chain (β-hydroxy-leucine) near anchor 1
I190W	See above; even larger residue
E191A	Removes an ionic lock with R202; may affect the protein structure of the binding site near anchor 1. E191 backbone is predicted to form hydrogen bonds with the free OH-group in YM and FR
P193C	Insp by $G\alpha_{16}$ protein; exchanging proline for another residue may affect the secondary structure near the binding site and therefore affect binding of YM and FR
R202H	Maintains ionic lock with E191; semi-homologous exchange. No direct interaction partner of anchor 2, minor impact expected
Anchor 2 mutants	
G74V	More voluminous lipophilic residue near the larger anchor 2 of FR; predicted to affect FR binding to a larger extent than YM binding
F75A	Removal of a major lipophilic interaction partner for anchor 2 of FR
F75K	Exchange of a lipophilic interaction partner to a charged residue; disruptive mutation
L78A	Removes a lipohilic interaction partner for anchor 2 of FR
V184M	Insp by $G\alpha_{16}$ protein; methionine is a lipophilic residues which is sterically different from valine, presumably interfering with anchor 2 binding of YM/FR by steric hindrance

Supporting Table 3: pIC_{50}- and ΔpIC_{50}-values (means ± SEM, number of independent experiments) for FR and YM in ATP-mediated calcium mobilization experiments performed in HEK293 cells expressing recombinant $G\alpha_q$ proteins. Experiments were performed in duplicate in at least three separate experiments (number of experiments provided in brackets).

	FR900359		**Y**	
	pIC_{50} ± SEM (n)	**ΔpIC_{50} ± SEM**	**pIC_{50} ± SEM (n)**	**ΔpIC_{50} ± SEM**
wt	8.20 ± 0.08 (5)	**0.00** ±	8.09 ± 0.07 (5)	**0.00** ±
I190F	7.10 ± 0.08 (5)	-1.10 ± 0.11	6.53 ± 0.07 (5)	-1.56 ± 0.10
I190W	7.73 ± 0.29 (4)	-0.47 ± 0.21	6.16 ± 0.49 (5)	-1.93 ± 0.49
E191A	8.63 ± 0.08 (3)	**0.43** ±	8.54 ± 0.16 (3)	**0.44** ±
P193C	7.97 ± 0.18 (4)	-0.24 ± 0.20	7.83 ± 0.21 (4)	-0.26 ± 0.22
R202H	8.38 ± 0.07 (4)	**0.18** ±	8.27 ± 0.16 (4)	**0.17** ±
G74V	8.69 ± 0.24 (4)	**0.50** ±	8.59 ± 0.37 (4)	0.44 0.38
F75K	7.17 ± 0.27 (4)	-1.04 ± 0.29	6.64 ± 0.44 (3)	-1.46 ± 0.45
L78A	8.64 ± 0.28 (4)	**0.44** ±	8.50 ± 0.28 (4)	**0.41** ±
V184M	8.52 ± 0.32 (4)	**0.32** ±	8.51 ± 0.40 (4)	**0.42** ±
G74V/L78A	7.94 ± 0.17 (3)	-0.26 ± 0.19	8.24 ± 0.33 (3)	0.15 ± 0.34

Supporting Table 4: Pseudo-pKD values (mean ± SEM) obtained from pseudo-homologous competition experiments (YM vs. [^{3}H]PSB-16254-YM) at HEK293 cell membrane preparations recombinantly expressing Gαq proteins (50 µg protein per well). Competition experiments were incubated for 90 minutes to reach equilibrium. Experiments were performed in duplicate in three independent experiments.

	YM-254890 vs. [^{3}H]PSB-16254-YM
	pseudo- pK_D ± SEM
wt	8.19 ± 0.17
E191A	8.41 ± 0.02
P193C	7.81 ± 0.17
R202H	8.31 ± 0.03
G74V	8.59 ± 0.26
L78A	8.00 ± 0.04
V184M	8.14 ± 0.22
G74V/L78A	7.79 ± 0.12

Supporting Table 5: Association half-life (mean ± SEM) of [^{3}H]PSB-15900-FR at wt and mutant Gq proteins. Experiments were performed in duplicate in three independent experiments if not indicated otherwise (number of experiments provided in brackets).

	Association $t_{1/2}$ (min) [^{3}H]PSB-15900	**x-fold of wt** ([^{3}H]PSB-15900-FR)	**Association $t_{1/2}$** (min) [^{3}H]PSB-16254	**x-fold of wt** ([^{3}H]PSB-16254-YM)
wt	2.18 ± 0.21	-	2.47 ± 0.54 (4)	-
E191A	3.22 ± 0.20	1	7.71 ± 0.70	0.3
P193C	1.21 ± 0.10	2	2.84 ± 0.68 (5)	1
R202H	1.61 ± 0.30	1	2.67 ± 0.51 (4)	1
G74V	1.65 ± 0.29	1	1.99 ± 0.30	1
L78A	1.45 ± 0.22 (4)	2	3.11 ± 0.65 (5)	1
V184M	1.28 ± 0.07	2	4.07 ± 0.44	1
G74V/L78A	1.11 ± 0.03	2	4.74 ± 1.14	1

Supporting Table 6: Dissociation half-life (mean ± SEM) of [^{3}H]PSB-15900-FR at wt and mutant Gq proteins. All experiments were performed in duplicate in three independent experiments.

	Diss. $t_{1/2}$ (min) [^{3}H]PSB-15900	**x-fold of wt** ([^{3}H]PSB-15900-FR)	**Diss. $t_{1/2}$** (min) [^{3}H]PSB-16254	**x-fold of wt** ([^{3}H]PSB-16254-YM)
wt	79.2 ± 1.5	-	3.89 ± 0.16	-
E191A	7.37 ± 0.11	11	0.95 ± 0.13	4
P193C	5.20 ± 0.73	15	0.70 ± 0.04	6
R202H	62.5 ± 3.34	1	3.45 ± 0.47	1
G74V	0.90 ± 0.10	88	0.86 ± 0.05	5
L78A	7.42 ± 0.35	11	0.72 ± 0.03	5
V184M	2.29 ± 0.07	35	0.37 ± 0.02	11
G74V/L78A	0.40 ± 0.15	198	0.30 ± 0.03	13

13.3. Appendix C – Agonist-dependent coupling of the promiscuous adenosine A_{2B} receptor to Gα protein subunits

The following pages include the article "Agonist-dependent coupling of the promiscuous adenosine A2B receptor to Gα protein subunits" and its supporting information as it was published in *ACS Pharmacology and Translational Science*. According to ACS, the re-use of this article for a thesis or dissertation is allowed, a legal note from the Copyright Clearance Center is presented below. The article is reprinted with permission from *ACS Pharmacol. Transl. Sci.* **2022**, 5, 5, 373-386.

ACS Pharmacology & Translational Science

pubs.acs.org/ptsci Article

Agonist-Dependent Coupling of the Promiscuous Adenosine A_{2B} Receptor to Gα Protein Subunits

Published as part of the ACS Pharmacology & Translational Science virtual special issue "GPCR Signaling".

Jan Hendrik Voss, Andhika B. Mahardhika, Asuka Inoue, and Christa E. Müller*

Cite This: *ACS Pharmacol. Transl. Sci.* 2022, 5, 373−386 Read Online

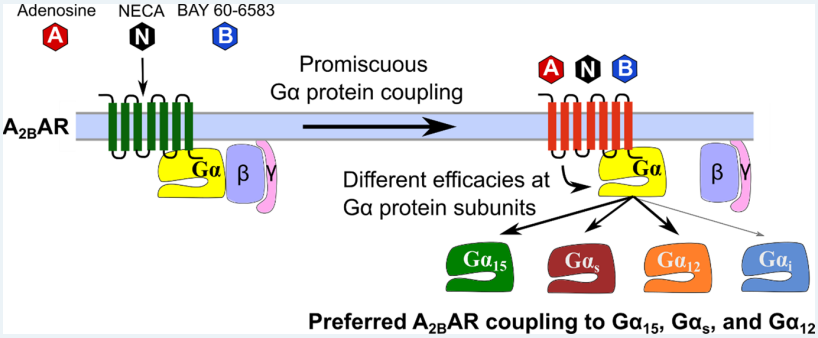

ABSTRACT: The adenosine A_{2B} receptor (A_{2B}AR) belongs to the rhodopsin-like G protein-coupled receptor (GPCR) family. It is upregulated under hypoxic conditions, in inflammation and cancer. Previous studies indicated the coupling of the A_{2B}AR to different G proteins, mainly G_s, but in some cases $G_{q/11}$ or G_i, depending on the cell type. We have now utilized novel technologies, (i) heterologous expression of individual members of the $Gα_{q/11}$ protein family ($Gα_q$, $Gα_{11}$, $Gα_{14}$, and $Gα_{15}$) in $Gα_{q/11}$ knockout cells, and (ii) the TRUPATH platform, allowing the direct observation of Gα protein activation for each of the Gα subunits by bioluminescence resonance energy transfer (BRET) measurements. Three structurally diverse A_{2B}AR agonists were studied: the cognate agonist adenosine, its metabolically stable analog NECA, and the non-nucleosidic partial agonist BAY 60-6583. Adenosine and NECA activated most members of all four Gα protein families ($Gα_s$, $Gα_{q/11}$, $Gα_i$, and $Gα_{12/13}$). Significant differences in potencies and efficacies were observed; the highest efficacies were determined at the $Gα_{15}$, $Gα_s$, and $Gα_{12}$ proteins, and for NECA additionally at the $Gα_{i2}$ protein. In contrast, the partial agonist BAY 60-6583 only activated $Gα_{15}$, $Gα_s$, and $Gα_{12}$ proteins. Adenosine deaminase, an allosteric modulator of ARs, selectively increased the potency and efficacy of NECA and BAY 60-6583 at the $Gα_{15}$ protein, while it had no effect or decreased efficacy at the other Gα proteins. We conclude that the A_{2B}AR is preferably coupled to the $Gα_{15}$, $Gα_s$, and $Gα_{12}$ proteins. Upon upregulation of receptor or Gα protein expression, coupling to further Gα proteins likely occurs. Importantly, different agonists can display different activation profiles.

KEYWORDS: *adenosine, BAY 60-6583, G protein coupling, $G_q/G_s/G_i/G_{12/13}$ proteins, HEK293 cells, NECA*

The adenosine A_{2B} receptor (A_{2B}AR) belongs to the α-branch of rhodopsin-like G protein-coupled receptors (GPCRs). Four different subtypes exist, designated A_1-, A_{2A}-, A_{2B}-, and A_3ARs. The alkaloid caffeine is a non-selective AR antagonist employed to improve lung function of pre-term babies and for pain management in combination with analgesics.[2,3] Moreover, the A_{2A}-selective antagonist istradefylline is used for the treatment of Parkinson's disease,[4,5] while the A_{2A}-selective agonist regadenoson and the cognate agonist adenosine are employed for cardiac imaging to induce vasodilation.[6] Moreover, adenosine is therapeutically applied to treat arrhythmia in paroxysmal supraventricular tachycardia.[1] All AR subtypes constitute promising drug targets, especially in the context of inflammation, immunity, and cancer.[2,3,7−12] The A_{2B}AR is mostly expressed in low density and only activated by relatively high, micromolar concentrations of adenosine, which are typically only present under pathological, e.g., inflammatory and hypoxic, conditions.[13,14] There are exceptions: e.g., some epithelial cells, particularly in the gut, display rather high expression levels of the A_{2B}AR.[15]

Received: February 5, 2022
Published: May 3, 2022

ACS Pharmacology & Translational Science pubs.acs.org/ptsci Article

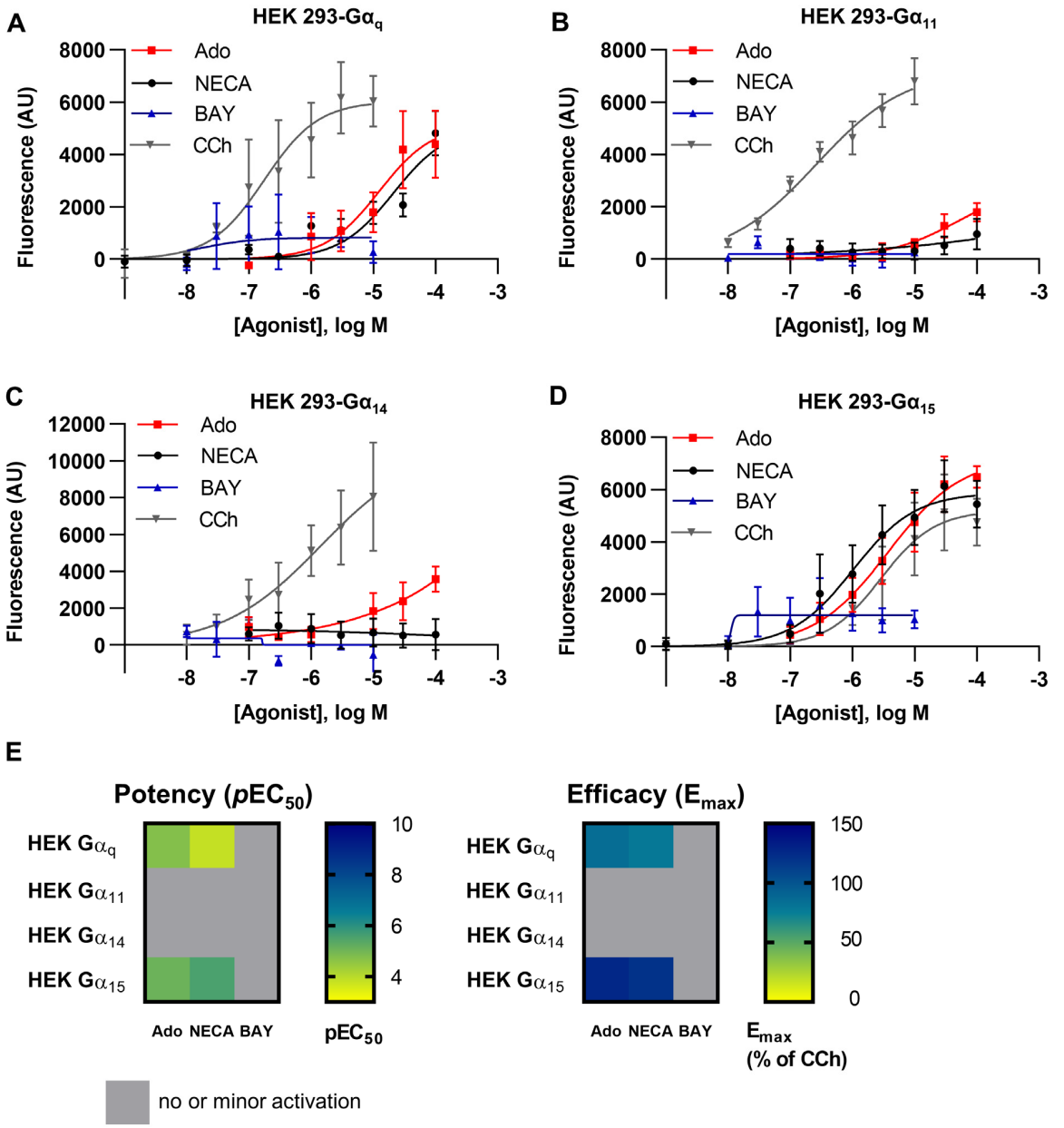

Figure 1. Concentration–response curves of NECA, adenosine (Ado), BAY 60-6583 (BAY), and carbachol (CCh) at HEK293 $\Delta G\alpha_{q/11}$ cells recombinantly expressing (A) $G\alpha_q$, (B) $G\alpha_{11}$, (C) $G\alpha_{14}$, or (D) $G\alpha_{15}$ proteins. Data points are from at least three separate experiments, each performed in triplicates. (E) Heatmaps of A_{2B}AR-mediated calcium signaling depicting potency (pEC_{50}, left) and efficacy (% of CCh signal at the highest tested concentration, right).

Moreover, A_{2B}AR expression is upregulated in inflamed tissues and on many cancer cells.[16−18] Therefore, A_{2B}ARs have significant potential as future drug targets for a range of diseases. Agonists have, e.g., been proposed for the treatment of stroke, obesity-induced diabetes, atherosclerosis, and wound healing, while antagonists have shown potential for treating inflammatory diseases (e.g., asthma, pulmonary and liver fibrosis, inflammatory bowel disease, multiple sclerosis), pain, cancer, and infections.[3,12] On the other hand, anti-inflammatory effects induced by A_{2B}AR activation have also been described.[14]

Agonists on GPCRs trigger intracellular signaling cascades by activation of heterotrimeric guanine nucleotide-binding proteins (G proteins), consisting of α-, β-, and γ-subunits. The $G\alpha$-subunits are crucial for the activation of various second messenger systems. They are subdivided into four families: $G\alpha_s$, $G\alpha_{i/o}$, $G\alpha_{q/11}$, and $G\alpha_{12/13}$.[19,20] During G protein activation, the helical and the Ras-like domains of the $G\alpha$-subunit separate from each other, thereby allowing the dissociation of the bound guanosine diphosphate (GDP), which is replaced by guanosine triphosphate (GTP).[21] The GTP-bound $G\alpha$-subunit then dissociates from the associated $G\beta\gamma$-dimer and subsequently interacts with its effector proteins. Depending on the $G\alpha$ protein subunit, specific effects are triggered in the cell, e.g., stimulation of adenylate cyclase (AC) by $G\alpha_s$ proteins, inhibition of AC by $G\alpha_{i/o}$

https://doi.org/10.1021/acsptsci.2c00020
ACS Pharmacol. Transl. Sci. 2022, 5, 373−386

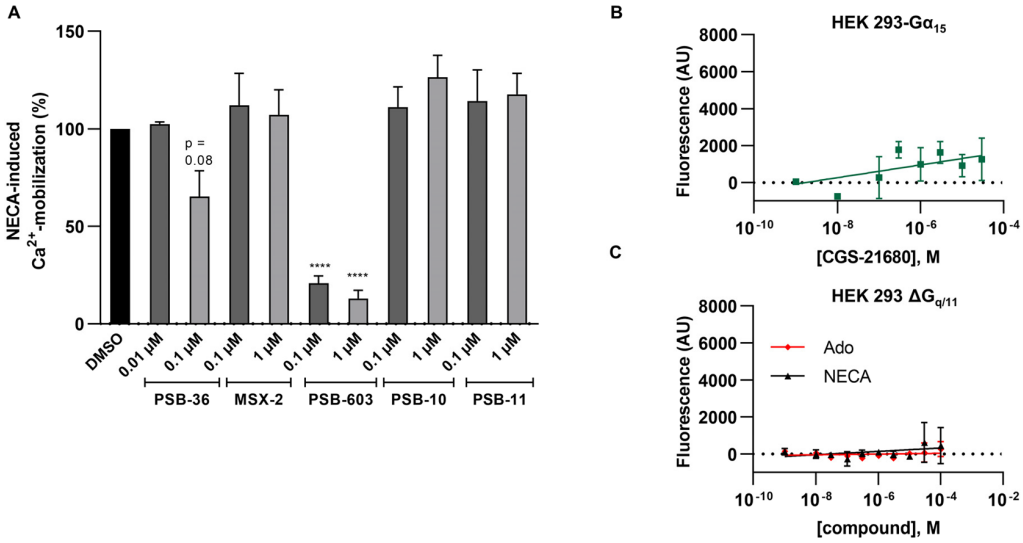

Figure 2. NECA-induced calcium mobilization in HEK293-Gα_{15} cells is inhibited by A_{2B}-selective AR antagonists. (A) NECA-induced calcium mobilization (8.8 μM NECA corresponding to its EC_{80} value) in the presence of the AR antagonists PSB-36 (A_1AR), MSX-2 (A_{2A}AR), PSB-603 (A_{2B}AR), PSB-10, and PSB-11 (both A_3AR) in HEK293-Gα_{15} cells. Cells were preincubated with the indicated concentrations of AR antagonist for 30 min before measurement. Values were normalized to controls in the absence of antagonist (100%) and in the absence of agonist (0%). Three (PSB-36) or four (all other) independent experiments were performed in triplicates; bars represent means ± SEM. (B) The A_{2A}AR-selective agonist CGS-21680 did not induce calcium mobilization in HEK293-Gα_{15} cells at concentrations of up to 30 μM. (C) Adenosine (Ado) and NECA did not induce calcium mobilization in HEK293-ΔG$\alpha_{q/11}$ cells.

proteins, calcium mobilization by G$\alpha_{q/11}$ proteins, or activation of Rho guanine exchange factors (Rho-GEFs) by G$\alpha_{12/13}$ proteins.[20,22]

In the past, it was challenging to investigate the activation of specific Gα protein subunits by GPCR subtypes and their agonists. Recent technological advances, namely the clustered regularly interspaced short palindromic repeats (CRISPR)-Cas9 technology,[23] and especially the development of novel biosensors for measuring G protein activation, have provided tools to unambiguously investigate the activation of individual Gα protein subunits. Human embryonic kidney (HEK) 293 cells depleted of Gα proteins by CRISPR-Cas9 knockout followed by heterologous expression of individual Gα protein subunits have enabled specific studies.[24−28] BRET sensors, e.g., the TRUPATH assay and similar previously described biosensors,[29,30] allow the measurement of BRET ratios between renilla luciferase-8 (RLuc8)-fused Gα protein subunits and a green fluorescent protein 2 (GFP2)-tagged Gγ subunit. This ratio decreases upon G protein activation due to the dissociation of the α- and β,γ-subunits, resulting in an increased distance between BRET donor and acceptor.[31] Further recently established methods for direct measurement of G protein activation include (i) split-luciferase assays (where Gα and, e.g., Gγ proteins are labeled by luciferase fragments that dissociate upon receptor activation, resulting in a decrease in luminescence),[32−35] (ii) effector-membrane translocator assays (EMTAs, in which luciferase-tagged effectors interact exclusively with GTP-bound Gα subunits and are thereby brought into close proximity to a membrane-anchored BRET acceptor),[36,37] and transforming growth factor-α (TGF-α) shedding assays (in which G$\alpha_{q/11}$ protein activation results in cleavage and release of a soluble alkaline phosphatase (AP) fragment from a membrane-bound TGF-α-AP fusion protein by the metalloprotease ADAM17).[34,38]

The A_{2B}AR was reported to couple to Gα_s and Gα_q proteins; however Gα_q protein coupling has only been observed in some of the investigated cell types,[39−41] and the reason for this has remained unclear. Few individual publications indicated additional coupling to G$\alpha_{i/o}$ proteins.[40,42,43] Thus, the A_{2B}AR appears to be endowed with an amazing, and at the same time confusing, promiscuity.[40,42] In the present study, we utilized novel techniques, that only recently became accessible, to monitor the activation of individual Gα protein subunits by the A_{2B}AR upon stimulation with structurally diverse agonists—namely the endogenous agonist adenosine, its metabolically stable analog NECA, and the A_{2B}-selective partial agonist BAY 60-6583[39] (for structures see Figure S1A). Our first approach was to stably express each G$\alpha_{q/11}$ protein family member (Gα_q, Gα_{11}, Gα_{14}, and Gα_{15}) in G$\alpha_{q/11}$-deficient HEK293 cells (HEK293-ΔG$\alpha_{q/11}$) that natively express a low level of the human A_{2B}AR[40,44] and then directly measure intracellular calcium mobilization (see Figure S1B). Next, we employed the BRET-based biosensor platform TRUPATH[31] to probe A_{2B}AR-induced activation of virtually each of the Gα protein subunits, directly at the G protein level (see Figure S1C). We discovered that the A_{2B}AR is preferably coupled to Gα_{15}, Gα_s, and Gα_{12} proteins. While the full A_{2B}AR agonists activated almost all Gα protein subunits, their potencies and efficacies were significantly different. Efficacy in particular appears to play a decisive role for the resulting physiological and pharmacological effects.

■ RESULTS

Calcium Mobilization Studies. Signaling via the $G_{q/11}$ protein family was initially studied by calcium mobilization assays in HEK293 cells, which natively express the A_{2B}AR.[40,44] In previously published experiments, Hinz et al.[39] and Gao et al.[40] demonstrated calcium mobilization upon A_{2B}AR stimulation with the adenosine analog NECA, while the A_{2B}AR-

https://doi.org/10.1021/acsptsci.2c00020
ACS Pharmacol. Transl. Sci. 2022, 5, 373−386

ACS Pharmacology & Translational Science pubs.acs.org/ptsci Article

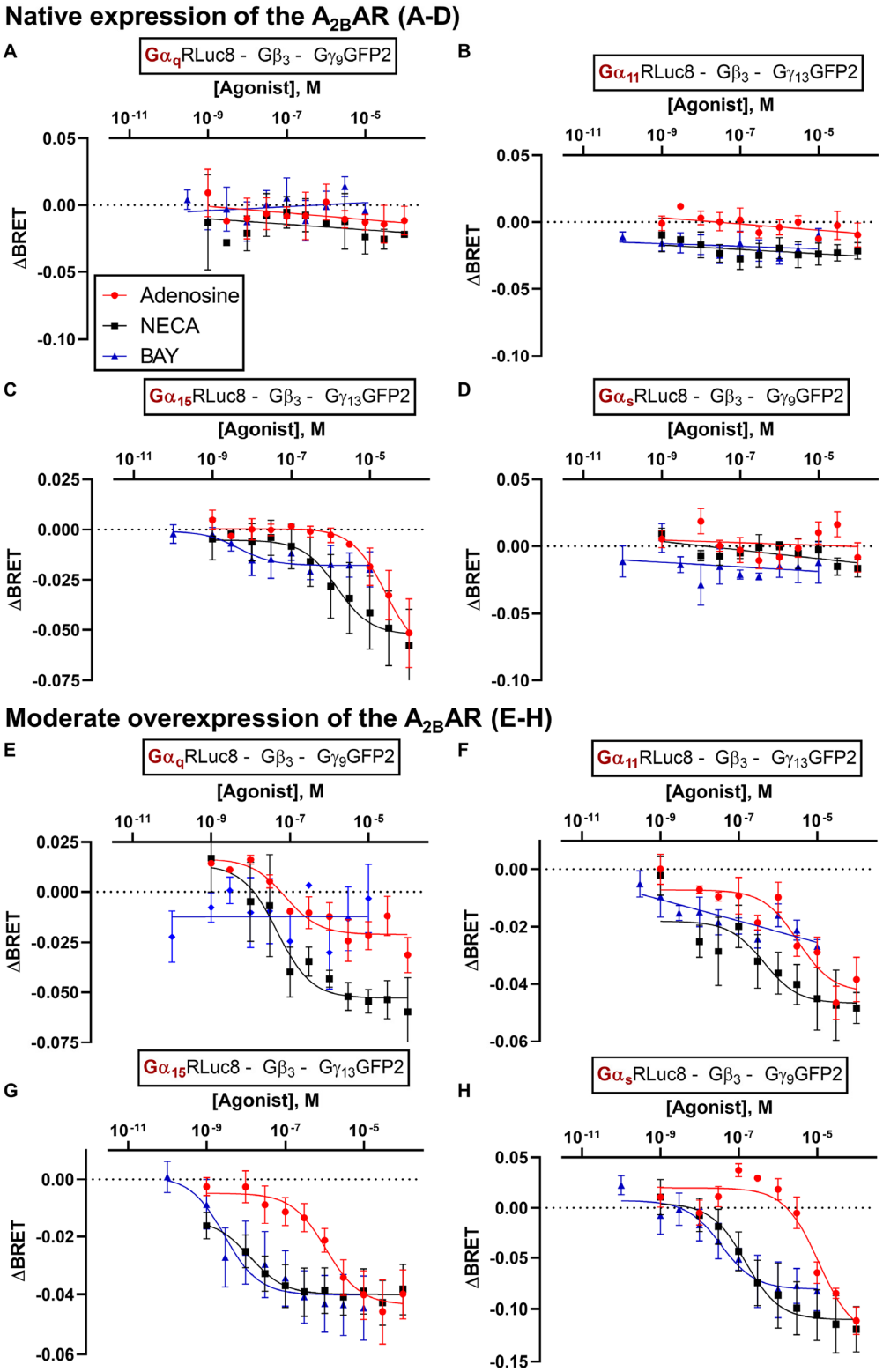

Figure 3. Concentration–response curves of the agonists adenosine, NECA and BAY 60-6583 at HEK293 cells transiently transfected with TRUPATH biosensors for the indicated G protein subunits. **A-D**. ΔBRET values measured in HEK293 cells with native $A_{2B}AR$ expression levels and overexpression of the indicated biosensors **A**. $G\alpha_q$, **B**. $G\alpha_{11}$, **C**. $G\alpha_{15}$, or **D**. $G\alpha_{s\text{-}s}$. **E-H**. ΔBRET values measured in HEK293 cells with overexpression of the $A_{2B}AR$ and the indicated biosensors $G\alpha_q$ (e), $G\alpha_{11}$ (f), $G\alpha_{15}$ (g), or $G\alpha_{s\text{-}s}$ (h) biosensors. Data points are presented as means ± SEM of three or more independent experiments; pEC_{50} values and efficacy values are listed in Tables S2 and S3 of Supporting Information.

https://doi.org/10.1021/acsptsci.2c00020
ACS Pharmacol. Transl. Sci. 2022, 5, 373−386

selective partial agonist BAY 60-6583 had not induced calcium mobilization in those studies. In order to investigate this discrepancy in more detail, we generated stable (polyclonal) cell lines that exclusively expressed a single Gα protein subunit of the Gα_q protein family, either Gα_q, Gα_{11}, Gα_{14}, or Gα_{15}, by retroviral transfection of HEK293-ΔG$\alpha_{q/11}$ cells, resulting in similar expression levels for Gα_q, Gα_{11}, and Gα_{14} proteins (the expression level of Gα_{15} could not be quantified on a protein level).[25] These cells were subsequently used to identify the Gα protein(s) involved in A_{2B}AR-induced intracellular calcium release. Our aim was to examine (i) whether the A_{2B}AR favors signaling via a specific Gα_q subfamily member and/or (ii) if structurally diverse A_{2B}AR agonists would result in specific or selective activation of certain Gα protein subunits and thus show biased signaling. Carbachol (CCh)-mediated activation of the muscarinic M_3 receptor (M_3R), which is endogenously expressed in HEK293 cells, was used as a control (for results see Figure 1A−E and Table S1).

In HEK293-ΔG$\alpha_{q/11}$ cells not expressing any G$\alpha_{q/11}$ family protein, calcium mobilization was neither induced by adenosine nor by NECA (see below). CCh exhibited a preference for signaling via Gα_q and Gα_{11} proteins, both of which were activated by submicromolar concentrations of the muscarinic receptor agonist. Higher CCh concentrations (20- to 30-fold) were required to activate calcium mobilization in HEK-Gα_{14} and HEK-Gα_{15} cells.

The physiological agonist adenosine and its closely related derivative NECA displayed similar activity showing a preference for Gα_{15}-induced intracellular calcium release (pEC_{50} adenosine: 5.52; NECA, 5.79) (see Figure 1A,D and Table S1) followed by Gα_q-mediated calcium mobilization (pEC_{50} adenosine: 4.84, NECA: 4.37). The efficacy also appeared to be higher for Gα_{15}- as compared to Gα_q-induced calcium release. Only minor or negligible activation of calcium mobilization via Gα_{11} or Gα_{14} proteins was observed (see Figure 1B,C). These results indicate that adenosine preferably activates Gα_{15} within the G$\alpha_{q/11}$ protein family. Interestingly, the A_{2B}-selective non-nucleosidic partial agonist BAY 60-6583 did not activate any of the G$\alpha_{q/11}$ family proteins in these calcium mobilization experiments (fluorescence monitored at the highest tested concentration of BAY 60-6583 did not significantly differ from basal values).

In order to confirm that the observed effects were actually due to the activation of A_{2B}ARs endogenously expressed in the HEK293 cells, we preincubated the cells with AR subtype-selective antagonists. Calcium mobilization induced by NECA was almost completely blocked by the A_{2B}AR-antagonist PSB-603 (Figure 2A), but not by selective A_1-, A_{2A}-, and A_3AR antagonists. The A_1AR-selective antagonist PSB-36 only inhibited calcium mobilization moderately at a concentration of 100 nM, but not at 10 nM, consistent with its affinity for the A_{2B}AR (K_i A_{2B}, 187 nM; K_i A_1 0.7 nM).[45] The A_{2A}AR-selective agonist CGS-21680 did not induce calcium mobilization (Figure 2B), nor did adenosine or NECA in G$\alpha_{q/11}$ knockout cells (Figure 2C).

Since the observed effects downstream of A_{2B}AR-mediated Gα protein activation might be modulated by unknown factors, we next measured direct activation of Gα protein subunits.

Direct Measurement of G Protein Activation. G protein activation by A_{2B}AR agonists was monitored using the TRUPATH assay platform, a BRET2-based method that allows to observe the dissociation of Gα from G$\beta\gamma$ protein subunits.[31] Biosensors are available for all Gα protein subunits with the exception of transducins, Gα_{14}, and Gα_{olf}. For each biosensor, the RLuc8-Gα subunit was paired with an optimized G$\beta\gamma$-GFP2 combination to yield maximum BRET2 ratio shifts upon GPCR activation.[31] The biosensors were transiently expressed in native HEK293 cells together with the receptor of interest, and the BRET ratio shifts in response to agonist stimulation were measured. To validate the assay, we expressed the Gα_{i1}-, and the Gα_q biosensor, respectively, together with a GPCR that is known to couple to the respective Gα protein subunits (Figure S2), namely the thromboxane receptor (TP) for the Gα_q biosensor, and the A_3AR for the Gα_{i1} biosensor. Transfected cells were activated by a full agonist of the respective receptor. The U46619-activated TP receptor elicited a maximum ΔBRET shift of −0.2. Using the Gα_{i1} biosensor, we measured a maximum ΔBRET shift of −0.23 for the NECA-activated A_3AR. The E_{max} values for the TP receptor and the A_3AR were nearly identical to the E_{max} values reported for model receptors (isoprotenerol-activated β_2 adrenoceptor for the Gα_s family, DAMGO-activated μ-opioid receptor for the G$\alpha_{i/o}$ family, neurotensin-activated neurotensin 1 receptor for the G$\alpha_{q/11}$ and G$\alpha_{12/13}$ families) in the original publication.[31] To assess the efficacy of receptor−G protein coupling we therefore decided to compare E_{max} values determined in the present study for the A_{2B}AR upon coupling to various Gα protein subunits to E_{max} values for the same subunits observed for full agonists with standard GPCRs reported in the original publication using the same procedures and conditions.[31]

We first investigated direct activation of the G$\alpha_{q/11}$ family members induced by A_{2B}AR agonists to enable comparison with our previous results from calcium mobilization assays. Next, we studied the A_{2B}AR's canonical effector, Gα_s (short isoform G$\alpha_{s\text{-}s}$). Endogenous A_{2B}AR expression in HEK293 cells was found to be not sufficient to trigger measurable activation of Gα_q, Gα_{11}, and G$\alpha_{s\text{-}s}$ biosensors in this system (Figure 3A-D; similarly, carbachol, an agonist at the endogenously expressed M_3R, failed to activate Gα_q, Gα_{11}, and Gα_{15} biosensors in the TRUPATH BRET2 assays, data not shown). Only the Gα_{15} biosensor was activated in these cells by adenosine and NECA in a concentration-dependent manner. BAY 60-6583 showed a very small effect typical of a weak partial agonist (Figure 3C).

Next, the A_{2B}AR was (moderately) overexpressed in HEK293 cells as recommended by the TRUPATH assay protocol[31] (100 ng pCDNA3.1-human ADORA2B per 10^6 cells, transient expression) (see Figure 3E-H; and Tables S2 and S3 in Supporting Information). Now, adenosine and NECA activated all four investigated Gα proteins, Gα_q, Gα_{11}, Gα_{15} and G$\alpha_{s\text{-}s}$, in a concentration-dependent manner, while BAY 60-6583 activated Gα_{15} and G$\alpha_{s\text{-}s}$ only. NECA appeared to be significantly more potent than adenosine in all cases, while BAY 60-6583 was equipotent to adenosine at Gα_{15} and G$\alpha_{s\text{-}s}$ proteins, where it showed activation. At the Gα_q protein, NECA was more efficacious than adenosine while at all other investigated Gα subunits both nucleosidic agonists displayed similar efficacy. BAY 60-6583 was as efficacious as adenosine at the Gα_{15} and G$\alpha_{s\text{-}s}$ subunit.

Since we had not observed any calcium mobilization induced by BAY 60-6583 in Gα_{15}-expressing HEK293 cells, we wondered whether this was due to the low A_{2B}AR expression level in this cell line combined with the partial agonistic properties of BAY 60-6583. Thus, we studied calcium mobilization in HEK293 cells overexpressing A_{2B}ARs by BAY

https://doi.org/10.1021/acsptsci.2c00020
ACS Pharmacol. Transl. Sci. 2022, 5, 373−386

ACS Pharmacology & Translational Science pubs.acs.org/ptsci Article

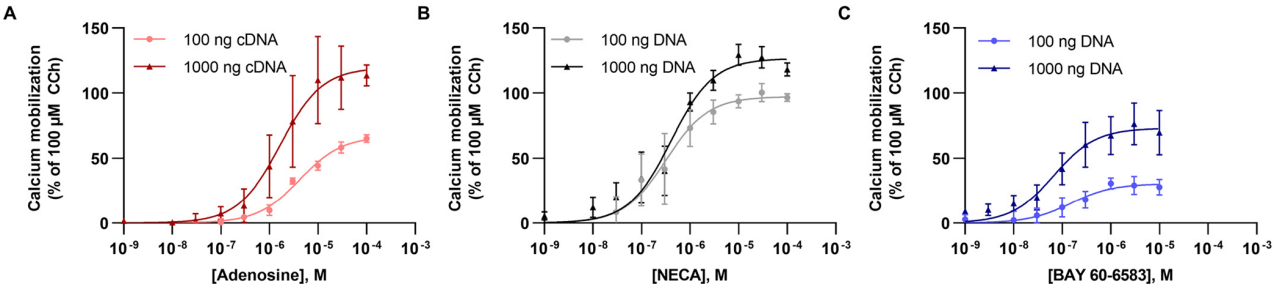

Figure 4. Calcium mobilization induced by A_{2B}AR agonists in HEK293-Gα_{15} cells transiently overexpressing A_{2B}ARs. The human A_{2B}AR was transiently overexpressed with either a low amount of cDNA (100 ng/well) or a high amount of cDNA (1000 ng/well). A_{2B}AR activation by **A**. adenosine (E_{max} adenosine: 100 ng DNA/well, 76 ± 10%; 1000 ng DNA/well, 119 ± 5%; pEC_{50} adenosine: 100 ng DNA/well, 5.38 ± 0.19; 1000 ng/well, 5.72 ± 0.21), **B**. NECA (E_{max} NECA: 100 ng DNA/well, 111 ± 3%; 1000 ng DNA/well, 122 ± 7%; pEC_{50} NECA: 100 ng DNA/well, 6.72 ± 0.36; 1000 ng/well, 6.37 ± 0.11), and **C**. BAY 60-6583 (E_{max} BAY 60-6583:100 ng DNA/well, 27 ± 1%; 1000 ng/DNA well, 71 ± 17%; pEC_{50} BAY 60-6583:100 ng DNA/well, 6.73 ± 0.11; 100 ng/well, 6.95 ± 0.15), normalized to the effect of 100 μM CCh. Data are means ± SEM of three individual experiments performed in duplicates.

60-6583 (Figure 4). To this end, we transiently overexpressed the A_{2B}AR using two different cDNA concentrations, and recorded concentration-dependent intracellular calcium release induced by adenosine, NECA, and BAY 60-6583. Adenosine showed an increase in efficacy with increasing amounts of cDNA (compared to the maximal effect of CCh) and a moderate increase in potency (E_{max} adenosine: 100 ng DNA/well, 76%; 1000 ng DNA/well, 119%; pEC_{50} adenosine: 100 ng DNA/well, 5.38; 1000 ng/well, 5.72; Figure 4A). NECA displayed a minor increase in efficacy and a similar potency with increasing cDNA concentrations (E_{max} NECA: 100 ng DNA/well, 111%; 1000 ng DNA/well, 122%; pEC_{50} NECA: 100 ng DNA/well, 6.72; 1000 ng/well, 6.37; Figure 4B). In HEK-Gα_{15} cells with overexpression of the A_{2B}AR, BAY 60-6583 was able to induce calcium mobilization; both potency and efficacy of BAY 60-6583 increased with increasing cDNA amounts used for transfection (E_{max}: BAY 60-6583 100 ng DNA/well = 27%, 1000 ng/DNA well = 71%; pEC_{50} BAY 60-6583 100 ng DNA/well = 6.73, 100 ng/well = 6.95, Figure 4C). Thus, the partial agonist BAY 60-6583 can induce calcium mobilization via Gα_{15}-activation in HEK cells, but requires high A_{2B}AR expression levels.

Effect of adenosine deaminase. The signaling molecule adenosine is ubiquitous and may be released by the cells or formed from ATP by ectonucleotidases.[46,47] To avoid an interfering effect of adenosine potentially present in the HEK293 cell culture, we additionally performed TRUPATH assays with the agonists NECA and BAY 60-6583 in the presence of adenosine deaminase (ADA) which converts adenosine to inosine, but has no effect on NECA or BAY 60-6583. NECA-induced Gα_q and Gα_{11} biosensor activation was not significantly different in terms of potency and efficacy in the presence and absence of ADA (Figure 5; Supp. Tables 2,3). At the Gα_{15} protein, the potency of NECA and BAY 60-6583 was enhanced by ADA (~10-fold for NECA, ~ 120-fold for BAY), while the efficacy was concomitantly increased by about 2-fold for BAY as well as for NECA. Potencies at the G$\alpha_{s\text{-}s}$ biosensor observed in the presence of ADA were again similar to those without ADA, but ADA reduced the efficacy of NECA- and BAY 60-6583-induced G$\alpha_{s\text{-}s}$ activation by approximately 2-fold (see Table S3). In summary, ADA selectively increased potency and/or efficacy of NECA and BAY 60-6583 in Gα_{15} protein activation, while it had no effect or decreased efficacy at the other Gα proteins.

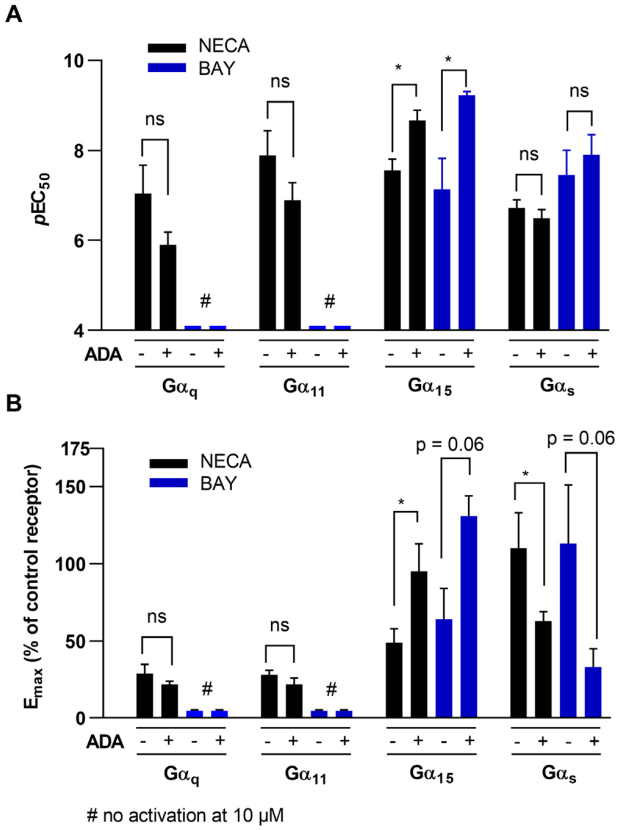

Figure 5. **A**. Potency and **B**. efficacy of NECA (black) or BAY 60-6583 (blue) for A_{2B}AR stimulation determined in TRUPATH BRET[2] assays using the Gα_q, Gα_{11}, Gα_{15}, or the G$\alpha_{s\text{-}s}$ biosensor in the absence (−) or presence (+) of ADA. Data are presented as means ± SEM of three or more independent experiments; pEC_{50} and E_{max} values are summarized in Table S2 and S3. Statistical analysis was performed with multiple unpaired *t*-tests corrected for multiple comparisons by the Holm-Sidak-method (as implemented in GraphPad PRISM v. 8.0; ns − $p > 0.05$, * − $p < 0.05$, *** − $p < 0.001$).

The promiscuous A_{2B}AR couples to all Gα protein families. Next, we investigated the potential coupling of the A_{2B}AR to further, noncanonical Gα protein subunits, specifically to members of the G$\alpha_{12/13}$ and the G$\alpha_{i/o}$ families

https://doi.org/10.1021/acsptsci.2c00020
ACS Pharmacol. Transl. Sci. 2022, 5, 373−386

ACS Pharmacology & Translational Science pubs.acs.org/ptsci Article

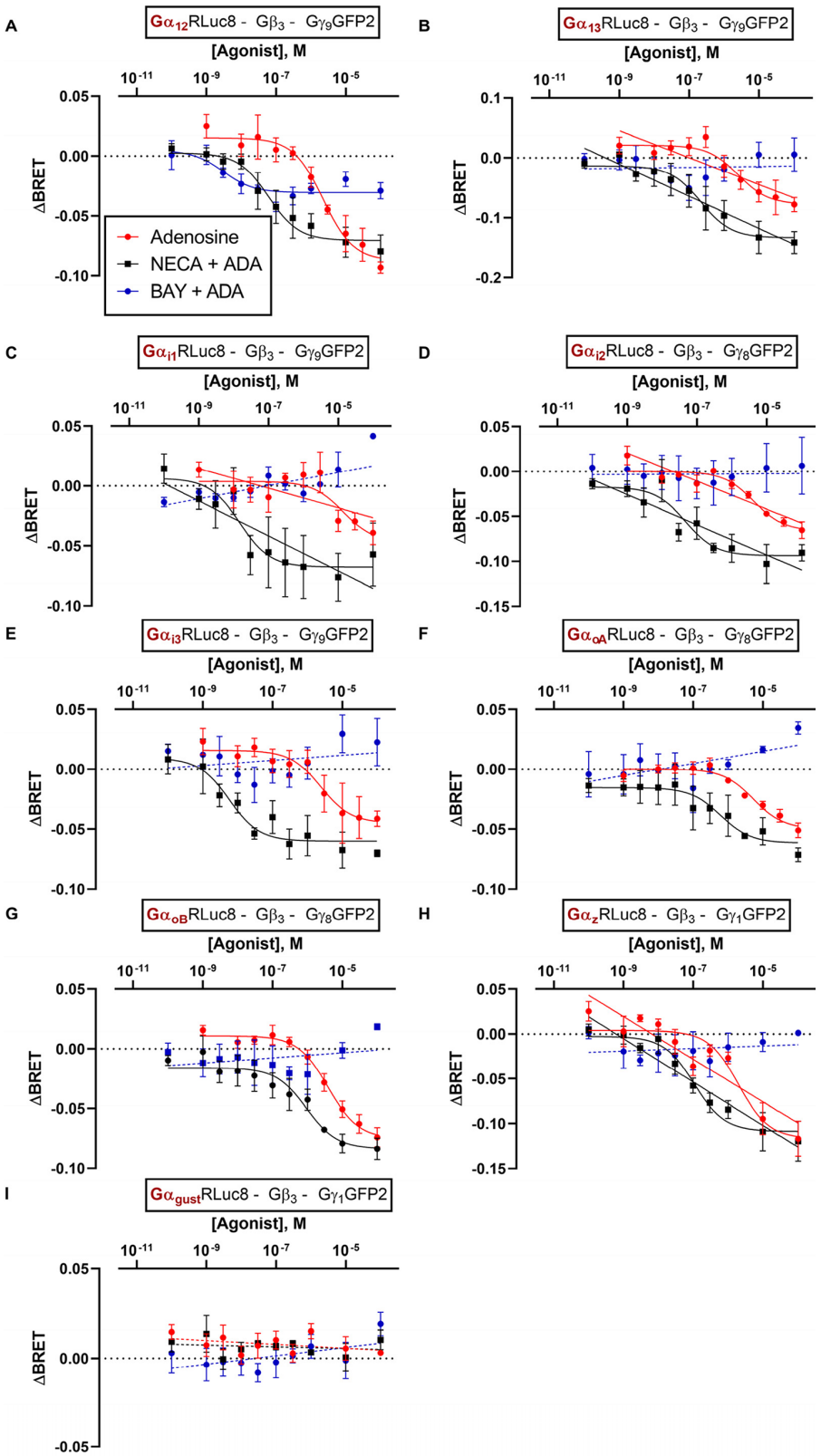

Figure 6. ΔBRET curves of the A_{2B}AR-agonists adenosine, NECA, and BAY 60-6583 at HEK293 cells transiently transfected with the A_{2B}AR and the indicated TRUPATH biosensors: A. $G\alpha_{12}$, B. $G\alpha_{13}$, C. $G\alpha_{i1}$, D. $G\alpha_{i2}$, E. $G\alpha_{i3}$, F. $G\alpha_{oA}$, G. $G\alpha_{oB}$, H. $G\alpha_{z}$, I. $G\alpha_{gust}$. Curves for NECA and BAY 60-6583 were determined in the presence of 2 U/ml ADA. Data points were obtained in 3−7 independent experiments, each performed with two technical replicates, and are represented as mean ± SEM. All pEC_{50} and E_{max} values are collected in Tables S2 and S3.

https://doi.org/10.1021/acsptsci.2c00020
ACS Pharmacol. Transl. Sci. 2022, 5, 373−386

ACS Pharmacology & Translational Science pubs.acs.org/ptsci Article

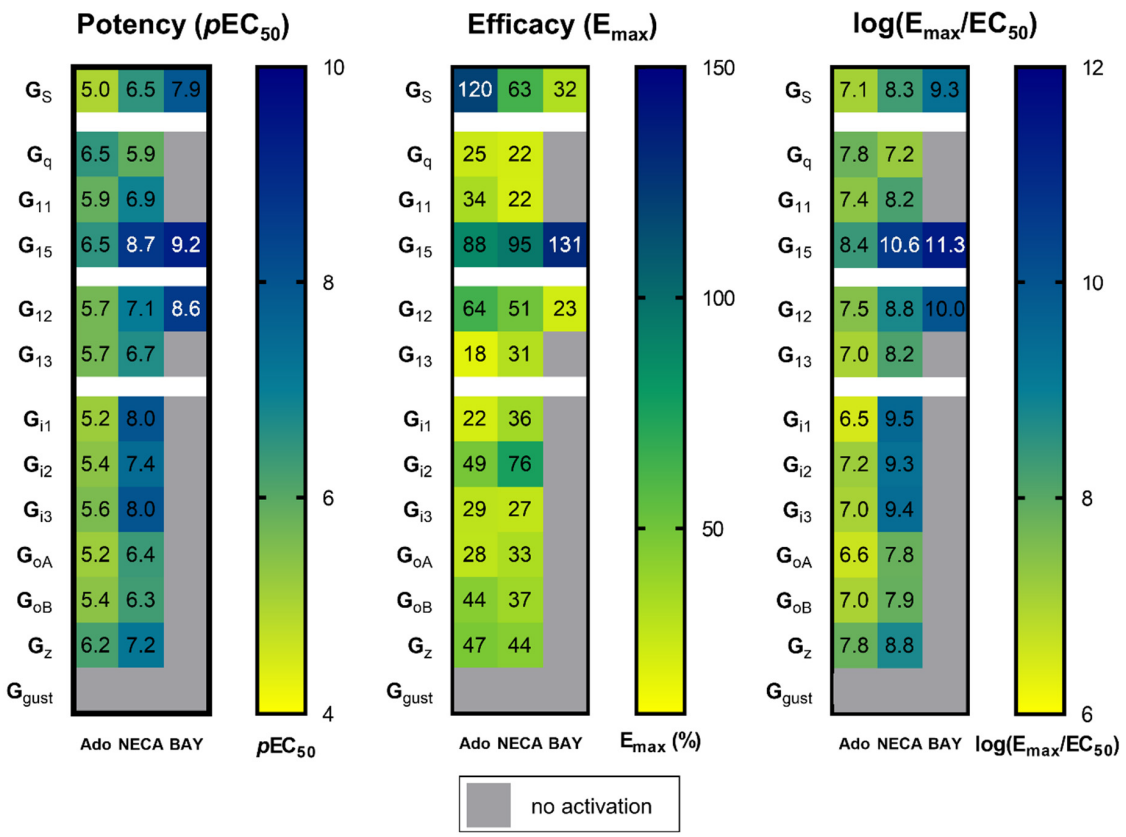

Figure 7. Heatmaps depicting potency (pEC_{50} values) and efficacy (E_{max} values given as % of maximal efficacy (E_{max}) of control receptors: isoprotenerol-activated β_2 adrenoceptor for the $G\alpha_s$ family, DAMGO-activated μ-opioid receptor for the $G\alpha_{i/o}$ family, neurotensin-activated neurotensin 1 receptor for the $G\alpha_{q/11}$ and the $G\alpha_{12/13}$ family), and a transduction coefficient expressed as log (E_{max}/EC_{50}).[31] Data for NECA and BAY 60-6583 (BAY) were determined in the presence of ADA. Units for log(E_{max}/EC_{50}): E_{max} is in %, EC_{50} in mol/L.

(see Figure 6; pEC_{50} and E_{max} values are collected in Tables S2 and S3).

All three agonists were able to activate the $G\alpha_{12}$ protein (Figure 6A). BAY 60-6583 acted as a partial agonist displaying ca. 36% efficacy relative to adenosine. Similar to the situation at $G\alpha_{15}$ and $G\alpha_{s\text{-}s}$ proteins, BAY 60-6583 and NECA were much more potent than adenosine. At the $G\alpha_{13}$ protein, adenosine and NECA displayed similar potency as at the $G\alpha_{12}$ protein, but adenosine was less efficacious than NECA, and BAY 60-6583 was inactive under the employed conditions (Figure 6B).

In further experiments, the $G\alpha_{i/o}$ protein family was investigated. Again, both adenosine and NECA displayed concentration-dependent $G\alpha_i$ protein activation. NECA was about 2 orders of magnitude more potent than adenosine in activating the $G\alpha_{i1-3}$, both agonists being similarly efficacious. In contrast, BAY 60-6583 did not activate any of the $G\alpha_i$ proteins (Figure 6C-E). Likewise, $G\alpha_{oA}$ and $G\alpha_{oB}$ biosensors were activated exclusively by adenosine and NECA, but not by BAY 60-6583; however, the potency of NECA was markedly lower at these $G\alpha$ protein subunits than at $G\alpha_{i1-3}$, while the potency of adenosine was similar in both cases (Figure 6F-G).

At the $G\alpha_z$ protein, a ubiquitously expressed, PTX-insensitive member of the $G\alpha_{i/o}$-family, adenosine displayed a slightly higher potency (Figure 6H) than at other $G\alpha_{i/o}$ proteins while the gustatory G protein $G\alpha_{gust}$ was not activated by any of the investigated $A_{2B}AR$ agonists (Figure 6I).

In summary, all $G\alpha$ protein subunits (with the exception of the $G\alpha_{gust}$ protein) could be activated by adenosine-stimulated $A_{2B}ARs$. The agonist NECA generally displayed higher potencies than adenosine, especially regarding the activation of $G\alpha_s$, $G\alpha_{i1-3}$, and $G\alpha_{15}$ proteins. BAY 60-6583 exclusively activated $G\alpha_s$, $G\alpha_{15}$, and $G\alpha_{12}$ protein subunits.

The extremely high promiscuity of the $A_{2B}AR$, activating virtually all $G\alpha$ protein subunits with pEC_{50} values for adenosine ranging from 5.0 to 6.5 as determined in the TRUPATH assay, raises the question: How does this actually translate into signal transduction? For example, $G\alpha_s$ proteins activate adenylate cyclase, while $G\alpha_{i/o}$ proteins inhibit the enzyme. Many of these G proteins, including $G\alpha_s$ and $G\alpha_i$, are coexpressed by a large number of cells. Why does G_s signaling in most cells win over G_i signaling induced by $A_{2B}ARs$? Besides differences in expression levels, different efficacies in activation of distinct $G\alpha$ proteins by the agonist-stimulated $A_{2B}AR$ might play a decisive role.

Efficacy of $A_{2B}AR$-Induced G Protein Activation. As demonstrated using the TRUPATH assay, the $A_{2B}AR$ induces activation, measured by dissociation from the $G\beta\gamma$-subunits, of nearly all $G\alpha$ protein subunits. However, the $A_{2B}AR$ is generally considered to be primarily a $G\alpha_s$-coupled and secondarily a $G\alpha_{q/11}$-coupled receptor. Besides potency (pEC_{50}), we additionally calculated efficacy (E_{max}) of agonist-induced $A_{2B}AR$-$G\alpha$ protein interactions. Thus, we compared the E_{max} values determined in the $A_{2B}AR$-dependent assays with the E_{max} values measured for model receptors, the

https://doi.org/10.1021/acsptsci.2c00020
ACS Pharmacol. Transl. Sci. 2022, 5, 373−386

isoproterenol-activated β_2 adrenoceptor for the $G\alpha_s$ family, the DAMGO-activated μ-opioid receptor for the $G\alpha_{i/o}$ family, and the neurotensin-activated neurotensin 1 receptor for the $G\alpha_{q/11}$ and the $G\alpha_{12/13}$ families.[31] The adenosine-activated $A_{2B}AR$ was observed to couple to $G\alpha_s$ proteins (efficacy: 120%) and also to the $G\alpha_{15}$ protein (88%) with an efficacy close to that of the control receptors (set at 100%); the efficacy in activating the $G\alpha_{12}$ protein was also still relatively high (64%) (see Figure 7 and Table S3; see Figure S3 for statistical analysis). A similar efficacy fingerprint was obtained for the $A_{2B}AR$ activated by NECA, but here we observed higher efficacy at the $G\alpha_{15}$ protein than at $G\alpha_s$ and $G\alpha_{12}$ proteins. NECA additionally activated the $G\alpha_{i2}$ subunit with relatively high efficacy (76%). At all other Gα proteins, the adenosine- and NECA-activated $A_{2B}AR$ displayed an efficacy below 50% of controls. The partial agonist BAY 60-6583 exclusively activated subunits displaying a high coupling efficacy for adenosine and NECA. It partially activated $G\alpha_s$ (32% efficacy) and the $G\alpha_{12}$ proteins (23%), and fully activated the $G\alpha_{15}$ protein (in comparison to the endogenous agonist adenosine as well as the control receptors).

The $\log(E_{max}/EC_{50})$ calculation is used to describe ligand bias toward a specific signaling pathway to provide a coefficient that includes both potency and efficacy.[48] These data are presented in Figure 7 for comparison. When this term is applied, the EC_{50} values appear to predominate while the efficacy values are underappreciated. Thus, we conclude that it is important to consider potencies and efficacies separately, in agreement with other authors.[31] Nevertheless, these data confirm the superior importance of the $G\alpha_{15}$ signaling pathway for all three investigated $A_{2B}AR$ agonists.

DISCUSSION

Previous studies on $A_{2B}AR$ signaling indicated that it could signal via multiple Gα proteins depending on the cell line studied.[14,39−42] However, only recently, novel methods have become available to unambiguously study the direct activation of specific Gα protein subunits upon stimulation with agonists.[31,35,37,38] In the present study, we determined agonist-dependent coupling of the human $A_{2B}AR$ to specific Gα protein subunits using two different approaches: (i) calcium mobilization assays utilizing CRISPR-Cas9-$G\alpha_{q/11}$-KO cells with re-expression of specific $G\alpha_q$ protein subunits ($G\alpha_q$, $G\alpha_{11}$, $G\alpha_{14}$, or $G\alpha_{15}$),[25] and (ii) TRUPATH BRET2 assays measuring dissociation of the G protein heterotrimer.[31] We investigated the coupling behavior induced by three different $A_{2B}AR$ agonists, the cognate agonist adenosine, its metabolically stable analog NECA, and the non-nucleosidic A_{2B}-selective partial agonist BAY 60-6583.[39] Based on our data, we conclude and confirm that the $A_{2B}AR$ is a promiscuous receptor. Upon activation with the full agonists adenosine or NECA it potentially interacted with all Gα protein subunits, with the exception of the $G\alpha_{gust}$ and the $G\alpha_{14}$ protein (the latter could only be tested in the calcium assays since a TRUPATH biosensor for $G\alpha_{14}$ has not been available). Activation of the $A_{2B}AR$ with the non-nucleosidic (partial) agonist BAY 60-6583, however, resulted exclusively in $G\alpha_{15}$, $G\alpha_s$, and $G\alpha_{12}$ coupling, with high efficacy at $G\alpha_{15}$, but low efficacy at the other Gα proteins.

Interestingly, the treatment of HEK293 cells with the adenosine-metabolizing enzyme ADA increased the potency of the agonists NECA (10-fold) and BAY 60-6583 (120-fold) exclusively at the $G\alpha_{15}$ subunit in TRUPATH BRET2 assays, while the efficacy of both agonists was approximately doubled (Figure 5). This may be explained by an allosteric modulation of the $A_{2B}AR$ by ADA as previously postulated.[49−51] ADA is proposed to act as an allosteric modulator facilitating a receptor conformation that exhibits high affinity for the $G\alpha_{15}$ protein. Another explanation could be that in cases where ADA appears to increase the potency of NECA, this could be due to the enzymatic activity of the enzyme.

It should be kept in mind that the employed test systems are highly artificial, the TRUPATH assays requiring overexpression of the $A_{2B}AR$ and control receptors. In calcium mobilization assays using HEK cells with low native $A_{2B}AR$ expression and recombinant expression of a single $G\alpha_q$ protein subunit, the full agonists adenosine and NECA sufficiently activated $G\alpha_{15}$ and $G\alpha_q$ proteins to induce calcium mobilization, but not $G\alpha_{11}$ and $G\alpha_{14}$ (see Figure 1). The partial agonist BAY 60-6583 only induced a calcium signal in cells recombinantly expressing a higher $A_{2B}AR$ level via the $G\alpha_{15}$ protein subunit (see Figure 4). These results point to a prominent role of the efficacy of a particular $A_{2B}AR$ agonist to activate a specific Gα protein subunit (see Figure 8). It appears

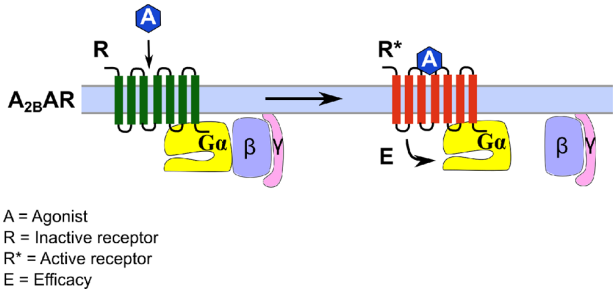

Figure 8. G protein dissociation induced by $A_{2B}AR$ activation. The agonist (A) binds to the receptor (R) with an agonist-specific affinity and induces an active conformation (R*). Different active conformations are conceivable depending on the employed agonist. The activated receptor binds to the heterotrimeric G protein (Gαβγ) with a receptor (R*)- and Gα-subunit-dependent affinity, and induces dissociation of the Gα- from the βγ-subunit with a specific efficacy (E) that depends on the nature and concentration of the agonist A, the receptor R*, and the Gα protein. The maximal efficacy (E_{max}) corresponds to the maximal effect observed for a specific agonist in a defined system.

that the efficacy fingerprint is an excellent indicator for the actual G protein coupling observed in native cells. Efficacies, however, can hardly be predicted at present, which may be the reason why computer programs have failed to correctly predict the G protein-coupling for the $A_{2B}AR$ (see precog.russel-lab.org).[52] Focus on potency rather than efficacy, or $\log(E_{max}/EC_{50})$ as previously proposed,[53] may not provide optimal results, at least for the $A_{2B}AR$.

The $A_{2B}AR$ couples most efficaciously to $G\alpha_s$ (E_{max} 120%), $G\alpha_{15}$ (88%) and $G\alpha_{12}$ proteins (64%) when activated by adenosine, and is therefore biased toward these signaling pathways. The (partial) agonist BAY 60-6583 only activated these three G proteins at all, with low efficacy in case of $G\alpha_s$ and $G\alpha_{12}$ (see Figure 7). Notably, the adenosine analog NECA additionally activated the $G\alpha_{i2}$ protein with relatively high efficacy (E_{max} 76%, compared to 49% for adenosine). Thus, the activation of specific G proteins is dependent on the employed agonist, and synthetic agonists do not necessarily imitate the activity of the physiological ligand.

https://doi.org/10.1021/acsptsci.2c00020
ACS Pharmacol. Transl. Sci. 2022, 5, 373−386

The preferential potent and efficacious coupling of the A_{2B}AR to $G\alpha_{15}$ proteins is of great importance in the context of immunology and immunotherapy since $G\alpha_{15}$ proteins are exclusively expressed on hematopoietic cells including immune cells.[54]

Studies on the Gα protein coupling of a large number of GPCRs have been recently published utilizing biochemical probes, such as the TRUPATH BRET2 assay,[31] the enhanced bystander BRET or EMTA assays,[37] and the TGFα shedding assay[34,38]). Inoue et al. employed the TGF-α shedding assay and found concentration-dependent coupling of the adenosine-activated A_{2B}AR to all investigated Gα protein subunits ($G\alpha_{i1}$, $G\alpha_{i3}$, $G\alpha_o$, $G\alpha_z$, $G\alpha_{12}$, $G\alpha_{13}$, $G\alpha_s$, $G\alpha_{olf}$, $G\alpha_q$, $G\alpha_{14}$) with the exception of the $G\alpha_{15}$ protein.[34] In contrast, the $G\alpha_{15}$ protein was potently and efficaciously activated by A_{2B}AR stimulation, both in TRUPATH BRET2 and calcium mobilization assays in the present study. The previously published study relied on chimeric $G\alpha_q$ proteins, which only harbored the six C-terminal residues of the $G\alpha_{15}$ protein to investigate its coupling. It appears likely that the interaction between the A_{2B}AR and the $G\alpha_{15}$ protein is based on other $G\alpha_{15}$-specific protein−protein interactions apart from the C-terminal residues. Thus, the $G\alpha_{15}$ protein is presumed to have a unique mode of engagement with and activation by the GPCR. In agreement with the present results, a study by Avet et al. using ebBRET/EMTA assays identified exclusively the $G\alpha_s$ and $G\alpha_{15}$ proteins as coupling partners for the adenosine-activated A_{2B}AR.[37] These proteins were likewise identified as the most efficacious coupling partners for the A_{2B}AR in the present study using TRUPATH BRET^2 assays (Figure 7).

At increasing A_{2B}AR or G protein density, e. g. in pathological scenarios such as inflammation and cancer,[12,14,55] A_{2B}AR activation by adenosine could result in efficacious activation of additional G proteins, such as $G\alpha_q$, $G\alpha_{11}$, $G\alpha_{i/o}$ or $G\alpha_{13}$ proteins.

In summary, each investigated agonist displays a characteristic signaling fingerprint regarding potency and especially efficacy at individual Gα protein subunits. The efficacy of the agonist-activated A_{2B}AR at certain Gα proteins appears to be decisive for biological significance of the respective signaling pathway. Since the cellular response to A_{2B}AR activation is dependent on the investigated cell type and the employed agonist, results from biological studies have to be interpreted with great care. BAY 60-6583 being a partial agonist does not imitate adenosine action, but nevertheless activates $G\alpha_{15}$, $G\alpha_s$, and $G\alpha_{12}$ proteins—presumably the most important downstream effectors of the A_{2B}AR. A highly potent A_{2B}-selective agonist that imitates adenosine action is currently not available, but would be most useful.

■ MATERIALS AND METHODS

Materials and Reagents. HEK293 $G\alpha_{q/11}$-KO cells were prepared by A. Inoue as previously described.[56] Dulbecco's modified Eagle medium (DMEM) and Hank's balanced salt solution (HBSS) buffer, supplemented with $CaCl_2$ and $MgCl_2$, were purchased from Sigma-Aldrich (Merck, Darmstadt, Germany). Fetal calf serum (FCS), G418, and penicillin-streptomycin were ordered from PAN Biotech (Aidenbach, Germany). Recombinant HEK293 cell lines stably expressing exclusively $G\alpha_{q/11}$ family subunits were created from CRISPR-Cas9-modified HEK293-Δ$G\alpha_{q/11}$ cells as previously described.[25] Fluo-4-AM was purchased from Invitrogen (ThermoFisher, Waltham, MA, USA). Adenosine and ATP disodium salt were from Sigma (St. Louis, MO, USA); NECA was purchased from SantaCruz (Dallas, TX, USA), carbachol was purchased from AlfaAesar (Haverhill, MA, USA), BAY 60-6583 was purchased from Tocris (Bristol, UK). PSB-10,[57] PSB-11,[58] PSB-36,[59] and PSB-603[60] were synthesized as previously described. Lipofectamine 2000 was ordered from ThermoFisher Scientific (Waltham, MA, USA). U46619 was ordered from SantaCruz.[61] Flat white-bottom 96-well plates were purchased from Greiner BioOne disposable materials such as pipet tips and cell culture flasks were purchased from Sarstedt (Nümbrecht, Germany).

Cultivation of Cells. Cells were cultured at 37 °C and 5% CO_2 in DMEM supplemented with 10% FCS, 0.1 mg/mL streptomycin, and 100 U/ml penicillin (growth medium). If cells stably expressed recombinant genes, G418 (200 μg/mL) was added to the medium. At 70−80% confluency, cells were detached by trypsination, diluted with growth medium, and transferred into a fresh cell culture flask. Retroviral transfection of HEK293-Δ$G\alpha_{q/11}$ cells was performed as previously described.[25]

Calcium Mobilization Assay. Calcium mobilization was measured as previously described for the $P2Y_2$ receptor.[62] In short, cells were trypsinized from cell culture flasks and seeded into a black clear-bottom 96-well plate (Corning 3340, Corning, Amsterdam, NL) in a final volume of 200 μL per well (40,000 cells per well) 1 day before the assay. Cells were incubated overnight in 96-well plates. On the next day, the supernatant medium was discarded and the following solution (40 μL) was added: HBSS buffer containing 3 μM fluo-4-AM + 0.075% w/v Pluronic F-127 ("dye solution"). All steps of the assay were performed at room temperature. The cells were incubated with the dye solution for 60 min while gently shaking. Then, the dye solution was removed and a mixture of 178 μL HBSS + 2 μL DMSO (without or with inhibitor) was added. If no inhibitor was present, the measurement was performed after a 2 min equilibration period. All assays in the presence of inhibitory compounds were preincubated for 30 min with the inhibitor before the measurement started. Cells were transferred to a plate reader (NovoStar, BMG Labtech, Offenburg, Germany). The A_{2B}AR was activated by the addition of 20 μL of agonist solution in HBSS (negative control: pure HBSS buffer). Fluorescence at 525 nm was measured for 40 s per well. Raw data were obtained in arbitrary fluorescence units (AU) and were corrected for the background signal (fluorescence intensity in the absence of agonist). If data were normalized, the normalization procedure was performed as indicated (see Figures). Each data point was recorded in duplicate or triplicate in three or more independent experiments. Dose−response curves were generated with Graph Pad Prism 8.0 (GraphPad, San Diego, CA, USA) using the "sigmoidal dose-response, variable slope" function. The assay principle is visualized in Figure S1B.

When the A_{2B}AR was transiently overexpressed for calcium mobilization assays, cells were transfected for 12 h with 100 or 1000 ng of hADORA2B-pcDNA3.1 per well in a 6-well plate (denoted as 100 ng DNA/well and 1000 ng DNA/well, respectively), 4 h after seeding the cells, using Lipofectamine 2000 according to the manufacturer's protocol. At the end of the 12 h period, the medium was exchanged. Transfected cells were harvested and transferred to 96-well plates 24 h after the end of the transfection, and from thereon the assay procedure was continued as described above.

https://doi.org/10.1021/acsptsci.2c00020
ACS Pharmacol. Transl. Sci. 2022, 5, 373−386

BRET2 TRUPATH Assay. G protein heterotrimer dissociation was measured in HEK293 cells using the TRUPATH assay kit.[31] TRUPATH plasmids were a gift from Bryan Roth (University of North Carolina on Chapel Hill, NC, USA) and shipped via Addgene (Addgene kit no. 1000000163). The measurements were performed as indicated in the original publication with minor modifications to the original protocol. On the first day, HEK293 cells cultivated in growth medium were detached from cell culture flasks by trypsination. Cells were seeded into 6-well plates at a density of approximately 500 000 cells per well in a volume of 2 mL, and incubated at 37 °C for 2 h before transfection. Transient transfection of HEK293 cells with the TRUPATH biosensors (100 ng of each pcDNA5/FRT/TO-Gα-RLuc8, pcDNA3.1-Gβ, and pcDNA3.1-Gγ-GFP2 per well) and the receptor of interest (100 ng receptor cDNA in pcDNA3.1 per well) was performed with Lipofectamine 2000 (2.5 μL per μg cDNA, ThermoFisher, Waltham, MA, USA). Lipofectamine was diluted in OptiMEM, incubated at room temperature for 10 min, and subsequently added to the DNA mixture in OptiMEM to a final volume of 500 μL per well. The mixture was added to the cells and the transfection was performed overnight. On the second day, media were removed, and cells were detached by pipetting and transferred to 96-well white bottom plates (Greiner BioOne, Frickenhausen, Germany) at a density of 30 000 cells per well in 60 μL of growth medium. On the third day, the medium was carefully aspirated, and cells were gently washed with assay buffer (HBSS + 20 mM HEPES pH 7.4). Assay buffer (60 μL per well; in experiments with adenosine deaminase (ADA), the buffer was supplemented with 5 μg ADA (Roche, Basel, Switzerland) per ml of buffer) and luciferase solution (50 μM coelenterazine 400a (Biomol, Hamburg, Germany) in assay buffer) were added to the cells. After a 5 min equilibration period, agonist solution (30 μL; 1% final DMSO concentration diluted in assay buffer) was added to the cells. After another 5 min equilibration period, luminescence and fluorescence were measured on a Mithras LB940 plate reader, using 395 and 510 nm emission filters for the RLuc8 and GFP2 signals, respectively. During assay optimization, the measurments were performed for several time points between 5 and 15 min after substrate addition.While BRET ratios remained stable, the absolute RLuc and GFP2 counts decreased over time probably due to degradation of the substrate. The ratio between the GFP2 and the RLuc8 signal intensity was computed and corrected for the baseline signal to obtain ΔBRET values, which were then fit to the "log (agonist) vs. response (three parameters)" equation in GraphPad PRISM 8 (GraphPad, San Diego, CA, USA) as suggested by Olsen et al.[31] to determine pEC_{50} values and maximum efficacy (top-bottom of the sigmoidal concentration–response curve). The assay principle is visualized in Figure S1C.

DATA ANALYSIS

All data are expressed as mean ± standard error of the mean (SEM) of at least three independent experiments performed with at least two replicates per experiment. To test for significant differences between two groups, an unpaired *t*-test was employed. To assess significant differences among three or more groups, a one-way analysis of variance (ANOVA) was used. Significant thresholds are defined as follows: not significant (ns) $p > 0.05$, * $p < 0.05$, ** $p < 0.01$, *** $p < 0.001$. Data analysis was performed with GraphPad PRISM v8.0 (GraphPad, San Diego, CA, USA).

To assess differences in potency and efficacy for each individual agonist across all Gα protein subunits for all results obtained in the TRUPATH BRET2 assays, mean efficacies and potencies of each agonist (depicted in Figure 7) were compared to each other by a one-way ANOVA. The mean of each column was compared with the mean of each other column and corrected for multiple comparisons by Turkey's test. All p-values, depicted in Figure S3, are multiplicity-adjusted.

ASSOCIATED CONTENT

Supporting Information

The Supporting Information is available free of charge at https://pubs.acs.org/doi/10.1021/acsptsci.2c00020.

Tables S1–S3, listing all determined potencies and efficacies in calcium and BRET^2 assays; Figures S1 and S2, displaying structures of the employed agonists, the assay principles, and reference curves obtained during establishment of TRUPATH BRET^2 assays (PDF)

AUTHOR INFORMATION

Corresponding Author

Christa E. Müller – *PharmaCenter Bonn, Pharmaceutical Institute, Pharmaceutical & Medicinal Chemistry, University of Bonn, D-53121 Bonn, Germany; Research Training Group GRK1873, University of Bonn, D-53121 Bonn, Germany;* orcid.org/0000-0002-0013-6624; Phone: +49-(0)-228-73-2301; Email: christa.mueller@uni-bonn.de; Fax: +49-(0)-228-73-2567

Authors

Jan Hendrik Voss – *PharmaCenter Bonn, Pharmaceutical Institute, Pharmaceutical & Medicinal Chemistry, University of Bonn, D-53121 Bonn, Germany;* orcid.org/0000-0003-0595-4607

Andhika B. Mahardhika – *PharmaCenter Bonn, Pharmaceutical Institute, Pharmaceutical & Medicinal Chemistry, University of Bonn, D-53121 Bonn, Germany; Research Training Group GRK1873, University of Bonn, D-53121 Bonn, Germany;* orcid.org/0000-0002-0456-1353

Asuka Inoue – *Graduate School of Pharmaceutical Sciences, Tohoku University, Sendai, Miyagi 980-8578, Japan*

Complete contact information is available at: https://pubs.acs.org/10.1021/acsptsci.2c00020

Funding

J.H.V., A.B.M., and C.E.M. were supported by the Deutsche Forschungsgemeinschaft (DFG, FOR2372, GRK1328). J.H.V., A.B.M., and C.E.M. are grateful for funding by the BMBF-funded Bonn International Graduate School Drug Sciences (BIGS DrugS). C.E.M. was supported by the EU COST Action ERNEST CA18133. A.B.M. is grateful for funding by the Ministry of Finance of Indonesia in the scheme of Indonesia Endowment Fund for Education (Lembaga Pengelola Dana Pendidikan (LPDP). A.I. was funded by the Japan Society for the Promotion of Science (JSPS) KAKENHI grants 21H04791 and 21H05113, FOREST JPMJFR215T from the Japan Science and Technology Agency (JST), LEAP JP20gm0010004 and BINDS JP20am0101095 from the Japan Agency for Medical Research and Development (AMED), the

Takeda Science Foundation, the Daiichi Sankyo Foundation of Life Science, and The Uehara Memorial Foundation.

Notes

The authors declare no competing financial interest.

■ ACKNOWLEDGMENTS

We thank Dr. Bryan Roth, University of North Carolina School of Medicine, Chapel Hill, NC, USA, for sharing the TRUPATH Biosensor Platform.

■ ABBREVIATIONS

A_1AR, adenosine A_1 receptor; A_{2A}R, adenosine A_{2A} receptor; A_{2B}AR, adenosine A_{2B} receptor; A_3R, adenosine A_3 receptor; AC, adenylate cyclase; ADA, adenosine deaminase; Ado, adenosine; AR, adenosine receptor; ATP, adenosine triphospate; $BRET^2$, bioluminescence resonance energy transfer type 2; CCh, carbachol; CRISPR-Cas9, clustered regularly interspaced short palindromic repeats - CRISPR-associated protein 9; EMTA, effector-membrane translocator assays; GDP, guanosine diphosphate; GFP2, green fluorescent protein-2; GPCR, G protein-coupled receptor; GTP, guanosine triphosphate; HEK293, human embryonic kidney type 293; M_3R, muscarinic M3 receptor; NECA, 5′-*N*-ethylcarboxamidoadenosine; Rluc8, Renilla luciferase; TGF-α, transforming growth factor-α; TP, thromboxane receptor

■ REFERENCES

(1) Müller, C. E.; Baqi, Y.; Namasivayam, V. Agonists and antagonists for purinergic receptors. *Methods Mol. Biol.* **2020**, *2041*, 45−64.

(2) Müller, C. E.; Baqi, Y.; Hinz, S.; Namasivayam, V. Medicinal chemistry of A_{2B} adenosine receptors. In *The adenosine receptors*; Borea, P. A., Varani, K., Gessi, S., Merighi, S., Vincenzi, F., Eds.; The Receptors Vol. *34*; Springer International Publishing, 2018; pp 137−168. DOI: 10.1007/978-3-319-90808-3_6

(3) Jenner, P.; Mori, A.; Aradi, S. D.; Hauser, R. A. Istradefylline - a first generation adenosine A_{2A} antagonist for the treatment of Parkinson's disease. *Exp. Rev. Neurother.* **2021**, *21* (3), 317−333.

(4) Chen, J.-F.; Cunha, R. A. The belated US FDA approval of the adenosine A_{2A} receptor antagonist istradefylline for treatment of Parkinson's disease. *Purinergic Signal.* **2020**, *16* (2), 167−174.

(5) Ghimire, G.; Hage, F. G.; Heo, J.; Iskandrian, A. E. Regadenoson: a focused update. *J. Nucl. Cardiol.* **2013**, *20* (2), 284−288.

(6) Rankin, A. C.; Brooks, R.; Ruskin, J. N.; McGovern, B. A. Adenosine and the treatment of supraventricular tachycardia. *Am. J. Med.* **1992**, *92*, 655−664.

(7) Borea, P. A.; Gessi, S.; Merighi, S.; Vincenzi, F.; Varani, K. Pharmacology of adenosine receptors: the state of the art. *Physiol. Rev.* **2018**, *98* (3), 1591−1625.

(8) Jamwal, S.; Mittal, A.; Kumar, P.; Alhayani, D. M.; Al-Aboudi, A. Therapeutic potential of agonists and antagonists of A_1, A_{2A}, A_{2B} and A_3 adenosine receptors. *Curr. Pharm. Des.* **2019**, *25* (26), 2892−2905.

(9) Chandrasekaran, B.; Samarneh, S.; Jaber, A. M. Y.; Kassab, G.; Agrawal, N. Therapeutic potentials of A_{2B} adenosine receptor ligands: current status and perspectives. *Curr. Pharm. Des.* **2019**, *25* (25), 2741−2771.

(10) Cacciari, B.; Pastorin, G.; Bolcato, C.; Spalluto, G.; Bacilieri, M.; Moro, S. A_{2B} adenosine receptor antagonists: recent developments. *Mini Rev. Med. Chem.* **2005**, *5* (12), 1053−1060.

(11) Kotańska, M.; Szafarz, M.; Mika, K.; Dziubina, A.; Bednarski, M.; Müller, C. E.; Sapa, J.; Kieć-Kononowicz, K. PSB 603 - a known selective adenosine A_{2B} receptor antagonist - has anti-inflammatory activity in mice. *Biomed. Pharmacother.* **2021**, *135*, 111164.

(12) Gao, Z.-G.; Jacobson, K. A. A_{2B} adenosine receptor and cancer. *Int. J. Mol. Sci.* **2019**, *20* (20), 5139.

(13) Ohta, A.; Sitkovsky, M. Extracellular adenosine-mediated modulation of regulatory T cells. *Front. Immunol.* **2014**, *5*, 304.

(14) Feoktistov, I.; Biaggioni, I. Role of adenosine A_{2B} receptors in inflammation. *Adv. Pharmacol.* **2011**, *61*, 115−144.

(15) Frick, J.-S.; MacManus, C. F.; Scully, M.; Glover, L. E.; Eltzschig, H. K.; Colgan, S. P. Contribution of adenosine A_{2B} receptors to inflammatory parameters of experimental colitis. *J. Immunol.* **2009**, *182*, 4957−4964.

(16) Xaus, J.; Mirabet, M.; Lloberas, J.; Soler, C.; Lluis, C.; Franco, R.; Celada, A. IFN-gamma up-regulates the A_{2B} adenosine receptor expression in macrophages: a mechanism of macrophage deactivation. *J. Immunol.* **1999**, *162* (6), 3607−3614.

(17) Sepúlveda, C.; Palomo, I.; Fuentes, E. Role of adenosine A_{2B} receptor overexpression in tumor progression. *Life Sci.* **2016**, *166*, 92−99.

(18) Long, J. S.; Crighton, D.; O'Prey, J.; Mackay, G.; Zheng, L.; Palmer, T. M.; Gottlieb, E.; Ryan, K. M. Extracellular adenosine sensing-a metabolic cell death priming mechanism downstream of p53. *Mol. Cell.* **2013**, *50* (3), 394−406.

(19) Simon, M. I.; Strathmann, M. P.; Gautam, N. Diversity of G proteins in signal transduction. *Science* **1991**, *252* (5007), 802−808.

(20) Milligan, G.; Kostenis, E. Heterotrimeric G-proteins: A short history. *Br. J. Pharmacol.* **2006**, *147* (Suppl 1), S46−S55.

(21) Dror, R. O.; Mildorf, T. J.; Hilger, D.; Manglik, A.; Borhani, D. W.; Arlow, D. H.; Philippsen, A.; Villanueva, N.; Yang, Z.; Lerch, M. T.; Hubbell, W. L.; Kobilka, B. K.; Sunahara, R. K.; Shaw, D. E. Signal Transduction. Structural basis for nucleotide exchange in heterotrimeric G proteins. *Science* **2015**, *348* (6241), 1361−1365.

(22) Suzuki, N.; Hajicek, N.; Kozasa, T. Regulation and physiological functions of $G_{12/13}$-mediated signaling pathways. *Neurosignals* **2009**, *17* (1), 55−70.

(23) Ran, F. A.; Hsu, P. D.; Wright, J.; Agarwala, V.; Scott, D. A.; Zhang, F. Genome engineering using the CRISPR-Cas9 system. *Nat. Protoc.* **2013**, *8* (11), 2281−2308.

(24) Annala, S.; Feng, X.; Shridhar, N.; Eryilmaz, F.; Patt, J.; Yang, J.; Pfeil, E. M.; Cervantes-Villagrana, R. D.; Inoue, A.; Häberlein, F.; Slodczyk, T.; Reher, R.; Kehraus, S.; Monteleone, S.; Schrage, R.; Heycke, N.; Rick, U.; Engel, S.; Pfeifer, A.; Kolb, P.; König, G.; Bünemann, M.; Tüting, T.; Vázquez-Prado, J.; Gutkind, J. S.; Gaffal, E.; Kostenis, E. Direct targeting of $G\alpha_q$ and $G\alpha_{11}$ oncoproteins in cancer cells. *Sci. Signal.* **2019**, *12* (573), aau5948.

(25) Kuschak, M.; Namasivayam, V.; Rafehi, M.; Voss, J. H.; Garg, J.; Schlegel, J. G.; Abdelrahman, A.; Kehraus, S.; Reher, R.; Küppers, J.; Sylvester, K.; Hinz, S.; Matthey, M.; Wenzel, D.; Fleischmann, B. K.; Pfeifer, A.; Inoue, A.; Gütschow, M.; König, G. M.; Müller, C. E. Cell-permeable high-affinity tracers for G_q proteins provide structural insights, reveal distinct binding kinetics, and identify small molecule inhibitors. *Br. J. Pharmacol.* **2020**, *177* (8), 1898−1916.

(26) Okashah, N.; Wan, Q.; Ghosh, S.; Sandhu, M.; Inoue, A.; Vaidehi, N.; Lambert, N. A. Variable G protein determinants of GPCR coupling selectivity. *Proc. Natl. Acad. Sci. U. S. A.* **2019**, *116* (24), 12054−12059.

(27) Patt, J.; Alenfelder, J.; Pfeil, E. M.; Voss, J. H.; Merten, N.; Eryilmaz, F.; Heycke, N.; Rick, U.; Inoue, A.; Kehraus, S.; Deupi, X.; Müller, C. E.; König, G. M.; Crüsemann, M.; Kostenis, E. An experimental strategy to probe G_q contribution to signal transduction in living cells. *J. Biol. Chem.* **2021**, *296*, 100472.

(28) White, A. D.; Jean-Alphonse, F. G.; Fang, F.; Peña, K. A.; Liu, S.; König, G. M.; Inoue, A.; Aslanoglou, D.; Gellman, S. H.; Kostenis, E.; Xiao, K.; Vilardaga, J.-P. $G_{q/11}$-dependent regulation of endosomal cAMP generation by parathyroid hormone class B GPCR. *Proc. Natl. Acad. Sci. U. S. A.* **2020**, *117* (13), 7455−7460.

(29) Galés, C.; van Durm, J. J. J.; Schaak, S.; Pontier, S.; Percherancier, Y.; Audet, M.; Paris, H.; Bouvier, M. Probing the activation-promoted structural rearrangements in preassembled receptor-G protein complexes. *Nat. Struct. Mol. Biol.* **2006**, *13*, 778−786.

(30) Galés, C.; Rebois, R. V.; Hogue, M.; Trieu, P.; Breit, A.; Hébert, T. E.; Bouvier, M. Real-time monitoring of receptor and G-protein interactions in living cells. *Nat. Methods* **2005**, *2*, 177−184.
(31) Olsen, R. H. J.; DiBerto, J. F.; English, J. G.; Glaudin, A. M.; Krumm, B. E.; Slocum, S. T.; Che, T.; Gavin, A. C.; McCorvy, J. D.; Roth, B. L.; Strachan, R. T. TRUPATH, an open-source biosensor platform for interrogating the GPCR transducerome. *Nat. Chem. Biol.* **2020**, *16*, 841.
(32) Laschet, C.; Dupuis, N.; Hanson, J. A dynamic and screening-compatible nanoluciferase-based complementation assay enables profiling of individual GPCR-G protein interactions. *J. Biol. Chem.* **2019**, *294* (11), 4079−4090.
(33) Wan, Q.; Okashah, N.; Inoue, A.; Nehmé, R.; Carpenter, B.; Tate, C. G.; Lambert, N. A. Mini G protein probes for active G protein-coupled receptors (GPCRs) in live cells. *J. Biol. Chem.* **2018**, *293* (19), 7466−7473.
(34) Inoue, A.; Raimondi, F.; Kadji, F. M. N.; Singh, G.; Kishi, T.; Uwamizu, A.; Ono, Y.; Shinjo, Y.; Ishida, S.; Arang, N.; Kawakami, K.; Gutkind, J. S.; Aoki, J.; Russell, R. B. Illuminating G protein-coupling selectivity of GPCRs. *Cell* **2019**, *177* (7), 1933−1947.e25.
(35) Dixon, A. S.; Schwinn, M. K.; Hall, M. P.; Zimmerman, K.; Otto, P.; Lubben, T. H.; Butler, B. L.; Binkowski, B. F.; Machleidt, T.; Kirkland, T. A.; Wood, M. G.; Eggers, C. T.; Encell, L. P.; Wood, K. V. NanoLuc complementation reporter optimized for accurate measurement of protein interactions in cells. *ACS Chem. Biol.* **2016**, *11* (2), 400−408.
(36) Wright, S. C.; Lukasheva, V.; Le Gouill, C.; Kobayashi, H.; Breton, B.; Mailhot-Larouche, S.; Blondel-Tepaz, É.; Antunes Vieira, N.; Costa-Neto, C.; Héroux, M.; Lambert, N. A.; Parreiras-E-Silva, L. T.; Bouvier, M. BRET-based effector membrane translocation assay monitors GPCR-promoted and endocytosis-mediated G_q activation at early endosomes. *Proc. Natl. Acad. Sci. U. S. A.* **2021**, *118* (20), e2025846118.
(37) Avet, C.; Mancini, A.; Breton, B.; Le Gouill, C.; Hauser, A. S.; Normand, C.; Kobayashi, H.; Gross, F.; Hogue, M.; Lukasheva, V.; St-Onge, S.; Carrier, M.; Héroux, M.; Morissette, S.; Fauman, E. B.; Fortin, J.-P.; Schann, S.; Leroy, X.; Gloriam, D. E.; Bouvier, M. Effector membrane translocation biosensors reveal G protein and β-arrestin coupling profiles of 100 therapeutically relevant GPCRs. *eLife* **2022**, *11*, 74101 DOI: 10.7554/eLife.74101.
(38) Inoue, A.; Ishiguro, J.; Kitamura, H.; Arima, N.; Okutani, M.; Shuto, A.; Higashiyama, S.; Ohwada, T.; Arai, H.; Makide, K.; Aoki, J. TGFα shedding assay: an accurate and versatile method for detecting GPCR activation. *Nat. Methods* **2012**, *9* (10), 1021−1029.
(39) Hinz, S.; Lacher, S. K.; Seibt, B. F.; Müller, C. E. BAY60-6583 acts as a partial agonist at adenosine A_{2B} receptors. *J. Pharm. Exp. Ther.* **2014**, *349* (3), 427−436.
(40) Gao, Z.-G.; Inoue, A.; Jacobson, K. A. On the G protein-coupling selectivity of the native A_{2B} adenosine receptor. *Biochem. Pharmacol.* **2018**, *151*, 201−213.
(41) Linden, J.; Thai, T.; Figler, H.; Jin, X.; Robeva, A. S. Characterization of human A_{2B} adenosine receptors: radioligand binding, western blotting, and coupling to G_q in human embryonic kidney 293 cells and HMC-1 mast cells. *Mol. Pharmacol.* **1999**, *56* (4), 705−713.
(42) Cohen, M. V.; Yang, X.; Downey, J. M. A_{2B} adenosine receptors can change their spots. *Br. J. Pharmacol.* **2010**, *159* (8), 1595−1597.
(43) Yang, X.; Xin, W.; Yang, X.-M.; Kuno, A.; Rich, T. C.; Cohen, M. V.; Downey, J. M. A_{2B} adenosine receptors inhibit superoxide production from mitochondrial complex I in rabbit cardiomyocytes via a mechanism sensitive to Pertussis toxin. *Br. J. Pharmacol.* **2011**, *163* (5), 995−1006.
(44) Atwood, B. K.; Lopez, J.; Wager-Miller, J.; Mackie, K.; Straiker, A. Expression of G protein-coupled receptors and related proteins in HEK293, AtT20, BV2, and N18 cell lines as revealed by microarray analysis. *BMC Genomics* **2011**, *12*, 14.
(45) Alnouri, M. W.; Jepards, S.; Casari, A.; Schiedel, A. C.; Hinz, S.; Müller, C. E. Selectivity is species-dependent: Characterization of standard agonists and antagonists at human, rat, and mouse adenosine receptors. *Purinergic Signal.* **2015**, *11* (3), 389−407.
(46) Ghiringhelli, F.; Bruchard, M.; Chalmin, F.; Rébé, C. Production of adenosine by ectonucleotidases: a key factor in tumor immunoescape. *J. Biomed. Biotechnol.* **2012**, *2012*, 473712.
(47) Zimmermann, H. History of ectonucleotidases and their role in purinergic signaling. *Biochem. Pharmacol.* **2021**, *187*, 114322.
(48) Winpenny, D.; Clark, M.; Cawkill, D. Biased ligand quantification in drug discovery: from theory to high throughput screening to identify new biased μ opioid receptor agonists. *Br. J. Pharmacol.* **2016**, *173* (8), 1393−1403.
(49) Herrera, C.; Casadó, V.; Ciruela, F.; Schofield, P.; Mallol, J.; Lluis, C.; Franco, R. Adenosine A_{2B} receptors behave as an alternative anchoring protein for cell surface adenosine deaminase in lymphocytes and cultured cells. *Mol. Pharmacol.* **2001**, *59* (1), 127−134.
(50) Gracia, E.; Farré, D.; Cortés, A.; Ferrer-Costa, C.; Orozco, M.; Mallol, J.; Lluís, C.; Canela, E. I.; McCormick, P. J.; Franco, R.; Fanelli, F.; Casadó, V. The catalytic site structural gate of adenosine deaminase allosterically modulates ligand binding to adenosine receptors. *FASEB J.* **2013**, *27* (3), 1048−1061.
(51) Moreno, E.; Canet, J.; Gracia, E.; Lluís, C.; Mallol, J.; Canela, E. I.; Cortés, A.; Casadó, V. Molecular evidence of adenosine deaminase linking adenosine A_{2A} receptor and CD26 proteins. *Front. Pharmacol.* **2018**, *9*, 106.
(52) Singh, G.; Inoue, A.; Gutkind, J. S.; Russell, R. B.; Raimondi, F. PRECOG: PREdicting COupling probabilities of G-protein coupled receptors. *Nucleic Acids Res.* **2019**, *47* (W1), W395−W401.
(53) Hauser, A. S.; Avet, C.; Normand, C.; Mancini, A.; Inoue, A.; Bouvier, M.; Gloriam, D. E. Common coupling map advances GPCR-G protein selectivity. *eLife* **2022**, *11*, 74107 DOI: 10.7554/eLife.74107.
(54) Amatruda, T. T.; Steele, D. A.; Slepak, V. Z.; Simon, M. I. G alpha 16, a G protein alpha subunit specifically expressed in hematopoietic cells. *Proc. Natl. Acad. Sci. U. S. A.* **1991**, *88* (13), 5587−5591.
(55) Onfroy, L.; Galandrin, S.; Pontier, S. M.; Seguelas, M.-H.; N'Guyen, D.; Senard, J.-M.; Gales, C. G protein stoichiometry dictates biased agonism through distinct receptor-G protein partitioning. *Sci. Rep.* **2017**, *7* (1), 7885.
(56) Schrage, R.; Schmitz, A.-L.; Gaffal, E.; Annala, S.; Kehraus, S.; Wenzel, D.; Büllesbach, K. M.; Bald, T.; Inoue, A.; Shinjo, Y.; Galandrin, S.; Shridhar, N.; Hesse, M.; Grundmann, M.; Merten, N.; Charpentier, T. H.; Martz, M.; Butcher, A. J.; Slodczyk, T.; Armando, S.; Effern, M.; Namkung, Y.; Jenkins, L.; Horn, V.; Stößel, A.; Dargatz, H.; Tietze, D.; Imhof, D.; Galés, C.; Drewke, C.; Müller, C. E.; Hölzel, M.; Milligan, G.; Tobin, A. B.; Gomeza, J.; Dohlman, H. G.; Sondek, J.; Harden, T. K.; Bouvier, M.; Laporte, S. A.; Aoki, J.; Fleischmann, B. K.; Mohr, K.; König, G. M.; Tüting, T.; Kostenis, E. The experimental power of FR900359 to study G_q-regulated biological processes. *Nat. Commun.* **2015**, *6*, 10156.
(57) Müller, C. E.; Burbiel, J.; Thorand, M. Improved, efficient synthesis for multigram-scale Production of PSB-10, a potent antagonist at human A_3 adenosine receptors. *Heterocycles* **2003**, *60* (6), 1425.
(58) Müller, C. E.; Diekmann, M.; Thorand, M.; Ozola, V. [^{3}H]8-Ethyl-4-methyl-2-phenyl-(8*R*)-4,5,7,8-tetrahydro-1*H*-imidazo[2,1-*i*]-purin-5-one ([^{3}H]PSB-11), a novel high-affinity antagonist radioligand for human A_3 adenosine receptors. *Bioorg. Med. Chem. Lett.* **2002**, *12* (3), 501−503.
(59) Weyler, S.; Fülle, F.; Diekmann, M.; Schumacher, B.; Hinz, S.; Klotz, K.-N.; Müller, C. E. Improving potency, selectivity, and water solubility of adenosine A_1 receptor antagonists: xanthines modified at position 3 and related pyrimido[1,2,3-*cd*]purinediones. *ChemMedChem.* **2006**, *1* (8), 891−902.
(60) Borrmann, T.; Hinz, S.; Bertarelli, D. C. G.; Li, W.; Florin, N. C.; Scheiff, A. B.; Müller, C. E. 1-Alkyl-8-(piperazine-1-sulfonyl)-phenylxanthines: development and characterization of adenosine A_{2B}

receptor antagonists and a new radioligand with subnanomolar affinity and subtype specificity. *J. Med. Chem.* **2009**, *52* (13), 3994−4006.
(61) Baqi, Y.; Alshaibani, S.; Ritter, K.; Abdelrahman, A.; Spinrath, A.; Kostenis, E.; Müller, C. E. Improved synthesis of 4-/6-substituted 2-carboxy-1H-indole-3-propionic acid derivatives and structure−activity relationships as GPR17 agonists. *Med. Chem. Commun.* **2014**, *5* (1), 86−92.
(62) Rafehi, M.; Neumann, A.; Baqi, Y.; Malik, E. M.; Wiese, M.; Namasivayam, V.; Müller, C. E. Molecular recognition of agonists and antagonists by the nucleotide-activated G protein-coupled P2Y2 receptor. *J. Med. Chem.* **2017**, *60* (20), 8425−8440.

https://doi.org/10.1021/acsptsci.2c00020
ACS Pharmacol. Transl. Sci. 2022, 5, 373−386

Supporting Information

Agonist-dependent coupling of the promiscuous adenosine A_{2B} receptor to Gα protein subunits

ACS Pharm. Transl. Sci., 2022

ACS Pharmacology & Translational Science

Agonist-dependent coupling of the promiscuous adenosine A_{2B} receptor to Gα protein subunits

Jan Hendrik Voss,[1] Andhika B. Mahardhika,[1,2] Asuka Inoue,[3] and Christa E. Müller[1,2]*

[1]PharmaCenter Bonn, Pharmaceutical Institute, Pharmaceutical & Medicinal Chemistry, University of Bonn, An der Immenburg 4, D-53121 Bonn, Germany

[2]Research Training Group GRK1873, University of Bonn, Germany

[3]Tohoku University, Graduate School of Pharmaceutical Sciences, Sendai, Miyagi, 980-8578 Japan

Keywords: adenosine, BAY 60-6583, G protein coupling, G_q/G_s/G_i/$G_{12/13}$ proteins, HEK293 cells, NECA

Running title: A_{2B} receptor Gα protein coupling

*To whom correspondence should be addressed: Prof. Dr. Christa E. Müller, Pharmaceutical Institute, Pharmaceutical & Medicinal Chemistry, University of Bonn, An der Immenburg 4, D-53121 Bonn, Germany, Phone: +49-(0)-228-73-2301; Fax: +49-(0)-228-73-2567; E-Mail: christa.mueller@uni-bonn.de

Table of contents

Table S1: Potency and efficacy of $A_{2B}AR$ agonists and CCh at HEK cells recombinantly expressing $G\alpha_{q/11}$ proteins determined by calcium mobilization assays. 3
Table S2: Potency (pEC_{50}) of $A_{2B}AR$ agonists at respective Gα proteins determined by TRUPATH BRET2 assays. 4
Table S3: Efficacy (E_{max}, % of maximum activation of a model receptor) of $A_{2B}AR$ agonists at respective Gα proteins determined by TRUPATH BRET2 assays. 5

Figure S1: Structures of the investigated $A_{2B}AR$ agonists, and assay principles of the calcium mobilization assay and the TRUPATH BRET2 assay. 7
Figure S2: Establishment of TRUPATH assay: concentration-response curves of standard agonists at control receptors. 8
Figure S3: Statistical analysis of TRUPATH BRET2 assay data. 9

Table S1: Potency and efficacy of $A_{2B}AR$ agonists and CCh at HEK cells recombinantly expressing $G\alpha_{q/11}$ proteins determined in calcium mobilization assays.

Cell line	**HEK-$G\alpha_q$**	**HEK-$G\alpha_{11}$**	**HEK-$G\alpha_{14}$**	**HEK-$G\alpha_{15}$**
Adenosine				
Potency (pEC_{50})	4.84 ± 0.17[b]	partial activation	partial activation	5.52 ± 0.29[c]
Efficacy (AU)	4398 ± 1290[b]	1800 ± 350[a]	3570 ± 680[b]	6480 ± 410[c]
NECA				
Potency (pEC_{50})	4.37 ± 0.34[b]	n.a.	n.a.	5.79 ± 0.21[c]
Efficacy (AU)	4820 ± 840[b]	n.a.	n.a.	5450 ± 900[c]
BAY 60-6583				
Potency (pEC_{50})	n.a.	n.a.	n.a.	n.a.
Efficacy (AU)	n.a.	n.a.	n.a.	n.a.
CCh				
Potency (pEC_{50})	6.61 ± 0.24	6.55 ± 0.18	5.12 ± 0.83	5.28 ± 0.32[a]
Efficacy (AU)	6160 ± 1370	6790 ± 890	8060 ± 2930	4750 ± 900[a]

Data are presented as means ± SEM from 3 independent experiments performed in duplicates if not otherwise indicated.
[a] Data from four independent experiments.
[b] Data from five independent experiments.
[c] Data from six independent experiments.
n.a. no activation at the highest tested concentration

Table S2: Potency (pEC_{50}) of $A_{2B}AR$ agonists at Gα proteins determined by TRUPATH BRET2 assays.

TRUPATH Biosensor	Adenosine	NECA -ADA	NECA +ADA	BAY -ADA	BAY 60-6583 + A A
$G\alpha_s$ subfamily					
$G\alpha_{s\text{-}s}$	4.99 ± 0.22	6.73 ± 0.18	6.50 ± 0.19[c]	7.46 ± 0.55	7.91 ± 0.45[a]
$G\alpha_{i/o}$ subfamily					
$G\alpha_{i1}$	5.19 ± 0.20	n.d.	7.97 ± 0.30	n.d.	n.a., <5
$G\alpha_{i2}$	5.38 ± 0.09	n.d.	7.43 ± 0.22	n.d.	n.a., <5
$G\alpha_{i3}$	5.58 ± 0.07	n.d.	8.00 ± 0.28	n.d.	n.a., <5
$G\alpha_{oA}$	5.18 ± 0.19[a]	n.d.	6.36 ± 0.71[a]	n.d.	n.a., <5
$G\alpha_{oB}$	5.39 ± 0.11[a]	n.d.	6.29 ± 0.49[b]	n.d.	n.a., <5
$G\alpha_{gust}$	n.a., <4	n.d.	n.a., <4	n.d.	n.a., <5
$G\alpha_z$	6.19 ± 0.48[a]	n.d.	7.17 ± 0.28[a]	n.d.	n.a., <5
$G\alpha_q$ subfamily					
$G\alpha_q$	6.48 ± 0.34[a]	7.05 ± 0.63[c]	5.90 ± 0.29[c]	n.a., <5	n.a., <5
$G\alpha_{11}$	5.85 ± 0.32[b]	7.89 ± 0.55[c]	6.90 ± 0.39[d]	n.a., <5	n.a., <5
$G\alpha_{15}$	6.51 ± 0.32[d]	7.56 ± 0.25[d]	8.67 ± 0.23[b]	7.14 ± 0.69[c]	9.23 ± 0.08
$G\alpha_{12/13}$ subfamily					
$G\alpha_{12}$	5.66 ± 0.03	n.d.	7.06 ± 0.48[a]	n.d.	8.61 ± 0.24[a]
$G\alpha_{13}$	5.66 ± 0.17	n.d.	6.67 ± 0.36[b]	n.d.	n.a., <5

Data are presented as means ± SEM from three independent experiments (unless otherwise noted) performed in duplicates.
pEC_{50} values calculated from experiments conducted with NECA and BAY 60-6583 were performed in the presence of ADA.
[a] Data from four independent experiments.
[b] Data from five independent experiments.
[c] Data from six independent experiments.
[d] Data from seven independent experiments.
n.a., no activation at the highest tested concentration
n.d., not determined

Table S3: Efficacy (E_{max}, % of maximum activation of a model receptor) of $A_{2B}AR$ agonists at respective Gα proteins determined by TRUPATH BRET2 assays.

TRUPATH Biosensor	Adenosine	NECA -ADA	NECA +ADA	BAY -ADA	BAY 60-6583 + A A
$G\alpha_s$ subfamily					
$G\alpha_{s\text{-}s}$	120 ± 15	110 ± 23	63 ± 6[c]	113 ± 38	32 ± 12[a]
$G\alpha_{i/o}$ subfamily					
$G\alpha_{i1}$	22 ± 5	n.d.	36 ± 6	n.d.	n.a., <10
$G\alpha_{i2}$	49 ± 18	n.d.	76 ± 12	n.d.	n.a., <10
$G\alpha_{i3}$	29 ± 2	n.d.	27 ± 4	n.d.	n.a., <10
$G\alpha_{oA}$	28 ± 4[a]	n.d.	33 ± 9[a]	n.d.	n.a., <10
$G\alpha_{oB}$	44 ± 4[a]	n.d.	37 ± 3[b]	n.d.	n.a., <10
$G\alpha_{gust}$	n.a., <4	n.d.	n.a., <4	n.d.	n.a., <10
$G\alpha_z$	47 ± 11[a]	n.d.	44 ± 11[a]	n.d.	n.a., <10
$G\alpha_{q/11}$ subfamily					
$G\alpha_q$	25 ± 6[a]	29 ± 6[c]	22 ± 2[c]	n.a., <10	n.a., <10
$G\alpha_{11}$	34 ± 4[b]	28 ± 3[c]	22 ± 4[d]	n.a., <10	n.a., <10
$G\alpha_{15}$	88 ± 24[d]	49 ± 9[c]	95 ± 18[b]	64 ± 20[c]	131 ± 13
$G\alpha_{12/13}$ subfamily					
$G\alpha_{12}$	64 ± 10	n.d.	51 ± 10[a]	n.d.	23 ± 2[a]
$G\alpha_{13}$	18 ± 6	n.d.	31 ± 2[b]	n.d.	n.a., <10

E_{max} values were calculated by dividing the maximum ΔBRET shift measured for the $A_{2B}AR$ by the maximum ΔBRET shift observed by a control receptor (β_2 adrenoceptor for the $G\alpha_s$ family, μ opioid receptor for the $G\alpha_{i/o}$ family, neurotensin 1 receptor for the $G\alpha_{q/11}$ and $G\alpha_{12/13}$ family). Means ± SEM from three independent experiments unless otherwise noted.

[a] Data from four independent experiments.

[b] Data from five independent experiments.

[c] Data from six independent experiments.

[d] Data from seven independent experiments.

n.a., no activation at the highest tested concentration

n.d., not determined

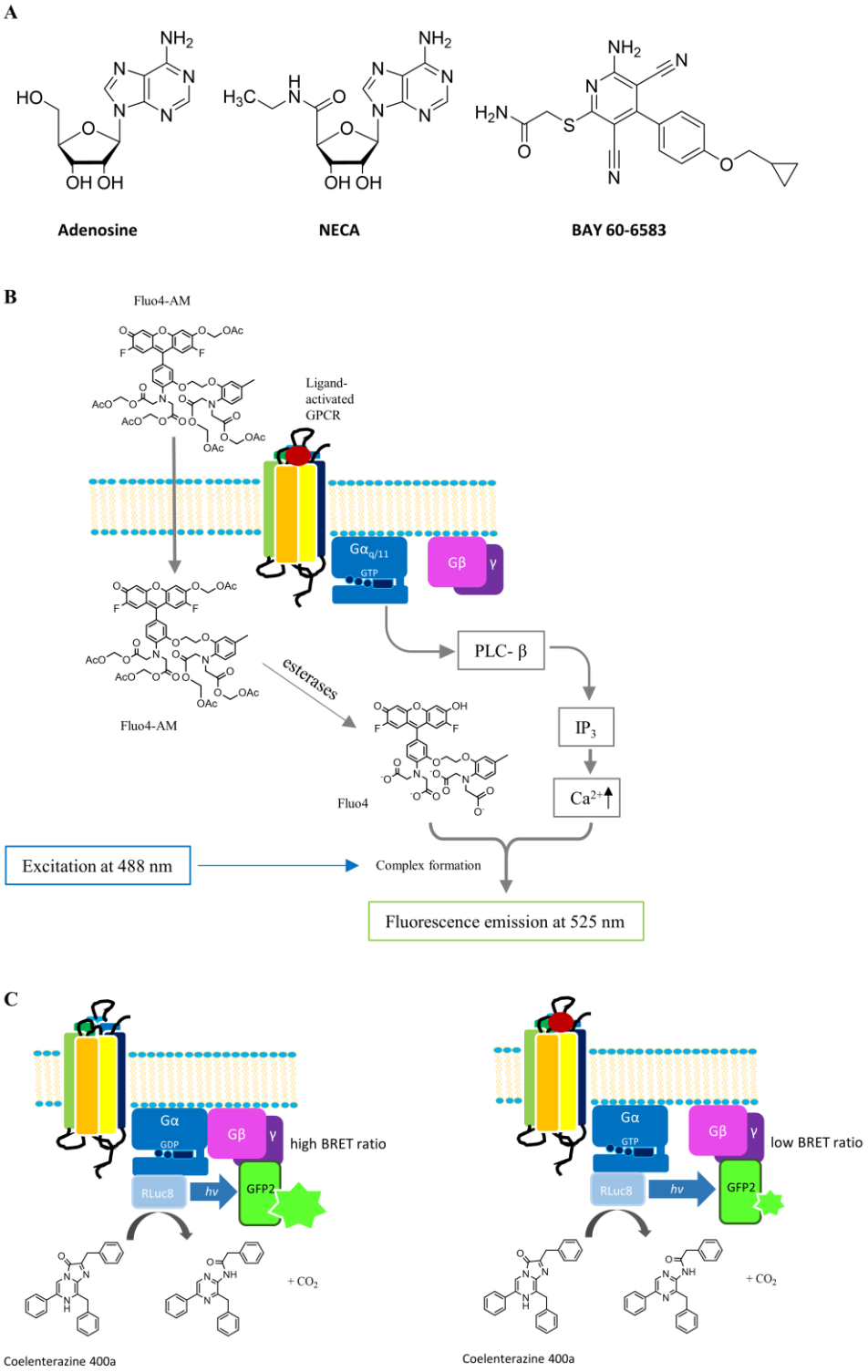
A
Adenosine
NECA
BAY 60-6583
B
Fluo4-AM
Ligand-activated GPCR
Gαq/11
GTP
Gβ
γ
PLC- β
esterases
Fluo4-AM
IP3
Ca2+
Fluo4
Excitation at 488 nm
Complex formation
Fluorescence emission at 525 nm
C
Gα
GDP
Gβ
γ
high BRET ratio
RLuc8
hv
GFP2
+ CO2
Coelenterazine 400a
Gα
GTP
Gβ
γ
low BRET ratio
RLuc8
hv
GFP2
+ CO2
Coelenterazine 400a

Figure S1: Structures of the investigated $A_{2B}AR$ agonists, and assay principles of the calcium mobilization assay and the TRUPATH BRET2 assay. **A**. Structural formulas of investigated $A_{2B}AR$ agonists. **B**. Calcium mobilization assay: Fluo-4-acetoxymethylester (Fluo-4-AM) penetrates the cell membrane. In the cytosol, the ester bonds are cleaved by esterases and the resulting anionic Fluo-4 is thereby trapped in the cytosol. Upon GPCR activation, $G_{q/11}$-family proteins release GDP and bind GTP instead, leading to calcium release from the endoplasmic reticulum via the phospholipase C-β (PLC-β) – inositol trisphosphate (IP_3) pathway. Free Ca^{2+} binds to Fluo-4 forming a fluorescent complex, which allows the monitoring of changes in the intracellular calcium concentration by fluorescence measurement at an emission wavelength of 520 nm after excitation of the complex at 488 nm. **C**. TRUPATH BRET2 assay: in the inactive receptor state, the RLuc8-tagged Gα subunit is bound to GDP and associated to the Gβγ dimer. The RLuc8 domain oxidizes coelenterazine 400a, emitting a constant signal of blue light, which in turn excites the proximate Gγ-GFP2 fusion protein resulting in a high BRET2 ratio (luminescence / fluorescence). In the active receptor state, the active, GTP-bound Gα-RLuc8 fusion protein separates from the Gβγ-GFP2 dimer. Due to the increased distance between RLuc8 and GFP2, energy transfer is reduced and the BRET2 ratio decreases.

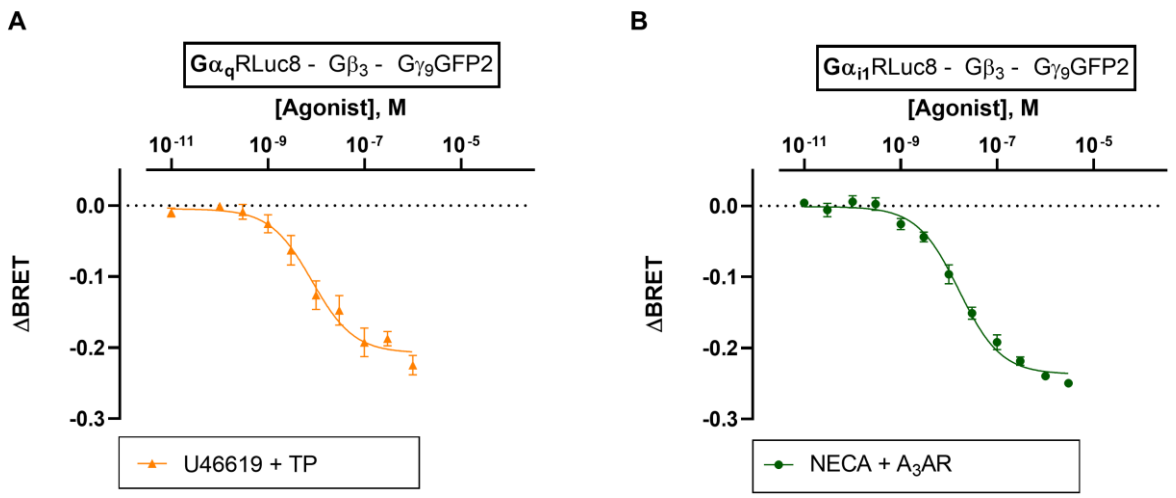

Figure S2: Establishment of TRUPATH assay: concentration-response curves of standard agonists at control receptors. **A**. $G\alpha_q$ biosensor, **B**. $G\alpha_{i1}$ biosensor, transiently expressed in HEK293 cells together with the investigated control GPCR. pEC_{50} values: $G\alpha_q$ - U46619 - TP = 8.02; $G\alpha_{i1}$ – NECA - A_3AR = 7.72. Data points are means ± SEM of three independent experiments performed in duplicates.

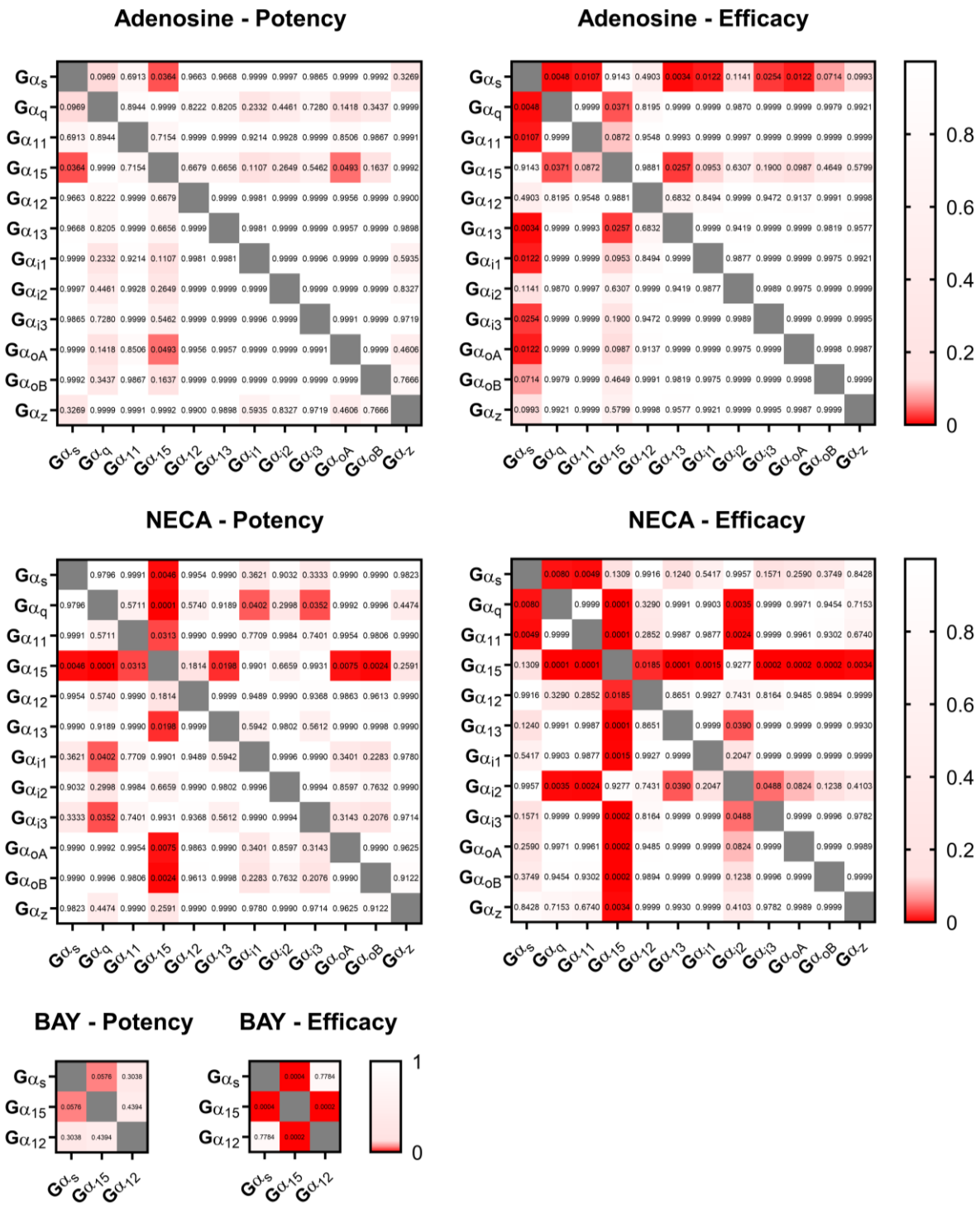

Figure S3: Statistical analysis of potency and efficacy values obtained from TRUPATH BRET2 assays. P-values were obtained from one-way analysis of variance (corrected for multiple comparisons using Turkey's test) comparing mean potencies and efficacies of adenosine (**A**, **B**), NECA (**C**, **D**), and BAY 60-6583 (**E**, **F**) at each investigated Gα subunit. High significance levels between means are indicated in red color.